Roles of the MAK-1 and MAK-2 MAP kinases modules in somatic cell fusion of filamentous fungi

Von der Fakultät für Lebenswissenschaften

der Technischen Universität Carolo-Wilhelmina zu Braunschweig

zur Erlangung des Grades eines

Doktors der Naturwissenschaften

(Dr. rer. nat.)

genehmigte

D i s s e r t a t i o n

von Antonio Serrano Salces

aus Córdoba / Spanien

1. Referent: Professor Dr. André Fleißner
2. Referent: Professor Dr. Norbert F. Käufer
eingereicht am: 03.04.2019
mündliche Prüfung (Disputation) am: 13.06.2019
Druckjahr 2019

Vorveröffentlichungen der Dissertation

Teilergebnisse aus dieser Arbeit wurden mit Genehmigung der Fakultät für Lebenswissenschaften, vertreten durch den Mentor der Arbeit, in folgenden Beiträgen vorab veröffentlicht

Publications

1. Fleißner, A. and Serrano, A. **The art of Networking: Vegetative Hyphal Fusion in Filamentous Ascomycete Fungi.** The Mycota Vol. I: Growth, Differentiation and Sexuality, 3rd ed., ed. by Jürgen Wendland. 2015

2. Serrano, A., Hammadeh, H., Herzog, S., Illgen, J., Schumann, M., Weichert, M., Fleißner, A., **The dynamics of signal complex formation mediating germling fusion in *Neurospora crassa***, Fungal Genetics and Biology (2017), doi: http://dx.doi.org/10.1016/j.fgb.2017.02.003

3. Serrano, A., Illgen, J., Brandt, U., Thieme, N., Letz, A., Lichius, A., Read, N.D., and Fleißner, A. (2018) **Spatio-temporal MAP kinase dynamics mediate cell behavior coordination during fungal somatic cell fusion**. J. Cell Sci. jcs.213462. doi:10.1242/jcs.213462

Conferences

1. Subcellular dynamics of MAPKs mediating tropism and cell fusion in *Neurospora crassa*. Oral presentation in the **ITN Fungibrain Network meeting II**. 19.09.14**,** Salamanca, Spain.

2. Subcellular dynamics of MAPKs mediating tropism and cell fusion in *Neurospora crassa*. Oral presentation in the **VAAM Mini-Symposium of the Special Group "Fungal Biology and Biotechnology".** 02.03.2015 Marburg, Germany.

3. Subcellular dynamics of MAPKs mediating tropism and cell fusion in *Neurospora crassa*. Oral presentation in the **ITN Fungibrain Network meeting III.** 15.06.15, Nice, France**.**

4. Role of different NAPDH oxidase components in the regulation of the MAP kinase MAK-2 during cell fusion in *Neurospora crassa*. Poster presentation in the **11th VAAM Conference Molecular Biology of Fungi,** 7-9.10.15, Berlin, Germany.

5. Role of different NAPDH oxidase components in the regulation of the MAP kinase MAK-2 during cell fusion in *Neurospora crassa*. Poster presentation in the **ITN Fungibrain Mid Term Review Meeting,** 16.10.15 Göttingen, Germany

6. Subcellular localization influences the activity of the MAP Kinase MAK-2 during cell fusion in *Neurospora crassa*. Oral presentation in the **European "Neurospora Meeting" at ECFG13 Workshop,** 3 April 2016, Paris, France.

7. Subcellular localization influences the activity of the MAP Kinase MAK-2 during cell fusion in *Neurospora crassa***.** Poster presentation in the **13th European Conference on Fungal Genetics (ECFG13),** 4-6 April 2016, Paris, France.

8. Roles of the MAP Kinase MAK-2 during cell fusion in *Neurospora crassa*. Oral presentation in the **ITN Fungibrain Network Meeting IV,** 16.09.16, Aberdeen, UK.

9. Subcellular dynamics of the MAP kinase MAK-2 correlate with its activity during germling fusion, thereby mediating a conserved cell-cell signaling mechanism. Oral and poster presentation in the **29th Fungal Genetics Conference.** 14-19 March 2017 in the Asilomar conference center, California, USA.

10. Cell fusion in filamentous fungi. Oral presentation in the **ITN Fungibrain Final Meeting**, 14-15.09.17, Córdoba, Spain.

11. Cell fusion in filamentous fungi. Oral presentation at the **12th conference of the VAAM special group Molecular Biology of Fungi**, 28-30 September 2017 in Jena, Germany.

12. Identification of novel functions of the cell wall integrity MAP kinase MAK-1 during cell polarity and cell fusion. Poster presentation at the **12th conference of the VAAM special group Molecular Biology of Fungi**, 28-30 September 2017 in Jena, Germany.

13. The cell dialog mechanism mediating vegetative cell fusion in fungi is conserved in the plant pathogen Botrytis cinerea. Oral presentation at the **Annual Conference 2018 of the Association for General and Applied Microbiology**, 15-18 April 2018 in Wolfsburg, Germany.

“We must not forget that when radium was discovered no one knew that it would prove useful in hospitals. **The work was one of pure science**. And this is a proof that scientific work must not be considered from the point of view of the direct usefulness of it. It must be done for itself, for the **beauty of science**, and then there is always the chance that a scientific discovery may become like the radium a benefit for humanity”

Marie Skłodowska Curie (7 November 1867 – 4 July 1934) was a Polish and naturalized French physicist and chemist who conducted pioneering research on radioactivity. She was the first woman to win a Nobel Prize, the first person and only woman to win twice, the only person to win a Nobel Prize in two different sciences and was part of the Curie family legacy of five Nobel Prizes. She was also the first woman to become a professor at the University of Paris, and in 1995 became the first woman to be entombed on her own merits in the Pantheon in Paris. Nowadays, the EU research council and the European commission honor her by naming the EU scientific program as Marie Curie Actions in which I, together with my other 13 colleagues from different European regions, joined as part of the Fungibrain consortium. With this little mention, I also want to honor her memory for its exceptional dedication and contribution to science.

A NATIVEL

Por todo el tiempo que nos ha robado, esta tesis es sólo tuya….

No estés lejos de mí un sólo día, porque cómo,
porque, no sé decírtelo, es largo el día,
y te estaré esperando como en las estaciones
cuando en alguna parte se durmieron los trenes.
No te vayas por una hora porque entonces
en esa hora se juntan las gotas del desvelo
y tal vez todo el humo que anda buscando casa
venga a matar aún mi corazón perdido.

Ay que no se quebrante tu silueta en la arena,
ay que no vuelen tus párpados en la ausencia:
no te vayas por un minuto, bien amada,

porque en ese minuto te habrás ido tan lejos
que yo cruzaré toda la tierra preguntando
sí volverás o si me dejarás muriendo.

Soneto 45, Cien sonetos de amor. Pablo Neruda.

…y que la distancia no nos vuelva a separar jamás.

Abbreviations

ºC	degree Celsius
1NM-PP1	1-(1,1-dimethylethyl)-3-(1-naphthalenylmethyl)-1H-pyrazolo[3,4-d]-pyrimidin-4-amine
ABP	Actin-binding protein
APS	Ammonium persulfate
ARP	Actin related protein
ATP	Adenosine triphosphate
bp	Base pair
BSA	Bovine serum albumin
CAT	Conidial anastomosis tube
cm	Centimeter
CWI	Cell wall integrity
DAD	Diaphanous-related formin autoregulatory domain
DID	Diaphanous-related formin inhibitory domain
DMSO	Dimethyl sulfoxide
DNA	Deoxyribonucleic acid
dsRED	*Discosoma* sp. red fluorescence protein
ER	Endoplasmic reticulum
erg	Ergosterol biosynthesis gene
FGSC	Fungal Genetics Stock Center
FH	Formin homology
GAPs	GTPase activating proteins
GDP	Guanosine diphosphate

GDIs	Guanine nucleotide dissociation inhibitors
GEFs	Guanine nucleotide exchange factors
GFP	Green fluorescence protein
GTP	Guanosine triphosphate
HGT	Horizontal gene transfer
hph	Hygromycine B phosphotransferase gene
HRP	Horseradish peroxidase
Hyg	Hygromycine
kb	kilobase
kDa	Kilodalton
KO	Knock-out
MAPK (2K) (3K)	Mitogen-activated protein kinase (kinase) (kinase)
mat	Mating type
MCS	Multiple cloning site
Min	minute
mL	milliliter
mm	milimiter
mM	millimolar
MM	minimal medium
µg	microgram
µl	microliter
µm	micrometer
µM	micromolar

nm	nanometer
NOX/Nox	NADPH-Oxidase
ORF	Open reading frame
PAK	p21-activated kinase
PCIA	Phenol:Chloroform:Isoamyl:Alcohol
PCR	Polymerase chain reaction
PEG	Polyethylene glycol
PKC	Protein kinase C
RBD	Rho-binding domain
Rho	Ras homologous
ROS	reactive oxygen species
rpm	rotations per minute
RT	room temperature
s	seconds
SD	standard deviation
SDS-PAGE	Sodium dodecyl sulfate polyacrylamide gel electrophoresis
SRM	Sterol-rich domain
SSPi	Single spore isolation
V	voltage
YRC	Yeast recombinational cloning

List of figures

List of tables

Introduction

1 Introduction

1.1 Cell fusion is essential for the development of eukaryotic organisms

Cell fusion (also termed cell-cell fusion) is a physiological process that plays an essential role in the development of most multicellular organisms. For example, cell fusion is fundamental during fertilization, in which the fusion of gametes initiates the development of a new individual organism (Zito et al., 2016). During muscle development, the fusion of myoblasts into multinucleate syncytia supports the formation of extended myofibrils and muscle regeneration (Abmayr and Pavlath, 2012). Very similar, cell fusion is needed for the creation of osteoclasts which are involved in bone formation and its misregulation might cause serious pathological conditions such as osteoporosis (Boyce, 2013). Interestingly, somatic cell fusion is also essential for the formation of syncytia in some organs (Shemer and Podbilewicz, 2000), or during the formation of the placenta of mammals through the fusion of trophoblast cells (Dittmar and Zänker, 2011).

In recent years, it has been shown that cell fusion is also crucial for the regeneration and reconnection of neuronal axons after injury, re-establishing the original axonal tract (Neumann et al., 2015, 2011). Cell fusion is also essential in some pathological conditions, such as virus infections. For example, infection by MPMV^{E}, a primate retrovirus that has no cytostatic or cytotoxic effects in humans, can cause cancer by inducing massive chromosomal instability through cell fusion of somatic cells (Duelli et al., 2007). In general, cell fusion is part of many fundamental processes in eukaryotic organisms, however the complex regulatory molecular machinery involved in the recognition of fusion partners, chemotaxis or chemotropism of the fusing cells, and plasma membrane fusion remain mostly unknown.

1.2 Fungal models to study cell fusion

Several models have been established to study the cell fusion process. Besides animal cell cultures models (originated from muscle cells and intestinal epithelial cells) and the nematode *Caenorhabditis elegans* (mostly for studying cell fusion during the epidermis formation), the organisms that have contributed more to understanding of this process

belong to the fungal kingdom. In fungi, cell fusion is observed generally in two different processes: sexual cell fusion (also known as mating) and somatic cell fusion (also known as vegetative cell fusion). The first is mediated by pheromones and occurs between two individuals of different mating type. It is usually performed by specialized cells that sense the gradient of pheromone produced by an opposite mating type cell. The cells grow towards each other until physical contact is established, after which both cytoplasms are fused and subsequently both nuclei are merged. This kind of cell fusion is observed in most fungal species, but it has been extensively studied in budding and fission yeast. In contrast, the second type of cell fusion occurs between non-specialized hyphae and/or spores and is mostly observed in filamentous fungi. Two spores or hyphae sense the presence of another cell (preferably from the same fungal colony) through a yet unknown molecule/peptide and grow towards each other in order to fuse. In this case, fusion of the cytoplasms does not necessarily induce karyogamie and a heterokaryon is formed if the original cells were genetically different. One of the most studied organisms of this fungal order is the filamentous fungus *Neurospora crassa*. In the next pages, the two type of cell fusion and the factors involved in this process are described in details.

1.2.1 Pheromone-mediated sexual cell fusion

Sexual reproduction requires two gametes that fuse and merge their DNA, resulting in a new individual organism. The mechanism behind the chemoattraction or chemotaxis, recognition between the partner cells, and fusion of the plasma membranes are studied in many different organisms. However, unicellular models such as the budding yeast *Saccharomyces cerevisiae* or the fission yeast *Schizosaccharomyces pombe* are the most extensively studied systems.

In both species, cell polarization is induced in response to secreted pheromones produced by the partner cells during the mating process. Cells of opposite mating type express the pheromones and their corresponding opposite pheromone-receptor. After binding of the pheromone to the receptor, the pheromone-response mitogen-activated protein (MAP) kinase module is activated, which controls cell cycle arrest and targets the transcription factors of mating-specific genes.

The pheromone response MAP (mitogen-activated protein) kinase pathway in budding yeast is one of the most studied signaling cascades in the MAP kinase field.

1.2.2 Fungal somatic cell fusion

The hallmark of filamentous fungi is their syncytial filaments, also known as hyphae. These hyphae form a highly interconnected network, known as the mycelial or fungal colony. Cross connections within this network are achieved through specific hyphae-to-hyphae interactions, which result in the fusion of hyphal branches and the formation of anastomoses. This entire process is termed hyphal fusion. Similarly, the early colony establishment involves the fusion between germinated (germlings) or ungerminated spores in a process generally known as germling fusion. Several spores, usually originated from the same fungal colony, germinate and fuse with each other thereby forming a merged functional unit, which later develops into the mycelial colony. Both processes occur in a pheromone-dispensable manner, which is one of the main differences between somatic and mating cell fusion. Although these processes were early described in the late 19. century, their physiological roles and molecular mechanisms are not fully understood.

1.2.2.1 Physiological roles of hyphal and germling fusion

In general, somatic cell fusion is certainly not essential for fungal propagation, since mutants defective in this process are usually still able to complete their life cycle. Interestingly, there are significant differences between the fusion rate of different isolates of the same fungal species, since some are able to fuse whilst others do not undergo somatic cell fusion (Heller et al., 2016; Hyakumachi and Ui, 1987). Different studies have found a correlation between fusion and spore yield in *N. crassa*, suggesting that cooperation and resource pooling within the functional fungal unit promotes competitiveness (Richard et al., 2012). In contrast, the formation of hundreds of colonies from all non-fusing spores results in competition for the resources and affects the healthiness of each fungal colony formed. Despite these functions, cell fusion seems to do not play any significant role in laboratory conditions, but its potential roles or significant advantages in nature cannot be excluded.

1.3 Molecular bases involved in mating and somatic cell fusion

Although the final purposes of these two fusion processes are different, the mechanisms and the molecular factors involved in both fusion types are partially shared, as have been already reviewed (Fleißner and Serrano, 2015; Herzog et al., 2015; Leeder et al., 2011; Martin and Arkowitz, 2014). For example, proteins such as MAP kinases, actin and polarity factors are involved in both somatic and sexual cell fusion besides their general role in polarized growth and sensing of environmental signals.

1.3.1 MAP kinases

Cellular communication often involves multiple pathways that coordinate the behaviour of the cell in response to extracellular stimuli. Sensing of these extracellular signals is mostly mediated by a highly conserved group of serine/threonine/tyrosine protein kinases so-called MAPK. These proteins are inactive in their base form. In order to be catalytically active, two phosphorylations events of the TxY (threonine-x-tyrosine) domain are neccesary. This activation is usually mediated by a phosphorylation cascade through two others components of the MAPK group: MAP2 kinase and MAP3 kinase. The group of the MAP2 kinase is often formed by members of the STE7 family. MAP2 kinases in turn, are activated by components of the serine/threonine MAP3 kinase. The three proteins work in a linear phosphorylation cascade which starts with the MAP3 kinase being phosphorylated at the membrane in presence of the stimulus and concludes with the activation of the MAPK and its translocation to different cellular compartments. In order to control the large variety of different cellular processes controlled by individual MAPKs, the kinases are well-regulated by phosphatases, interactions with other activating/deactivating factors and their subcellular localization (Wainstein and Seger, 2016). Activation of the MAPK often occurs at the plasma membrane, where maximal outputs are generated from low-level inputs, allowing the cells to respond accordingly to the extracellular stimuli (Harding et al., 2005). Upon activation, MAPK activity is regulated by its subcellular localization and inactivating phosphatases.

For example, the mammalian MAPK Erk1 is translocated to the nucleus through the importin7 upon activation. Preventing its translocation by using analogs based on the protein interaction domains of importin7 is nowadays used as a anticancer therapy (Plotnikov et al., 2015). In the nucleus, MAPK are known to phosphorylate many different transcription factors needed to respond to the extracellular signals (Chen and Thorner, 2007). Phosphatases that specifically regulate MAPK activation are often located inside the nucleus and act as negative regulators to control the signal output mediated by MAPK (Kondoh and Nishida, 2007). For example, restriction of MAPK to the plasma membrane and its prevention to translocate to the nucleus provokes a hyper-phosphorylation state of the protein, although no activation signal is provided (Chen et al., 2010). The regulation mediated by inactivating phosphatases is as important as the activation of the MAPK. When phosphatases are surpressed, cells do not respond properly to activating signals and MAPK activation leads to permanent and severe defects in the cells (Zhan et al., 1997). MAP kinases are problably the most intensively studied signaling factors within eukaryotic organisms due to their central and key roles in extracellular signals reception. As a consequence of the central role of these proteins, the study of knock-out mutants often does not reveal information on the function of the protein in all processes. Many different tools have been established in order to understand the different functions of MAP kinases. One of the most powerful tools is the use of analog-sensitive kinases, also known as Shokat alleles (Bishop et al., 2000). The use of these analog-sensitive versions can be extended to all protein kinases, including MAP kinases. All protein kinases need to hydrolyze ATP (adenosine triphosphate) in order to transfer the phosphate group to their protein target, yielding a phosphorylated protein. The three-dimensional structure and the amino acid sequence of the ATP binding pocket of protein kinases are highly conserved. The region which interacts with the adenosine moiety of the ATP contains a bulky hydrophobic residue, such as threonine, leucine, methionine, phenylalanine or isoleucine (Bishop et al., 2000). This amino acid is also called gatekeeper and is not essential for the ATP binding function of the domain. Interestingly, exchange of this residue to a small amino acid such as glycine or alanine results in additional space which allows the binding of larger ATP-analogs, such as 1-NM-PP1 (Fleißner, 2013; Wohlbold et al., 2012).

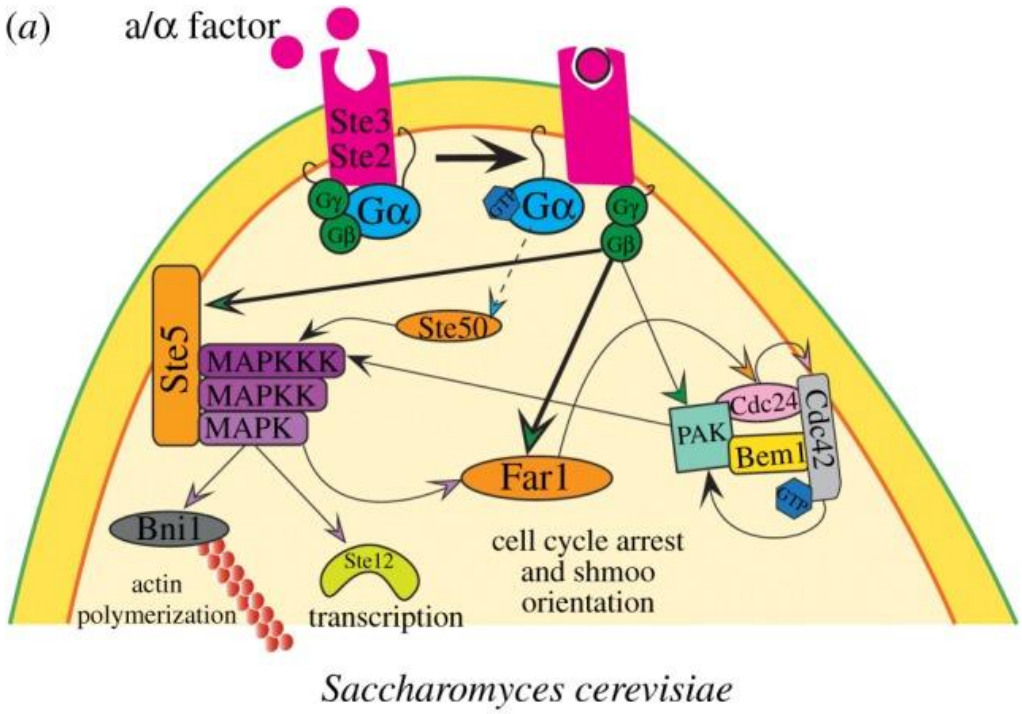

Figure 1.1. Pheromone response signaling in budding yeast. Depicted are the MAPK signaling cascade and some of the pathways activated after binding of the pheromone to the corresponding receptor (adapted from Merlini et al., 2013).

The chemical 4-Amino-1-tert-butyl-3-(1'-naphthylmethyl) pyrazolo [3, 4-d] pyrimidine (1-NM-PP1) (Toronto Research Chemicals) is a non-hydrolysable ATP-analog that can bind to mutated kinases with an enlarged ATP-binding site. In wild-type kinases, binding of the ATP-analog is sterically hindered. In contrast, the gatekeeper mutation inserted into the analog-sensitive kinase variants increases the binding affinity of the chemical, which now can compete with ATP during the enzymatic reaction. The use of this chemical and other analogs in budding yeast has revealed new functions and has helped to identify the Fus3p phosphorylation targets and phosphatases that would not have been identified by simple classical genetics (Alonso-Rodríguez et al., 2016; Genetics et al., 2007; Wohlbold et al., 2012)

1.3.1.1 MAP kinase activation in budding yeast

In yeast, pheromones (called a- and α-factor) are produced naturally by the cells on rich medium. Each pheromone binds to its cognate receptor, Ste3 for a- and Ste2 for α-factor, and both activate the Gαβγ heterotrimeric G-protein. Activation by a GDP (guanosine diphosphate) to GTP (guanosine triphosphate) exchange leads to the release of the Gβγ heterodimer. Specifically, Gβ promotes the activation of the scaffold protein Ste5 and binds physically to the p21-activated kinase (PAK)-like kinase Ste20. The scaffold protein Ste5 stimulates the interactions between the three-tiered MAP kinase cascade components and increases the efficiency of their interactions. The Ste20 kinase is the upstream component of the Fus3p MAP kinase cascade and triggers the phosphorylation of the MAPKKK Ste11. This activation occurs at the plasma membrane and induces the phosphorylation cascade, which leads to activation of the MAPKK Ste7 and the MAP kinase Fus3p. Once activated, Fus3p phosphorylates Ste5 to disassociate the protein complex and phosphorylates different targets, such as the transcription factor Ste12 or the cyclin-dependent kinase Cdk1, which overall promotes cell cycle arrest in G1. The cell polarizes its growth in the direction of the pheromone by redirecting the actin polarization through Fus3 phosphorylation of different cytoskeleton organizing factors, such as the formin Bni1. Shmoo projections are the consequence of this polarization. Once the two cells of opposite mating type establish contact, cell fusion and subsequent karyogamy occur (Fig. 1.1).

1.3.2 Actin assembly

Actin is a structural protein highly conserved in most living organisms. This protein can be present as a free monomer named G-actin or as part of a microfilament called F-actin. F-actin is composed by assembled G-actin. The assembly is highly dynamic and regulated by ATP hydrolyses and a large number of actin-binding proteins (ABPs). F-actin is organized in supra-structures that can be differentiated by their localization patterns and dynamics: actin patches, actin rings and actin cables (Berepiki et al., 2011).

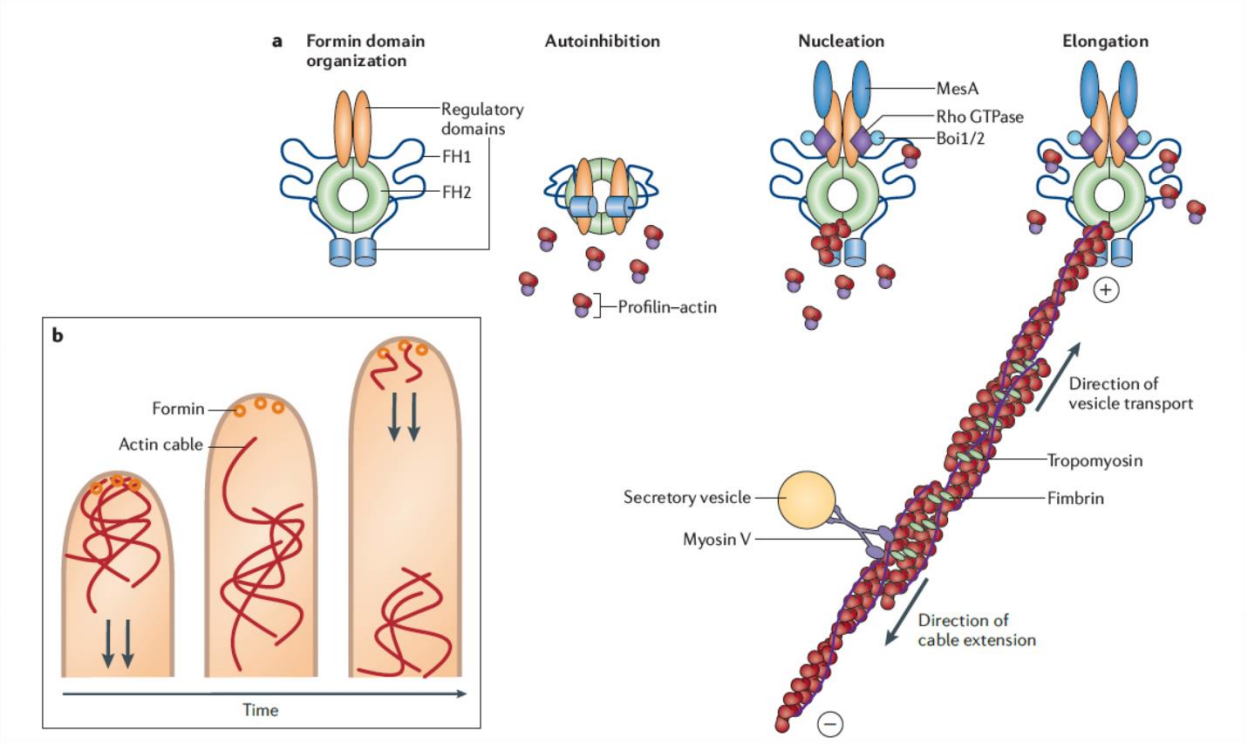

Figure 1.2. Actin cable polymerization mediated by formin. Representation of the factors involved in actin cable assembly (adapted from Berepiki et al., 2011).

Actin patches are formed by the accumulation of branched actin filaments in a major complex with other proteins, and they function in mediating endocytosis (Mooren et al., 2012; Robertson et al., 2009; Young et al., 2004). Recruitment of clathrin proteins to the plasma membrane induces the recruitment of the endocytic machinery, in which the actin-related protein 2/3 (Arp2/3) is part of. Activation of upstream components leads to the formation of a filamentous-actin network regulated by Arp2/3 and subsequent invagination and scission of the endocytic vesicle. Multiple reviews has summarized this process in budding yeast (Smythe and Ayscough, 2006), in fission yeast (Mishra et al., 2014), filamentous fungi (Berepiki et al., 2011), mammalian cells (Galletta et al., 2010) and plant cells (Fan et al., 2015). Actin rings are typically composed of actin filaments and myosin motors (actomyosin). After activation, these motor structures trigger ring constriction. In fungi, actin rings are part of the contractile actomyosin ring, which is formed by the recruitment of multiple signaling proteins (Bud-3, Bni-1, Bud-4, etc.).

Upon activation of the complex, the actomyosin ring contracts and produces membrane invagination, which also triggers cell wall biosynthesis resulting in septum formation. (Berepiki et al., 2011; Roh et al., 2002; Willet et al., 2016).

Actin cables function as tracks for the transport of multiples cargoes, such as actin patches, organelles, secretory vesicles, etc. The transport of cargoes is often mediated by myosin V motor proteins. They translocate along actin filaments and transport the cargoes usually to the plasma membrane for secretion (exocytosis). The assembly of the actin cables is mediated by a specialized group of proteins known as formins. These are conserved nucleators of actin filaments and are composed by two domains: formin homology 1 (FH1) domain and formin homology 2 (FH2) domain. The FH1 domain contains binding sites to actin-profilin complexes, and the FH2 domain controls the polymerization of the actin cable. Three more domains are found in formin proteins: the diaphanous-related formin inhibitory domain (DID), the Rho-binding domain (RBD) and the diaphanous-related formin autoregulatory domain (DAD). In budding yeast, the formin Bni1 is catalytically inactive in its base form due to autoinhibitory interactions between the DID and DAD domains. (Sagot et al., 2002). The members of the Rho (Ras homologous) small GTPase family are activators of formin proteins and regulate the actin cable polymerization. Indeed, the activation of formins occurs by interaction of the Rho proteins with the RBD domain of the formin, relieving the auto-inhibitory interaction of the DID and DAD domain and allowing the formin to be catalytically active. Three members of the family have been studied in detail in several organisms: Cdc42, Rac1 and RhoA (Fig. 1.2).

1.3.3 Rho-GTPases

Rho GTPases are small signaling G proteins which regulate several processes related to actin dynamics, such as cellular morphogenesis, phagocytosis, mitosis, cell polarity, etc. These proteins are molecular switches and perform their function by switching from an inactive GDP-bound state to an active GTP-bound state in response to extracellular stimuli. Several upstream regulators of Rho GTPases have been described.

These regulators are categorized as GTPase activating proteins (GAPs), Guanine nucleotide exchange factors (GEFs) and Guanine nucleotide dissociation inhibitors (GDIs).

While GAPs and GEFs proteins activate the Rho-GTPases in response to stimuli, the GDIs inhibit this activation. One of the most important GEF proteins is CDC-24, which is specific for both RAC-1 and CDC-42 in *N. crassa* (Araujo-Palomares et al., 2011). Interestingly, inactive Rho GTPases may be associated with the perinuclear endoplasmic reticulum (ER) and, upon activation, are accumulating to sterol-rich domains of the plasma membrane, usually at the cell tips of filamentous fungi (Araujo-Palomares et al., 2011; A. Lichius et al., 2014), although similar observations have also been made in yeasts, such as *S. pombe* (Tatebe et al., 2008) or *Candida albicans* (Corvest et al., 2013). Cdc42, Rac1 and RhoA have different roles and functions during development and growth. For example, in *N. crassa* RHO-A is essential for septa formation (also known as septation) but dispensable for general polarized growth (Rasmussen and Glass, 2005). In addition, CDC-42 and RAC-1 are essential for vegetative growth, but RAC-1 only functions during cell fusion-related polarization, while CDC-42 works in general polarity of non-interacting cells (Araujo-Palomares et al., 2011; A. Lichius et al., 2014).

1.3.4 Actin dynamics and cell fusion

The polarized growth of cells to chemoattractants, for example pheromones, is mediated through a highly regulated machinery which involves the activation of MAP kinases and spatial focalization of polarity core factors, such as formins, or Rho-GTPases. (Berepiki et al., 2010; A. Lichius et al., 2014; Martin and Arkowitz, 2014; Merlini et al., 2013). The concentration of formin-created actin at the cell tip is also known as a formin-nucleated actin aster. In fission yeast, formation of the actin aster is controlled by the formin Fus1 and type V myosins. The formin is needed for nucleation of the actin aster, and type V myosins are essential for the release of cell wall hydrolases, which degrade the cell wall between the interacting cells and allow the completion of the cell fusion process (Dudin et al., 2015). In budding yeast, actin aster and cable assembly are essential for recruitment of the MAP kinase Fus3p (Qi and Elion, 2007).

In addition, Fus3p positively regulates actin cable assembly through phosphorylation of the formin bni1p (Matheos et al., 2004), yielding a regulatory feedback loop that increases the phosphorylation of Fus3p and therefore the response to the pheromone signal.

In filamentous fungi, actin is essential for all types of growth (polarized hyphal extension or cell fusion). Disruption of actin during hyphal extension leads to rapid tip swelling, indicating an important function of actin into polarized growth (Berepiki et al., 2010). A highly dynamic actin aster is also observed in *N. crassa* cells undergoing cell fusion, and disruption of actin also arrests the growth of the interacting cells (Berepiki et al., 2010). Many actin-related proteins have been identified as essential for cell fusion. For example, the nucleation promoting factor BUD-6, BNI-1, the only formin identified in *N. crassa,* and the scaffolding protein that mediates BUD-6/BNI-1 interactions, SPA-2, are essential for cell fusion. All three proteins (which are part of the polarisome complex) localize to the cell tips of the interacting cells during cell fusion (Lichius et al., 2012). BUD-6 works as a promoter of actin nucleation that enhances actin cable extension through physical interactions with the formin BNI-1 and through the scaffolding protein SPA-2 (Graziano et al., 2011; Lichius et al., 2012). Actin is, overall, the main component of the polarization during cell fusion and many regulators tightly control its assembly and subcellular localization.

1.4 Neurospora crassa as a model organism

One of the best-known model organisms for studying somatic cell fusion is the red bread mold *N. crassa*. This fungus is part of the *Ascomycota* phylum and the order of *Sordariales*. It was first described from an infestation of French bakeries in 1843. This fungus became a model organism after the experiments performed by the Nobel laureates (Physiology or Medicine, 1958) Edward Tatum and George Well Beadle. They exposed *N. crassa* cells to x-rays, causing failures in metabolic pathways by mutation of specific enzymes. These data lead them to propose the “one gene, one enzyme” hypothesis. In recent years, this fungus has become a model organism and has been employed to study circadian rhythms, epigenetics, cell polarity, cell fusion and has very recently been used as a host for heterologous protein production (Havlik et al., 2017).

More interesting information on the history and the scientific achievement obtained with this fungus has been reviewed (Biosciences et al., 2014; Davis and Perkins, 2002).

As mentioned above, several different research topics have been developed by using this fungus due to its advantages as a model organism. For example, the genome has been fully sequenced and annotated since 2003 (Galagan et al., 2003) and an ongoing collaborative project is aiming to produce mutants for every single gene, with more than 9.600 genes knocked-out at the moment (Colot et al., 2006) (www.fgsc.net) (Fungal Genetics Stock Center). Another advantage of *N. crassa* is its very quick life cycle and its incapacity for causing diseases in animals or plants (Perkins and Davis, 2000). Like other ascomycete fungi, *N. crassa* possesses two mating types, named as “A“ and “a” with no morphological differences. Under laboratory conditions, the sexual female structure (protoperithecia) is formed under nitrogen starvation (Westergaard and Mitchell, 1947).

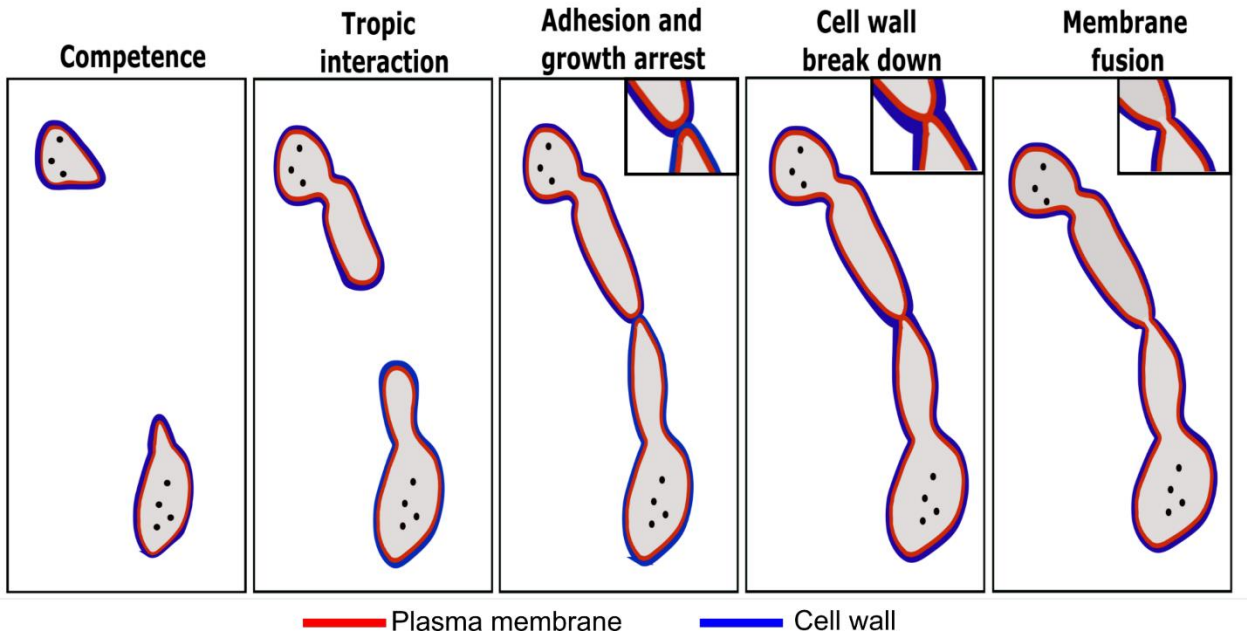

Figure 1.3. Steps of the cell fusion process. Initially, cells acquire a cell fusion competence and germinate. Afterwards, cells recognize the presence of a fusion-partner in their surroundings, and the cell communication mediated by MAK-2 and SO alternating membrane recruitment is started. Once cells establish physical contact, the growth is arrested and the machinery for degrading the cell wall is activated. Once the cell wall is degraded, the plasma membrane of both cells fuse, which allows the mixing of the cytoplasms

A specialized hypha named trichogyne is formed by the protoperithecium that senses pheromone secreted by cells of the opposite mating type and chemotropically grows towards the signal source.

Once fusion of the trichogyne and the male cell is completed and fertilization has been taking place (sexual cell fusion, similar to yeast) the perithecium matures and forms the sexual haploid ascospores. After a heat shock, these spores germinate and establish the fungal colony. When nitrogen becomes deficient, the cycle restarts by the induction of protoperithecia. A more extended description of the life cycle of *N. crassa* is provided by (Seale, 1973). In nature, the fungus is mostly found around the tropical region, growing on dead plant matter after fires, it is currently also discussed as an endophyte of plants, such as pine trees (Kuo et al., 2014).

1.5 Cell fusion in the filamentous fungus N. crassa

The establishment of the fungal colony depends in part on the ability of the fungal cells to undergo cell fusion. The first step of colony establishment is the germination of spores. In the laboratory, spores from the same strain (genetically identical) are incubated together in conditions that allow the observation of cell fusion. Germination is therefore induced and directly after, spores start to grow towards each other in order to fuse. Successive fusion events result in the formation of an interconnected cellular network. As a consequence, the individual germlings cooperate within one functional unit instead of competing for the available nutrients. Mechanistically the fusion process can be divided into five discernable steps: (1) acquisition of a cell fusion competent state, (2) cell communication between the two fusion partners and tropic growth towards each other, (3) cell growth arrest upon the physical contact, (4) cell wall remodeling at the contact area and (5) plasma membrane fusion and subsequent cytoplasm mixing (Fig. 1.3).

Throughout recent years the work of several research groups has identified more than 60 mutants affected in the fusion process. The respective factors include MAP kinase signaling cascades, reactive oxygen-generating systems, Ca^{2+} signaling, polarity factors and other signaling complexes conserved in eukaryotes.

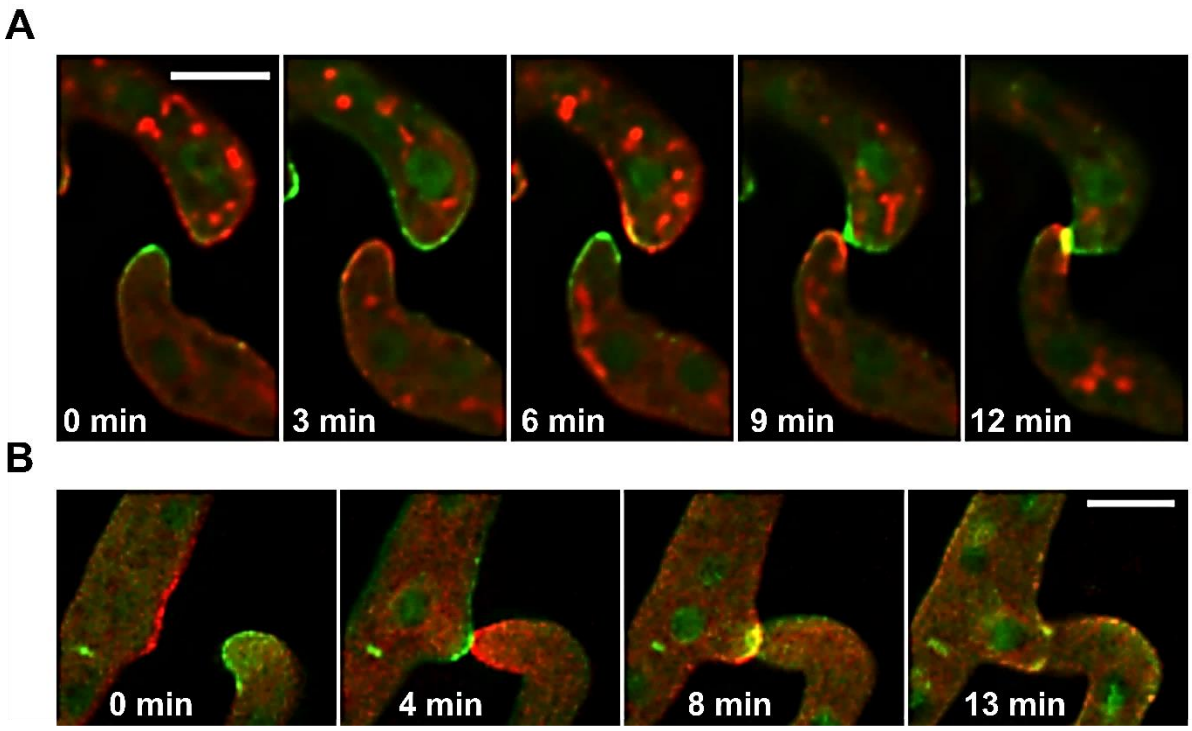

Figure 1.4. MAK-2-GFP and dsRed-SO localization during cell fusion. (A) Alternating oscillatory recruitment of MAK-2 and SO during germling fusion. Figure obtained from the movie published in Serrano et al., 2017. (B) Alternating oscillatory recruitment of MAK-2 and SO during hyphal fusion. This figure has been published in Serrano et al., 2018.

A complete overview of the reported factors and its function in cell fusion have been reviewed in (Fleißner and Serrano, 2015; Fu et al., 2011; Herzog et al., 2015). An important question on the vegetative cell fusion process is related to the communication process.

Since the cells undergoing cell fusion are genetically identical, they must somehow avoid self-signaling and control their response to the extracellular signals, in order to grow in the right direction. In 2009, it was described that this communication process was under control of two proteins: the MAP kinase MAK-2 and the protein of unknown function SO (Fleissner et al., 2009). While the study of knock-out mutants of these genes showed that they are essential for the cell fusion process (Fleißner and Glass, 2007; Pandey et al., 2004), the localization exposed a very unusual mode of communication. During the communication process (Fig. 1.4), both proteins localize to opposing cell tips of the interacting cells.

Surprisingly, this localization switches after 3-6 minutes and both MAK-2 and SO alternate in their localization to the cell tips. As a consequence, both proteins are recruited in an antiphase-manner. The switching process continues until the cells establish physical contact, when both proteins accumulate at the contact area (Fleissner et al., 2009; Serrano et al., 2017).

This communication has been interpreted as a kind of dialog between the cells. The current working model states that in order to avoid self-signaling, the cells coordinate their behavior and while one cell is sending a signal, the other cell is only receiving the signal. The roles then switch, and the cell that was sending the signal is now receiving, and the cell that was receiving is now sending the signal. Interestingly, this hypothesis is supported by mathematical modeling which states that the presence of MAK-2 at the cell tip is related to signal receiving, while the presence of SO is related to signal sending (Goryachev et al., 2012). So far, however, the nature of the signal and the cognate receptor remain unknown (Herzog et al., 2015).

A second MAP kinase is responsible for the cell growth arrest after cells establish physical contact: the cell wall integrity (CWI) MAP kinase MAK-1. This kinase is only recruited once the cells establish physical contact. Interestingly, partial inhibition of MAK-1 activity leads to a very unique phenotype in which cells continue to interact and grow even after establishing contact (Weichert et al., 2016).

1.5.1 Signal-receiving cell

The MAP kinase MAK-2 is homologous to the pheromone response MAP kinase Fus3p of budding yeast. During the cell communication process in germling/hyphal fusion, the kinase is recruited to the plasma membrane at the cell tip together with its MAK2P MEK-2, MAP3K NRC-1, the scaffolding adapter HAM-5 and the protein activating kinase STE50 (Dettmann et al., 2014, 2012; Jonkers et al., 2014). Upon reception of the signal and membrane recruitment of the MAK-2 complex, the kinase is likely phosphorylated by MEK-2 in the conserved phosphorylation sides T180 (Threonine) and Y182 (Tyrosine). This activation might lead to the disassembly of the complex and release of the kinase (Jonkers et al., 2014; Schürg et al., 2012; Weichert et al., 2016).

After nuclear translocation of the kinase, the expression of fusion-associated genes is induced through phosphorylation of the Ste12-like transcriptional factor PP-1 and the dimeric transcriptional factor RCO-1/RCM-1 (Aldabbous et al., 2010; Leeder et al., 2013). By using an analog-sensitive MAK-2 variant (MAK-2^{Q100A}) several phosphorylation targets that are involved in cell fusion, such as the scaffold protein HAM-5 or the adapter HAM-14 (Jonkers et al., 2016, 2014), were identified.

In addition, although not much is known about the regulatory relationship between MAK-2 and SO, it is known that MAK-2 activity is needed for the detachment of SO from the plasma membrane during cellular communication and directed growth (Fleissner et al., 2009). Potential upstream activators of the MAPK module have been identified in previous studies, such as the bud emergence protein BEM-1. The lack of BEM-1 leads to defects in MAK-2 phosphorylation, which also affects the cell fusion efficiency of the mutant strain (Schürg et al., 2012). In the endophytic fungus *Epichloë festucae*, BEM-1 has been identified as part of the ROS (reactive oxygen species) generating system (also known as NADPH oxidase complex) (Takemoto et al., 2011). In addition, the ROS generating system is essential for cell fusion in the plant pathogen *Botrytis cinerea* (Roca et al., 2012). In this thesis, the roles of the ROS generating system during cell fusion and its involvement in MAK-2 activation will be further elucidated.

1.5.2 Signal-sending cell

As mention above, mathematical modeling suggested that the presence of SO at the cell tip is related to signal sending during the communication process (Goryachev et al., 2012). SO is a protein conserved in all filamentous ascomycete fungi, however its roles are not very well understood (Fleißner et al., 2005). In the filamentous plant pathogen fungus *Alternaria brassisicola*, the mutation of *so1* leads to disruption of cell fusion and the loss of pathogenicity (Craven et al., 2008). In contrast, mutation of *fso* gene in *Fusarium oxysporum f. sp. Lycopersici* results in disruption of cell fusion while pathogenicity remains unaffected (Prados Rosales and Di Pietro, 2008). Interestingly, the deletion of the *so* gene in the plant endophyte *E. festucae* leads to disruption of the mutualistic symbiosis with the host plant and the fungus becomes pathogenic (Charlton

et al., 2012). Regarding the molecular function of the protein, the SO homolog in the filamentous fungus *Sordaria macrospora*, PRO40, has been described as a scaffold of the previously mentioned CWI MAP kinase MAK-1 cascade, linking the activation of the protein MAPK with the protein kinase C (PKC1) (Teichert et al., 2014). However, during germling/hyphal fusion in *N. crassa*, MAK-1 is only recruited to the membrane after cells establish physical contact, while SO is recruited already before, during the communication process, which suggest that SO might have MAK-1-related and unrelated functions depending on the phase of the cell fusion process (Weichert et al., 2016).

1.6 Cell fusion in the plant pathogen fungus Botrytis cinerea

Although somatic cell fusion has been reported in several fungal species, the unusual mode of communication in which two proteins oscillate to the cell tips in an antiphase manner has only been shown in *N. crassa*. The study of the localization of MAK-2 and SO homologs in different fungal species would help to understand how conserved the molecular bases of somatic cell fusion are and the relevance of the cell fusion process in different biological niches. Among all of the potential fungal species, one of the most studied, with molecular and cloning tools developed and an increasing number of knock-out mutants generated, is the plant pathogen *B. cinerea.*

B. cinerea is an airborne plant pathogenic fungus with a necrotrophic lifestyle infecting more than 200 crop plants (Williamson et al., 2007). This ascomycete fungus is responsible for the gray mold disease and is considered the second most important phytopathogenic fungus based on its important economic loss in agriculture (Dean et al., 2012). Due to its genetic plasticity, the extensive variety of modes of attack and its successful survival rate in nature make the control measures in preventing infection unlikely to succeed (Williamson et al., 2007). In its life cycle, this fungus also undergoes somatic cell fusion in a manner very similar to *N. crassa* cell fusion. Some molecular system involved in cell fusion in *N. crassa*, are also important for *B. cinerea*, such as the ROS generating system which is essential for the cell fusion process in both fungi (Roca et al., 2012; Serrano et al., 2018) . Surprisingly, *B. cinerea* behaves differently depending on the surface where it grows, while *N. crassa* does not. On hydrophobic surfaces the cell fusion process is completely inactive, while it is promoted in hydrophilic surfaces,

which has been correlated to the infectious behavior of *B. cinerea* and the hydrophobicity of plant leaves (Roca et al., 2012). These data showed for the first time a relationship between somatic cell fusion and a biological fundamental process like plant infection, opening the question about a potential relationship between cell fusion and pathogenicity and therefore making *B. cinerea* a suitable model to answer this question.

1.7 Objectives of this study

The filamentous fungus *N. crassa* employs an unusual mode of cell communication during the process of cell-cell fusion, in which the fusion partners appear to take turns in signal sending and signal receiving. During this process, the MAP kinase MAK-2 and the protein SO are recruited to the plasma membrane of the growing cell tips in an alternating manner, such that when MAK-2 is present at one tip, SO is present at the other one. One primary research aim of this thesis is to gain a better understanding of the relationship between the subcellular spatial and temporal dynamics of the MAP kinase and its activity and function during the cell fusion process. To investigate this, we will manipulate the localization of the MAP kinase to understand how changes in its dynamics influence the cell fusion process. The outcome of this manipulation will be studied by phospho-Western blot analysis, live-cell imaging and co-localization with different factors that are known to be involved in the process.

Earlier studies had shown that a second MAP kinase (MAK-1) is recruited to the fusion point, once the cells establish physical contact. The current working hypothesis states that this kinase controls cell wall remodeling during fusion pore formation. Commonly, MAP kinases functions are studied by analyzing the respective gene deletion mutants. Mutant analysis revealed that both MAP kinases, MAK-2 and MAK-1, are essential to acquire cell fusion competence, since the strains lacking the respective genes are unable to initiate the communication process. Therefore, the function of both proteins during the subsequent steps of the cell fusion process, such as fusion pore formation, could not be directly addressed. In this thesis, we will use a chemical genetics approach, that will allow us to investigate the protein function by controlling the MAP kinase activity in a reversible

manner at specific steps of the cell communication and fusion process and to decipher the specific contributions of the individual kinases.

In addition, previous studies revealed potential inter-species interactions between spore germlings of the two different fungi *N. crassa* and *B. cinerea*. In this thesis, we will investigate if the unusual communication mode identified in *N. crassa* is conserved in *B. cinerea* and if it also mediates the interspecies interaction. Therefore, we will identify the homologs of the *mak-2* and *so* genes in *B. cinerea* and localize the respective proteins during the cell fusion process. In addition, we will follow up on the interspecies interactions in order to understand how conserved the signals mediating this inter-species communication are. Furthermore, we will also investigate how cell fusion influences the plant pathogenic development of *B. cinerea*.

Some of the key questions that will be answered in the different result chapters of this thesis are:

1. How important are the subcellular spatial and temporal dynamics of MAK-2 for the function of the protein?
2. Where and how is MAK-2 controlling SO localization?
3. What is the role of MAK-2 activity during the different phases of the cell fusion process?
4. What is the importance of BEM-1 and NADPH oxidases for cell fusion and MAK-2 activation?
5. What is the role of the CWI MAP kinase MAK-1 during the communication phase?
6. What are the consequences of MAK-1 inhibition for the actin-mediated polarity machinery?
7. How interconnected are the subcellular dynamics of MAK-2, MAK-1, and SO?
8. How conserved is the cell communication process mediated by MAK-2 and SO in other filamentous fungi?
9. Are the (so far unknown) signal and receptor mediating the cell-cell interaction conserved?
10. Does cell fusion contribute to the pathogenic growth and development of *B. cinerea*?

MATERIALS AND METHODS

2 Materials and methods

2.1 Materials

2.1.1 Strains used in this study

Strain	Genotype	Source
N1-01 (FGSC #2489)	*Mat A*	FGSC
N1-02 (FGSC #988)	*Mat a*	FGSC
N1-03 (FGSC #6103)	*his-3; Mat A*	FGSC
MAL-1	Δ*mak-2::hph; his-3*$^{+}$*::pccg1-mak-2*^{Q100G}*; Mat A*	(Fleissner et al., 2009)
R23-20	*Dip-1; his-3; Mat A*	(Hutchison et al., 2009)
*his-3;*Δ*mek-2* (N2-41)	Δ*mek-2::hph; his-3 Mat A*	(Dettmann et al., 2012)
*his-3;*Δ*nrc-1* (N2-42)	Δ*nrc-1::hph; his-3 Mat a*	(Dettmann et al., 2012)
Δ*mek-2* (FGSC #11524)	Δ*mek-2::hph; Mat a*	FGSC
Δ*nrc-1* (FGSC #18162)	Δ*ncr-1::hph; Mat a*	FGSC

Δ*nox1* (FGSC #12867)	Δ*nox1::hph; Mat a*	FGSC
Δ*mak-2* (FGSC #21728)	Δ*mak-2::hph; Mat a*	FGSC
Δ*ham-6* (FGSC #16903)	Δ*ham-6::hph, Mat a*	FGSC
Δ*mak-1* (FGSC #11321)	Δ*mak-1::hph, Mat a*	FGSC
715	Δ*nor-1::hph; Mat a*	This study
21-A1	Δ*bem-1::hph;* Δ*mus52::bar+; Mat a*	(Schürg et al., 2012)
2-A1	Δ*bem-1::hph; his-3;* Δ*mus52::bar+; his-3 Mat a*	(Schürg et al., 2012)
P611-3	Δ*mak-2::hph; his-3*$^{+}$*::Pmak-2-mak-2-gfp Mat A*	(Fleissner et al., 2009)
N1-05 (FGSC #9720)	Δ*mus-52::bar+, his-3*, mat A	FGSC
N1-06 (FGSC #9719)	Δ*mus-52::bar+*, mat a	FGSC
N1-42	*his-3::Pmak-2-mak-2-gfp Mat A*	(Fleissner et al., 2009)
MW_488	Δ*mak-1::hph; his-3*$^{-}$ *Mat a*	(Weichert et al., 2016)
691	Δ*nox1::hph; his-3 Mat A*	This study
724	Δ*nor-1::hph; his-3 Mat A*	This study
267	*his-3*$^{+}$*::Ptef-1-mak-2-gfp-caax; Mat A*	Illgen, 2017

279	Δ*mek-2::hph; his-3^{+}::Pmek-2-mek-2-gfp-caax; Mat a*	Illgen, 2017
286	Δ*mek-2::hph; his-3^{+}::Ptef-1-mek-2-gfp-caax; Mat A*	Illgen, 2017
330	*his-3^{+}::Ptef-1-mek-2-gfp-caax; Mat A*	Illgen, 2017
353	*his-3^{+}::Pmak-2-mak-2-gfp-caax; Mat A*	Illgen, 2017
361	*his-3^{+}::Ptef-1-mak-2-gfp-saax; Mat A*	Illgen, 2017
381	Δ*mak-2::hph; his-3^{+}::Ptef-1-mak-2-gfp-saax; Mat A*	Illgen, 2017
384	Δ*mek-2::hph; his-3^{+}::Ptef-1-mak-2-gfp-caax; Mat a*	Illgen, 2017
404	Δ*mak-2::hph; his-3^{+}::Pmak-2-mak-2-gfp-saax; Mat A*	Illgen, 2017
406	*his-3^{+}::Ptef-1-mek-2-gfp; Mat A*	(Dettmann et al., 2012)
423	Δ*mek-2::hph; his-3^{+}::Ptef-1-mek-2-gfp; Mat a*	Illgen, 2017
437	*his-3^{+}::Ptef-1-nrc-1-gfp; Mat A*	Illgen, 2017
549	*his-3^{+}::Ptef-1-mek-2-gfp-saax; Mat A*	Illgen, 2017
569	Δ*bem-1::hph; his-3^{+}::Ptef-1-mak-2-gfp-caax; Mat A*	Illgen, 2017
598	Δ*mak-2::hph; his-3; Mat A*	(Fleissner et al., 2009)
607	Δ*mak-2::hph; his-3^{+}::Ptef-1-mak-2-$^{T180A-Y182F}$-gfp; Mat A*	Illgen, 2017
610	Δ*mak-2::hph; his-3^{+}::Ptef-1-mak-2-^{T180A}-gfp; Mat A*	Illgen, 2017
613	Δ*mak-2::hph; his-3^{+}::Ptef-1-mak-2-^{Y182F}-gfp; Mat A*	Illgen, 2017
618	Δ*mek-2::hph; his-3^{+}::Ptef-1-mek-2-gfp-caax; Mat a*	Illgen, 2017

633	Δ*mak-2::hph; his-3*$^{+}$*::Ptef-1-mak-2-gfp; Mat A*	Illgen, 2017
640	Δ*mak-2::hph; his-3*$^{+}$*::Ptef-1-mak-2-gfp-caax; Mat A*	Illgen, 2017
642	Δ*mak-2::hph; his-3::Pmak-2-mak-2-gfp-caax; Mat A*	Illgen, 2017
665	*his-3*$^{+}$*::Ptef-1-mak-2-gfp; Mat A*	Generated in Illgen, 2017 and homokaryon isolation done for this study
670	Δ*nrc-1::hph; his-3*$^{+}$*::Ptef-1-mak-2-gfp-caax; Mat a*	This study
714	*his-3*$^{+}$*::Ptef-1-so-gfp, mat A.*	Schumann, 2018
719	Δ*nor-1::hph; his-3*$^{+}$*::Ptef-1-mak-2-gfp-caax; Mat A*	This study
723	Δ*nox1::hph; his-3*$^{+}$*::Ptef-1-mak-2-gfp-caax; Mat A*	This study
743	Δ*ham-5::hph*; *his-3*$^{-}$*, mat A*	(Dettmann et al., 2014)
750	*his-3*$^{+}$*::Pccg1-ham5-mCherry, mat A*	(Dettmann et al., 2014)
754	*his-3*$^{+}$*::Ptef-1-Lifeact-gfp; Δmus-51::bar+; mat A*	(Berepiki et al., 2010)
770	Δ*ham-5::hph; his-3*$^{+}$*::Ptef-1-mak-2-gfp-caax; Mat A.*	This study
773	Δ*ham-6::hph, his-3*$^{+}$*::Ptef-1-mak-2-gfp-caax; Mat A*	This study
785	B05.10. *Botrytis cinerea* wild-type strain (teleomorph *Botryotinia fuckeliana*)	(Büttner et al., 1994)
787	*hph::bmp1*	(Doehlemann et al., 2006)
797	*his-3*$^{+}$*::Ptef-1-mak-2-*$^{T180A-Y182F}$*-gfp-caax; Mat A*	This study
800	*his-3*$^{+}$*::Ptef-1-gfp-caax; Mat A.*	This study

802	*Δmak-2::hph; his-3^{+}::Ptef-1-mak-2-Q100A-gfp; Mat A*	This study
809	*his-3^{+}::Pmak-2-mak-2-Y182F-gfp; Mat A*	This study
813	*his-3^{+}::Pmak-2-mak-2-T180A-gfp; Mat A*	This study
816	*his-3^{+}::Pmak-2-mak-2-T180A-Y182F-gfp; Mat A*	This study
843	*his-3^{+}::Ptef-1-dsred-so; Mat A*	This study
848	*mak-1::hph-mak-1-e104g, his-3; Mat a*	This study
849	*mak-1::hph-mak-1-e104g; Mat a*	This study
854	*bcniiA::PoliC-bcso-gfp-Tgluc-hph*	This study
856	*bcniiA::hph-PoliC-bmp-1-mCherry*	This study
857 (bcbmp1_gfp)	*bcniiA::nat-PoliC-bmp-1-gfp*	(Marschall and Tudzynski, 2016)
860	*mak-1::hph-mak-1-e104g; his-3::Ptef-1-mek-2-gfp; mat A*	This study
862	*mak-1::hph-mak-1-e104g; his-3::Ptef-1-nrc-1-gfp; mat A*	This study
865	*mak-1::hph-mak-1-e104g; his-3::Ptef-1-mak-2-gfp; mat A*	This study
869	*mak-1::hph-mak-1-e104g; his-3::Ptef-1-lifeact-gfp; mat A*	This study
874	*mak-1::hph-mak-1-e104g; his-3::Ptef-1-so-gfp; mat A*	This study
882	*Pmak-2-mak-2::Ptef-1-mak-2-q100a-hph; his-3-, bar+::mus5; mat A*	This study
889 (CBS101525)	*Trichoderma atroviride* wild-type isolate	CBS
891	*mak-1::hph, his-3::Ptef-1-lifeact-gfp mat a*	This study
899	*Pmak-2-mak-2::Ptef-1-mak-2-q100a-hph; mat a*	This study

908	*hph::bcso*	This study
909	*hph::bcso*	This study
910	*bcniaD::hph-Pbcso-bcso*	This study
912	*Pmak-2-mak-2::Ptef-1-mak-2-q100a-hph; his-3+::Ptef-1-so-gfp*	This study
915	*pmak-2-mak-2::Ptef-1-mak-2-q100a-hph; his-3+::Ptef-1-lifeact-gfp*	This study
926	*pmak-2-mak-2::Ptef-1-mak-2-q100a-hph; mak-1::hph-mak-1-e104g; his-3+::Ptef-1-lifeact-gf; mat A*	This study
927	*Pccg1::crib^cla-4-gfp::bar+ Mat A*	(Alexander Lichius et al., 2014)
929	*bcniaD::PgdpA-bcso-gfp-nat; bcso::hph*	This study
943	*mak-1::hph-mak-1-e104g;Pccg1::crib^cla-4-gfp::bar+*	This study
949	*pmak-2-mak-2::Ptef-1-mak-2-q100a-hph;Pccg1::crib^cla-4-gfp::bar+*	This study

2.1.2 Plasmids

Number	Plasmid	*N. crassa* strain generated	Description
701	*Pmak-2-mak-2^{Y182F}*	809	Exchange of *Ptef-1* promoter with *Pmak-2* with enzymes NotI / XbaI from plasmid pUB0375
702	*Pmak-2-mak-2$^{T180A/Y182F}$*	816	Exchange of *Ptef-1* promoter with *Pmak-2* with enzymes NotI / XbaI from plasmid pUB0376
703	*Pmak-2-mak-2^{T180A}*	813	Exchange of *Ptef-1* promoter with *Pmak-2* with enzymes NotI / XbaI from plasmid pUB0377
843	*mak-2$^{T180A/Y182F}$-caax*	797	Plasmids UB396 and p25c were cut with PacI/XbaI. Fragment and plasmid, respectively, were recovered, ligated and cloned.
692	*Ptef-1-mak-2^{Q100A}-gfp*	802	*Mak-2*^{Q100A}-gfp were cloned together by YRC. The full fragment was cloned into pMF272 + tef plasmid with XbaI/PacI.
723	*Ptef-1-dsRed-so*	843	SO amplified from genomic DNA of *N. crassa* and cloned into the vector 722 (pMF334-Tef-dsRed) with enzymes AscI/XbaI

711	*bcso-gfp-hph*	854	Fragments generated with overlapping regions and cloned by YRC in the plasmid pNAH_OGG.
727	*bmp-1-mcherry-hph*	856	BMP-1 fragment cloned in plasmid pUB0619 with enzymes AscI/PacI
774	*bcso-gfp; nat+*	929	Fragments generated with overlapping regions and cloned by YRC in the plasmid pNDN_OGG
737	*hph::bcso*	908	Upstream, downstream and hph cassette were amplified with overlapping regions and cloned in plasmid pUB595.
799	*Pbcso-bcso-gfp-hph*	910	PgdpA from plasmid 711 was exchanged with 1 kb upstream of the bcso gene with enzymes PacI/SpeI.
846	*Ptef-1-mak-2q100a*	882	*Ptef-1-mak-2-Q100A* fragment amplified from plasmid 692 and cloned with 5’ and 3’ region of the MAK-2 DNA sequence
738	*mak-1-e104g*	848, 849	Two pairs of primers were used to amplify the mak-1 5’ genomic region and the 3’ genomic region including the exchange in the base pairs for E104G. Also, the hph cassette and a recombinant sequence at the 5’ and 3’ region was cloned together by YRC.

93*	pNAH_OGG	(Schumacher, 2012) *General laboratory plasmid list
94*	pNDN_OGG	
661	pNAH_OGG with Poly-linker (pUB0563)	Addition of a Poly-linker region to the sequence of the original pNAH-OGG plasmid.
710	mCherry in pUB0563 (pUB0602)	GFP removed with *Nco*I and *Not*I and mCherry cloned in it.

2.1.3 Oligonucleotides

All oligonucleotides used in this study were purchased from Sigma.

number	Name	Nucleotide sequence	Plasmids generated with the primers	Strains generated with the plasmids
1327	pmak-2-Not1 fw	aatgtagcggccgctgggacctga gacataggcacgc	701, 702 and 703	809, 813 and 816
1328	pmak-2-Xba1 rev	aatgtatctagattcgacgtgtcccg aaaagttgct	701, 702, 703	809, 813 and 816
1271	Q100A-MAK-2inh-Pr2	tcaacgaagtgtatctcatcgccga actgatggagactga	692	802
1272	Q100A-MAK-2inh-Pr3	tcagtctccatcagttcggcgatgag atacacttcgttga	692	802
1273	PacI-MAK-2inh-Pr4	gcggataacaatttcacacaggaa acagcttaattaacctcataatctcct ggtagatcaactgc	692	802
1274	PacI-MAK-2inh-Pr5	gtaacgccagggttttcccagtcac gacgttaattaacatgagcagcgca caaagaggc	692	802
1275	XbaI-MAK-2inh-Pr6	gcggataacaatttcacacaggaa acagctctagatcacctcataatctc ctggtagatca	692	802
1296	B-MP1-AscI F	aatgtaggcgcgccatgacagctc gtgcgcctaat	727	856
1297	B-MP1 PacI R	aatgtattaattaatctcatgatctcat cataaat	727	856
1419	SO-AscI-Fw	aatgtaggcgcgcccatgtctcgat cccgcggtgttc	723	843
1420	SO-XbaI-Rv	aatgtatctagactaatgcccatact ccaaatgcggc	723	843

1415	YRC GFP Bot soft R	gattacttacctcacccttggaaaccattctgccaaactccaaactgggtac	711	854
1416	YRC PoliC Bot soft F	ctcaactccatcacatcacaatcgatccaaatggctcggcgcactggaaaac	711	854
1296	B-MP1-AscI F	aatgtaggcgcgccatgacagctcgtgcgcctaat	727	856
1297	B-MP1 PacI R	aatgtattaattaatctcatgatctcatcataaat	727	856
1505	RS_soft 5prime F	gtaacgccagggttttcccagtcacgacgccaaggtctgttccccaaggtg	774	929
1509	soft3´R_RS	gcggataacaatttcacacaggaaacagcgaagtcatttatttgtgttacg	774	929
1451	Bot so KO 5´F	gtaacgccagggttttcccagtcacgacggattgttagattctatagggttata	737	908
1452	Bot so KO 5´R	gtccgagggcaaaggaatagcttgtacagataccagcgctc	737	908
1453	hph F	ctattcctttgccctcggacgag	737	908
1454	hph R	gatattgaaggagcatttttg	737	908
1455	Bot so KO 3´F	caaaaaatgctccttcaatatcgagtttggcagatgatgaggaag	737	908
1456	Bot so KO 3´R	gcggataacaatttcacacaggaaacagccgagagaatttaaattggaag	737	908
1431	YRC PtrpC Bot nat Prom softF	gccaagcccaaaaaatgctccttcaatatccaccatttacctgtctttgta	799	910

1415	YRC GFP Bot soft R	gattacttacctcacccttggaaaccattctgccaaactccaaactgggtac	799	910
1529	bcniaD-hi5F	cgcatatcagcatatcgagatgtcc	Primer to detect integration of transformant construct *	
1530	bcniiA-hi5F	gcggggtatggcagcatgagtg	Primer to detect integration of transformant construct *	
1531	bcniiA-hi3R	cttatagcaagcgcgatgtgtatc	Primer to detect integration of transformant construct *	
1532	bcniaD-hi3R	gagtacccatccgatggagttgttg	Primer to detect integration of transformant construct *	
1533	bcniaD-WT-F	gccacagactccgccagattctaatg	Primer to detect integration of transformant construct *	
1534	bcniaD-WT-R	caaccatttcacgctgcgaccacc	Primer to detect integration of transformant construct *	
1535	bcniiA-WT-F	ggttgaggtggtggaagatttg	Primer to detect integration of transformant construct *	
1486	mak-2 pRS--Q100G F	gtaacgccagggttttcccagtcacgacgctgttacactgcatccgttcca	846	882
1487	mak-2 Q100G R	gagccagcacgcgatcatacgccgatgagatacacttcgttga	846	882
1488	mak-2 Q100G F	tcaacgaagtgtatctcatcggcgtatgatcgcgtgctggctc	846	882
1489	mak2 5strichF--pRS	gtaacgccagggttttcccagtcacgacgtctctctggttgttctgttcgga	846	882
1490	mak2 5srichR--tef Promotor	tagttcagtggtcacgggatatccaactacttcacccttcacaca	846	882

1492	MAK-2-Pr1.Rv	tcacctcataatctcctggtagatcaactgc	846	882
1304	Mak1.knockin.1	gtaacgccagggttttcccagtcacgacgcgagacctatctctacggcggtacgtcatggctcat	848, 849	738
1305	Mak1.knockin.2	atccacttaacgttactgaaatcaaacattctttttggctttttgtactaatctgg	848, 849	738
1306	Mak1.knockin.3	gctccttcaatatcatcttctgtgaaccgccgacgccatgcag	848, 849	738
1307	Mak1.knockin.4	gcggataacaatttcacacaggaaacagctcctctctctctccgtcgtcgcc	848, 849	738
1329	MAK-1 control wild type f	ggctcgccattgaggcgg	848, 849	738
1330	MAK-1 control wild type r	cacgtccacaagcagcccgtct	848, 849	738
82	HPH F	gtcggagacagaagatgatattgaaggagc	hph cassette	
83	HPH R	gttggagatttcagtaacgttaagtggat	hph cassette	
1411	mCherry Not R	aatgtagcggccgcctacttgtacagctcgtccatg	mCherry for pNAH_OGG	
1412	mCherry Pac F	aatgtattaattaagatggtgagcaagggcgaggag	mCherry for pNAH_OGG	

* (Schumacher, 2012)

2.1.4 Enzymes

All restriction enzymes used for cloning were purchased from Thermo Scientific. For analyses of the primary transformants, the PCR (polymerase chain reaction) test was performed with the DreamTaq polymerase (Fermentas). In contrast, for amplification of inserts used in cloning or sequencing, the Phusion Taq (Thermo Scientific) was used. For ligation of plasmid and insert, the T4-DNA-Ligase (Thermo Scientific) was used. And for elimination of RNA from our samples, the TE-buffer was supplemented with RNase (Serva) enzymes.

2.1.5 Antibodies

Antibody	Species	Source
Anti-GFP	Mouse	Roche, Cat#11814460001
Anti-mouse,HRP-conjugate	Goat	Invitrogen, G21453
Anti-mouse,HRP-conjugate	Goat	Novex, A24512
Anti-Phospho p44/42	Rabbit	Cell Signaling Technology, #9101
Anti-Rabbit, HRP-conjugate	Goat	Cell Signaling Technology, #7074

2.1.6 Buffers and solutions

Name	Preparation	
20x BDES	200 g 10 g 10 g 1 L Sterilize by autoclavation.	Sorbose Sucrose Fructose ddH_2O
Biotin solution	5 mg 50 mL	Biotin ddH_2O
Blocking solution	5 g 50 mL	BSA TBS-T 0.1%
Coomassie solution	60 mg 1 L Shake for three hours 3 mL	Coomassie Brilliant Blue G ddH_2O HCl 37% w/w
DNA extraction buffer	10 mL 30 mL 2 g 10 mL Adjust to 100 mL	1 M Tris-HCl buffer pH 7.5 5 M NaCl CTAB 0.5 M EDTA ddH_2O
0.5 M EDTA solution pH 8	146.12 g 15 g 800 mL Adjust to pH 8 with NaOH pellets	EDTA NaOH ddH_2O

0.5 M EGTA solution pH 8	146.12 g 15 g 800 mL Adjust to pH 8 with NaOH pellets	EGTA NaOH ddH_2O
10x FIGS solution	200 g 5 g 5 g Add to 1 L Sterilize by autoclavation	Sorbose Fructose Glucose ddH_2O
1M HEPES solution pH 7.5	238.31 g Adjust to 1 L	HEPES ddH_2O
KCl buffer	0.6 M 50 mM Sterilize by filtration with 0.20 µm filters	KCl $CaCl_2$ $2H_2O$
5x Laemmli buffer	3.12 mL 1 g 5 mL 1.5 mL 2 mg Adjust to 10 ml with ddH_2O at 60ºC (water bath).	1 M Tris-HCl buffer pH 6.8 SDS (pellets) Glycerin β-Mercaptoethanol Bromophenol blue
NaOAc solution (3 M, pH 6.3)	246.03 g Add to 1 L Adjust pH to 6.3 with 1 M HCl	NaOAc ddH_2O

Protein extraction buffer	50 mM 5 mM 2 mM 100 mM 1% (v/v) 10% (v/v) 1 mM 10 mM 60 mM 15 mM 1 Tablet Adjust to 20 mL	HEPES solution pH 7.5 EDTA solution pH 8 EGTA solution pH 8 NaCl Triton X-100 Glycerin Na_3VO_4 NaF β-Glycerol phosphate para-Nitrophenyl phosphate Cocktail protease-inhibitor ddH_2O
Stripping solution	57.3 g 1.14 mL Adjust to 100 mL	Guanidine HCl Acetic acid TBS-T 0.1%
10x TBS buffer	60.6 g 87.7 g pH to 7.5 with 1 M HCl Adjust to 1 L	Tris NaCl ddH_2O
TBS-T 0.1% buffer	100 mL 0.1% (v/v) Adjust to 1 L	10x TBS buffer Tween 20 ddH_2O
TBS-T 0.05% buffer	100 mL 0.05% (v/v) Adjust to 1 L	10x TBS buffer Tween 20 ddH_2O
TE-RNase buffer	10 mM 1 mM 200 µg/mL	Tris-HCl buffer pH 8 EDTA RNase (20 mg/mL)

Trace metals	50 g 50g 10 g 2.5 g 0.5 g 0.5 g 0.5 g Adjust to 1 L Sterilize by filtration with 0.2 µm filters	Citric acid $ZnSO_4 \cdot 7\ H_2O$ $(NH_4)_2Fe(SO_4)_2 \cdot 6\ H_2O$ $CuSO_4 \cdot 5\ H_2O$ $MnSO_4 \cdot H_2O$ H_3BO_3 $Na_2MoO_4 \cdot 2\ H_2O$ ddH_2O
50x Vogel's solution	125 g 250 g 100 g 10 g 5 g 2.5 mL 5 mL Adjust to 1 L	Na_3 Citrate - $2H_2O$ KH_2PO_4 NH_4NO_3 $MgSO_4$ - 7 H2O $CaCl_2$ - 2 H2O Biotin solution Trace metals ddH_2O
2x Westergaard's solution	6 g 4.2 g 3 g 3 g 0.6 g 0.6 g 0.3 mL 0.6 mL Adjust to 3 L	KNO_3 K_2HPO_4 KH_2PO_4 $MgSO_4 \cdot 7\ H_2O$ NaCl $CaCl_2 \cdot 2\ H_2O$ Biotin solution Trace elements ddH_2O

Western transfer buffer	3.03 g 14.41 g 200 mL Adjust to 1 L	Tris Glycine Methanol ddH_2O

2.1.7 Media

Media	Preparation	
BDES	20 mL 15 g Adjust to 950 mL Sterilize by autoclavation Add 50 mL	50x Vogel's solution Agar ddH_2O 20x BDES solution
Bottom agar media	20 mL 15 g Adjust volume to 900 mL Sterilize by autoclavation Add 100 mL	50X Vogel's solution Agar 10X FIGS solution
Complex media	10 mL 10 g 2.5 g 2.5 g 7.5 g Adjust to 500 mL Sterilize by autoclavation	50x Vogel's solution Sucrose Yeast extract Peptone Bacto-agar ddH_2O

LB media	10 g 5 g 10 g 15 g Adjust to 1 L Sterilize by autoclavation	Peptone Yeast extract NaCl Agar (optional) ddH_2O
Malt medium	5 g 15 g 1 g 1 g 1 g Adjust to 1 L Sterilize by autoclavation	Glucose Malt extract Casein peptone Yeast extract Casamino acids ddH_2O
SC-Ura- media	26.7 g 2 g 15 g Adjust to 1 L and pH 6.5 Sterilize by autoclavation	Drop-out Glucose D9500 Drop-out mix Ura- D9535 Agar ddH_2O
SH medium	1 mM 0.6 M 5 mM 10 g Adjust to 1 L Sterilize by autoclavation	$NaNO_3$ Sucrose Tris HCl pH 6.5 Bacto-agar ddH_2O

Top agar media	20 mL 10 g Adjust volume to 900 mL Sterilize by autoclavation Add 100 mL	50X Vogel's solution Agar 10X FIGS solution
Vogel's minimal media (MM)	20 mL 20 g 15 g 0.5 mg/mL 0.3 mg/mL Adjust to 1 L Sterilize by autoclavation	50x Vogel's solution Sucrose Agar (optional) L-Histidine (optional) Adenine (optional) ddH_2O
Westergaard's media	500 mL 15 g 15 g Adjust to 1 L Sterilize by autoclavation	2x Westergaard's solution Sucrose Agar ddH_2O
YPD media	10 g 20 g 20 g Adjust to 1 L and pH 6.5 Sterilize by autoclavation	Yeast extract Peptone Glucose ddH_2O

2.1.8 Electronic devices

Name	Provider	Detailed description and function
Electroporation	Bio-Rad	Gene Pulser II, used for transformation of *N. crassa* and *E. coli*.
Gel doc visualizer	Bio-Rad	Gel Doc. UV-light screen to visualize ethidium bromide agarose gels.
Microscope	Zeiss	Zeiss Observer 2.1 (Nomarski optics). Plan-Neofluar 100x/1.30 oil immersion objective (420493-9900). Light source: LED (CoolLED pE4000). Camera: PCO Edge 5.5 Gold (16 bits). Software: 4-D microscopy programmed by Ralf Schnabel and Christian Hennig (Schnabel et al., 1997)
	Leica	M60-Stereomicroscope with a DFC295 camera (from Leica) and controlled with the software of the provider: Leica Application Suite (version 3.5.0).
Thermocycler	Eppendorf	PCR
UV-VIS spectrometer	Pharmacia Biotech	Quantification of DNA (OD 270) and Bradford (OD 595)
Mechanical cell disruptor (bead beater)	Peqlab	Cell lysis and homogenization.
Chemiluminiscence detection system	Bio-Rad	ChemiDoc MP. Developing of western blot membranes.

2.2 Methods

2.2.1 Culturing of N. crassa and B. cinerea

N. crassa strains were typically grown on slant tubes containing minimal medium. Supplements were added when required. To obtain conidia, cultures were incubated for 3 days at 30ºC under dark conditions, and later incubated for one more day at room temperature with natural light, which induced sporulation of the fungus. *B. cinerea* strains were inoculated and grown in complex media plates and incubated for 7 days at room temperature under full spectrum light, which induced sporulation of the fungus. Conidia of both fungi were harvested using sterile wooden sticks and transferred into tubes containing ddH_2O water in order to prepare conidial suspensions.

2.2.2 DNA extraction

This method was only used to extract DNA for simple analyses, such as PCR. A mix of mycelium and spores were harvested from the slant tubes or media plates and mixed with 200 µl of glass beads in 800 µl of DNA extraction buffer, freshly supplemented with 8 µl of β-Mercaptoethanol. The fungal material was disrupted mechanically by using a beat beater (5.7 m/sec 2x30 sec). The solution was pelleted by centrifugation at max speed for 5 minutes, and 80 µl of NaOAc 3M pH 6.5 and 500 µl of PCIA (Phenol:Chloroform:Isoamyl:Alcohol) were added and mixed by vortexing. The aqueous phase was separated by centrifugation at maximum speed for 10 minutes and transferred to a new reaction tube together with 1 ml of 100% ethanol. The DNA was precipitated by centrifugation and washed with 70% ethanol. Finally, the DNA was resuspended with 50 µl of TE with RNAse.

2.2.3 PCR

PCR analyses were performed in order to check the presence or absence of wild-type genes, resistant cassettes, or to amplify genes for cloning. To test the integration of constructs into strains, the Taq polymerase Dreamtaq (Thermo) was used. In contrast, for amplification of genes used for cloning purpose, the high fidelity Phusion Taq (NEB) was chosen. The following recipes and protocols were used for each polymerase:

Dreamtaq protocol (for a final volume of 50 µl)

Buffer 10x	5 µl
dNTP (10 mM)	1 µl
Primer forward (10 mM)	2 µl
Primer reverse (10 mM)	2 µl
Dreamtaq polymerase	0.25 µl
DNA (≥100 nm)	
ddH_2O up to 50 µl.	

Cycles	Temperature	Time
x1	94ºC	30 secs
	94ºC	30 secs
x34	58-64ºC*	30 secs
	72ºC	≥1 min
x1	72ºC	10 mins

Phusion Taq protocol (for a final volume of 50 µl)

Buffer 5x	10 µl
dNTP (10 mM)	1 µl
Primer forward (10 mM)	2 µl
Primer reverse (10 mM)	2 µl
Dreamtaq polymerase	0.5 µl
DNA (≥100 nm)	
ddH_2O up to 50 µl.	

Cycles	Temperature	Time
x1	94ºC	30 secs
	94ºC	30 secs
x34	58-64ºC*	30 secs
	72ºC	≥1 min
x1	72ºC	10 mins

For both protocols, the annealing temperature was adjusted to the average temperature calculated for the forward and the reverse primer.

2.2.4 Agarose electrophoresis

The separation of the PCR product was performed with agarose gels prepared as 0.8% (w/v) with ethidium bromide to visualize the DNA band. The 1 kb DNA GeneRuler ladder (Fermentas) was used as DNA size standard. Gels were migrated at 100V for 45 minutes and observed under UV light (Bio-Rad). When required, the DNA band was excised from the agarose gel and purified by using the GeneJET Gel Extraction kit (Thermo) and DNA was resuspended in 50 µl of TE-RNAse.

2.2.5 Plasmid cloning

For cloning of PCR fragments into plasmids, we usually digested plasmid and fragment with the same restriction enzymes in order to ligate them together. For all restriction enzyme reactions, we mixed 0.2 µl of the corresponding enzymes, together with at least 200 ng of the DNA fragment and 2 µl of the 10x Fast digestion buffer (Thermo). Sterilized ddH_2O was added up to 20 µl. The reaction tube was incubated 2 hours at 37ºC.

For the ligation of treated fragment and plasmid, 0.5 µl of a T4-DNA Ligation enzyme was used, together with 1 µl of 10X T4 DNA ligase buffer, 1 µl of plasmid and 7.5 µl of the PCR fragment. The mix was incubated overnight at room temperature.

2.2.6 Transformation in E. coli XL1-Blue

1 µl of the ligation sample was usually used for transformation of a 50 µl suspension of competent *E. coli* XL1-Blue bacterial. The transformation was mediated through electroporation, in cuvettes of 2 mm. The settings used were 200 Ω, 25 µF and 2.3 Kv (Bio-Rad). Directly after electroporation, the bacteria were shaken for 1 hour at 37ºC in 1 ml of LB. Selection of positive colonies was done on ampicillin containing plates.

2.2.7 Plasmid purification

Positive colonies were inoculated in 5 ml of LB with antibiotic selection and incubated overnight at 37ºC. Afterwards, the bacterial culture was pelleted and resuspended in 100 µl of solution I (50 mM Glucose, 25 mM Tris pH 8 and 10 mM EDTA). Later, the same reaction tube was slowly mixed with 200 µl of solution II (0.2 M NaOH and 1% SDS) by inverting. After an incubation of 5 minutes on ice, 150 µl of solution III (5 M Calcium Acetate and Glacial acetic acid) was added and mixed slowly. A following centrifugation of 15 min at 16.000 rpm was performed and the supernatant was transferred to another reaction tube containing 1 ml of pure ethanol. DNA was precipitated by centrifugation at 16.000 rpm for 10 minutes and the precipitated DNA was mixed with 500 µl of 70% ethanol and centrifuging for 5 minutes. The DNA pellet was resuspended in 65 µl of TE RNAse. Successful cloning was usually tested by restriction analysis.

2.2.8 Yeast recombinational cloning

For preparation of plasmids for *B. cinerea* transformations, or knock-in plasmids for *N. crassa*, yeast recombinational cloning (YRC) was used. Primers were generated with overlapping regions at the end of the sequence. The obtained PCR fragments and a linearized plasmid (pNAH_OGG/pNDN_OGG for *B. cinerea* or pRS426 for *N. crassa*) were transformed together into the *S. cerevisiae* strain (FY834). For transformation, a colony of the FY834 strain (from a YPD + adenine plate) was inoculated in YPD liquid medium and incubated overnight at 30ºC with shaking at 125 rpm. 1 ml of this pre-culture was inoculated in 50 ml of YPD. The culture was incubated until OD_{600} reached the value 1. Cells were then pelleted by centrifugation (3.500 rpm, 5 min) and resuspended in 25 ml of sterilized ddH_2O.

Cells were pelleted for at least 2 more times and resuspended in 1 ml of 100 mM LiOAc. In a final step, cells were pelleted but resuspended in 400 µl of 100 mM LiOAc. 50 µl of this cell suspension were used for each transformation and mixed with the transformation mix (240 µl 50% PEG (polyethylene glycol) 3350 (w/v), 36 µl of 1 M lithium acetate (LiOAc), 50 µl of carrier DNA (salmon sperm), 1 µg of inserts plus 100 ng of linearized plasmid and filled up to a final volume of 360 µl with ddH_2O. The suspension of cells with the transformation mix was mixed by inverting the reaction tube and directly incubated for 30 minutes at 42ºC (heat shock). Later, cells were spun down by centrifugation (13.300 rpm, 5 minutes) and the supernatant was discarded. The pellet was resuspended in ddH_2O and spun down again for washing of the cells. Finally, the pellet was resuspended in 200 µl of fresh YPD medium, plated on SC Ura^- plates with glass beads (4 mm), and incubated at 30ºC for 3 days.

The plasmids generated by YRC were purified by a miniprep of all growing colonies obtained from the transformation plates. All colonies were recovered and pelleted in a reaction tube. 200 µl of glass beads (0.5 mm) and 200 µl of solution 1 (50 mM Glucose, 50 mM Tris pH 8 and 10 mM EDTA) were mixed with the cell suspension. The fungal material was disrupted mechanically by using a beat beater (5.7 m/sec 2x30 sec). 400 µl of solution II (0.2 M NaOH and 1% SDS) were added and mixed by inverting. Then, 300 µl of solution III (5 M potassium acetate (300 ml), 57.5 ml of acetic acid and 142.5 ml of H_2O) were added and mixed by inverting of the reaction tube. DNA was separated by centrifugation at max speed (16.000 rpm) for 15 minutes and 500 µl of the supernatant were recovered. DNA was precipitated by mixing with 100% Ethanol and centrifugation for 12 minutes at maximum speed, followed by discard of the supernatant and a new centrifugation after mixing with 500 µl of Ethanol 70%. The DNA pellet was dissolved in 50 µl of TE+RNAse. For *N. crassa*, the resulting plasmid was used as a template for amplification of the corresponding insert that was used for the subsequent transformation. For *B. cinerea*, a large amount of DNA was needed for transformation. Therefore, the resulting plasmid from the YRC was transformed into *E. coli* for a larger production of plasmid. Transformation and purification of the plasmid from *E. coli* was performed as previously explained.

2.2.9 Transformation of N. crassa

The strain to transform was usually incubated for 3 days at 30ºC under dark conditions and for 7 more days at room temperature and natural light conditions in 250 ml Eppendorf flasks (supplemented when required with histidine). Spores were harvested, mixed with cold sorbitol 1M and separated from the mycelium by cheesecloth filtration. 4 following rounds of centrifugation (5 minutes, 3.500 rpm) and resuspension in sorbitol of the pellet were performed in order to wash the spores. Finally, the pellet was resuspended in 1 ml of sorbitol and separated in 90 µl aliquots. 2-3 µg of DNA were mixed with the aliquots and transferred to an electroporation cuvette (1 mm) in order to electroporate the sample with the following settings: 1.5 KV, 600 Ω and 25 µF. The spore solution was then mixed with top agar (with or without histidine) and inoculated into bottom agar plates (supplemented with antibiotic when needed). Transformants were observed after a 3 days incubation at 30ºC.

2.2.10 Transformation of B. cinerea

The wild-type strain B05.10 was usually used as the recipient strains for all transformations (except for complementation of Δ*bcso*). Frozen mycelia from glycerol stocks was inoculated on complex media plates and incubated for 10-12 days at room temperature under full spectrum light, with a dark/light cycle of 12/12 hours. Spores were harvested with 10 ml of sterilized ddH_2O and separated from the mycelium by Nytex filtration. The fresh spores were inoculated in 100 ml of liquid malt medium (see table 5.1.7) and incubated for 24 hours at 19ºC, shaking at 150 rpm. The developed mycelium was collected with Nytex and washed twice with 30 ml of KCl buffer (0.6 M KCl and 50 mM $CaCl_2$). The washed mycelium was mixed with 200 mg of Glucanex and 20 mg of Lyticase, which were previously sterilized by filtration through 0.20 µm filters. The solution was incubated for 2 hours at 27ºC with 90 rpm., The suspension was then filtered through Nytex in order to separate protoplasts from the mycelium. The protoplasts were washed with 20 ml of KCl twice with two rounds of centrifugation (10 minutes with 4.000 rpm and at 4ºC) and resuspension. After the last centrifugation, the pellet was resuspended in 1 ml of KCl and the volume was adjusted to 10^7 protoplasts per 100 µl. 30 to 60 µg of linearized DNA were mixed with the protoplast suspension and incubated in ice for 5

minutes. Afterwards, 100 µl of PEG 6000 (previously sterilized by filtration through 0.20 µm filters) were added to the solution and incubated for 10 minutes at room temperature. 100 µl of PEG 6000 were added and incubated for 10 more minutes on ice. Finally, KCl buffer was added to a final volume of 1 ml. 100 µl of the protoplast solution were inoculated per plate together with SHA without selection pressure and incubated overnight. Afterwards a top layer of SHA media supplemented with the corresponding antibiotic was added and colonies were observed after 6 days. This protocol is adapted from (Schumacher, 2012).

2.2.11 Isolation of homokaryotic strains

For *N. crassa* homokaryons were isolated from primary transformants, either by sexual crossing or by single spore isolation (SSPi). For sexual crosses, wild-type strains (N1-01 or N1-02) were inoculated in Westergaard plates and incubated for 10 days at 26ºC under 12 hours light/dark conditions (Westergaard and Mitchell, 1947). This condition promotes the formation of the female sexual reproductive structures, the protoperithecia. Spores of opposite mating type from the transformant were harvested and inoculated on the crossing plate. Plates were incubated for 20 more days at room temperature, and cells underwent the formation of the perithecia and ascus development. Ascospores are haploid and homokaryotic, which allowed us to obtain homokaryon strains. Ascospores were activated by a heat shock (20 minutes at 59ºC) and incubated overnight on MM supplemented with selection antibiotics if required. Only resistant strains grew, whose genotypes were tested by PCR and fluorescence microscopy when possible. For SSPi, 5 µl of a 1:1000 diluted spore suspension was inoculated by streaking technique and incubated overnight at room temperature. Single spores were isolated from the agar plate and inoculated in MM slant tube for further analyses (PCR/fluorescence microscopy).

For *B. cinerea,* primary transformants were selected by single spore isolation. The spores were incubated overnight in MM under antibiotic pressure and germinated spores were isolated. Those spores were incubated in complex media again supplemented with selection antibiotics: nourseothricin (100 µg/ml) or hygromycin (70 µg/ml).

2.2.12 Live-cell imaging

To observe cell fusion, 300 µl of a 10^7 suspension of freshly harvested spores of *N. crassa* were inoculated on MM agar plates and incubated for 2 hours at 30ºC in the dark. Afterwards, 4 cm^2 agar slides were cut out and were inverted on a coverslip. For very long acquisition times, 10 µl of sterilized ddH_2O water were added on top of the agar slide, in order to prevent the sample to dry out. For fluorescence imaging, the standard values for the intensity of the LED were 50% and the exposure of the camera up to 1 second, but these parameters changed for some of the proteins observed (range between 20-80% LED intensity and 0.1 to 1.4 seconds of exposure time). For the recording of movies, a z-stack (up to 200 nm) of pictures was taken every minute and folded together with the open platform for scientific image analyses ImageJ. For observation of hyphal fusion in *N. crassa*, 5 µl of a 10^7-spore suspension were inoculated on the side of a MM agar plate and incubated for 15 hours at 30ºC. The preparation of the sample was performed in a similar way than for the spores. For *B. cinerea*, 300 µl of a 10^6-spore suspension was inoculated in a MM plate and incubated in the dark at 21ºC for 12-15 hours. The preparation of the sample for microscopy was performed as explained above. For observation of interspecies interactions between *N. crassa* and *B. cinerea*, 300 µl of a 10^6-spore suspension of *B. cinerea* were inoculated in MM plates and incubated for 12 hours at 21ºC. Afterwards, 300 µl of a 10^7-spore suspension of *N. crassa* was dropped in the center of the plate. To spread the suspension the plate was slowly moved and inclined to their sites and the extra volume was dried under the clean bench. The plate was incubated for another 3 hours at 21ºC in the dark. Afterwards, *B. cinerea* and *N. crassa* cells were in a similar vegetative state and interspecies cell interactions were observed. For all microscopy observations the x100 objective was used.

2.2.13 Deconvolution analyses

Deconvolution is an algorithm-based process, which is used to reverse the effects of convolution on recorded data. All fluorescence images shown in this thesis were processed by the widely used commercial deconvolution software Huygens (by Scientific Volume Imaging), more specifically the Huygens Essential version. Z-stacks (usually n=10) up to 200 nm of all fluorescence images were captured and assembled as a single

.tiff file by using ImageJ (image-stacks-image to stack). The composite images were processed through the deconvolution software with the following parameters (40-100 iterations, 12 signal/noise ratio and 0.01% of quality change thresh).

2.2.14 Microscopy analyses

For quantification of cell fusion in *N. crassa*, 300 µl of a 10^7 spore/ml suspension was inoculated in MM plates and incubated for 4 hours. Afterwards, a 2x2 cm^2 agar slide was cut off and placed inverted in the glass coverslip. Under the microscope, the number of germinated and ungerminated spores was counted to obtain the germination rate. Similarly, the number of cell interactions was quantified and divided by the total number of cells, resulting in the interaction rate, represented as a percentage. For all experiments at least 100 spores were quantified per sample/condition, and at least three independent repetitions were studied. Quantification of *B. cinerea* cell fusion was performed in a similar way but spores were incubated for 12h (except when indicated).

2.2.15 Pathogenicity test

For testing of the virulence of *B. cinerea*, pathogenicity tests were performed. Fresh spores of the strains tested were harvested and filtered and their concentration was adjusted to 10^5 spores/ml, in 1 ml of SMB media (40 g/l maltose, 10 g/l peptone, solution pH 5.6). 10 µl droplets of this suspension were placed on the backside of the leaves and incubated in humidity chambers. Test and control strains were placed on the same leaf, with at least 10 leaves tested from 5 independent plants. To obtain the plant material, French beans (Marschall and Tudzynski, 2016) were seeded in commercial soil (Preisfuxx) and grown inside of the greenhouse of the Genetics department for at least 10-15 days. Primary leaves were selected depending on similar size and healthiness and placed inside the humidity chamber for inoculation with the fungal strains.

The pathogenicity test aimed to study the influence of *N. crassa* on *B. cinerea* virulence was performed on *Arabidopsis thaliana* plants, in collaboration with Konstantin Kanofsky and Reinhard Hehl. *A. thaliana* plants were grown and prepared for infection as described in (Lehmeyer et al., 2016). Spores from *B. cinerea* were prepared as previously indicated in this section, with a concentration of 10^5 spores/ml in SMB medium.

N. crassa spores were harvested and the concentration was adjusted to 10^6 spores/ml in 1 ml of SMB medium. The spore solution of both species was mixed, spin down and resuspended in 1 ml of SMB medium. In contrast to the French bean infection, for the *A. thaliana* infection every plant was infected with a single strain by adding a single droplet of spore suspension per leaf.

2.2.16 Protein extraction

A total amount of $5x10^7$ spores were inoculated in 50 ml of liquid MM (placed in 250 ml plastic flasks). The cultures were incubated at 26ºC, shaking at 120 rpm for 24h. Afterwards, the mycelia were recovered by filtration with Miracloth, covered with aluminum foil and immediately frozen with liquid nitrogen. A mortar and pestle were chilled with liquid nitrogen and a portion of the frozen mycelium was ground to a fine powder. 500 µl of homogenized mycelium were transferred to a reaction tube and mixed with 300 µl of glass beads (0.5 mm) and 500 µl of protein extraction buffer (2.1.6). All samples were always kept on ice to keep the stability of the proteins. The fungal material was disrupted mechanically in a bead beater system (5.7 m/sec 2x30 sec), which was cooled to 4ºC with liquid nitrogen. Samples were then incubated for 30 minutes on ice, and vortexed every 10 minutes. Finally, samples were centrifuged for 8 minutes, 13.000 rpm at 4ºC. 350 µl of the supernatant were transferred into a new reaction tube placed on ice. For quantification of the protein content, a Bradford was performed as described (Bradford, 1976; Havlik et al., 2017). The protein concentration was always adjusted to 25 µg in a volume of 20 µl, mixed with 5 µl of Laemmli buffer (2.1.6). Afterwards, the proteins samples were boiled for 10 minutes at 104.5ºC in water bath and stored at -80ºC.

2.2.17 SDS-PAGE and Coomassie

SDS (sodium dodecyl sulfate)-PAGE gels were used to separate proteins by their molecular weight. The separating gel was created at a concentration of 8% of acrylamide and the stacking gel at 5%. For the lower gels, the following mixes were used:

	8%	
	1 gel	**10 gels**
dH_2O (ml)	2.4	24
30% Acrylamide (ml)	1.2	12
1.5 Tris HCl pH 8.8(ml)	1.3	13
10% SDS (µl)	50	500

For polymerization of the gels, the following volume of ammonium persulfate (APS) and TEMED were used depending on the volume of gel mix:

	1 gel	**2 gels**	**3 gels**	**4 gels**	**5 gels**	**6 gels**	**7 gels**	**8 gels**
Separating mix (ml)	5	10	15	20	25	30	35	40
APS (µl)	50	100	150	200	250	300	350	400
TEMED (µl)	2.5	5	7.5	10	12.5	15	17.5	20

4,4 ml of the solution were pipetted into the gap between the glass plates, previously folded together. To keep the top of the separating gel even, 1 ml of isopropanol was filled into the gap. 30 minutes later, the isopropanol was removed and the gap was washed with ddH_2O.

For the stacking gel, the following acrylamide mix and APS/TEMED volumes were used:

	1 gel	**20 gels**
dH_2O (ml)	1.3	26
30% Acrylamide (ml)	0.35	7
1 M Tris HCl pH 6.8 (ml)	0.27	5.4
10% SDS (µl)	20	400

	1 gel	**2 gels**	**3 gels**	**4 gels**	**5 gels**	**6 gels**	**7 gels**	**8 gels**
Concentrating mix (ml)	2	4	6	8	10	12	14	16
APS (µl)	20	40	60	80	100	120	140	160
TEMED (µl)	2.7	5.4	8.1	10.8	13.5	16.2	18.9	21.6

As previously described, the mix of acrylamide and APS/TEMED was pipetted into the gap and the well-forming comb was inserted avoiding air under the teeth. After 30 minutes, the comb was removed and 25 µl of the samples were loaded into the wells. If the gel was later used for Coomassie, 6 µl of the PageRuler Unstained Protein Ladder (CAT 26614; Thermo Fisher Scientific) were loaded in one well. In contrast, 6 µl of the PageRuler Plus Prestained Protein Ladder (CAT 26619; Thermo Fisher Scientific) were loaded in the gels used for Western blot analysis. After loading of all samples into the gels, the chamber was filled with the electrophoresis buffer (2.1.6), the top of the chamber was covered and electrodes connected. For electrophoresis of the SDS-PAGE gels, 150 V were applied for 1 hour. To visualize the general amount of proteins after electrophoresis of the gels, Coomassie staining was performed. The gels were removed carefully from the glass and placed in small plastic chambers filled with ddH_2O. Gels were heated up in the microwave at maximum power for 10 seconds and shake for 5 minutes.

Afterward the water was removed and the chamber was filled up again with more ddH_2O. This process was performed at least 3 times. Finally, the water was again removed and 20 ml of the Coomassie solution were added, fully covering the gels. A following heating was done again in the microwave and the gels with the Coomassie solution were shaken for at least 30 minutes. Later, the solution was exchanged with ddH_2O and the stained gels were photographed in the Bio-Rad gel doc.

2.2.18 Western blot analyses

After the electrophoresis, the gels aimed for Western blot analysis were washed twice with ddH_2O (shaking for 5 minutes). Finally, gels were incubated for 5 minutes with Western transfer buffer (2.1.6). For blotting of the gels, we used a PVDF membrane (Immobilon-P, Roth). The membrane was previously activated with methanol and subsequently washed twice with ddH_2O for 2 minutes, and finally incubated for 5 minutes with Western transfer buffer. After activation, the foam pad was placed primary on the cassette. Later, one sheet of filter paper and the gel on top were carefully positioned without bubbles in between the layers. The membrane was placed on the top of the gel, together with another sheet of filter paper and the second foam pad. The cassette holder was closed and placed inside the transfer tank. The tank was filled up with Western transfer buffer, the top of the tank was covered and the electrodes were connected. The blotting was performed always overnight at 4ºC, with 50 V. Afterwards, membranes were removed from the cassette holder and incubated with blocking solution (2.1.6) for 8 hours at 4ºC. To detect the phosphorylation of the MAP kinases, the membrane was washed 3 times with 20 ml of TBS-T 0.1% (2.1.6) shaking at 4ºC. After the buffer was discarded, the membrane was incubated with 10 ml of the phospho antibody (p44/42, 2.1.5) in a dilution of 1:1000, at 4ºC overnight. The membrane was subsequently washed 6 different times for 10 minutes with TBS-T 0.1%, shaking at 4ºC. Afterwards, the membrane was incubated with a 1:120.000 dilution of the secondary antibody (anti-rabbit, 2.1.5) at 4ºC for 90 minutes. Six additional washing steps (each of 10 minutes) were performed with TBS-T 0.1% at 4ºC. Afterwards, the membrane was ready for developing, and the developing kit (Super Signal West Femto Maximum Sensitivity Substrate, Thermo Scientific) was used as specified in the commercial instructions.

The developing of the membrane was visualized in a Gel-doc system from Bio-Rad (2.1.8) When the experiment required subsequent detection of the GFP (green fluorescence protein) signal, the same membrane was stripped by incubating it with 20 ml of stripping solution (2.1.6), shaking at room temperature for one hour. To recover the properties of the membrane, it was washed 3 times for 5 minutes with 20 ml of TBS-T 0.5% (2.1.6) and finally incubated again with blocking solution overnight at 4ºC. After the membrane was blocked, it was washed 3 times for 5 minutes each with TBS-T 0.1% at room temperature. Later, the membrane was incubated with the primary GFP detection antibody (2.1.5) for 90 minutes at room temperature and shaking. Afterwards, the membrane was washed 4 times for 5 minutes with TBS-T 0.1%, incubated now with the anti-mouse HRP secondary antibody (2.1.5) for 45 minutes, and washed again 4 times for 5 minutes each with TBS-T 0.1%. Finally, the membrane was developed as previously described with the anti-phospho detection. In a few cases, only the GFP was of interest to detect, therefore the membrane was directly incubated with the primary anti-gfp antibody after the blotting/blocking step. The analyses of the results were quantified and analyzed with the commercial software provided by Bio-Rad, Image Lab version 5.2.1.

2.2.19 Inhibitor assays

Three different chemicals were used for the corresponding experiments. Latrunculin A was used to test the consequences of actin-polymerization inhibition, 1-NM-PP1 was used to test the inhibition of the analog-sensitive kinases, and NSC23766 was used for specific inhibition of the Rho-GTPase RAC-1. The concentration of each chemical is detailed in the results section. For all inhibitor experiments, fresh spores were harvested and incubated for 2 hours at 30ºC in MM plates. A 1 cm^2 piece was cut from the agar plate and inverted onto a coverslip. 10 µl of the chemical were pipetted on one side of the agar block and the effect was directly observed under the microscope.

2.2.20 Statistics applied to the data

All quantitative data were statistically analyzed by performing a two-tailed paired t-test using Excel. The P values were calculated for 0.001, 0.05 or 0.01, and indicated as ***, ** or * respectively. To analyze whether the variances were paired or unpaired, F-test analyses were performed.

RESULTS

3 Results

3.1 Fine-tuned spatiotemporal dynamics of MAPK mediate fungal somatic cell fusion

3.1.1 A permanently membrane-tethered variant of MAK-2 does not complement the Δmak-2 phenotype

One of the most striking features of the cellular communication mediating cell fusion is the highly regulated dynamic localization of MAK-2 and SO. In order to understand the role and regulation of this process, we decided to interrupt the dynamics of MAK-2 and SO permanently. In the first step, a membrane-tethering tool based on farnesylation was established for *N. crassa* (Illgen, 2017; Serrano et al., 2018). Farnesylation is a posttranslational modification of proteins, in which an isoprenyl group is added to a cysteine residue embedded in a -CaaX domain at the C-terminal region of the protein. This modification mediates among others protein-membrane interactions. In her PhD Thesis, Julia Illgen established this tool for *N. crassa*. The DNA sequence encoding the last 20 amino acids of the BAND-1 protein (also known as *ras-1*, NCU08823.2) from *N. crassa* was fused downstream to a commercial *gfp* and expressed in *N. crassa* wild-type N1-01, resulting in strain 800. This strain showed a clear permanently membrane-tethered localization of the GFP fluorescence signal (Illgen, 2017; Serrano et al., 2018). The same plasmid was used, to fuse the coding region of *mak-2* with *gfp-caax*, resulting in a *mak-2-gfp-caax* plasmid controlled by either the commonly used overexpression promoter *tef-1* (Berepiki et al., 2010) or the native *mak-2* promoter, plasmids p22 and p25, respectively (Illgen, 2017). Both plasmids were transformed into the *mak-2* knock out mutant (strain 598) generating the strains 642 (native expression promoter) and 640 (overexpression promoter). As a control, the cysteine residue was exchanged by a serine residue, which is not recognized by the farnesyltransferase enzymes. These new plasmids (containing the native and the *tef-1* promoter) were also transformed into Δ*mak-2*, resulting in strains 404 and 381, respectively (Illgen, 2017).

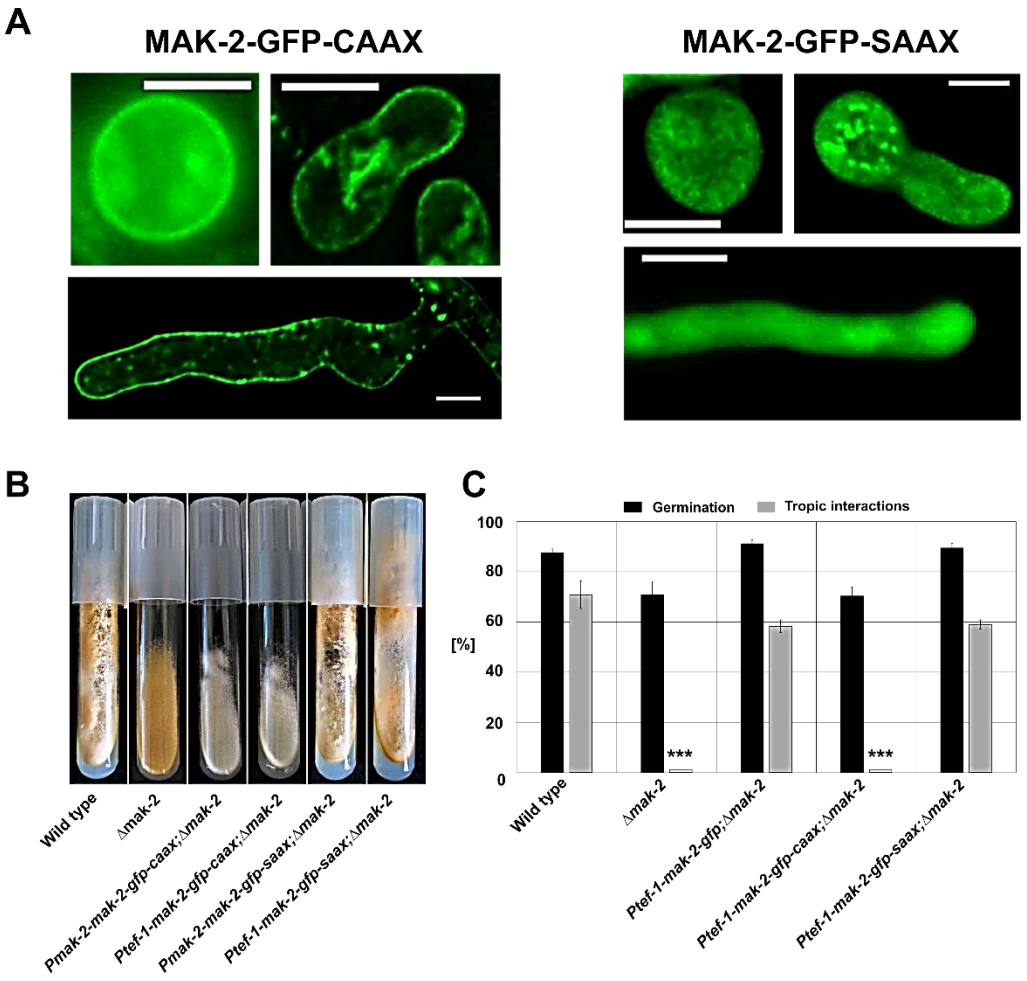

Figure 3.1.1. A permanently membrane-tethered variant of MAK-2 does not complement the Δ*mak-2* phenotype. (A) Left: membrane tethered localization of MAK-2 in spores, germlings and hyphae of strain 640. Right: cytoplasmic localization of MAK-2 in the control - SaaX domain strain (strain 381). Scale bars: 5 µm. (B) Macroscopic growth of the following strains: Wild type (FGSC 2489), Δ*mak-2* (NCU02393), 640 (*Ptef-1-mak-2-gfp-caax, mak-2::hph*), 404 (*Pmak-2-mak-2-gfp-saax, mak-2::hph*) and 381 (*Ptef-1-mak-2-gfp-saax, mak-2::hph*). (C) Quantification of tropic interactions and germination of the following strains: Wild type (FGSC 2489), Δ*mak-2* (NCU02393), 633 (*Ptef-1-mak-2-gfp, mak-2::hph*), 640 (*Ptef-1-mak-2-gfp-caax, mak-2::hph*) and 381 (*Ptef-1-mak-2-gfp-saax, mak-2::hph*) (n = 150 pairs per strain). The error bars represent the standard deviation observed between at least 100 germlings per strain in three independent experiments. Statistics analyses show significant differences between strains Δ*mak-2* and 640 with the wild type ($p<0.01$).

A more detailed description of the cloning and the generation of these strains can be found in the dissertation of Julia Illgen (Illgen, 2017)**.** As part of this thesis, some of the key experiments were repeated to test their reproducibility (Serrano et al., 2018).

As was previously reported by Julia Illgen, the addition of a -CaaX domain to the C-terminal region of the MAK-2-GFP protein resulted in its permanent tethering to the plasma membrane in different cell types representing the vegetative life cycle of *N. crassa*: spores, germlings and hyphae (Fig. 3.1.1A). Only the strains overexpressing the constructs were used for all microscopy images shown in Figure 3.1.1A and 3.1.1B. Native expression of the CAAX box-tagged MAK-2-GFP (642) resulted in a very weak fluorescence signal and no unambiguous localization was possible. For the control strains, fluorescence imaging revealed that the GFP signal remained mostly cytoplasmic, and no accumulation at the membrane was observed (Fig. 3.1.1A). Interestingly, we found that the permanently membrane-tethered MAK-2 variant (strains 642 and 640) did not complement the Δ*mak-2* macroscopic phenotype, while the control strains expressing MAK-2-GFP (404 and 381) exhibited full complementation (Fig. 3.1.1B). In addition, we observed no influence of the expression level of the constructs (*Pmak-2* or *Ptef-1*) (Fig. 3.1.1B) on the phenotype of the strains. During cell fusion, MAK-2 is recruited to the cells tips of the interacting cells in an antiphase manner. The permanent tethering of the protein to the plasma membrane in both cells disrupts this dynamics, and therefore might impair cell fusion. To test this hypothesis, a quantification of the cell fusion rate (represented as the percentage of cells exhibiting tropic interactions) was conducted for the different strains. As a result we observed that the MAK-2-GFP-CAAX construct did not complement the Δ*mak-2* mutant regarding its cell communication defect, while the control strains 633 (*Ptef-1-mak-2-gfp, mak-2::hph*) and 381 (*Ptef-1-mak-2-gfp-saax, mak-2::hph*) showed full complementation. In addition to the rate of tropic interactions, we also quantified the germination rate of the spores, to test the general healthiness of the strains. No significant differences were observed between all tested strains (Fig. 3.1.1C).

3.1.2 The permanent membrane tethering of MAK-2 results in hyper-phosphorylation of the protein

In baker's yeast, Fus3p is recruited to the plasma membrane of the Shmoo after pheromone binding to the receptors (Ste2/Ste3). There, the protein is phosphorylated and subsequently released from the complex formed. After activation, Fus3p translocates into the nucleus, where it phosphorylates different transcription factors that regulate the response of the cells to the pheromone secreted by the mating partner (Merlini et al., 2013). In *N. crassa*, MAK-2 is also recruited to the cell tips of the two interacting cells during somatic cell fusion, however in an alternating fashion. The membrane-tethering of MAK-2 disrupted its subcellular dynamic localization, which prevents translocation of the protein to the nucleus and phosphorylation of its targets (Fig. 3.1.1A). In order to understand whether the phosphorylation of MAK-2 was also affected, we performed Western blot analyses testing the MAP kinase phosphorylation. Surprisingly, we found that the MAK-2-GFP-CAAX fusion protein was hyper-phosphorylated compared to the controls (-GFP or -SAAX). The expression level of the construct did not influence this activation (Fig. 3.1.2A). To test the total amount of the MAP kinase present in each sample, the Western blot membranes were also hybridized with an anti-GFP antibody. In all CAAX samples the GFP signal was reduced, suggesting that the membrane tethering of the protein had a negative influence on its stability. The anti-GFP signal was used for normalization of the anti-phospho signal to allow a proper comparison of the different samples (Fig. 3.1.2B). As for most MAP kinases, MAK-2 phosphorylation is mediated by a classical three-tiered pathway (Fig. 3.1.2C). To test whether MAK-2-GFP-CAAX phosphorylation was mediated by the upstream kinases of the MAK-2 module, we tested phosphorylation of the construct in the following deletion mutants: Δ*ham-5,* Δ*nrc-1* and Δ*mek-2*. The *Ptef-1-mak-2-gfp-caax* plasmid was transformed into the histidine auxotrophic deletion mutants (strains 743, N2-42 and N2-41, respectively), generating the following strains: 770, 670 and 384, respectively. In these strains, MAK-2 was efficiently tethered to the membrane (Fig. 3.1.2D and E). Western blot analysis revealed that phosphorylation of all tested MAK-2 constructs had vanished or was highly reduced in absence of the MAK-2 module components (Fig. 3.1.2F and G).

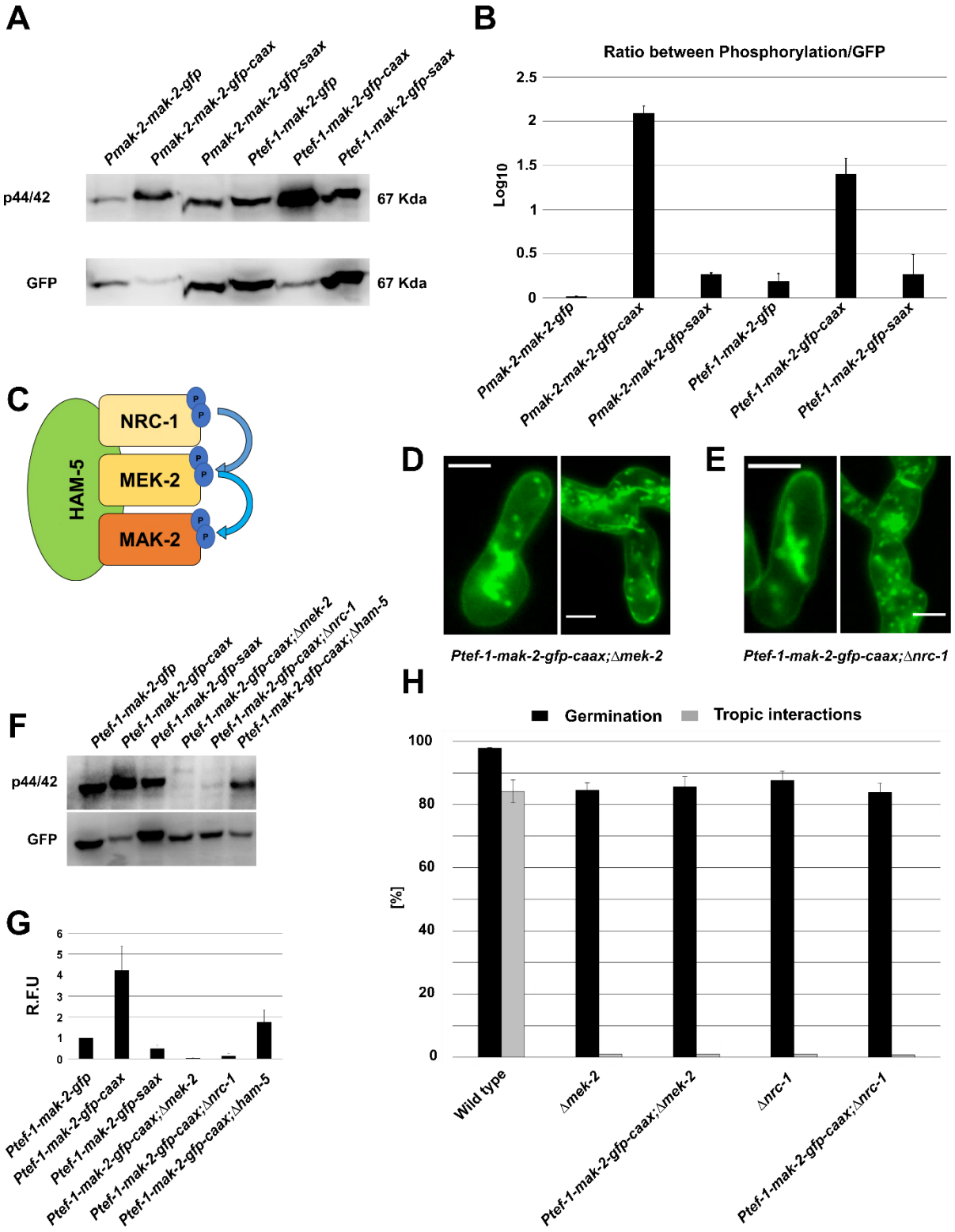
A
Pmak-2-mak-2-gfp
Pmak-2-mak-2-gfp-caax
Pmak-2-mak-2-gfp-saax
Ptef-1-mak-2-gfp
Ptef-1-mak-2-gfp-caax
Ptef-1-mak-2-gfp-saax
p44/42
67 Kda
GFP
67 Kda
B
Ratio between Phosphorylation/GFP
Log10
2.5
2
1.5
1
0.5
0
C
HAM-5
NRC-1
MEK-2
MAK-2
D
Ptef-1-mak-2-gfp-caax;Δmek-2
E
Ptef-1-mak-2-gfp-caax;Δnrc-1
F
Ptef-1-mak-2-gfp
Ptef-1-mak-2-gfp-caax
Ptef-1-mak-2-gfp-saax
Ptef-1-mak-2-gfp-caax;Δmek-2
Ptef-1-mak-2-gfp-caax;Δnrc-1
Ptef-1-mak-2-gfp-caax;Δham-5
p44/42
GFP
G
R.F.U
6
5
4
3
2
1
0
Ptef-1-mak-2-gfp
Ptef-1-mak-2-gfp-caax
Ptef-1-mak-2-gfp-saax
Ptef-1-mak-2-gfp-caax;Δmek-2
Ptef-1-mak-2-gfp-caax;Δnrc-1
Ptef-1-mak-2-gfp-caax;Δham-5
H
Germination
Tropic interactions
[%]
100
80
60
40
20
0
Wild type
Δmek-2
Ptef-1-mak-2-gfp-caax;Δmek-2
Δnrc-1
Ptef-1-mak-2-gfp-caax;Δnrc-1

Figure 3.1.2. The membrane tethering of MAK-2 results in hyper-phosphorylation of the protein through its upstream MAPKKK (NRC-1) and MAPKK (MEK-2). (A) Phospho Western blot analysis of the following strains: GN5-17 (1; *Pmak-2-mak-2-gfp, mak-2::hph*), 642 (2; *Pmak-2-mak-2-gfp-caax; mak-2::hph*), 404 (3; *Pmak-2-mak-2-gfp-saax, mak-2::hph*), 633 (4; *Ptef-1-mak-2-gfp, mak-2::hph*), 640 (5; *Ptef-1-mak-2-gfp-caax; mak-2::hph*) and 381 (6; *Ptef-1-mak-2-gfp-saax; mak-2::hph*). (B) Quantification of the ratio between the phosphorylation and the GFP signal, represented under Log_{10}. Error bars represent the standard deviation in the quantified phosphorylation/gfp signals observed in 3 independent experiments. (C) Representation of the proteins involved in MAK-2 activation: the MAP3K (NRC-1), the MAP2K (MEK-2), the MAP kinase (MAK-2) and the scaffolding protein HAM.5. (D) Subcellular localization of MAK-2-GFP-CAAX in the deletion mutant background of *mek-2* (Δ*mek-2*), strain 384 (*Ptef-1-mak-2-gfp-caax, mek-2::hph*) (E) Subcellular localization of MAK-2-GFP-CAAX in the Δ*nrc-1* background, strain 670 (*Ptef-1-mak-2-gfp-caax, ncr-1::hph*). (F) Phospho Western blot analysis of the activation of MAK-2 in the following strains: 665 (*Ptef-1-mak-2-gfp*), 267 (*Ptef-1-mak-2-gfp-caax*), 361 (*Ptef-1-mak-2-gfp-saax*), 384 (*Ptef-1-mak-2-gfp-caax, mek-2::hph*), 670 (*Ptef-1-mak-2-gfp-caax, ncr-1::hph*) and 770 (*Ptef-1-mak-2-gfp-caax, ham-5::hph*). (G) Quantification of the ratio between the phosphorylation and the GFP signal. Error bars represent the standard deviation of the phosphorylation/gfp signals in 3 independent Western blots. (H) Quantification of tropic interactions and germination of the following strains: WT (FGSC 2589), Δ*mek-2* (NCU04612), 384 (*Ptef-1-mak-2-gfp-caax, mek-2::hph*), Δ*nrc-1* (NCU06182) and 670 (*Ptef-1-mak-2-gfp-caax, ncr-1::hph*). Error bars represent the standard deviation observed between 100 germlings analyzed per strain in three independent experiments.

This indicates that the hyper-phosphorylation of the membrane-tethered MAK-2 variant is mediated by its usual upstream factors.

To test the function of membrane-tethered MAK-2 in these mutant backgrounds, we quantified the tropic interactions. As expected, we observed that MAK-2-GFP-CAAX did not restore the cell fusion-deficient phenotype (Fig. 3.1.2H). Taken together these data suggest that membrane recruitment of MAK-2 results in increased phosphorylation through the upstream components and that the subcellular spatial dynamics of the kinase are essential for its normal functioning during the cell-cell interaction process.

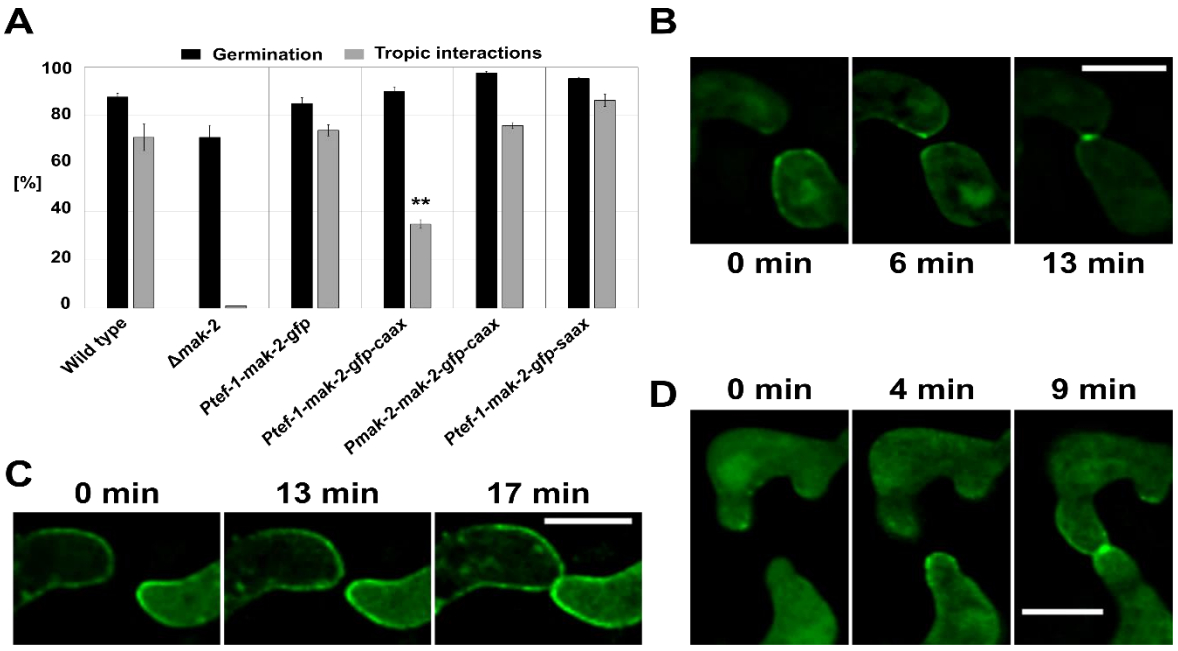

Figure 3.1.3. The presence of permanently membrane-tethered MAK-2 disrupts the normal functioning of the wild-type MAP kinase. (A) Quantification of the tropic interactions and germination of the following strains: WT (N1-01), Δ*mak-2* (NCU02393), 665 (*Ptef-1-mak-2-gfp*), 267 (*Ptef-1-mak-2-gfp-caax*), 353 (*Pmak-2-mak-2-gfp-caax*) and 361 (*Ptef-1-mak-2-gfp-saax*). Error bars represent the standard deviation observed between 100 germlings analyzed in three independent experiments. ** Significant differences are observed between *Ptef-1-mak-2-gfp-caax* and the wild-type strain. (B) Localization of the MAK-2-GFP overexpressed (*Ptef-1*) construct in strain 665 during cell-cell interaction. (C) Subcellular localization of the membrane tethered MAK-2 during cell-cell interaction in strain 267. (D) Localization of the overexpressed control construct MAK-2-GFP-SAAX during cell-cell interaction in strain 361. All scales bar: 5 µm

3.1.3 The permanent membrane tethering of MAK-2 has a negative dominant effect in the wild-type background

Once we found that the subcellular dynamic localization of MAK-2 was essential for its function during cell fusion, we decided to test the consequences of the membrane tethering in a wild-type background. The *Ptef-1-mak-2-gfp-caax* and the *Pmak-2-mak-2-gfp-caax* plasmids (p22 and p25) (Illgen, 2017) were transformed into the wild-type strain (N1-03), resulting in strains 267 and 353, respectively.

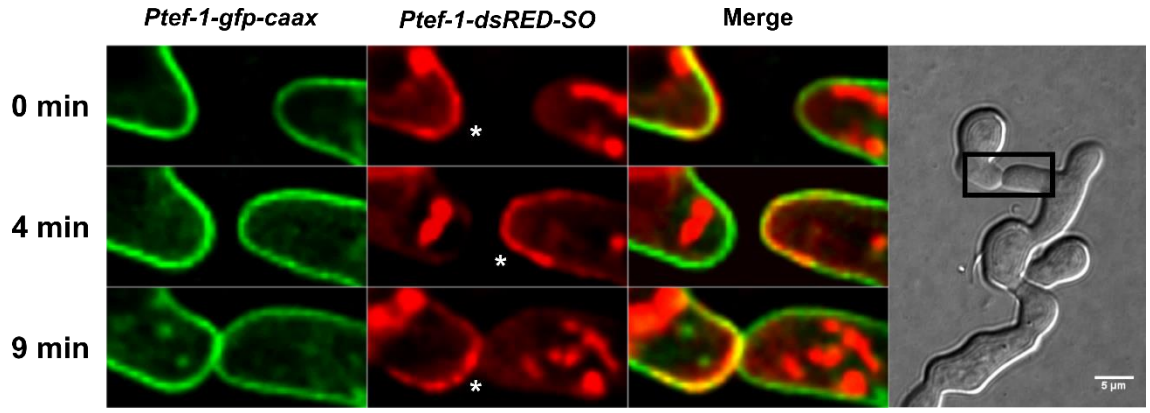

Figure 3.1.4. Localization of SO when GFP is permanently membrane tethered during a cell fusion interaction. SO-dsRed is localized at the opposite cell tips in an oscillatory manner, while GFP is continuously membrane tethered in both cell tips. The images were acquired from a heterokaryon created by mixing of spores from strains 802 and 843. Scale bar: 5 µm. Similar observations were made at least 4 more times.

Unfortunately, the native expression of the *mak-2-gfp-caax* construct was, however, too weak to allow unambiguous observations by microscopy. Therefore as a control the *Ptef-1-mak-2-gfp* and *Ptef-1-mak-2-gfp-saax* (p76 and p66, from (Illgen, 2017)) plasmids were transformed into N1-03, resulting in the strains 665 and 381, respectively. In a first step, germling interactions were quantified in the different strains. Interestingly, the number of tropic interactions was significantly reduced in the MAK-2-GFP-CAAX overexpression, strain 267, compared to the wild type and the control strains (Fig. 3.1.3A). This suggests that the presence of membrane-tethered MAK-2 has a dominant negative effect on the number of tropic interactions.

It is known that the dynamic, alternating membrane localization of MAK-2 and SO is a highly coordinated process, in which the two proteins never colocalize until the cells establish physical contact. While MAK-2 and MAK-2-GFP-SAAX showed the normal oscillation pattern, MAK-2-GFP-CAAX was permanently present at the plasma membrane, even during the tropic interactions (Fig. 3.1.3B, C and D). In light of the reduced number of interactions in the wild-type background strain expressing MAK-2-GFP-CAAX, we therefore hypothesized that membrane recruitment of SO might be disturbed in the presence of membrane-tethered MAK-2.

To test this hypothesis, SO dynamics were determined in the wild-type background strain expressing MAK-2-GFP-CAAX.

3.1.4 Only the presence of phosphorylated MAK-2 disrupts the dynamic localization of SO during cell-cell interactions

As a control, we first tested the localization of dsRed-SO when only GFP is membrane-tethered in a heterokaryon of strains 843 and 800 (*Ptef-1-dsRed-so* and *Ptef-1-gfp-caax,* respectively), to exclude the possibility that the presence of a mislocalized protein at the membrane has a general effect on SO recruitment. Spores from strain 843 and 800 were mixed, in order to obtain the heterokaryon containing both fluorescent proteins. The germinated spores from both strains fuse and the nuclei are mixed, which results in the expression of both constructs, that are located at the same genomic locus but in independent nuclei, within the same cell.

While the GFP signal was continuously detected at the plasma membrane, we observed the typical SO dynamic localization during the cell fusion process (Fig. 3.1.4). In all observations, the SO signal was present at only one cell tip. After around 4 minutes the signal switched to the opposite cell tip and after around 10 minutes, both cells established physical contact and the signal accumulated at the contact area.

Next, we tested the localization of SO when MAK-2 is permanently tethered at the plasma membrane. To form the test heterokaryon, we mixed spores of strain 843 (*Ptef-1- dsRed-so*) with spores of 267 (*Ptef-1-mak-2-gfp-caax*). When analyzing the subcellular dynamics of the proteins, we observed that while MAK-2 was permanently tethered to the plasma membrane, SO recruitment was not detected during the cell communication phase and only appeared when cells established physical contact (Fig. 3.1.5).

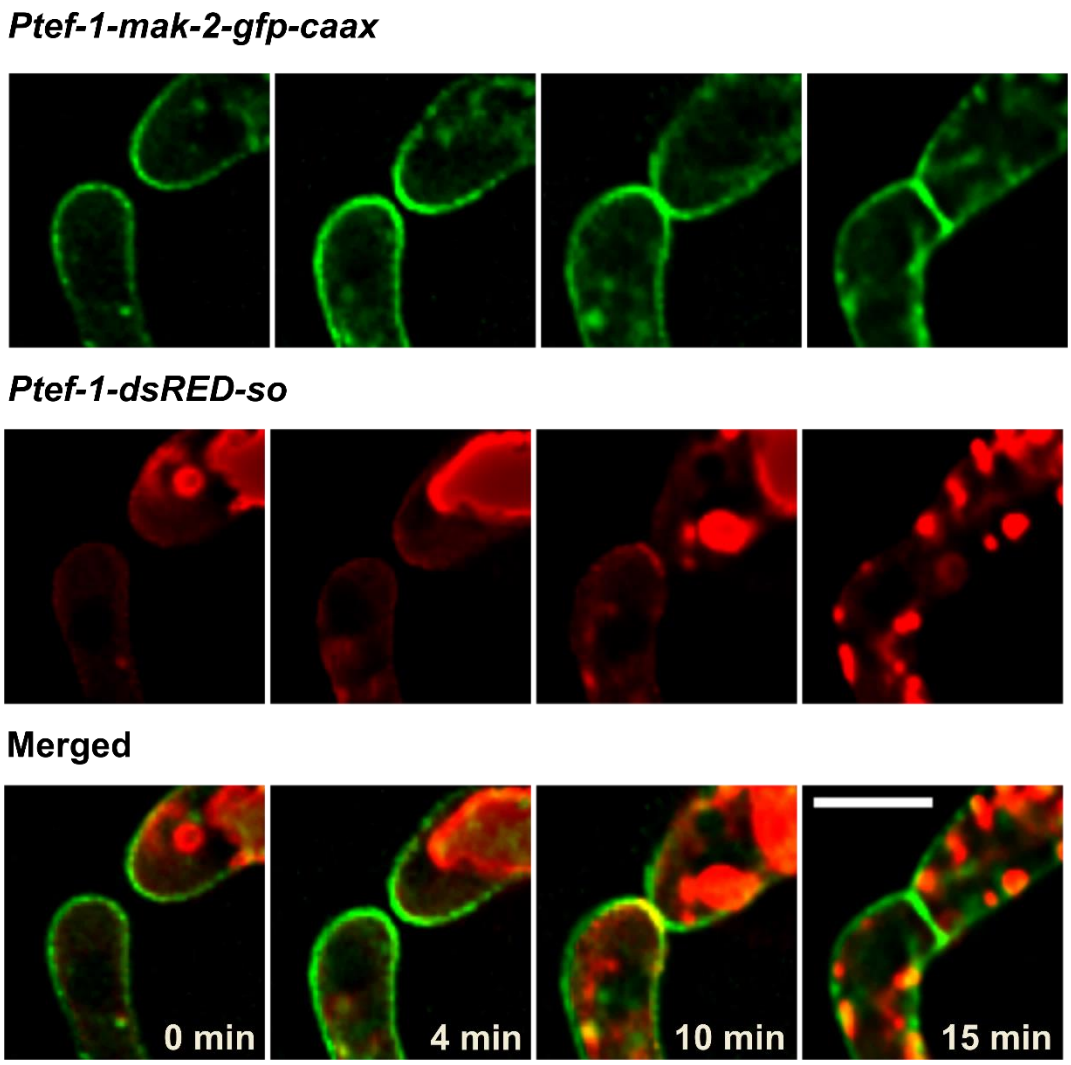

Figure 3.1.5. The dynamic localization of SO is disrupted when MAK-2 is permanently tethered at the plasma membrane. Images acquired from a heterokaryon created by mixing spores from strains 267 and 843. Scale bar: 5 µm.

We quantified the number of cells in which SO was recruited when MAK-2 was either present as the -GFP-CAAX or the -GFP variant (as a control). We found that in all tested cell pairs expressing MAK-2-GFP-CAAX (n=120), the presence of MAK-2 at the plasma membrane disrupted the recruitment of SO during the communication phase. Interestingly, in all 120 pairs SO was recruited after the cells established physical contact. In the control, SO was recruited in a wild-type manner in all pairs tested (n=60).

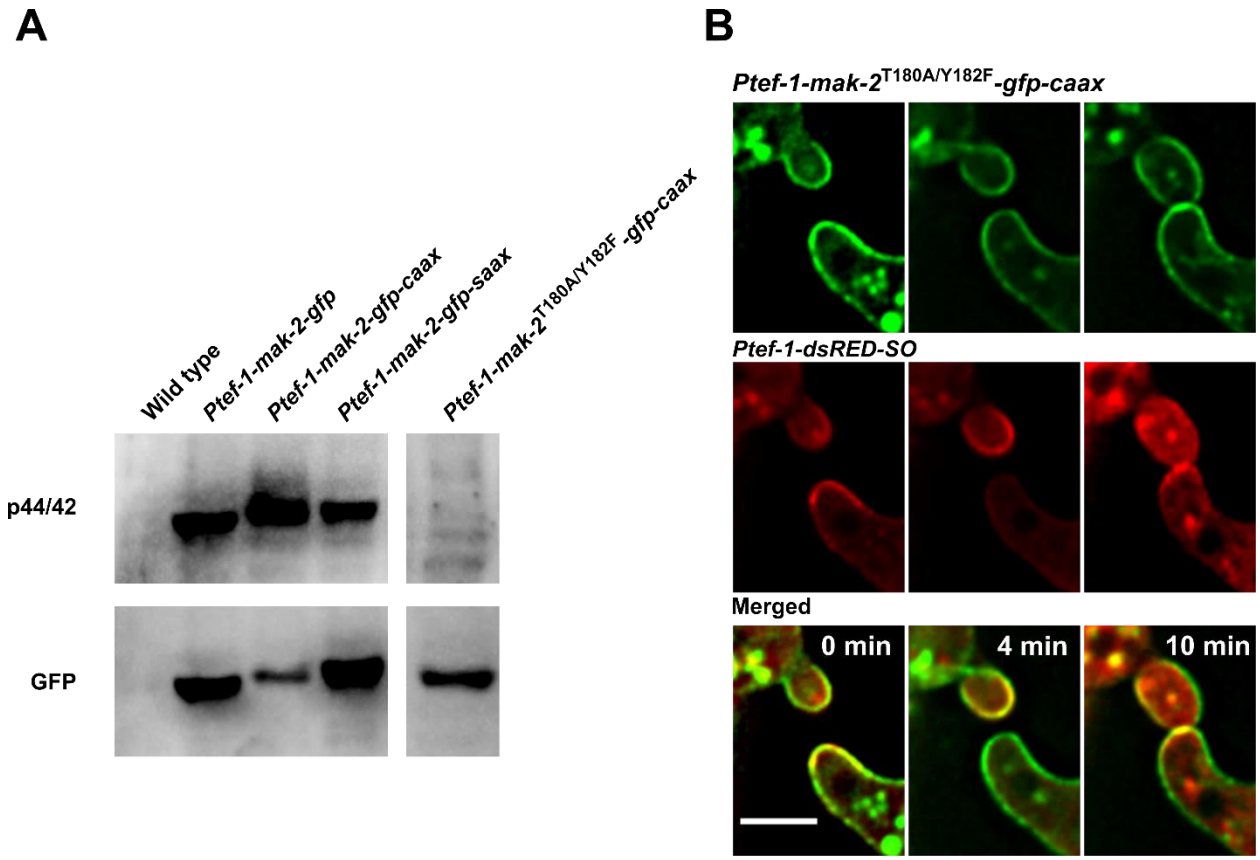

Figure 3.1.6. The membrane tethering of the non-phosphorylatable MAK-2 version (MAK-2$^{T180A/Y182F}$) do not influence the SO dynamic localization during cell interactions. (A) Phospho western blot analyses of the MAK-2 phosphorylation of the following strains: WT (N1-01), 665 (*Ptef-1-mak-2-gfp*), 267 (*Ptef-1-mak-2-gfp-caax*), 361 (*Ptef-1-mak-2-gfp-saax*) and 797 (*Ptef-1-mak-2-*$^{T180A/Y182F}$*-gfp-caax*). p44/42 detects phosphorylation signal of the conserved T180 and Y182 residues of the MAP kinase MAK-2. This western blot only shows the interested parts of the blotting membrane for this figure. (B) Microscopy analyses of a cell fusion interaction in a heterokaryon created by mixing spores from strains 797 (*Ptef-1-mak-2-*$^{T180A/Y182F}$*-gfp-caax*) and 843 (*Ptef-1-dsRed-so*). Scale bar: 5 µm. Similar observations were made at least 5 times.

These data indicate that MAK-2 only controls the localization of SO during the communication phase, but allows co-localization of both proteins after cells establish physical contact.

As shown above, the permanent membrane-tethering of MAK-2 induced hyper-phosphorylation of the protein. We therefore decided to test if this activation of MAK-2 is causing the effect on the SO recruitment. MAK-2 is a MAP kinase with two highly conserved phosphorylation sites: T180 (Threonine) and Y182 (Tyrosine). By yeast recombinational cloning, we created a plasmid in which both MAK-2 phosphorylation sites were mutated: T180 to A (Alanine) and Y182 to F (Phenylalanine). The new plasmid (*Ptef-1-mak-2*$^{T180A/Y182F}$*-gfp-caax*; number 843) was transformed into the wild-type background (N1-03), resulting in strain 797.

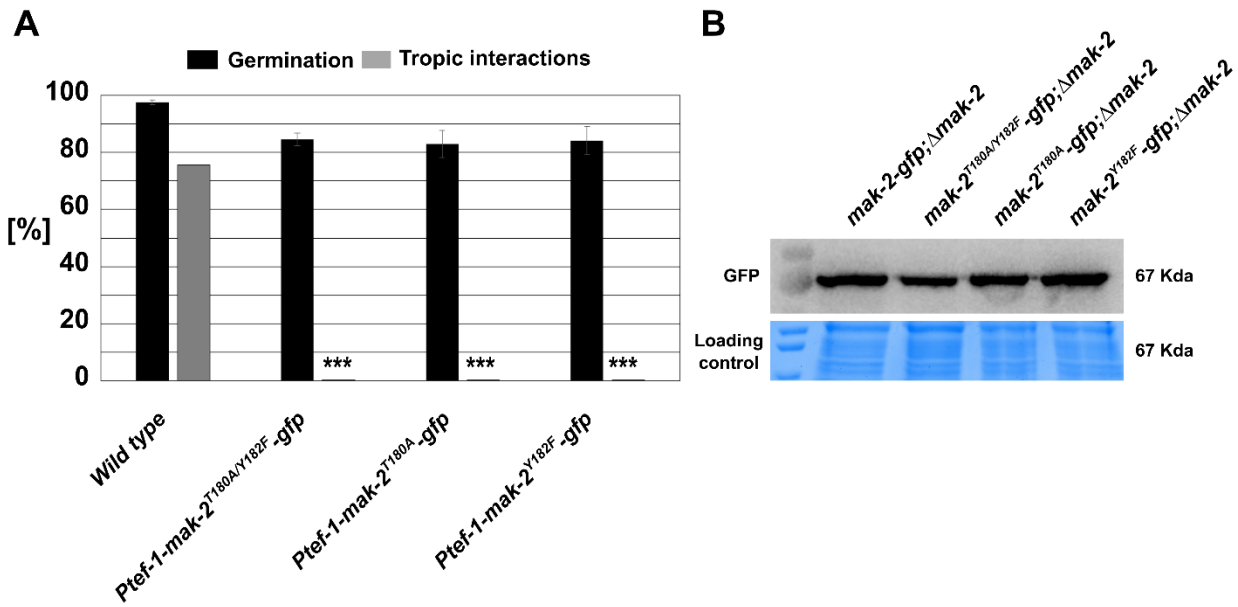

Figure 3.1.7. Quantification of tropic interactions of spores expressing mutated MAK-2 versions in the Δ*mak-2* background. (A) Quantification of the following strains: WT (N1-01), 607 (*mak-2::hph; Ptef-1-mak-2-*$^{T180A/Y182F}$*-gfp*), 610 (*mak-2::hph; Ptef-1-mak-2-*^{T180A}*-gfp*) and 613 (*mak-2::hph; Ptef-1-mak-2-*^{Y182F}*-gfp*). Error bars represent the standard deviation observed between at least 100 germlings analyzed in three independent experiments. (B) Western blot analysis of the expression level of the various constructs using an anti-GFP antibody. Comparable observations were made in at least in 3 independent experiments.

Macroscopically, the new strain had a wild-type phenotype. In a Western blot analyses no phosphorylation was detected by antibody p44/42, which recognizes the double but also both single phosphorylated versions of MAK-2 (Fig. 3.1.6A). To determine the influence of this construct on the SO dynamics, a heterokaryon was created by mixing spores of strains 797 (*Ptef-1-mak-2-*$^{T180A/Y182F}$*-gfp-caax*) and 843 (*Ptef-1-dsRed-so*). As previously described, the subcellular localization of SO was observed by fluorescence live-cell imaging. SO membrane recruitment and its oscillation were fully wild-type like when MAK-2 was not phosphorylated but present at the plasma membrane (Fig. 3.1.6B). These data suggest that only phosphorylated MAK-2 disrupts SO dynamic localization and clearly suggests a link between MAK-2 activation and SO membrane recruitment. However, SO regulation may change when cells establish physical contact, since its localization is no longer influenced by the phosphorylation status of MAK-2.

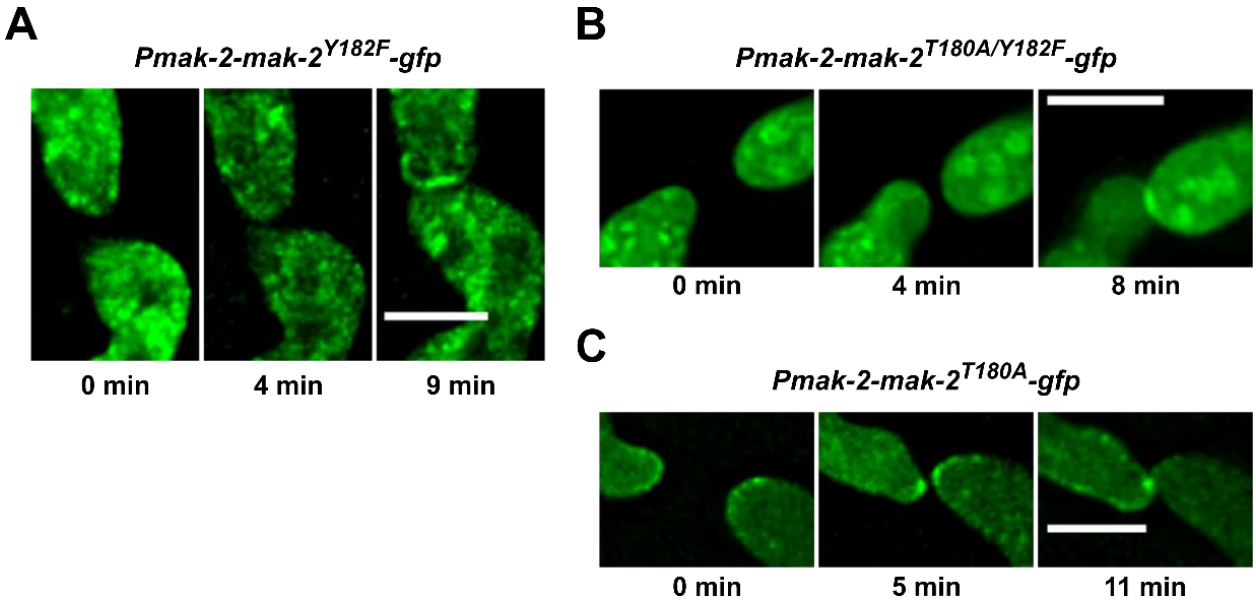

Figure 3.1.8. Localization of the different phosphorylation truncated versions of MAK-2. (A) Subcellular localization of the MAK-2^{Y182F}-GFP version in the strain 809 (*Pmak-2-mak-2-*^{Y182F}*-gfp*). Scale bar: 5 µm. (B) Subcellular localization of the MAK-2$^{T180A/Y182F}$-GFP in the strain 816 (*Pmak-2-mak-2-*$^{T180A/Y182F}$*-gfp*). Scale bar: 5 µm. (C) Subcellular localization of the MAK-2^{T180A}-GFP from the strain 813 (*Pmak-2-mak-2-*^{T180A}*-gfp*). Scale bar: 5 µm.

3.1.5 MAK-2 phosphorylation and activity are essential for the dynamic subcellular localization of the kinase during the cell-cell communication phase

Earlier in this study, we have shown that subcellular dynamic localization of MAK-2 is essential for the function of this MAP kinase. In addition, we observed that the phosphorylation of MAK-2 is strongly influenced by its subcellular localization. To gain a better understanding on the interrelation between subcellular localization and activity, we next followed two approaches: 1) analyzing the dynamics of various MAK-2 variants with mutated phosphorylation sites and 2) testing the influence of MAK-2 activity inhibition on its subcellular localization. In her dissertation, J. Illgen previously created the non-phosphorylatable MAK-2 variants in the Δ*mak-2* background. As reported in her thesis, three plasmids were generated by yeast recombinational cloning: p400 (*Ptef-1-mak-2-*^{T180A}*-gfp*), p398 (*Ptef-1-mak-2-*^{Y182F}*-gfp*) and p399 (*Ptef-1-mak-2-*$^{T180A/Y182F}$*-gfp*). These three constructs were transformed into the Δ*mak-2* background (strain 598), resulting in strains that she named as 610, 613 and 607, respectively.

We used these strains to test that all three isolates behaved comparable to Δ*mak-2*, showing no complementation of the Δ*mak-2* mutation, although all constructs showed similar protein expression levels (Fig. 3.1.7A and B). Since the goal of this experiment was to test the subcellular localization of the mutated MAK-2 versions during cell fusion, we also transformed the constructs in the wild-type background N1-01, which allowed cell-cell interactions. We created three new plasmids where the overexpressed promoter was replaced by the native promoter *Pmak-2*, as a control to potential artefacts due to overexpression. By yeast recombinational cloning, the *Ptef*-1 promoter was replaced by the native *Pmak-2,* resulting in the plasmids: 703 (*Pmak-2-mak-2-*^{T180A}*-gfp*), 701 (*Pmak-2-mak-2-*^{Y182F}*-gfp*) and 702 (*Pmak-2-mak-2-*$^{T180A/Y182F}$*-gfp*). Transformation of these plasmids generated the strains 813, 809 and 815, respectively. Macroscopically, the new strains grow comparable as the wild type. Cell fusion was observed in a wild type-like manner, a no significant differences were observed. Localization of the constructs was tested by fluorescence microscopy.

Interestingly, in the strains expressing the constructs with the mutated Y182F phosphorylation site, strains 809 (*Pmak-2-mak-2-*^{Y182F}*-gfp*) and 816 (*Pmak-2-mak-2-*$^{T180A/Y182F}$*-gfp*), no membrane recruitment of the MAP kinase variant was observed during cell interactions, although the signal accumulated at the fusion point after the cells established physical contact (Fig. 3.1.8A and B). In contrast, the mutation of the T180A phosphorylation site of the strain 813 (*Pmak-2-mak-2-*^{T180A}*-gfp*) still allowed membrane recruitment of the protein, however, it appeared at both interacting tips at the same time, suggesting that membrane release was deficient. This construct also accumulated at the fusion point when cells had established physical contact (Fig. 3.1.8C). These data show that the full activation of MAK-2 is necessary for the oscillatory dynamic recruitment of the protein to the plasma membrane during the communication phase. Furthermore, the localization of the protein is independent of its phosphorylation state after the cells establish physical contact, which might indicate that at this state of the fusion process the protein plays a different function than in the previous communication phase.

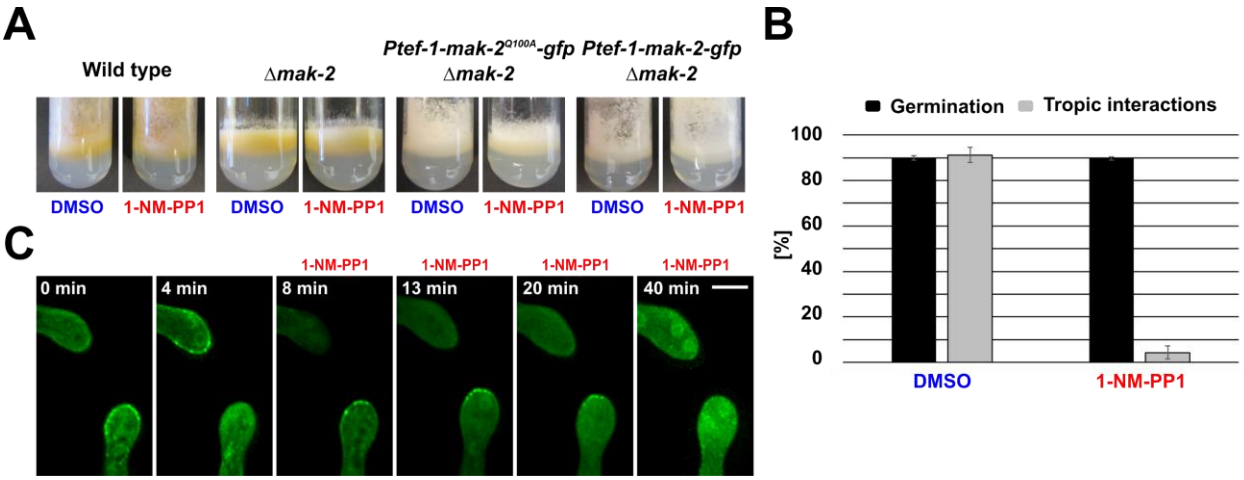

Figure 3.1.9. MAK-2 activity is essential for the subcellular dynamic localization of the kinase during cell fusion. (A) Macroscopic phenotype of the tested strains either with 1-NM-PP1 (+) or DMSO (-). The strains tested were the following: WT (N1-01), Δ*mak-2* (NCU02393), 802 (*mak-2::hph;Ptef-1-mak-2*^{Q100A}*-gfp*) and 633 (*mak-2::hph;Ptef-1-mak-2-gfp*). (B) Quantification of tropic interactions and germination of strain 802 (*mak-2::hph;Ptef-1-mak-2*^{Q100A}*-gfp*). Error bars represent the standard deviation observed in at least 100 germlings per condition, in three independent experiments. (C) Fluorescent microscopy images of an interaction of cells of strain 802 (*mak-2::hph;Ptef-1-mak-2*^{Q100A}*-gfp*). +Inh represents the addition of 1-NM-PP1. Scale bar: 5 µm.

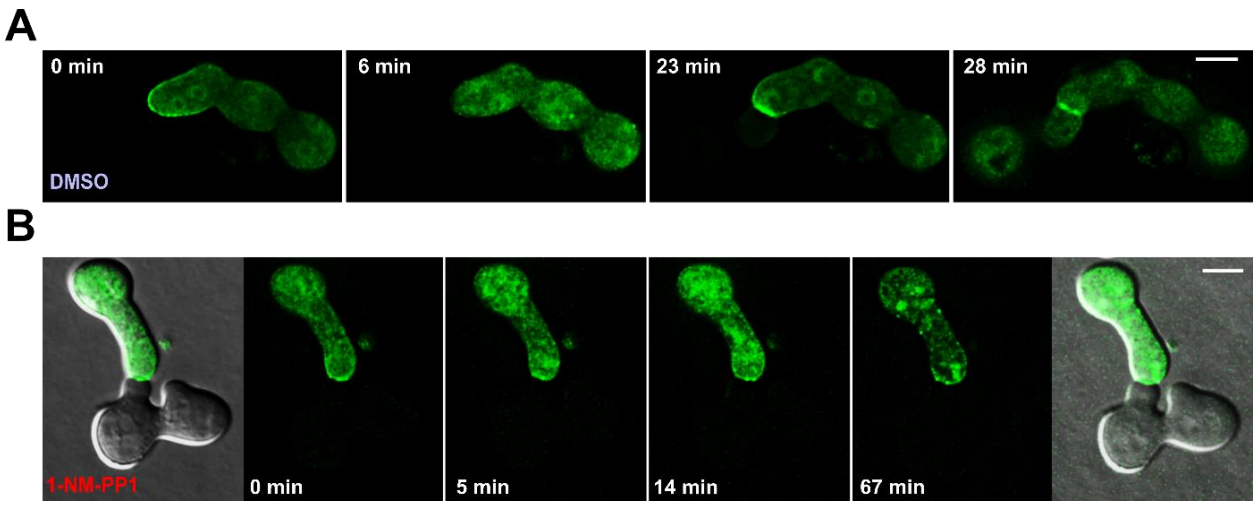

Figure 3.1.10. MAK-2 activity is essential during cell wall degradation and membrane fusion. (A) Mix of spores from strains 802 (*mak-2::hph;Ptef-1-mak-2^{Q100A}-gfp*) and N2-01 (*mak-2::hph;Pcgg-1-mak-2^{Q100G}*). DMSO was added in time 0 min. Green cytoplasmic flow from the upper cell to the lower cell is observed at time 23'. Scale bar: 5 µm. (B) Mix of spores from strains 802 (*mak-2::hph;Ptef-1-mak-2^{Q100A}-gfp*) and N2-01 (*mak-2::hph;Pcgg-1-mak-2^{Q100G}*). 1-NM-PP1 (+ Inh) was added at time 0'. No cytoplasmic flow is observed. Scale bar: 5 µm. Comparable observations were made in 5 additional cell pairs.

In a second approach, we followed a chemical genetics strategy to specifically manipulate the MAK-2 activity within the living cells. In a previous study, Fleißner et al created an analog-sensitive variant of MAK-2^{Q100A} that resulted in full complementation of the Δ*mak-2* phenotype in the absence of the inhibitor. However, the localization of the protein after inhibition was not analyzed (Fleissner et al., 2009). By yeast recombinational cloning an analog-sensitive version of MAK-2 tagged to GFP was created by substituting the gatekeeper amino acid (Q100) by an Alanine, resulting in the plasmid 692 (*Ptef-1-mak-2^{Q100A}-gfp*). This plasmid was transformed into the Δ*mak-2* background (strain 598) resulting in strain 802 (*mak-2::hph; his-3::Ptef-1-mak-2^{Q100A}-gfp*). In the absence of the chemical inhibitor (1-NM-PP1), the strain 802 behaved as wild type, indicating that the point mutation did not disturb the general function of the kinase. Upon addition of 1-NM-PP1 to the growth medium, however, the strain developed a clear *mak-2* knock-out phenotype, indicating that MAK-2^{Q100A}-GFP was fully inhibited (Fig. 3.1.9A). Consistent with this finding, the addition of the chemical also completely disrupted the cellular tropic interactions in strain 802 (Fig. 3.1.9B).

For the subsequent live-cell imaging experiments, the cells were incubated for 2 hours at 30ºC in MM. A 1x1cm agar slice was placed under the microscope and cell pairs undergoing cell fusion were observed. By adding the inhibitor specifically during MAK-2 oscillation, we found that the oscillation was fully interrupted and MAK-2^{Q100A}-GFP remained stable at the plasma membrane of one cell, suggesting that the current state of the cells was arrested. The kinase remained at the plasma membrane for up to 40 minutes; afterwards a clear accumulation of the kinase in the nucleus was observed. (Fig. 3.1.9C). Together, these data indicate that the subcellular dynamic localization of MAK-2 influences but at the same time is controlled by its phosphorylation state and its enzymatic activity.

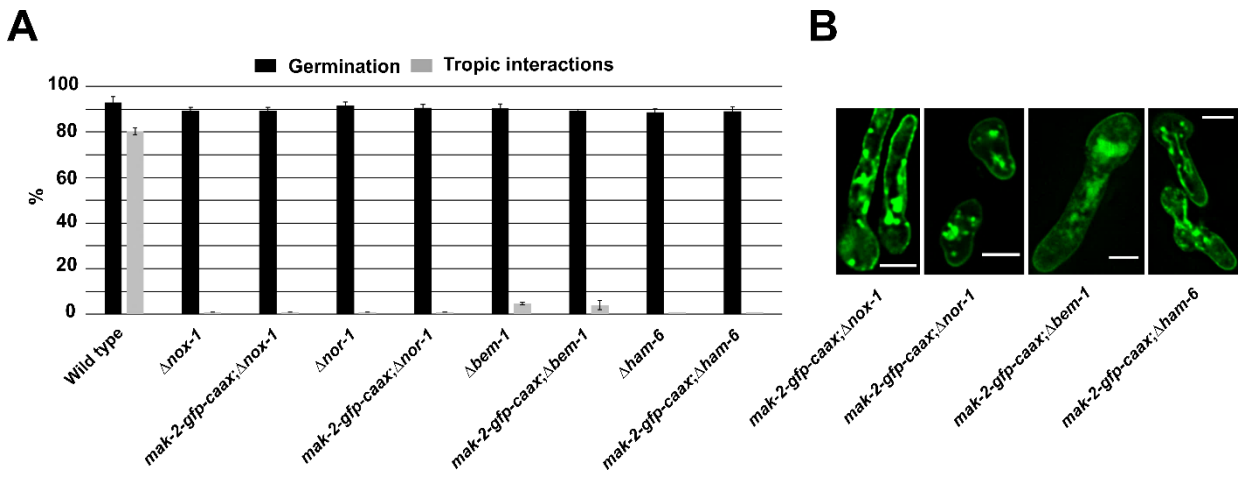

Figure 3.1.11. The cell fusion defects of the NOX complex mutants are not restored by the membrane-tethering of MAK-2. (A) Quantification of tropic interactions and germination of the following strains: WT (N1-01), Δ*nox-1* (NCU02110), 723 (*nox-1::hph;Ptef-1-mak-2-gfp-caax*), Δ*nor-1* (NCU07850), 719 (*nor-1::hph;Ptef-1-mak-2-gfp-caax*), Δ*bem-1* (NCU06593), 569 (*bem-1::hph;Ptef-1-mak-2-gfp-caax*), Δ*ham-6* and 773 (*ham-6::hph;Ptef-1-mak-2-gfp-caax*). Error bars represent the standard deviation observed in at least 100 germlings per strain in three independent experiments. (B) Fluorescence microscopy images from strains 723 (*nox-1::hph;Ptef-1-mak-2-gfp-caax*), 773 (*ham-6::hph;Ptef-1-mak-2-gfp-caax*), 719 (*nor-1::hph;Ptef-1-mak-2-gfp-caax*) and 569 (*bem-1::hph;Ptef-1-mak-2-gfp-caax*). Scale bars: 5 µm.

3.1.6 MAK-2 activity is also essential for the late steps of the cell fusion process: cell wall degradation and membrane fusion

In the previous sections, we have addressed the functions of the MAP kinase MAK-2 during the cell-cell interaction process. Interestingly, it was previously reported that MAK-2 also accumulates at the cell-contact area after cell contact, where it remains until fusion is completed and the cytoplasms have mixed (Fleissner et al., 2009). However, it is not fully understood whether MAK-2 plays any role at these very last steps of the cell fusion process.

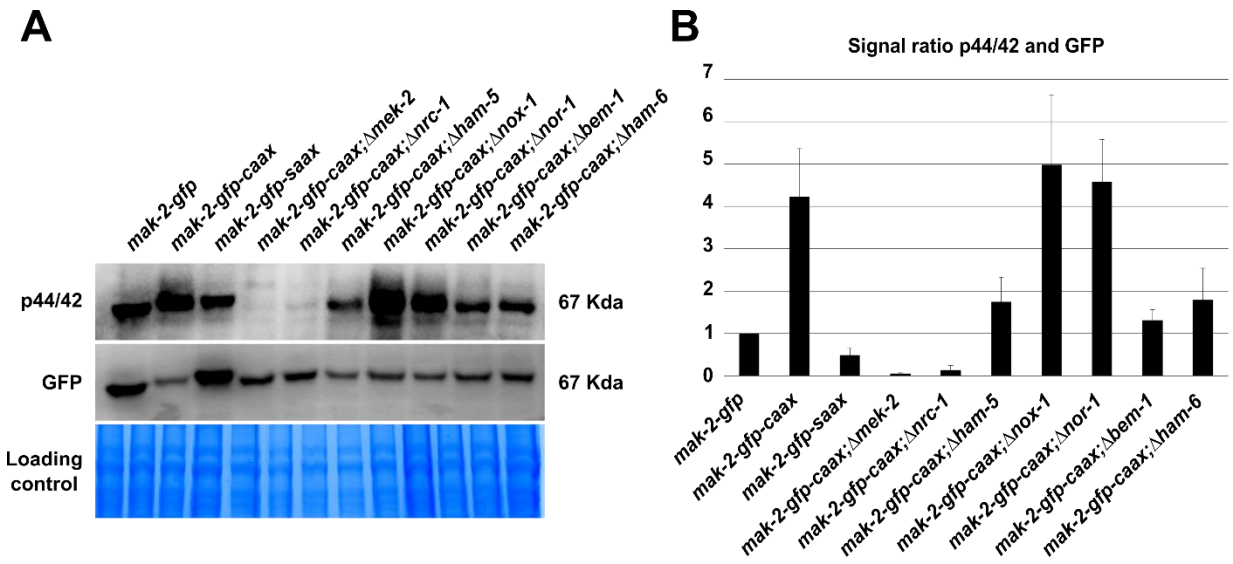

Figure 3.1.12. Phospho Western blot analysis of MAK-2-GFP-CAAX in different NOX complex mutants. (A) Phospho Western blot of the following strains: 665 (*Ptef-1-mak-2-gfp*), 267 (*Ptef-1-mak-2-gfp-caax*), 361 (*Ptef-1-mak-2-gfp-saax*), 384 (*mek-2::hph;Ptef-1-mak-2-gfp-caax*), 670 (*nrc-1::hph;Ptef-1-mak-2-gfp-caax*), 770 (*ham-5::hph;Ptef-1-mak-2-gfp-caax*), 723 (*nox-1::hph;Ptef-1-mak-2-gfp-caax*), 719 (*nor-1::hph;Ptef-1-mak-2-gfp-caax*), 569 (*bem-1::hph;Ptef-1-mak-2-gfp-caax*), 773 (*ham-6::hph;Ptef-1-mak-2-gfp-caax*). p44/42 corresponds to the signal obtained for the phosphorylation state of the proteins. GFP corresponds to the anti-gfp antibody. (B) Quantification of the ratio between the signals for the phosphorylation and for GFP from the same strains tested above. Error bars represent the standard deviation calculated from 4 independent experiments.

By using the chemical genetics approach, we tested the role of MAK-2 activity after cell contact in two different strains: 802 (*mak-2::hph;Ptef-1-mak-2^{Q100A}-gfp*) from this study and N2-01 (*mak-2::hph;Pcgg-1-mak-2^{Q100G}*) from (Fleissner et al., 2009). Both strains are MAK-2-inhibited when 1-NM-PP1 is added.

The experimental approach consisted of mixing spores of both strains and investigating cell pairs of 802 (expressing GFP) and N2-01 (cell unlabeled). Successful fusion could be detected by the transfer of GFP from the labeled to the unlabeled cell. The inhibitor was added to cell pairs that had already successfully established their interaction and had just touched, to test specifically for the role of MAK-2 at the late fusion stage. As a control, DMSO was added (Fig. 3.1.10A). While in the control cytoplasmic mixing was readily observed, the addition of 1-NM-PP1 resulted in a lack of fusion although MAK-2 remained recruited at the contact area (Fig. 3.1.10B). These data clearly indicate that MAK-2 activity is essential for cell-cell merger, either by controlling cell wall degradation or membrane fusion, or playing other so far unknown additional functions.

3.1.7 The yeast polarity factor BEM-1 is essential for MAK-2 phosphorylation in a NOX complex-independent manner

In an earlier study, Schürg *et al* identified potential functions of the polarity factor BEM-1 in MAK-2 activation during vegetative cell fusion. The *bem-1* knock-out strain (Δ*bem-1*) shows reduce activation of MAK-2 that correlates with highly reduced, delayed and instable germling interactions (Schürg et al., 2012). Interestingly, the BEM1 homologue in the plant symbiotic fungus *E. festucae* has been described as a component of the NADPH oxidase complex (NOX complex) (Takemoto et al., 2011). Moreover, the NOX complex is essential for cell fusion in the filamentous fungus *B. cinerea* (Roca et al., 2012) and *S. macrospora* (Dirschnabel et al., 2014). However, the direct link between cell fusion and NOX regulation is still unknown. We therefore asked whether the function of NOX in cell fusion involves the MAK-2 MAP kinase and specifically BEM1 and its potential regulation of MAK-2. First, we decided to test the cell fusion defects previously reported in closely related filamentous fungi. The components of the NOX complex in *N. crassa* were identified and characterized (except for their role in cell fusion) in the following study

(Cano-domı et al., 2008). General cell fusion defects of these strains were reported in an independent study but were not quantified (Lichius, 2010). Recently, a new subunit of the NOX complex, NoxD, was identified in *Podospora anserina* (Lacaze et al., 2015). After conducting a BLAST search with the NoxD protein sequence from *P. anserina*, we identified HAM-6 as the *N. crassa* homolog. HAM-6 is a transmembrane protein with a potential role in the reception of the signal that triggers MAK-1 activation (Fu et al., 2014; Maddi et al., 2012). Mutants for the following components of the NOX complex were obtained from the *N. crassa* gene knock-out collection (FGSC): Δ*nor-1* (NCU07850), Δ*nox-1* (NCU02110), Δ*nox-2* (NCU10775) and Δ*ham-6* (NCU02767), together with the Δ*bem-1* (NCU06593) strain. The Δ*nor-1* mutant was purified by single spore isolation in order to obtain a homokaryotic strain. We were unable to get a pure homokaryon of the Δ*nox-2* deletion strain (suggesting a lethal mutation), so it was disregarded for this study. We first quantified the cell fusion defects previously reported in *N. crassa*. All of the knock-out mutants showed a complete cell fusion defect and no interactions were observed in the spore populations (Fig. 3.1.11A). Furthermore, all knock-out mutants were crossed with the strain 267 (*Ptef-1-mak-2-gfp-caax*) in order to test the consequences of MAK-2 membrane tethering in the various NOX defective strains. Strain 267 was always used as a female whilst the mutants as males.

The following strains were obtained from the sexual crosses: 723 (*nox-1::hph;Ptef-1-mak-2-gfp-caax*), 719 (*nor-1::hph;Ptef-1-mak-2-gfp-caax*), 773 (*ham-6::hph;Ptef-1-mak-2-gfp-caax*). Strain 569 (*bem-1::hph;Ptef-1-mak-2-gfp-caax*) was previously obtained in another study from our laboratory (Schürg, 2012). Since Δ*nor-1* is ascospore lethal, we previously crossed the strain with the DIP (N2-10) mutant. This mutant is commonly used to generate ascospores which are diploid, and therefore the ascospolethality can be rescued by a wild-type copy of the respective gene (Hutchison et al., 2009). Afterwards, a single spore isolation must be performed to obtain a homokaryotic, haploid strain. Once a Δ*nor-1 his-3*$^{-}$ strain was obtained, a transformation with the plasmid *Ptef-1-mak-2-gfp-caax* (p25, from (Illgen, 2017)) was performed and the primary transformants were purified by single spore isolation. All of the newly constructed strains were tested for cell fusion (Fig. 3.1.11A). Interestingly, no influence on the cell fusion defects by the presence of MAK-2-GFP-CAAX was observed. The typical localization of the MAK-2-GFP-CAAX at the

plasma membrane was, however, found in the knock-out mutant strains (Fig. 3.1.11B). In order to test potential changes in MAK-2 activation, a phospho Western blot with all of the mentioned strains was performed (Fig. 3.1.12A and B). As previously observed, no phosphorylation signal was detected in strains lacking the MAK-2 cascade components MAP2K MEK-2 (strain 384, *mek-2::hph;Ptef-1-mak-2-gfp-caax*), MAP3K NRC-1 (strain 670, *nrc-1::hph;Ptef-1-mak-2-gfp-caax*) or the scaffold protein HAM-5 (strain 770*, ham-5::hph;Ptef-1-mak-2-gfp-caax*). In contrast, no negative influence on the phosphorylation intensity was observed in the absence of the NOX components: NOX-1 or NOR-1. Overall, the absence of a proper NADPH oxidase complex did not have any effect on MAK-2 phosphorylation.

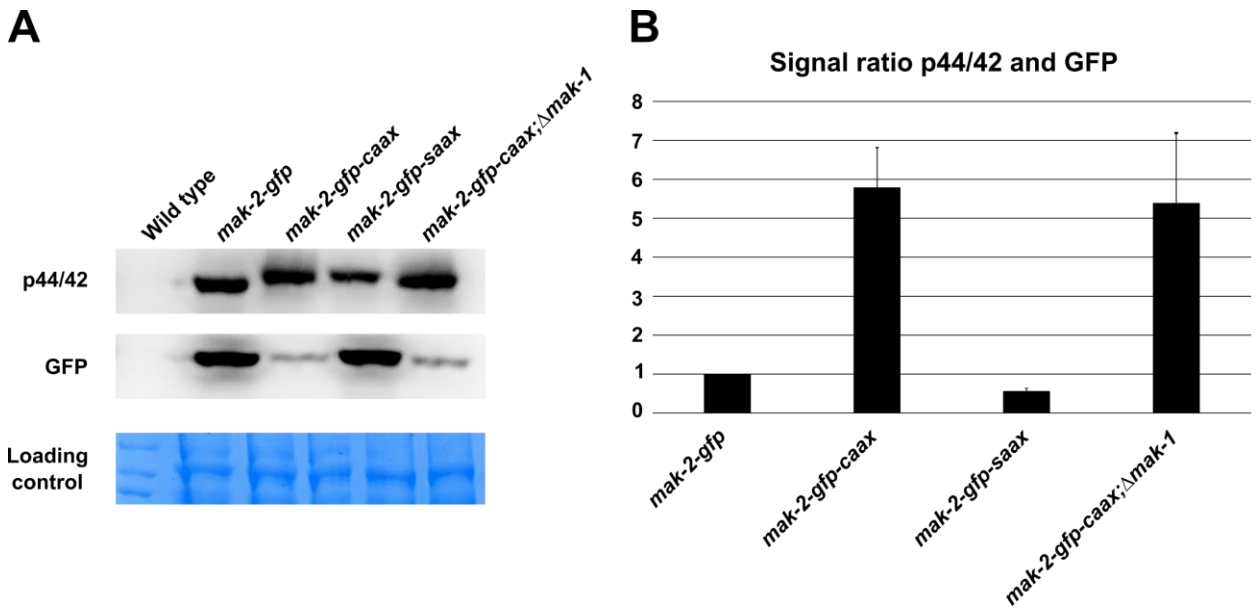

Figure 3.1.13. Western blot analysis of the MAK-2-CAAX phosphorylation in the Δ*mak-1* background. (A) Antibody staining detecting the phosphorylation level of MAK-2 (p44/42) and the GFP signal (α-gfp). The strains used are: WT (N1-01), 665 (*Ptef-1-mak-2-gfp*), 267 (*Ptef-1-mak-2-gfp-caax*), 361 (*Ptef-1-mak-2-gfp-saax*) and 775 (*hph::mak-1;Ptef-1-mak-2-gfp-caax)*. (B) Coomassie staining performed with the samples used for the antibodies staining. (C) Quantitative analyses of the ratio between the phosphorylation signal and the GFP signals. Error bars represent the standard deviation calculated from 3 independent experiments.

However, the mutation of either *bem-1* or *ham-6* significantly reduced the activation of MAK-2-GFP-CAAX. These two factors might therefore play a role in MAK-2 phosphorylation in a NOX-independent manner. Taken together these data suggest that the NOX complexes function downstream or independent of the MAK-2 signaling cascade. In addition, BEM-1 and HAM-6 appear to have functions independent of their role in the NOX complexes and these functions are required for the full activation of MAK-2.

3.1.8 The cell wall integrity MAP kinase MAK-1 does not influence MAK-2 phosphorylation

Cross-talk regulation between MAP kinases has been widely reported in many different organisms, including *S. cerevisiae* (McClean et al., 2007), *A. thaliana* (Wurzinger et al., 2011), *Cryptococcus neoformans* or *C. albicans* (Román et al., 2007).

In *N. crassa* there are no reports of potential cross-talk in MAP kinase regulation. Only, in 2014 it was shown by Ci Fu *et al* that MAK-2 phosphorylation was not affected by mutation of the MAP3K *mik-1* gene, which is part of the MAK-1 phosphorylation cascade (Fu et al., 2014). By using the permanently membrane-tethered version of MAK-2, we decided to test whether phosphorylation was affected by the mutation of the *mak-1* gene. The strain MW488 (*mak-1::hph;his-3-*) generated by Martin Weichert (Weichert et al., 2016), was used as a recipient strain for the (*Ptef-1-mak-2-gfp-caax*) plasmid p25 (Illgen, 2017), generating the strain 775 (*mak-1::hph; his-3::Ptef-1-mak-2-gfp-caax*). The MAK-2 phosphorylation in 775 was tested by phospho Western blot analysis, together with the usual control strains: 665 (*Ptef-1-mak-2-gfp*), 267 (*Ptef-1-mak-2-gfp*-caax) and 361 (*Ptef-1-mak-2-gfp-saax*). Interestingly, no significant differences were observed in the MAK-2 phosphorylation levels in the strains 775 and 267 (Fig. 3.1.13A and B). Together, these results suggest that MAK-1 does not influence MAK-2 phosphorylation in our experimental setup. However, it might still play important roles in the reception or processing of MAK-2 activating signals. Unfortunately, it cannot be tested in our experimental conditions where MAK-2 is permanently activated even without the presence of the fusion signals.

Together, all the data of this chapter clearly indicate an intricate regulation of the MAP kinase MAK-2 during the cell fusion process. The dynamic localization of the protein, its phosphorylation state and its activity are essential for the successful completion of the cell fusion process. Our data also show a different signaling regulation after cells establish physical contact. While SO is affected by the presence the permanent phosphorylated MAK-2 at the plasma membrane during the cell communication phase, it is clearly accumulated when cells establish physical contact, independently of MAK-2. Similarly, the phosphorylation state of MAK-2 is not important after cells establish contact. These data support the hypothesis that the cells completely switch their signaling regulation after establishment of physical contact, when MAK-2 activity is absolutely essential. We also found that activation of MAK-2 is promoted by HAM-6 and BEM-1, but in an NADPH independent manner, suggesting additional functions that will be investigated in future experiments.

3.2 MAK-1 activity is essential during the cell-cell communication process

As described in the introduction, cell fusion is a highly coordinated cellular process, in which 5 different steps are distinguished: gain of fusion competence, cell-cell communication and directed growth, cell growth arrest after physical contact, cell wall remodeling and finally fusion pore formation and plasma membrane merger. In all of these different steps, MAPK signaling plays a crucial role. For example, the MAP kinases MAK-2 and MAK-1 are essential for germling and hyphal fusion and the analysis of the respective knock-out mutants showed that the mutants fail to gain fusion competence (Fu et al., 2011; Maerz et al., 2008; Pandey et al., 2004). During the cell-cell communication step, MAK-2 is alternatively recruited to the plasma membrane of the interacting cells, while MAK-1 remains mostly cytoplasmic and is only recruited, together with MAK-2, after the cells establish physical contact (Weichert et al., 2016). While these data indicate that MAK-1 is required for the onset of the fusion process and after cell-cell contact, it remains unclear if this MAP kinase also plays a role during the tropic interaction of the fusion partners. In order to answer this question, we turned to a chemical genetics approach, which allows inactivation of the kinase at any specific stage of the fusion process.

3.2.1 Generation of an analog-sensitive genome-integrated version of mak-1 encoded at the original gene locus

We decided to introduce the point mutation, which renders the encoded kinase analog sensitive, at the original gene locus. By site-directed mutagenesis, the gatekeeper amino acid of the MAK-1 ATP binding pocket was exchanged by a glycine residue (E104G) yielding a kinase sensitive to ATP-analogs such as 1-NM-PP1. This strategy allowed using of the usually employed *his-3* expression locus for the integration of additional gene constructs, such as expression cassettes for fluorescently labelled cell fusion factors. In the resulting strains the influence of MAK-1 inhibition on the dynamics of these factors can be studied. In order to construct the *mak-1*^{E104G} (analog-sensitive) knock-in cassette, a fragment containing a 5´ upstream region together with the *mak-1* open reading frame was PCR amplified using the primers 1304 and 1305 and using the previously generated

mak-1^{E104G}*-gfp* plasmid as a template (Weichert et al., 2016). By yeast recombinational cloning, the resulting fragment was fused to the hygromycin resistance cassette (amplified with primers 82 and 83) and a 1 kb fragment homologous to the 3' downstream region of *mak-1* (generated with primers 1306 and 1307). The construct was assembled by yeast recombinational cloning resulting in plasmid 738. By using this plasmid as a template, the full-length knock-in fragment was amplified by PCR and transformed into the *N. crassa* strain N1-06 (FGSC 9719).

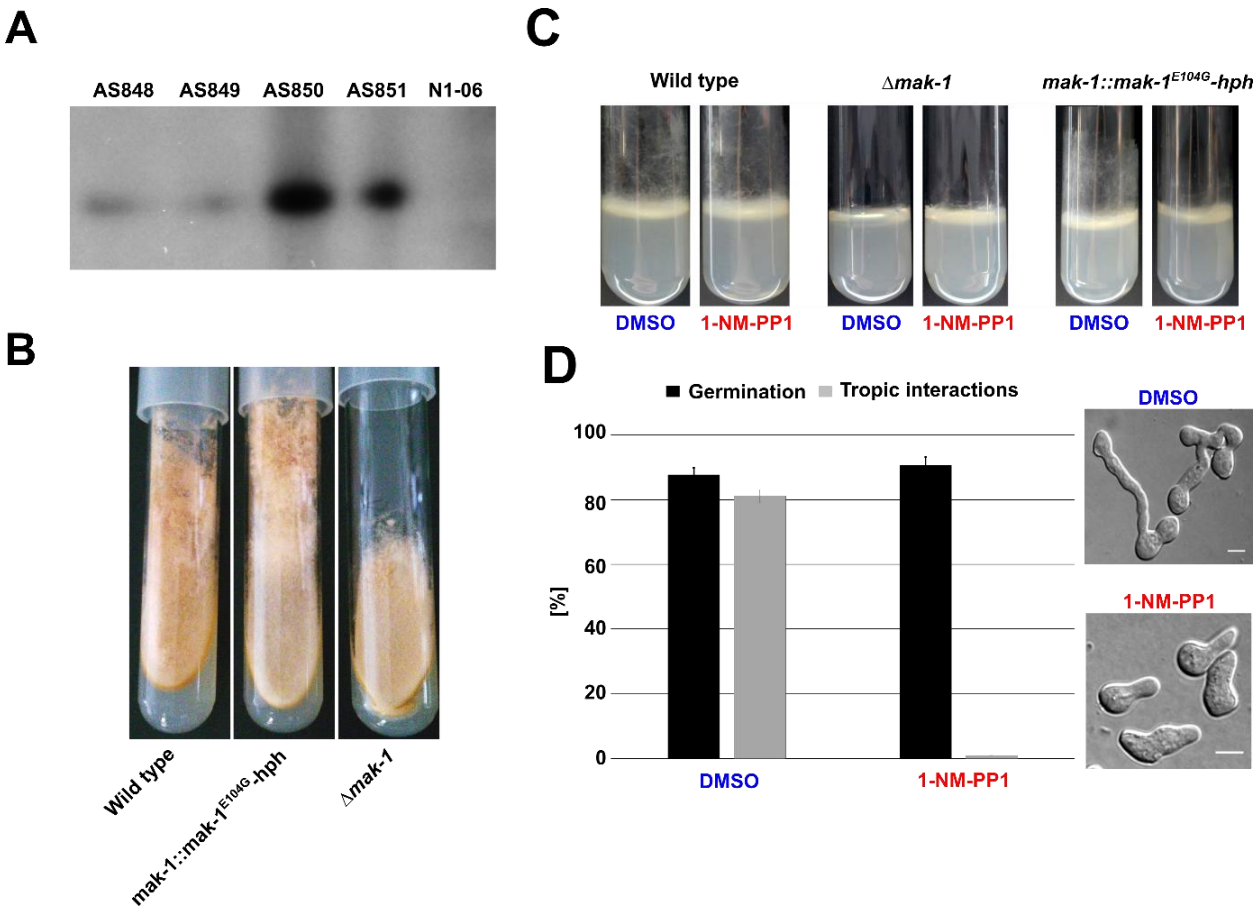

Figure 3.2.1. Creation of an analog-sensitive MAP kinase MAK-1 variant. (A) Southern blot of the homokaryon transformed *mak-1::mak-1*^{E104G}*-hph* strains into the N1-06 recipient strain. (B) Macroscopic phenotype of the following strains: Wild type (N1-01), 849 (*mak-1::mak-1-E104G-hph*) and Δ*mak-1* (NCU09842). (C) Macroscopic effect of the presence of either DMSO 0.2% (-) or 1-NM-PP1 40 µM (+). (D) Quantification of the microscopic effect of the presence of 1-NM-PP1 (40 µM) or DMSO (0.2%). Error bars represent the standard deviation observed in at least 100 germlings per condition in three independent experiments.

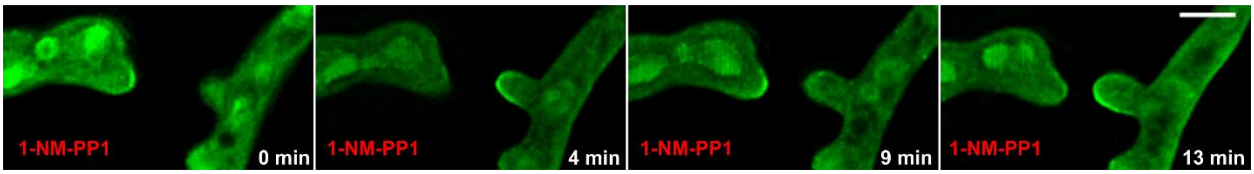

Figure 3.2.2. The presence of the bulky ATP-analog 1-NM-PP1 do not affect the normal functioning of the wild-type kinases. Image composition of MAK-2-GFP oscillation under the presence of 40 µM 1-NM-PP1 in the media. Strain genotype: *Ptef-1-mak-2-gfp*; wild-type background. Comparable observations were made multiple times (n=15). Scale bar: 5 µm.

This recipient strain possesses a mutation in the gene *mus52* (*mutagen sensitive 52*), whose gene product is required for DNA repair by nonhomologous end-joining .The mutation results in an increase in the frequency of homologous recombination up to almost 100% (Ninomiya et al., 2004). The resulting transformants were first tested by PCR by amplifying the *mak-1* locus and the fragment was sequenced to confirm the base pair exchange (E104G; CAG to GGC). The proper integration of the transforming DNA and the absence of additional heterologous integrations were successfully tested by Southern blot of homokaryotic isolates obtained from a sexual cross of the primary transformants with the wild-type strain (Fig. 3.2.1A). The resulting homokaryotic strain, 849 (similar observation was made in 848, 850 and 851), appeared macroscopically wild type-like, indicating that the mutated kinase is functional in absence of the inhibitor. (Fig. 3.2.1B). In contrast, addition of the inhibitor to the growth medium resulted in a Δ*mak-1*-like phenotype, whilst the wild-type control strain remained unaffected (Fig. 3.2.1C). Microscopically, the presence of the inhibitor drastically reduced the cell fusion rate, proving that the strain can be inhibited, allowing us to analyze the functions of MAK-1 at specific stages of the cell fusion process, such as the tropic growth phase (Fig. 3.2.1D).

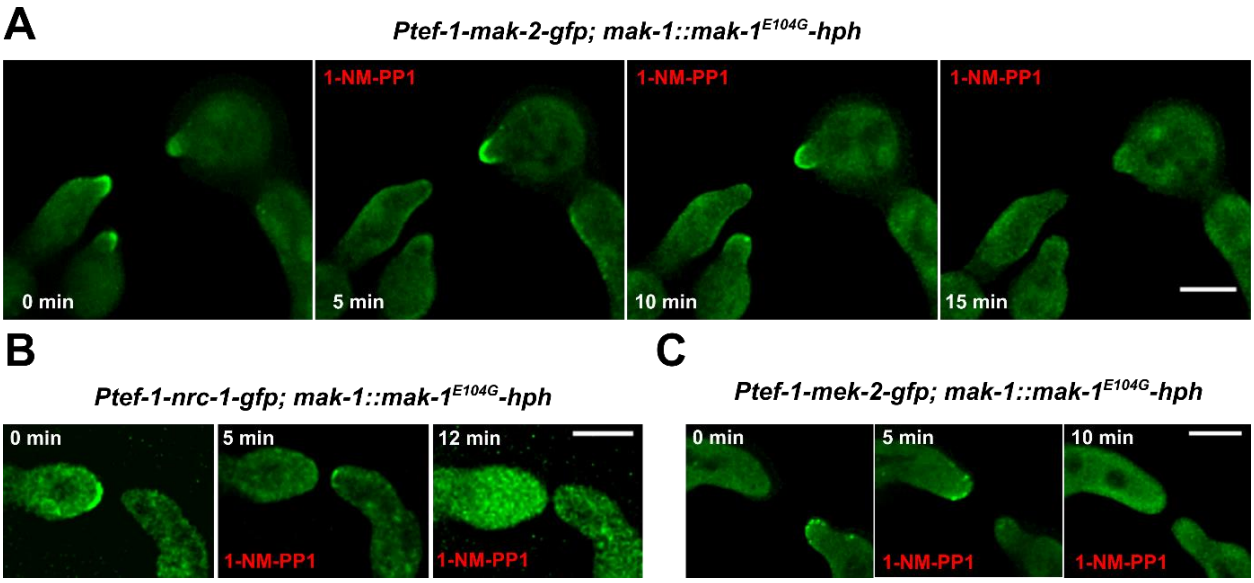

Figure 3.2.3. The inhibition of the MAP kinase MAK-1 disrupt the cell fusion process and the dynamic localization of the MAK-2 kinase complex. (A) Cell fusion between interacting germlings from strain 865 (*his-3::Ptef-1-mak-2-gfp;mak-1::mak-1^{E104G}-hph*). Inhibitor is added at 5 minutes. (B) Cell fusion between interacting germlings from strain 862 (*his-3::Ptef-1-nrc-1-gfp;mak-1::mak-1^{E104G}-hph*). Inhibitor is added at 5 minutes. (C) Cell fusion between interacting germlings from strain 860 (*his-3::Ptef-1-mek-2-gfp;mak-1::mak-1^{E104G}-hph*). Inhibitor is added at 5 minutes. All scale bars: 5 µm. Comparable observations were made multiple times (n=10).

3.2.2 *The addition of the ATP-analog 1-NM-PP1 does not disrupt the cell fusion process in wild-type cells*.

As a control for the following experiments, the effects of the bulky ATP-analog 1-NM-PP1 on wild-type cells was tested. As expected, no significant changes were observed in the macroscopic growth of the wild type when the inhibitor was present (Fig. 3.2.1C). Also, the cell fusion rate of the wild type was unaffected, and the normal oscillatory recruitment of MAK-2 was clearly observed in multiple interactions (Fig. 3.2.2). Together, these data indicate that the inhibitor is innocuous at the used concentration (40 µM) in wild-type cells.

3.2.3 The inhibition of MAK-1^{E104G} disrupts the membrane recruitment of the MAK-2 kinase complex

In order to test the consequences of MAK-1 inhibition during the cell-cell communication steps, multiple strains were created. The strain carrying the *mak-1::mak-1^{E104G}-hph* (849) genotype was independently crossed with the strains *his-3::Ptef-1-mak-2-gfp* (665), *his-3::Ptef-1-mek-2-gfp* (MT406) and *his-3::Ptef-1-nrc-1-gfp* (MT437), resulting in strains 865, 860 and 862, respectively. All strains showed comparable MAK-1 inhibition phenotypes at the presence of 1-NM-PP1. When cell-cell communication was observed with the microscope, the addition of DMSO did not affect the normal oscillatory recruitment of any of the three proteins of the MAK-2 kinase complex. However, addition of the ATP-analog 1-NM-PP1 completely disrupted the cell-cell communication process, and the usual dynamic localization of MAK-2/MEK-2/NRC-1 was interrupted. The kinases remained blocked at the membrane and no detachment was observed after almost 10 minutes.

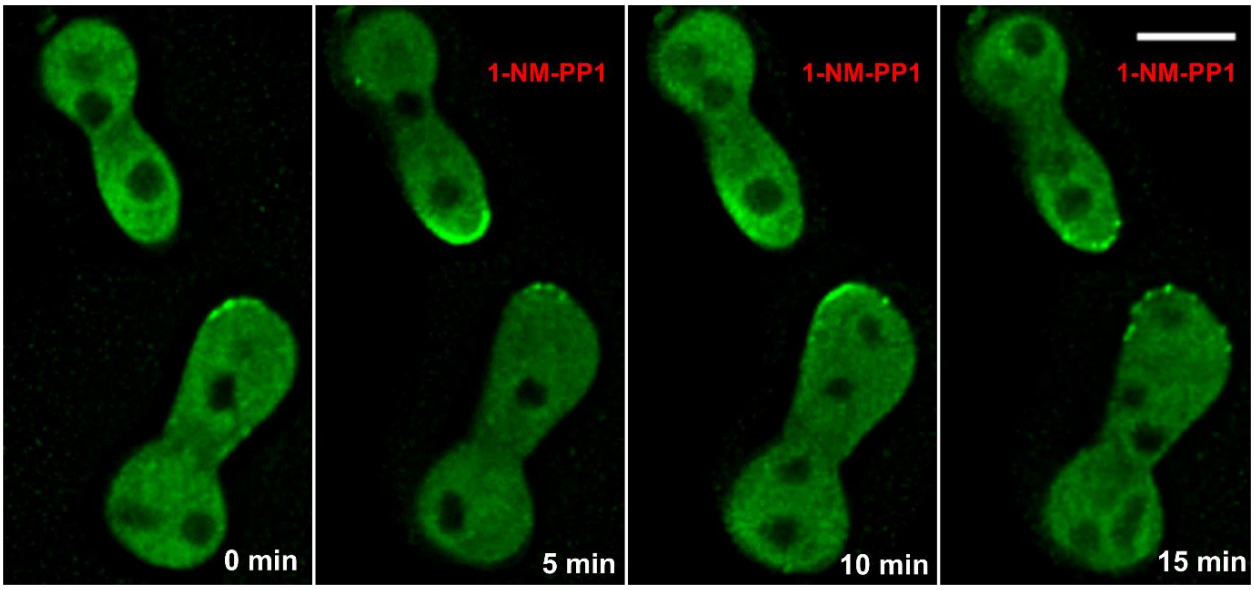

Figure 3.2.4. Inhibition of the MAP kinase MAK-1 disrupts the oscillatory localization of the SO protein. Cell communication process observe between two interacting cells from 874 strain (*his-3::Ptef-1-so-gfp;mak-1::mak-1^{E104G}-hph).* Inhibitor is added after 5 minutes. Scale bar: 5 µm. Comparable observations were made multiple times (n=10).

At the opposite cell, no kinase recruitment was observed and the signal remained mostly cytoplasmic (Fig. 3.2.3A, B and C, respectively).

3.2.4 The inhibition of MAK-1^{E104G} disrupts the membrane recruitment of the SO protein

In order to test the behavior of SO after MAK-1 inhibition, a cross of the strains 849 (*mak-1::mak-1^{E104G}-hph*) and 714 (*his-3::Ptef-1-so-gfp*) was performed, resulting in strain 874 (*mak-1::mak-1^{E104G}-hph*; *his-3::Ptef-1-so-gfp*). The strain showed the typical macroscopic MAK-1 inhibition phenotype in the presence of 1-NM-PP1.

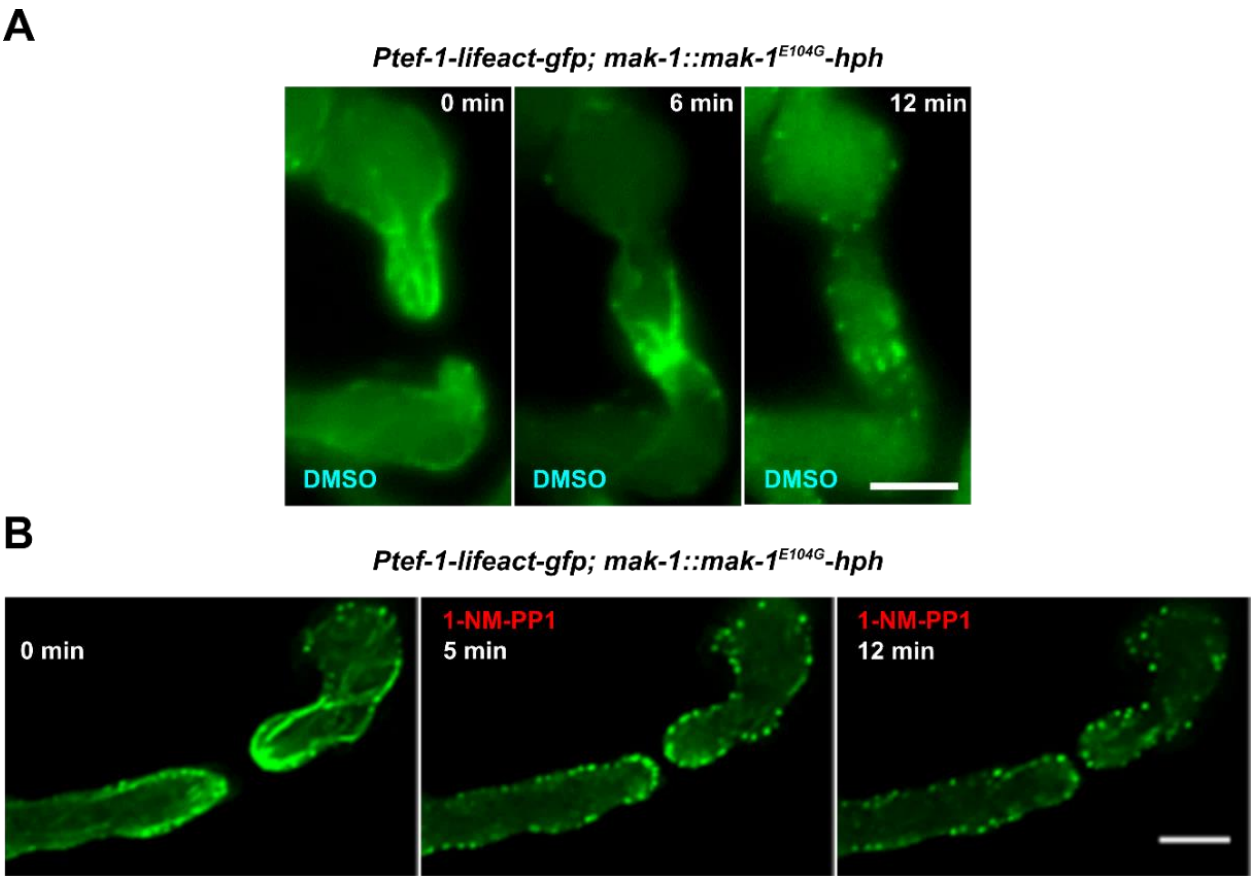

Figure 3.2.5. Inhibition of the MAP kinase MAK-1 disrupts the actin accumulation at the cell tips during cell-cell fusion. (A) Actin localization during cell-cell fusion. Actin is visualized with the actin-reporter Lifeact, linked to a -GFP. The DMSO was present in all images. Scale bar: 5 µm. (B) Effect of MAK-1^{E104} inhibition by 1-NM-PP1 on actin localization during cell-cell fusion. 1-NM-PP1 was added at time 5 minutes. Scale bar: 5 µm. Comparable observations were made at least 5 more times.

In the control assays, the addition of DMSO did not affect the usual dynamic localization of SO. Without the inhibitor, SO localized at the cell tip of one of the interacting cells and oscillated in a wild-type manner. The addition of 1-NM-PP1 still allowed one more switch.

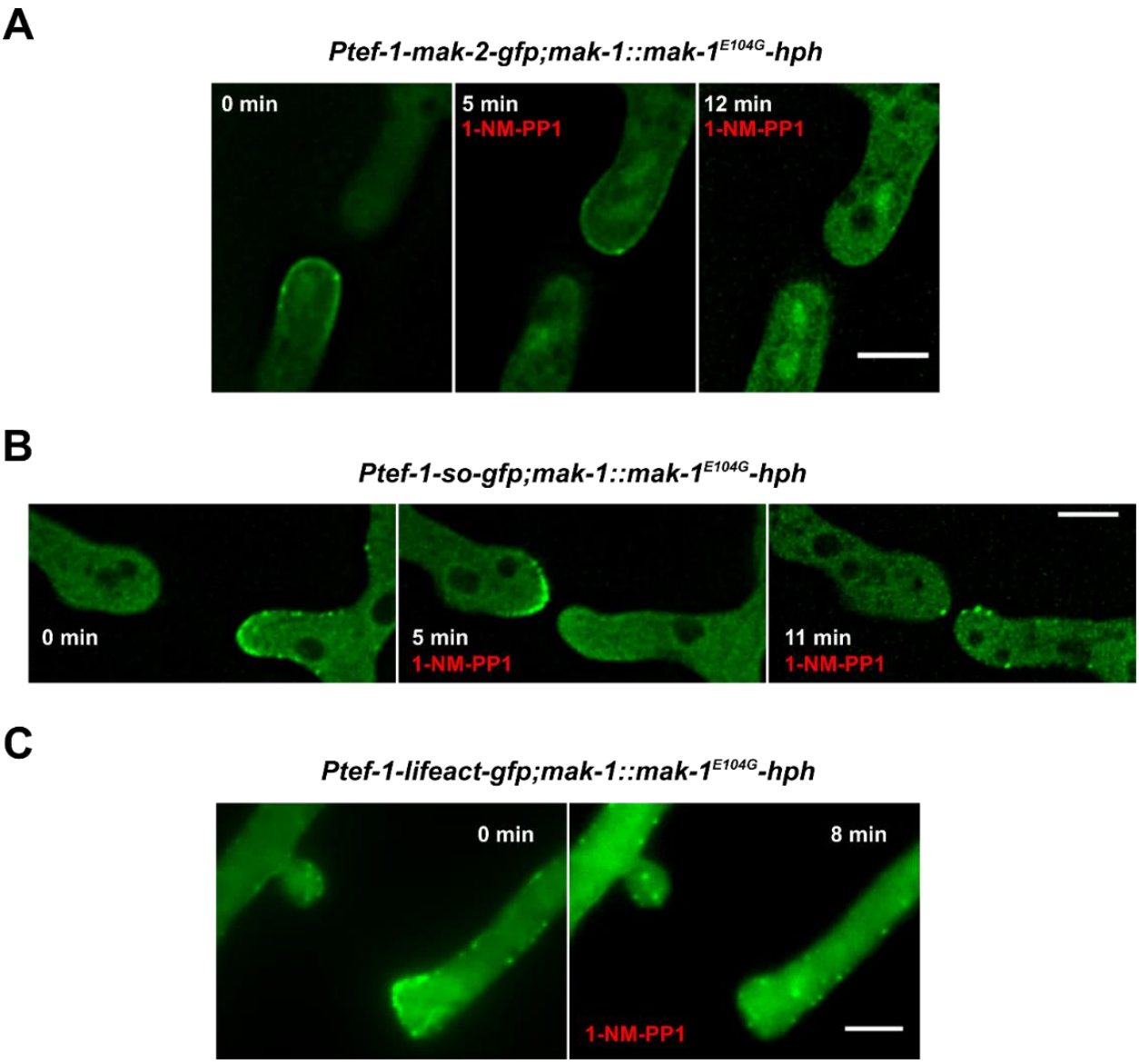

Figure 3.2.6. Effect of MAK-1 inhibition during hyphal fusion. (A) MAK-1^{E104G} inhibition disrupts the typical MAK-2 dynamic localization. The inhibitor is added at time 5 minutes. Scale bar: 5 µm. (B) MAK-1^{E104G} inhibition disrupts the SO dynamic localization. SO remains at single dots around the cell tip. Inhibitor is added after 5 minutes. Scale bar: 5 µm. (C) MAK-1^{E104G} inhibition disrupts the accumulation of actin cables and actin patches at the cell tips. The inhibitor is added after 5 minutes. Scale bar: 5 µm. Comparable observations were made multiple times (n≥3).

However, 10 minutes after addition of the inhibitor, SO was accumulated at the membrane in both cell tips at the same time, although the gfp signals were more widely distributed around the cell tips (Fig. 3.2.4). The growth of the cells was disrupted and SO remained attached to the membrane for more than one hour, suggesting that the protein is deficient to translocate to the cytoplasm once the cellular interaction has been disrupted. Taken together these data indicate that MAK-1 activity is essential for the tropic growth phase and for proper MAK-2 and SO dynamics.

3.2.5 The inhibition of the MAK-1^{E104G} disrupts the accumulation of actin at the tips of interacting cells

In fungi, proper actin organization is crucial for polarized hyphal extension. In *N. crassa*, Berepiki *et al* established a method for indirect actin visualization: the actin-reporter lifeact linked to GFP (Berepiki et al., 2010). Lifeact is a small peptide (17 amino-acid), which represents the N-terminus of the actin-binding protein Abp140 from *S. cerevisiae*. (Riedl et al., 2008). In non-interacting cells of *N. crassa* expressing this reporter, actin is mainly found at the tips of growing germ tubes, in the form of actin patches localized around the cell tips and actin cables. During cell fusion, actin is present at the tips of both interacting cells and no specific dynamics are observed during the process (Berepiki et al., 2010; Richthammer et al., 2012). Disruption of actin assembly results in failure of polarized, directed growth of the fusion tips, while microtubules are dispensable for this process (Roca et al., 2010). Additionally, in *S. pombe* mating fusion, actin also accumulates at the Shmoo of the interacting cells in a structure termed actin fusion aster complex. This accumulation has been shown to mediate the release of cell wall degrading enzymes involved in fusion pore formation (Dudin et al., 2015). All these data indicate that actin is essential for tropic growth and cell fusion, but its regulation remains mostly unknown. In order to test whether MAK-1 influences actin assembly and dynamics, we created a strain carrying the *mak-1::mak-1^{E104G}-hph* construct together with the *his-3::Ptef-1-lifeact-gfp* expression cassette, by crossing of strains 849 and 754, resulting in strain 869. This isolate behaved as wild type in the absence of 1-NM-PP1, and typical actin cables were present at the cell tips during the communication phase and during cell merger comparable to wild-type cells (Fig. 3.2.5A).

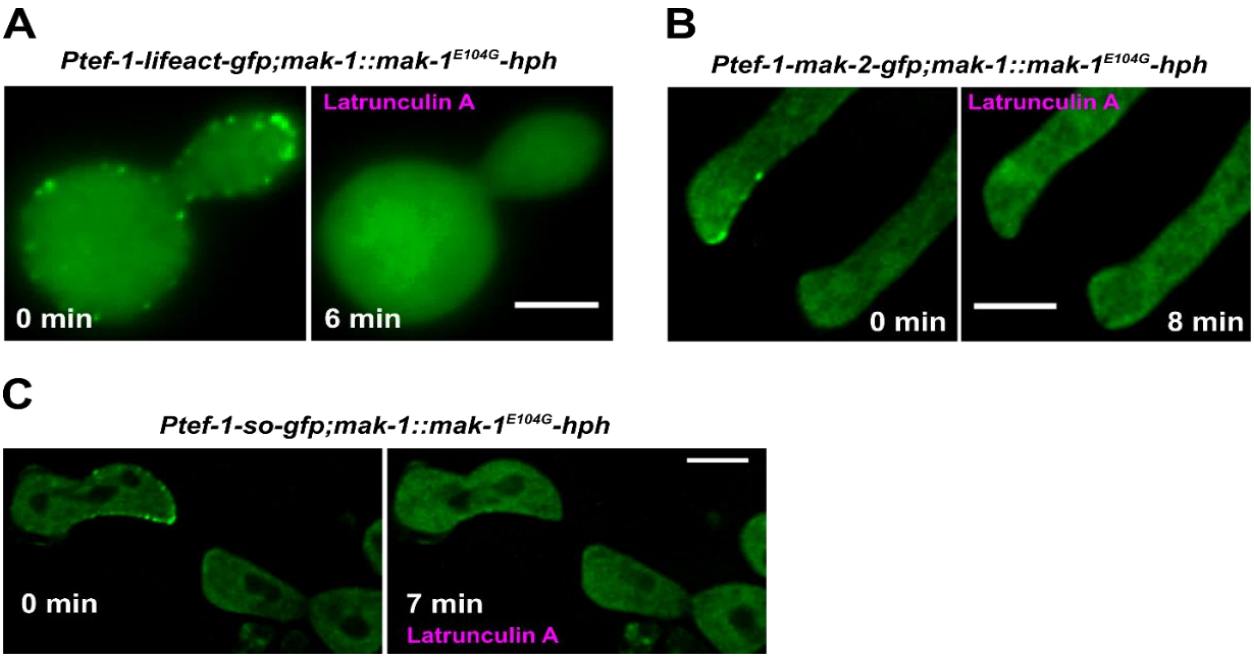

Figure 3.2.7. Effect of the actin polymerization inhibitor latrunculin A in the recruitment of the cell fusion proteins MAK-2 and SO. (A) After 6 minutes, the effect of the actin inhibitor latrunculin A is observed and actin accumulation is disrupted. (B) The use of the actin inhibitor results in a disruption in MAK-2 accumulation at the membrane of interacting cells. (C) The inhibition of actin polymerization results in the banishing of SO from the plasma membrane of the interacting cell tips. All scale bars: 5 µm. Comparable observations were made multiple times (n≥5).

When MAK-1^{E104G} was inhibited by addition of the chemical, actin accumulation was clearly affected. Interestingly, the accumulation of actin cables from the tips disappeared. In addition, actin patches were not focused anymore around the cell tips, but localized in a wider distribution around the cell membrane of the entire cell body (Fig. 3.2.5B). These data suggest for the first time that MAK-1 might be involved in the regulation of the actin cytoskeleton during the cell fusion process.

An alternative explanation might be that the actin misregulation represents an indirect effect of the disruption of the cell fusion process in the cells. These two hypotheses will be addressed in the following sections.

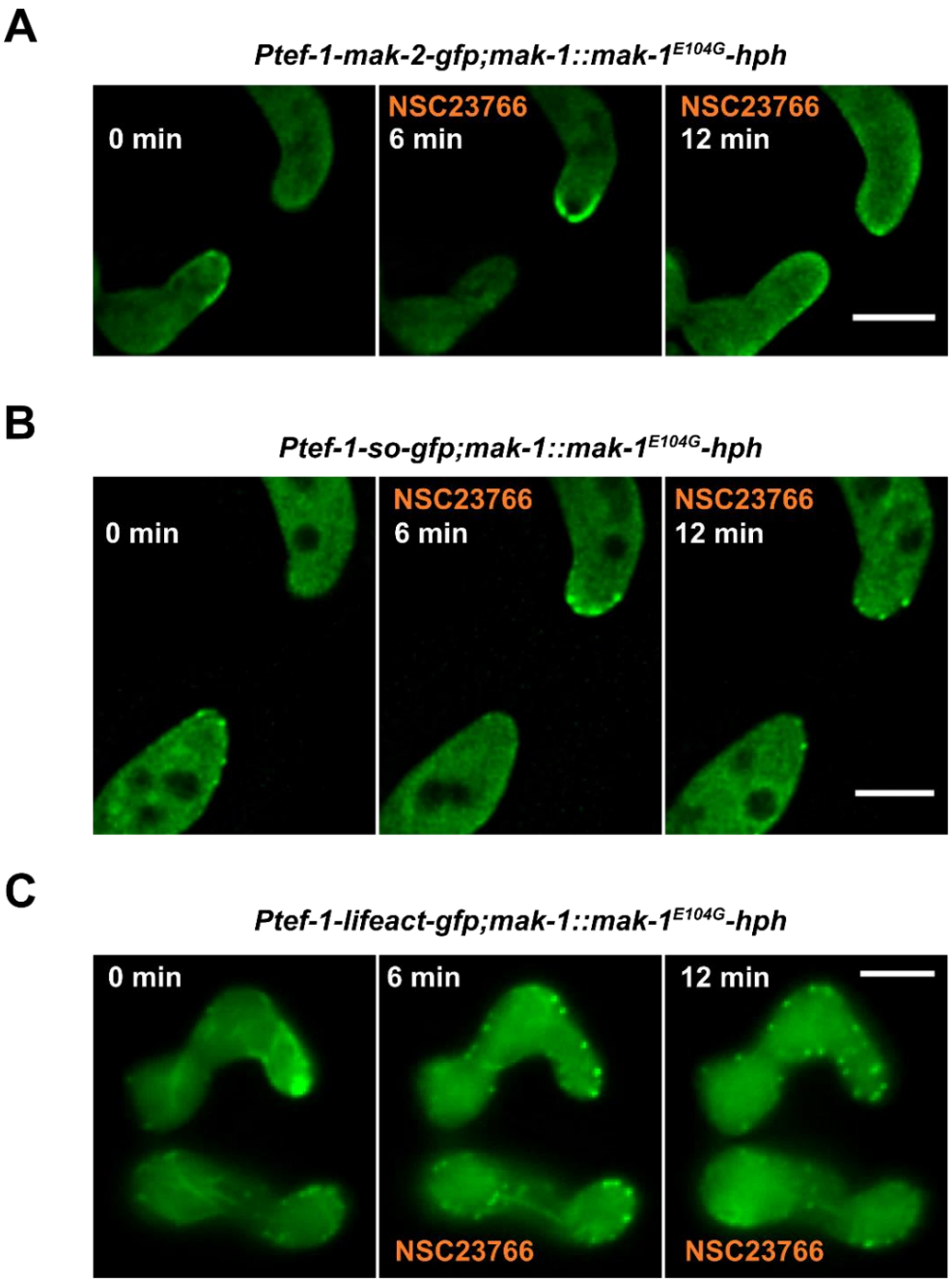

Figure 3.2.8. Effect of the RAC-1 inhibitor NSC23766 (200 µM) during cell fusion. (A) MAK-2-GFP dynamics are disrupted by the addition of 200 µM of the RAC-1 inhibitor NSC23766. The inhibitor is added after obtaining the first image. (B) SO dynamics are disrupted by the addition of the RAC-1 inhibitor NSC23766 (200 µM). The inhibitor is added after obtaining the first image. (C) Actin accumulation at the cell tips was disrupted and actin cables disappeared after addition of the RAC-1 inhibitor NSC23766 (200 µM). All scale bars: 5 µm. Comparable observations were made multiple times (n=5).

3.2.6 Inhibition of MAK-1^{E104G} produces the same effect observed in germlings during hyphal fusion

As previously described, cell fusion is observed at the early stage of colony establishment between germinated and ungerminated spores, but also later in development between hyphae in the inner part of the fungal colony in a process known as hyphal fusion.

We had shown that the characteristic MAK-2/SO dynamics also occur during hyphal fusion (Fig. 1.4B). In order to test whether MAK-1 also plays a role during hyphal fusion, we tested the consequences of MAK-1 inhibition by microscopic analysis of hyphal fusion events. When MAK-1^{E104G} was inhibited, MAK-2 and SO showed a disruption of their dynamics similar to the findings in germlings (Fig. 3.2.6A and B). MAK-2 completely vanished from the hyphal tip, while SO remained as single dots distributed widely around the plasma membrane of both interacting hyphae. Inhibition of MAK-1^{E104G} also disrupted actin accumulation at the hyphal tips as previously observed in germling fusion (Fig. 3.2.6C). These data indicate that the function played by MAK-1 during germling fusion is also conserved in hyphal fusion.

3.2.7 Accumulation of actin at the cell tips is essential for MAK-2/SO membrane recruitment

MAK-1^{E104G} inhibition disrupts the proper MAK-2 and SO membrane recruitment. At the same time, actin accumulation at the cell tips is also disturbed, and actin cables disappear while actin patches are more widely distributed around the cell membrane. Actin cables serve as tracks for the transport of multiple cargoes, including potential secretory vesicles, which might be involved in the cell fusion process (Berepiki et al., 2011; Dudin et al., 2015). Our data support two alternative hypotheses: either MAK-1 activity is directly involved in both MAK-2/SO recruitment and actin organization, or it is only involved in actin organization, but actin disruption results in a disturbed MAK-2/SO localization. A third option could be that MAK-2 or SO are involved in actin assembly, and its mislocalization after MAK-1 recruitment might lead to the actin disassociation.

In yeast, Fus3p recruitment is mainly mediated through actin cables organized at the Shmoo of the mating cells (Qi and Elion, 2007). In order to test whether actin is needed for proper MAK-2/SO recruitment, we employed the actin disrupting drug latrunculin A. This toxin originating from the Red Sea sponge *Latrunculia magnifica* binds to actin monomers, thereby preventing the formation of F-actin (Martine et al., 1987). In *N. crassa*, it has been used to demonstrate that actin is essential during the cell fusion process, but without testing of MAK-2/SO dynamics (Roca et al., 2010).

In a pretest we determined that a concentration of 10 µM resulted in the disassociation of F-actin in germinating spores within 6 minutes (Fig. 3.2.7A). When MAK-2 localization was tested, we observed that actin disruption resulted in the loss of MAK-2 dynamics after 8 minutes, and no further MAK-2 membrane recruitment was observed in the cells (Fig. 3.2.7B). In addition, the dynamic localization and membrane recruitment of SO were also affected by F-actin inhibition (Fig. 3.2.7C). In contrast to MAK-1^{E104G} inhibition, SO fully vanished from the plasma membrane, and no single dots were observed, suggesting different causes of SO membrane disassociation. These data suggest that actin is essential for membrane recruitment of MAK-2 and SO. Tu further understand the implications of MAK-1 in this process, we decided to investigate the roles of the upstream regulators of actin polymerization, the Rho-GTPases.

3.2.8 Inhibition of the Rho GTPase RAC-1 results in a MAK-1-like cell fusion defect

Rho GTPases are signaling G proteins conserved in all eukaryotic organisms that regulate intracellular actin dynamics. These proteins cycle between an active (GTP-bound) and an inactive (GDP-bound) conformation. Upon activation, the Rho GTPases translocate from the cytosol to the plasma membrane, where they interact with actin polymerization proteins, such as formins, that regulate the formation of actin cables (Michaelson et al., 2001, (Berepiki et al., 2011; Buchsbaum, 2007).

In previous experiments, we have observed that MAK-1^{E104G} inhibition resulted in disruption of actin cable polymerization, suggesting that MAK-1 activity is needed for proper assembly of actin cables at the interacting tips. To further elucidate the link between MAPK activity and actin dynamics we investigated the roles of one Rho-type

GTPase and how its dynamics are influenced by MAK-1 ^{E104G} inhibition. In *N. crassa* the Rho-type GTPase RAC-1 is essential for cell fusion, while the Rho-type GTPase CDC-42 plays a role in germination and normal polarized germ tube growth. Both proteins localize to the tips of growing cells (A. Lichius et al., 2014). To differentiate the functions of both Rho-type GTPases, the specific RAC-1 inhibitor NSC3766 was employed in an earlier study (Lichius et al. 2014). This molecule was identified by a structure-based virtual screening of molecules that can bind to a critical domain for GEF specification.

The drug only affects RAC-1 but not CDC42 and had already been used and proved functional in *N. crassa* (Gao et al., 2004; A. Lichius et al., 2014). In our experiments, we tested if the specific inhibition (with NSC3766) of RAC-1 would affect the dynamics of actin and the recruitment of MAK-2, SO and actin assembly. In interacting cell pairs expressing MAK-2-GFP (865), the protein was recruited to the membrane in a wild-type manner before addition of NSC3766. The addition of NSC23766 at a concentration of 200 µM resulted in defects in the recruitment of MAK-2 after 12 minutes. MAK-2 fully disappeared from the membranes of both cells and the interaction ended (Fig. 3.2.8A). When SO dynamics were tested (strain 874), the usual membrane accumulation at the cell tips was observed. Like the previous experiment, defects in the localization of SO were observed 12 minutes after the addition of the inhibitor. However, in contrast to MAK-2, SO remained widely distributed at the membranes of both cells although the interaction had ended (Fig. 3.2.8B). This mislocalization of SO was comparable to the one observed after MAK-1 inhibition.

Actin localization was also tested in the presence of the inhibitor in strain 869. Without NSC23766, actin strongly accumulated at the tips of the interacting cells. When the inhibitor was added, the number of actin cables declined and actin patches were distributed more widely around the plasma membrane. After 12 minutes, actin cables fully disappeared and directed cell growth halted (Fig. 3.2.8C). The disruption of MAK-2 dynamics caused by RAC-1 inhibition was already reported by Lichius and colleagues (A. Lichius et al., 2014).

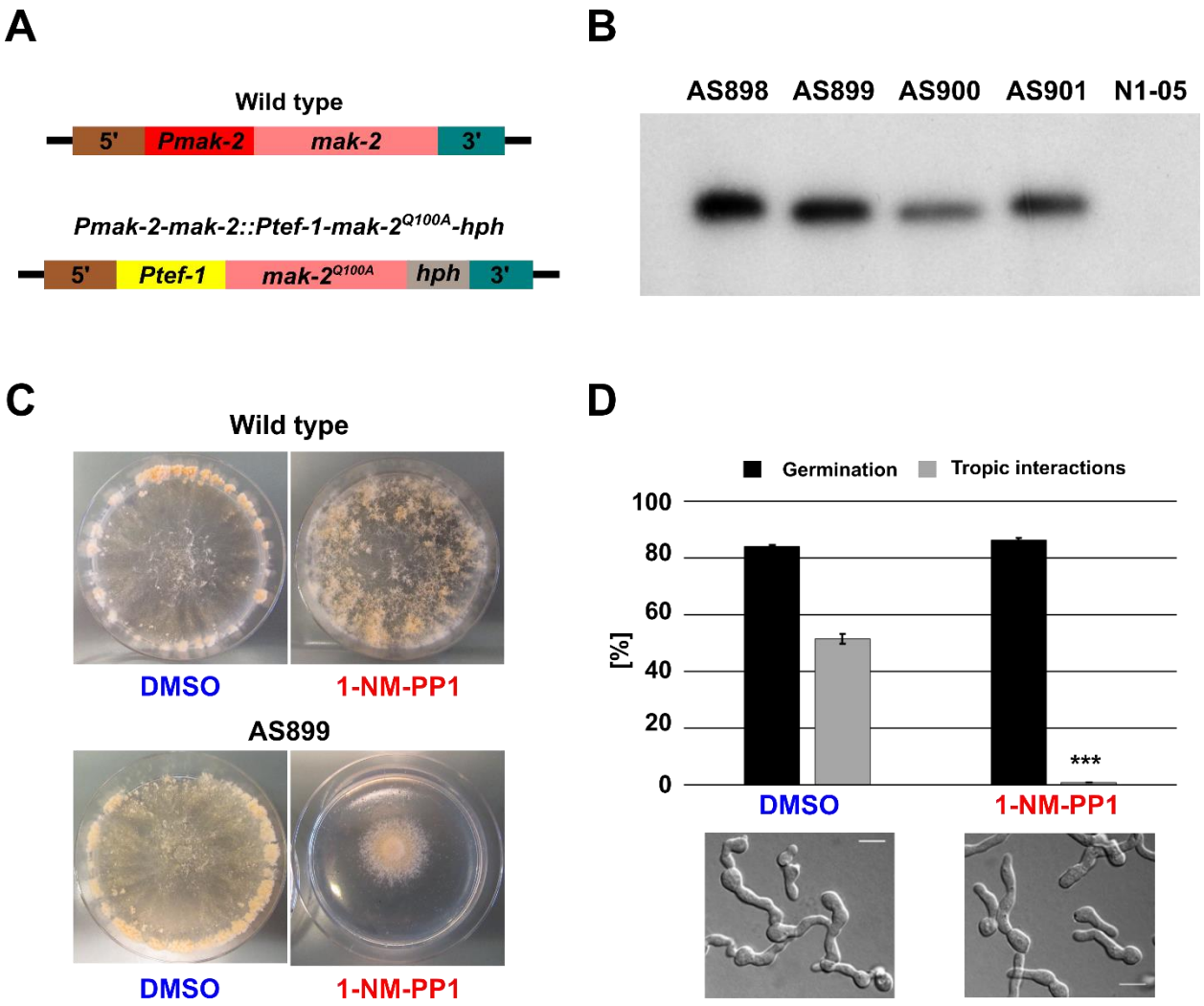

Figure 3.2.9. Creation of a *mak-2* analog-sensitive variant integrated at the original locus. (A) Representation of the differences between the wild type and the MAK-2^{Q100A} construct. By homologous recombination the *Pmak-2::mak-2* is replaced by the *Ptef-1-mak-2^{Q100A}-hph* fragment. (B) Southern blot of the homokaryon *Pmak-2::mak-2::Ptef-1-mak-2^{Q100A}-hph* strains. The bands observed represent the result of the developing of the membrane after incubation with the radioactive-labelled *Ptef-1-mak-2^{Q100A}-hph* PCR fragment. (C) Macroscopic phenotype of the tested strains wild type and MAK-2^{Q100A} with DMSO (0.2%) or 1-NM-PP1 (40 µM). (D) Quantification of tropic interactions and germination of the strain 899 with DMSO (0.2%) or 1-NM-PP1 (40 µM). The error bars represent the standard deviation observed in more than 100 germlings per condition in three independent experiments. Significant differences were observed between tropic interactions with 1-NM-PP1 and tropic interactions with DMSO ($p<0.01$).

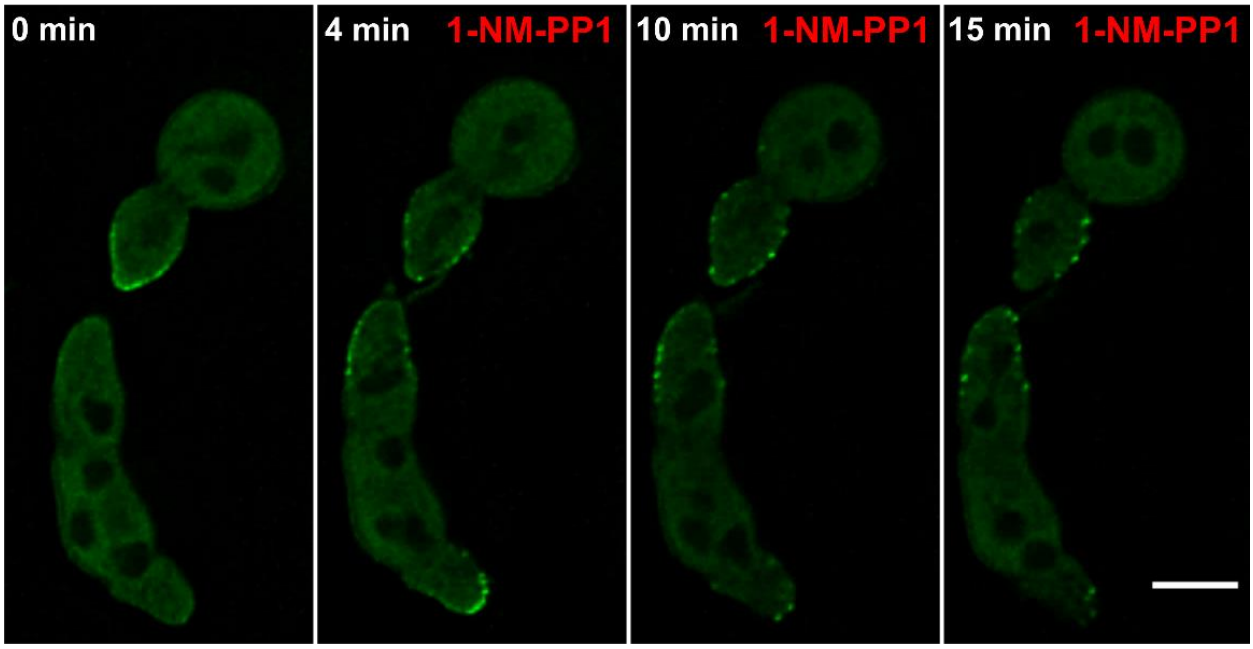

Figure 3.2.10. The inhibition of MAK-2 disrupts the dynamic localization of SO. Inhibition of MAK-2^{Q100A} while SO-GFP was observed under the fluorescence microscope in the strain *Pmak-2-mak-2*::*Ptef-1-mak-*2^{Q100A}*-hph*; *his-3::Ptef-1-so-gfp*, 912. The inhibitor 1-NM-PP1 was added after obtaining the first image (time 0 min). Scale bar: 5 µm. Comparable observations were made in 5 independent germling pairs.

In their study, the authors hypothesized that a signaling complex comprising the Rho-type GTPase RAC-1, together with BEM-1 and other factors might be needed for the plasma membrane association of the MAK-2 MAPK module (NCR-1/MEK-2/MAK-2), and that MAK-2 might be directly implicated in the regulation of F-actin cable assembly and polar growth of the cells during cell fusion. However, our data suggest that MAK-1 might be implicated in this process, while MAK-2 is not involved.

Taken together, these data suggest that MAK-1 serves as a main regulator of actin assembly and directed growth through the Rho-GTPase RAC-1 during the cell-cell interaction. However, as earlier mentioned, the observed disassembly of actin could also be just an indirect consequence of a growth arrest caused by the inhibition of MAK-1/RAC-1. In order to solve this conundrum, we decided to inhibit the cell fusion in a different way by inhibiting the second MAPK essential for the cell-cell interaction, MAK-2, in a chemical genetics approach.

3.2.9 Generation of an analog-sensitive genome-integrated version of MAK-2

Similar to the design of the *mak-1*^{E104G}*-hph* construct, a *mak-2*^{Q100A}*-hph* gene knock in cassette was created and integrated at the original gene locus of strain N1-06. However, this construct proved to be not functional and the respective transformants exhibited a Δ*mak-2*-like phenotype (data not shown). In previous studies, we found that the Δ*mak-2* phenotype of the knock-out mutant was only fully complemented when the analog-sensitive version was overexpressed by using strong promoters such as *Pccg-1* or *Ptef-1* (Fleissner et al., 2009; Serrano et al., 2018). We therefore decided to replace the promotor at the original gene locus by the P*tef-1* sequence. The fragments required for the construction of the gene knock in cassette were amplified by PCR. A 1 kb genomic region positioned 2 kb upstream of the *mak-2* promoter (considering it to be the 1 kb region upstream of the coding read frame) was amplified with primers 1489 and 1490. The *Ptef-1-mak-2*^{Q100A}*-gfp* plasmid created previously in this dissertation (Serrano et al., 2018) served as a template for the amplification of the *Ptef-1-mak-2*^{Q100A} PCR fragment with primers 1488 and 1487. The resistance cassette used was *Hyg*^{R}, which was amplified with primers 82 and 83. Finally, the 1 kb genomic region downstream of the *mak-2* Stop codon was amplified with primers 1489 and 1492. The four fragments were fused by yeast recombinational cloning (Fig. 3.2.9A).

The linear *Ptef-1-mak-2*^{Q100A}*-hph* knock-in cassette was transformed into N1-05 (Δ*mus-52* like N1-06, but different mating type) resulting in strain 882 (*Pmak-2-mak-2::Ptef-1-mak-2*^{Q100A}*-hph*). The primary transformants were tested by PCR of the *mak-2* locus and sequencing of the resulting fragment. In order to obtain a homokaryotic strain, a sexual cross was performed between wild type *mat a* (N1-02) and one of the primary transformants, 882 (*mat A*). Four of the resulting progenies were tested by Southern blot analysis for single integration of our construct. All four isolates showed a clear band corresponding to the *Ptef-1-mak-2*^{Q100A} radioactive-labelled fragment, while it was absent in the recipient strain (N1-05) (Fig. 3.2.9B). No additional bands were detected, which indicated that no heterologous integration events have happened.

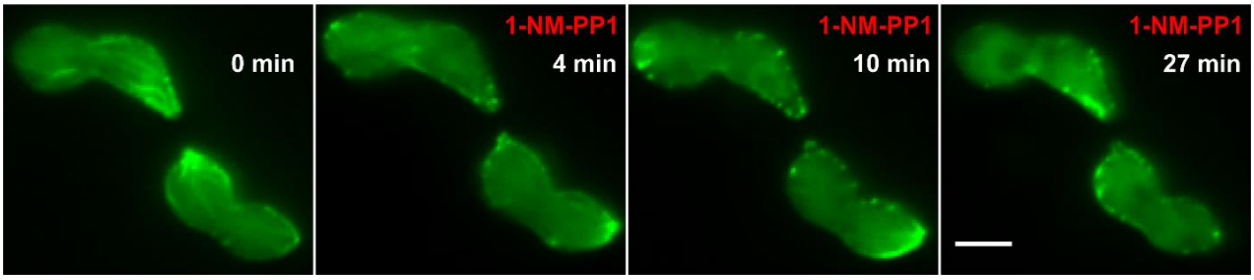

Figure 3.2.11. Effect of MAK-2 inhibition in actin localization. Inhibition of MAK-2^{Q100A} while actin (*lifeact-gfp*) was observed under the fluorescence microscope (strain 915, *Pmak-2-mak-2::Ptef-1-mak-2^{Q100A}-hph; his-3::Ptef-1-lifeact-gfp*). The inhibitor 1-NM-PP1 was added after obtaining the first image (time 0 min). Scale bar: 5 µm. Comparable observations were made in 5 independent germling pairs.

Macroscopically, strain 899 (*Pmak-2-mak-2::Ptef-1-mak-2^{Q100A}-hph*) growth as wild type. When the inhibitor 1-NM-PP1 was present in the growth medium, the strain showed clear defects in growth, comparable to the Δ*mak-2* phenotype, while the wild type was not affected by the inhibitor. (Fig. 3.2.9C). Similar observations were made for all the other strains. Microscopic analysis revealed, that 899 behaved like wild type when only the solvent DMSO was added to the medium and no defects on cell fusion were observed. In presence of 1-NM-PP1, however, the tropic interactions rate was significantly decreased. In both cases the germination rate was not affected (Fig. 3.2.9D). Together, these data indicate that strain 899 is well suited to study the specific consequences of MAK-2 inhibition.

3.2.10 Inhibition of MAK-2 disrupts the dynamic localization of SO

In order to test the influence of MAK-2 on the localization of SO, we set up a sexual cross between the strains 714 (*his-3::Ptef-1-so-gfp)* and the MAK-2^{Q100A} inhibitable strain 899 (*Pmak-2-mak-2::Ptef-1-mak-2^{Q100A}-hph*), resulting in strain 912 (*his-3::Ptef-1-so-gfp; Pmak-2-mak-2::Ptef-1-mak-2^{Q100A}-hph*). Under the microscope and with DMSO, the dynamic localization of SO was wild-type like and no significant differences to the reference strain were observed. When the inhibitor was added, the oscillation rapidly ceased (after around 4 minutes) and the localization of SO surprisingly changed to another area of the cell, but the protein remained associated to the plasma membrane.

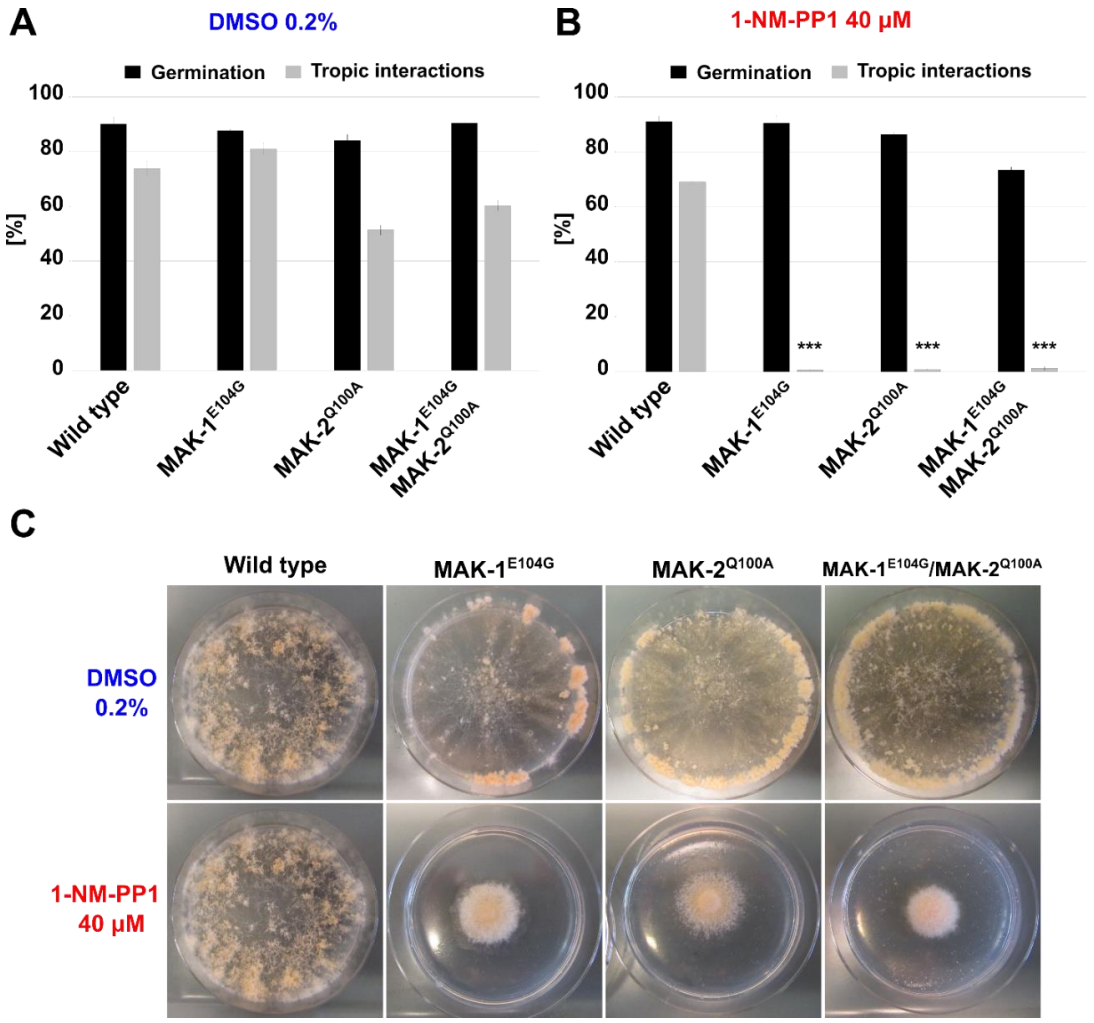

Figure 3.2.12. Creation of a double analog-sensitive kinases MAK-1E104G/MAK-2Q100A. (A) All strains behaved as wild type when the kinases were not inhibited (DMSO 0.2%). The error bars represent the standard deviation between 100 germlings observed per strain in three independent experiments. (B) When 1-NM-PP1 (40 µM) was in the media, the MAK-1^{E104G} and MAK-2^{Q100A} were inhibited and no tropic interactions were observed. No significant differences are observed in the germination rate. The error bars represent the standard deviation between 100 germlings observed per strain in three independent experiments. Significant differences are observed in the tropic interaction rate between the MAK-1^{E104G}, MAK-2^{Q100A} and MAK-1^{E104G}/MAK-2^{Q100A} strains compared to the wild type ($p=0.01$). (C) Macroscopically, all strains behaved as wild type when the inhibitor is absent in the media (DMSO 0.2%). When 1-NM-PP1 is present, MAK-1^{E104G}, MAK-2^{Q100A} and MAK-1^{E104G}/MAK-2^{Q100A} show clear defects in their growth and significant differences are observed with the wild type, which remain unaffected. Comparable observations were made multiple times (n=3 plates per strain and condition).

After 10 minutes of MAK-2 inhibition, the protein was no longer only accumulated at the tips but wider distributed around the cell membrane, suggesting that the inhibition of MAK-2 and MAK-1 share similar consequences (Fig. 3.2.10).

3.2.11 The inhibition of MAK-2 does not disrupt actin cable assembly but affects positioning of the actin aster

In order to test the influence of MAK-2 on the actin cytoskeleton, we set up a sexual cross between strains 754 (*his-3::Ptef-1-lifeact-gfp*) and 899 (*Pmak-2-mak-2::Ptef-1-mak-2^{Q100A}-hph*), generating strain 915. With DMSO, the strain fully behaved as wild type. Under the microscope, a clear accumulation of actin patches and actin cables was observed at the tips of the interacting cells.

When the inhibitor 1-NM-PP1 was added to the sample, the actin localization switched to a different spot within the cell away from the cell tip. After 10 minutes, actin was still accumulated at the new spots although the tropic interaction and directed growth were already terminated.

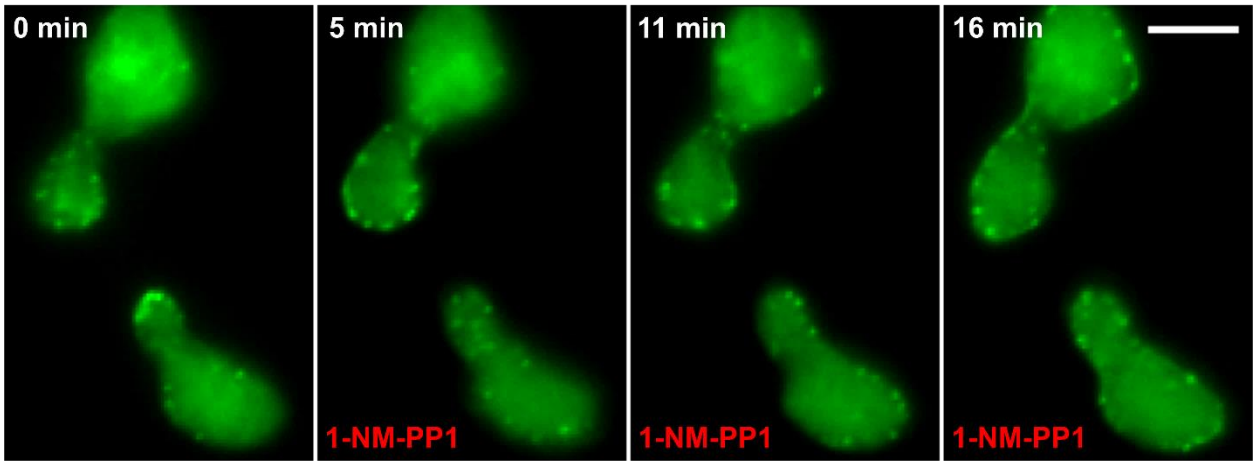

Figure 3.2.13. The inhibition of the double analog sensitive kinase MAK-1/MAK-2 results in a MAK-1-like actin disruption. Simultaneous inhibition of MAK-1^{E104G} and MAK-2^{Q100A} while actin (*lifeact-gfp*) was observed under the fluorescence microscope. The inhibitor 1-NM-PP1 was added after obtaining the first image (time 0 min). The strain used was 926 (*his-3::Ptef-1-lifeact-gfp; mak-1::mak-1^{E104G}-hph; Pmak-2-mak-2::Ptef-1-mak-2^{Q100A}*-hph). Scale bar: 5 µm.

Even after around 30 minutes, actin localization changed again to a different spot, but not to the original localization at the cell tips (Fig. 3.2.11). Interestingly, the presence of actin patches and the general actin cable assembly was not affected by MAK-2^{Q100A} inhibition, although the cell communication process was completely disrupted. This observation differs highly from the consequences of the MAK-1^{E104G} inhibition described above.

Together, these findings suggest that MAK-1 activity is needed for structurally maintaining an actin aster, while MAK-2 controls its proper position within the cell. In other words, MAK-1 is needed to establish and maintain the machinery for polarized growth, while MAK-2 is needed for integration of signal transduction and growth directionality. This experiment, therefore, excludes the hypothesized indirect effects of cell fusion inhibition in the localization of the fusion factors and support the hypothesis in which MAK-1 is directly involved in the control of the actin polymerization and its organization at the cell tips during cell fusion.

3.2.12 Creation of a strain carrying both inhibitable MAPK variants (MAK-1^{E104G} and MAK-2^{Q100A})

Inhibition of MAK-1 resulted in actin cable disassembly and subsequent termination of the cell fusion process by disrupting the MAK-2/SO actin-mediated membrane recruitment. Inhibition of MAK-2 resulted in disruption of the cell communication process, whilst actin filament remained intact but their cellular positioning became unstable. In order to understand whether MAK-2 and MAK-1 functions are interconnected, we created a strain carrying both analog sensitive variants (*mak-1^{E104G}* and *mak-2^{Q100A}*), whose expression constructs were integrated in the original *mak-1* and *mak-2* genes loci, respectively. A sexual cross between strains 869 (*his-3::Ptef-1-lifeact-gfp;mak-1::mak-1^{E104G}-hph mat A*) and 898 (*Pmak-2-mak-2::Ptef-1-mak-2^{Q100A}-hph mat a*) was set up, resulting in the progeny strain 926 (*his-3::Ptef-1-lifeact-gfp;mak-1::mak-1^{E104G}-hph; Pmak-2-mak-2::Ptef-1-mak-2^{Q100A}-hph mat A*). As shown before for the MAK-1^{E104G} and MAK-2^{Q100A} single mutants, the strain behaved like wild type in absence of the inhibitor. No significant differences were observed in the germination or interaction rate and no additive effect was observed compared to the single MAP kinase MAK-1 or MAK-2 inhibition (Fig.

3.2.12A). When the inhibitor was tested, we observed a significant reduction in the tropic interaction rate of MAK-1^{E104G}, MAK-2^{Q100A} and MAK-1^{E104G}/MAK-2^{Q100A}, while wild type remained unaffected by the presence of the inhibitor (Fig. 3.2.12B). To observe the macroscopic phenotype, petri dishes were filled with MM plus 0.2% of DMSO or 40 µM of the inhibitor 1-NM-PP1. With DMSO, all strains behaved like wild type and no significant differences were observed. With 1-NM-PP1, the inhibitable MAP kinase strains showed clear growth defects compared to the wild type, which remained unaffected (Fig. 3.2.12C). Together, these findings suggest that the kinase variants MAK-1^{E104G}/MAK-2^{Q100A} can be inhibited in the double mutant to study the function of both kinases during the cell fusion process.

3.2.13 Simultaneous inhibition of MAK-1^{E104G} and MAK-2^{Q100A} results in a MAK-1^{E104G}-like phenotype

In addition to the two inhibitable kinases, the strain 926 express Lifeact-GFP, thereby allowing the analysis of actin dynamics after the simultaneous inhibition of MAK-1 and MAK-2. Like the previous experiments, spores were incubated in MM plates and observed under the microscope after 2 hours. Afterwards, cell fusion pairs were photographed and solvent (control) or inhibitor was added. Pictures were later obtained every 3 minutes. In all fusing cells, actin was accumulated at the cell tips of both interacting cells before addition of any chemical. When only the solvent (0.2% DMSO) was added, actin was present at the growing cell tips in a wild-type-like manner and cell fusion was successfully completed. When the inhibitor was added and after approximately 5 minutes of incubation, actin cables were no longer detectable and actin patches were distributed around the cell tips.

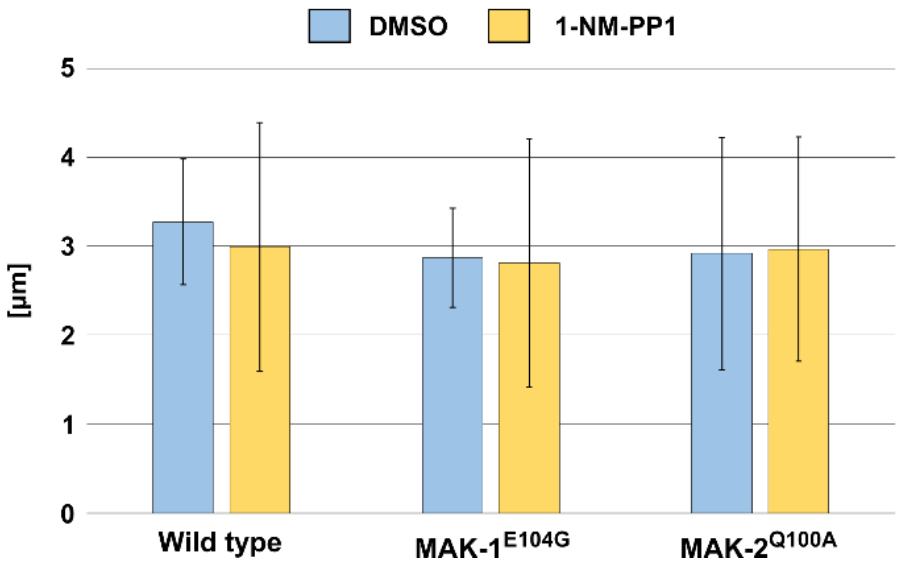

Figure 3.2.14. Inhibition of either MAK-1 or MAK-2 do not disrupt vegetative growth. The growth distance of germlings from the tested strains was calculated before and after addition of either DMSO (0.2 %) or 1-NM-PP1 (40 µM). The error bars represent the variability of the growth distance from at least 10 non-interacting cells. Although cells were previously incubated for 2 hours, its germination and growth are not synchronized between all the spore population.

After 10 minutes, actin patches were widely distributed and finally, after around 15 minutes, actin patches were observed everywhere around the cell membrane (Fig. 3.2.13), and cell growth was disrupted. These observations are comparable to the effect seen after the single inhibition of MAK-1^{E104G}, where actin cables were also disassembled and actin patches no longer accumulated around the cell tips. These results indicate that the inhibition of MAK-1 have a dominant effect over MAK-2, which clearly support our hypothesized model. While MAK-1 is under controlled of actin formation and maintenance, MAK-2 only controls the directionality of the growing cell, by redirecting the actin aster subcellular localization.

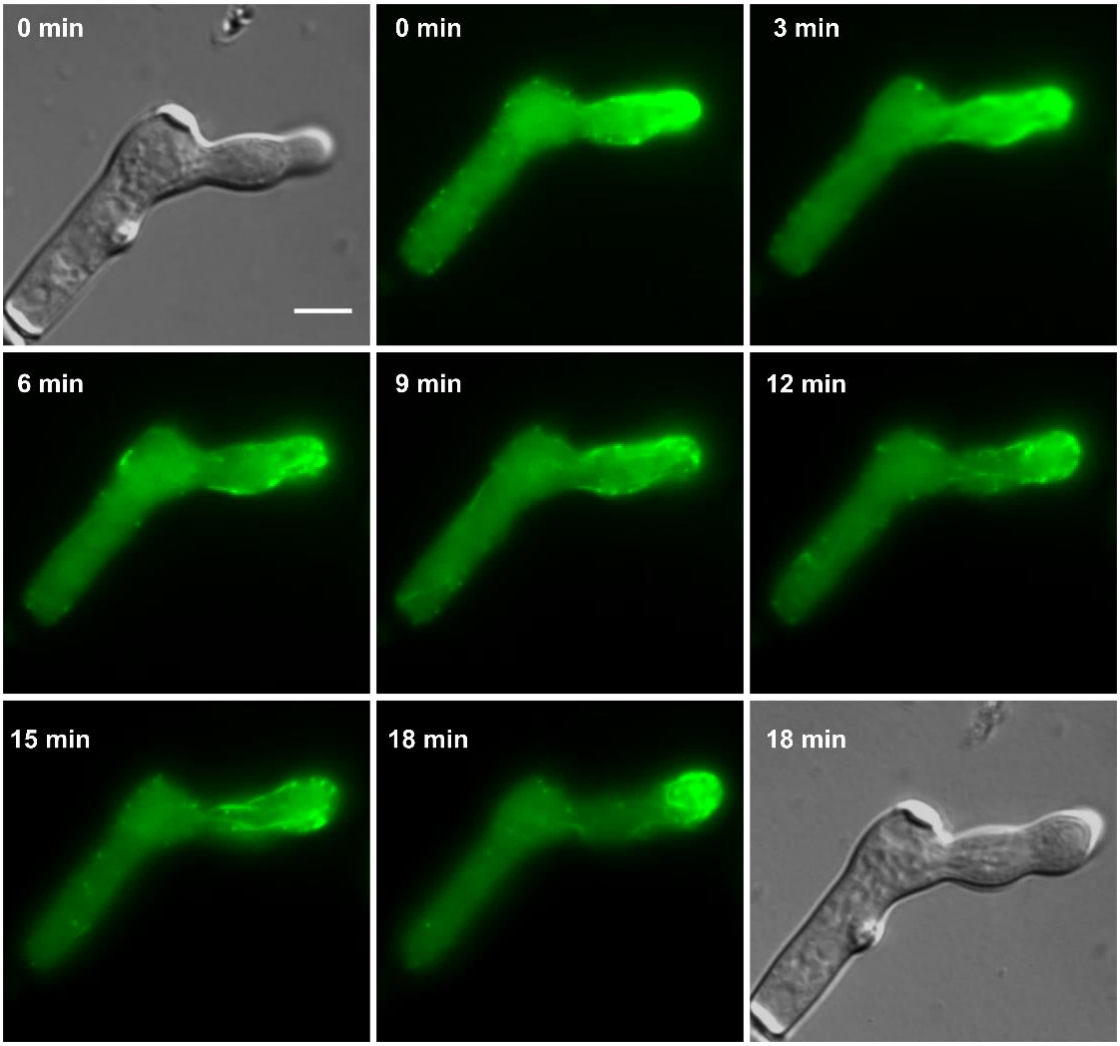

Figure 3.2.15. Actin organization during vegetative growth of Δ*mak-1*. Vegetative growth of an isolated and non-interacting cell and visualization of actin organization in the cell tip. Strain 891 (*hph::mak-1; his-3::Ptef-1-lifeact-gfp*. Scale bar: 5 µm.

3.2.14 MAK-1^{E104G} inhibition does not disrupt general polar growth

As shown above, MAK-1 is essential for polymerization of the actin cables in the interacting cells. Since actin is an essential part of the general polarity machinery, this observation raised the question whether MAK-1 functions are specific for directed growth or if they are also involved in general polar growth. Earlier studies already indicated that the two kinds of polar growth (directed polar growth and general polar growth) are differently regulated.

For example, while RAC-1 controls the directed growth during cell fusion, CDC-42 controls general polar growth during spore germination and hyphal growth (A. Lichius et al., 2014). In order to test whether MAK-1 activity is also needed for general polar growth, we decided to observe the effect of the inhibitor 1-NM-PP1 in non-interacting cells. The strains tested were MAK-1^{E104G} (849) and the wild type (N1-01) as a control. To ensure that only non-interacting cells were tested, only germlings with a distance of more than 30 µm to the nearest cell were analyzed. In order to determine the growth rate, the distance between the cell tip and the opposite site of the cell were measured before and 30 minutes after the addition of the inhibitor or DMSO. As a result, no significant differences were observed between the DMSO and the inhibitor treated cells of the test and the control strain (Fig. 3.2.14).

These data indicate that MAK-1 activity is dispensable for the general establishment and maintenance of cell polarity. This also suggests that MAK-1 functions might be related to RAC-1 while it seems that no relationship to CDC-42 exists.

3.2.15 Actin organization is not affected in the mak-1 knock-out strain

Our data indicate that MAK-1 is only necessary for polar growth during cell fusion but dispensable for general polar growth. In order to confirm this finding from the chemical genetics approach, we also studied the actin organization in the *mak-1* knock-out mutant. The knock-out strain was obtained from the *N. crassa* gene knock-out collection (NCU09482). As previously reported, the mutant showed a cell fusion-deficient phenotype (Fu et al., 2011). In order to obtain an actin-labelled Δ*mak-1* strain, a sexual cross was set up between the strains 754 (*his-3::Ptef-1-lifeact-gfp*) and Δ*mak-1*, resulting in strain 891 (*mak-1::hph;his-3::Ptef-1-lifeact-gfp*). Spores of this isolate were incubated in MM for 2 hours and actin organization was studied by fluorescence microscopy.

In the wild-type cells, actin is organized at the growing cell tips and actin cables are expanding from the growing tip (Berepiki et al., 2010). In the Δ*mak-1* mutant cells, germ tube elongation and actin assembly at the growing cell tips was comparable to wild type (Fig. 3.2.15). These data further confirm that MAK-1 is not involved in actin assembly during vegetative growth and has specific functions during cell fusion.

3.2.16 MAK-1 inhibition disrupts the membrane recruitment of RAC-1

All previous experiments suggest a potential connection between MAK-1 activity and RAC-1 activity. First of all, MAK-1 activity is necessary for the maintenance of actin accumulation at the cell tips of interacting cell, but dispensable for general vegetative growth. Similarly, RAC-1 activity is essential for maintaining the polarized growth of interacting cells, but dispensable for general vegetative growth, where the Rho-type GTPase CDC-42 plays the crucial role (A. Lichius et al., 2014). In addition, a comparable mislocalization of actin patches and disassembly of actin cables is observed when either MAK-1 or RAC-1 are inhibited, suggesting that these factors work together in a common pathway. In contrast, MAK-2 inhibition does not disrupt actin assembly, while the cell communication process also ceases. Actin cables and actin patches remain in a wild-type-like manner, but the localization of the actin aster within the cell becomes unstable.

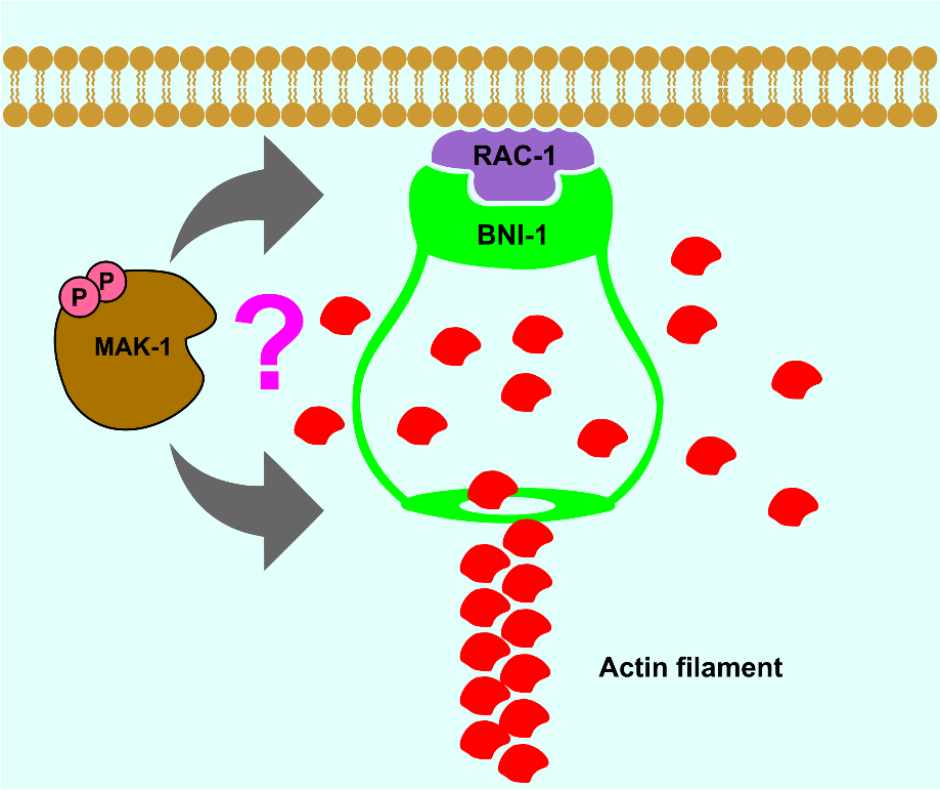

Figure 3.2.16. Hypothetical model of MAK-1 activity regulation during the actin cable assembly. Activated MAK-1 might regulates, direct or indirectly, the assembly of the actin cable. There are two potential targets: the formin BNI-1 or the Rho-type GTPase RAC-1.

Together, these data support two potential hypotheses: MAK-1 and RAC-1 function in the same pathway (either upstream/downstream), which controls actin polymerization, or RAC-1 and MAK-1 regulate, independently, a common target that is essential for actin assembly (e.g. BNI-1) (Fig. 3.2.16). To test these hypotheses, we decided to analyze active RAC-1 dynamics after MAK-1 inhibition through visualization by the Cdc42-Rac-interacting-binding (CRIB) reporters (see below).

If our first potential hypothesis is correct, the outcome of the experiment will show that MAK-1 inhibition results in inactivation of RAC-1 and therefore membrane detachment of the reporter. This will also indicate that MAK-1 might be an upstream regulator of RAC-1.

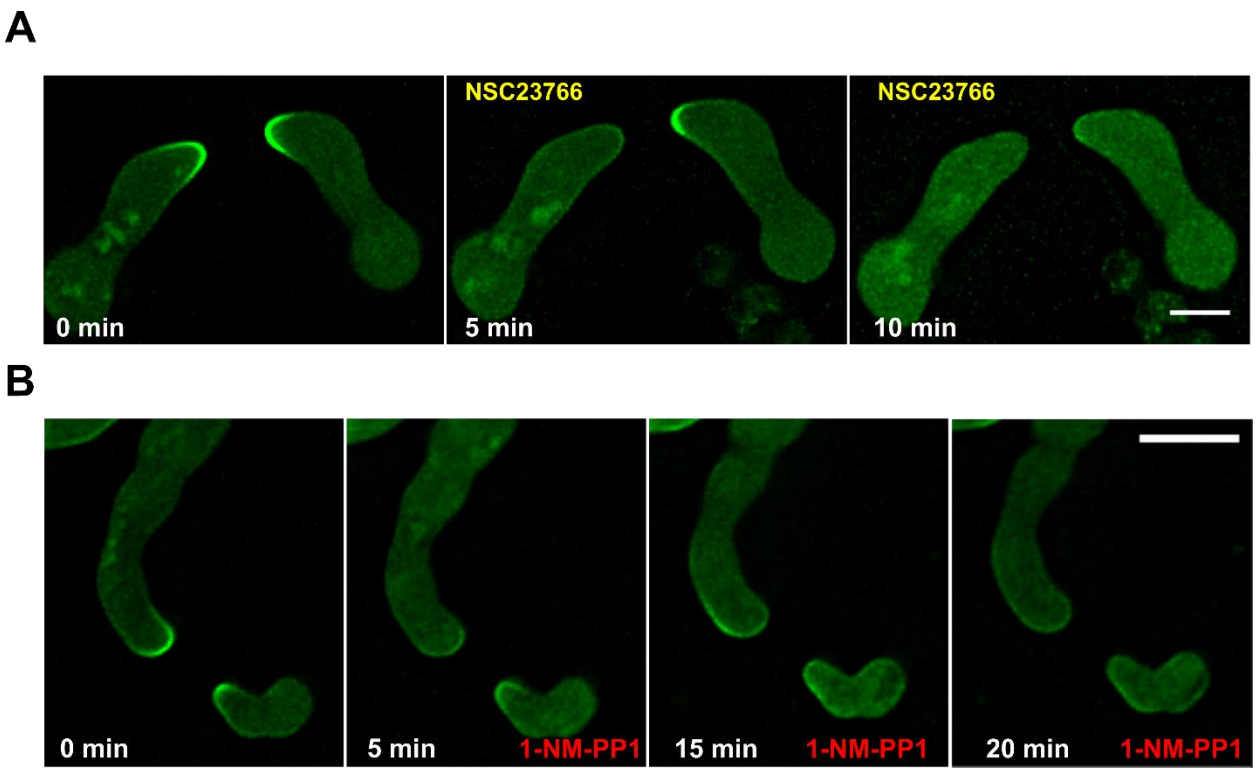

Figure 3.2.17. Effects of RAC-1 inhibitor and MAK-1 activity inhibition in the localization of the CRIB reporter. (A) Inhibition of RAC-1 with 200 µM of NSC23766 provoke the release of the activated Rho GTPase from the plasma membrane as previously reported. (B) Inhibition of MAK-1 provoke a similar effect than inhibition of RAC-1 in interacting cells. The CRIB reporter disappears in the tips of the interacting cells. All scale bars: 5 µm. Similar observations were made multiple times (n=3).

If the second hypothesis is correct, we should observe that MAK-1 inhibition does not have any effect on RAC-1 activation, and therefore the reporter should remain activated and attached at the plasma membrane. It would mean that MAK-1 and RAC-1 control independently the same factor, that is involved in actin polymerization during cell fusion.

The use of CRIB reporters in *N. crassa* was established by Lichius and colleagues (A. Lichius et al., 2014), who studied the different functions of the Rho-type GTPases RAC-1 and CDC42. To observe the localization of active GTP-bound GTPases, they identified the p21-binding domain of the PAKs (STE-20 and CLA-4) of *N. crassa* and cloned it together with membrane-interaction domains (PH or BR of CLA-4 and STE-20) and fused it to a GFP. In summary, they created a GFP-labelled reporter that binds as a GEF protein to activated Rho-GTPases without disrupting their function, thereby allowing to localize both activated RAC-1 and CDC-42 at the same time (A. Lichius et al., 2014).

The use of the RAC-1 inhibitor allowed them to distinguish the functions of both proteins. The CLA-4 CRIB reporter strain (927) was obtained from the FGSC. This strain was crossed with the MAK-1^{E104G} strain (849), resulting in strain 943 (*mak-1::mak-1^{E104}G-hph; Pal1-crib^{cla-4}-bar*). As a control we first tested the already reported effects of RAC-1 inhibition on the CRIB reporter. As previously shown by Lichius and colleagues, the addition of the RAC-1-specific inhibitor NSC23766 (200 µM) to interacting cells resulted in vanishing of the reporter from the apical tip and cell growth arrest (Fig. 3.2.17A). The complete disappearance of the reporter from the tips of the interacting cells indicates that only RAC-1 and not CDC-42 are present at the growth cone of interacting and directly growing cells, since CDC-42 is not affected by the RAC-1 inhibitor.

When in the next step, MAK-1 was inhibited, an effect similar to the consequences of RAC-1 inhibition was observed. In cells tropically interacting, the CRIB reporter disappeared from the plasma membrane after addition of the inhibitor and cell growth was arrested (Fig. 3.2.17B). Interestingly, both RAC-1 and MAK-1 inhibition showed a similar effect on the CRIB reporters, suggesting that the inhibition of MAK-1 specifically affect RAC-1 activity, and therefore disrupting the actin assembly, membrane recruitment of MAK-2 and SO and the general fusion process.

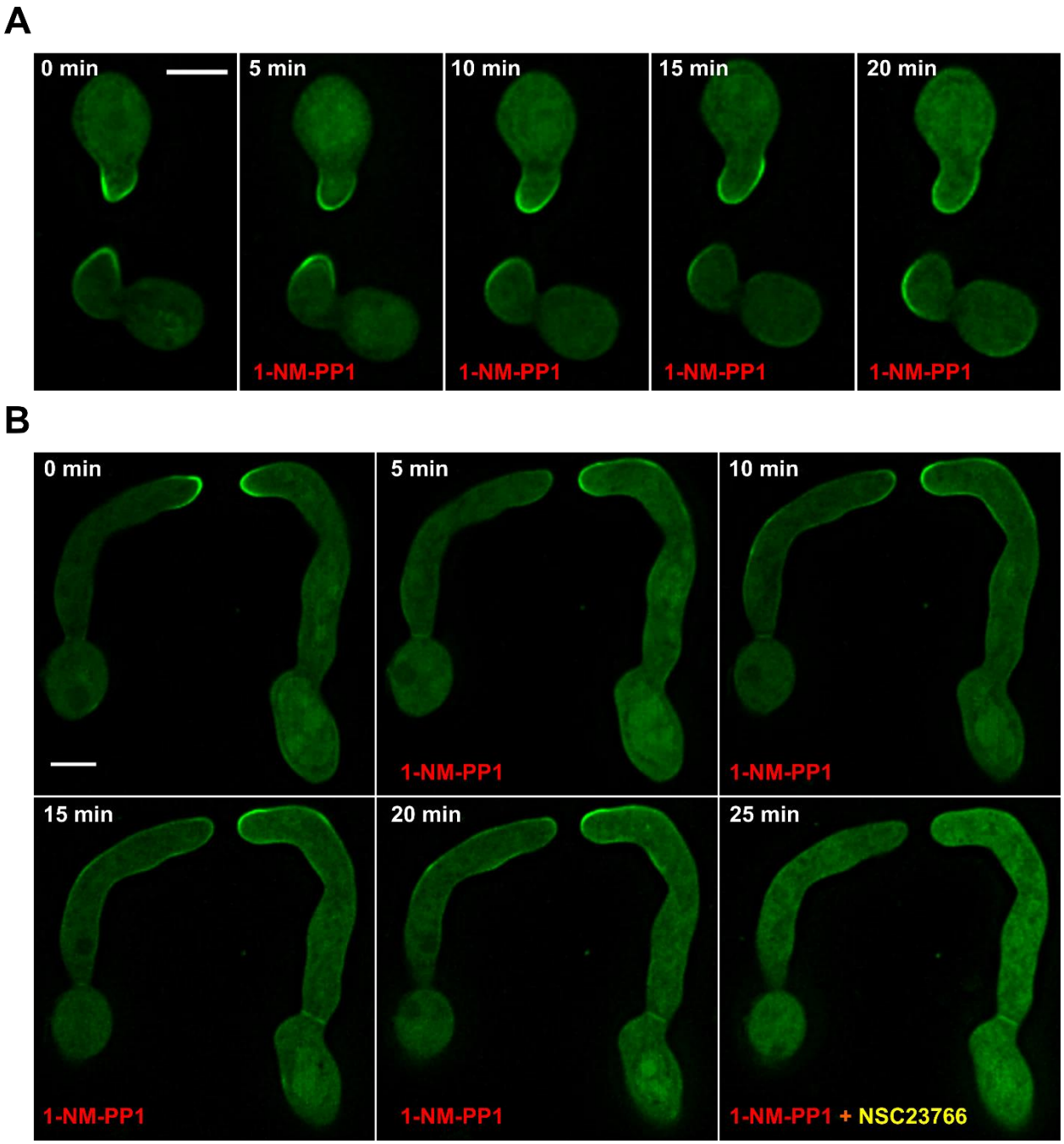

Figure 3.2.18. Inhibition of MAK-2 effect the localization of RAC-1. (A) Inhibition of MAK-2 do not affect the membrane recruitment of the CRIB reporter, but its localization and cells redirect its growth after inhibition. (B) The subsequent inhibition of RAC-1 after inhibition of MAK-2 shows that MAK-2 inhibition specifically effects the RAC-1 membrane localization. All scale bars: 5 µm.

3.2.17 MAK-2 inhibition leads to repositioning of RAC-1 around the plasma membrane

Consistent with our hypothesis, MAK-2 inhibition should not affect the activity of RAC-1, but rather its localization, as we have observed with the actin in previous experiments. To test this, the CRIB reporter strain (927) was crossed with MAK-2^{Q100A} (899), resulting in strain 949 (*Pmak-2-mak-2::Ptef-1-mak-2^{Q100A}-hph;Pal1-crib^{cla-4}-bar*).

Like in previous experiments, fusing cells were observed under the microscope and the inhibitor was added at the same concentration. When MAK-2 was inhibited, the CRIB reporter remained recruited to the plasma membrane but its localization switched to different spots in the cell. These data suggest that MAK-2 might be controlling the localization, and therefore growth directionality, of the Rho-GTPase RAC-1 (Fig. 3.2.18A).

However, we already mentioned that the CRIB reporter allows the localization of the activated forms of RAC-1 and CDC-42 at the same time. To decipher if RAC-1, and not CDC-42, is switching its position after MAK-2 inhibition, we used the RAC-1 inhibitor after inhibition of MAK-2. Like the previous experiments, fusing cells were observed under the microscope and the 1-NM-PP1 inhibitor (which inhibits MAK-2^{Q100A}) was added to the media. After observing again the switching in the position of the CRIB reporter provoked by the inhibition of MAK-2, the RAC-1 inhibitor was added to the media. Interestingly, the CRIB reporter fully disappeared from the plasma membrane, indicating that MAK-2 inhibition of fusing cells affects exclusively the position of RAC-1 at the plasma membrane (Fig. 3.2.18B). These data indicate that MAK-2 inhibition in tropically growing cells specifically affects the localization of RAC-1 (that stays active), which remains recruited to the plasma membrane but loses growth directionality towards the cell fusion partner and changes its position to another area in the cell.

Together, all the data presented in this chapter support a model in which inhibition of MAK-1 specifically affects RAC-1 membrane recruitment, which then results in disassembly of the actin focus organized by the Rho-GTPase and arrest growth of the interacting cells.

In addition, MAK-2 inhibition affects the localization of RAC-1 at the cell tips, which now become dispersed around the plasma membrane, resulting in an instable localization of the actin aster. Both MAP kinases are essential for cell fusion, but in a completely different mode of action.

3.3 The cell dialog mechanism mediating vegetative cell fusion is conserved in the plant pathogenic fungus *Botrytis cinerea*

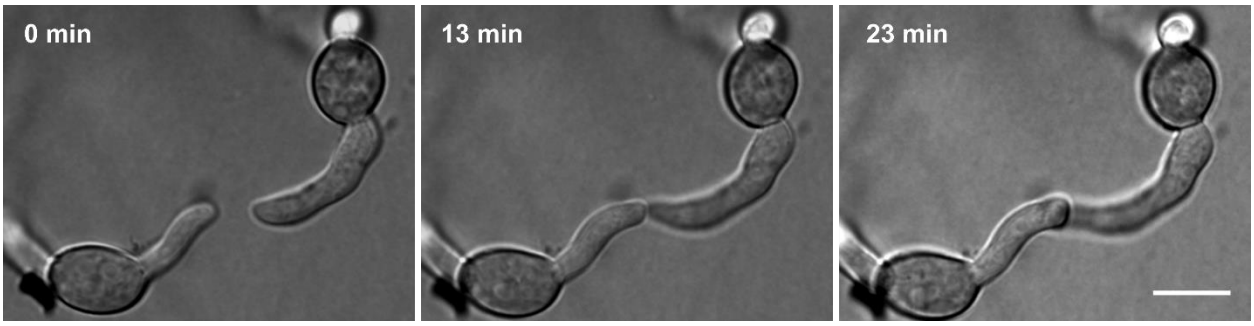

Figure 3.3.1. Cell fusion between germinated spores of *B. cinerea*. Spores were plated on minimal medium and images were taken at the indicated time points. Scale bar: 10 µm**.**

The oscillatory recruitment of SO and MAK-2 has so far been only described in *N. crassa* (Fleissner et al., 2009). However, vegetative cell fusion has been reported for numerous other fungal species, such as *F. oxysporum*, *S. macrospora*, *A. brassisicola*, *E. festucae*, *Aspergillus flavus*, *Colletotrichum lindemuthianum* and *B. cinerea* (Becker et al., 2014; Bernhards and Pöggeler, 2011; Charlton et al., 2012; Craven et al., 2008; Prados Rosales and Di Pietro, 2008; Roca et al., 2012, 2004; Zhao et al., 2017). In these organisms, cell fusion serves many different functions. For example, cell fusion seems to be essential for sclerotial development in *A. flavus*, and mutations causing disruption of genes involved in cell fusion results in a highly reduction in virulence (Zhao et al., 2017). However, mutation of the *N. crassa* SO-homolog in *F. oxysporum*, *Fso,* does not affect the pathogenicity on the host plant tomato (Prados Rosales and Di Pietro, 2008).

In addition, deletion of the *soft* gene in *E. festucae* results in a cell fusion deficient phenotype and turns the mutualistic interaction between the symbiotic fungus and the host plant *Lolium arundinaceum* into a pathogenic one (Charlton et al., 2012). Although germling and hyphal fusion are common in fungi, the mode of communication between the interacting cells in all of the exampled mentioned above remains unknown.

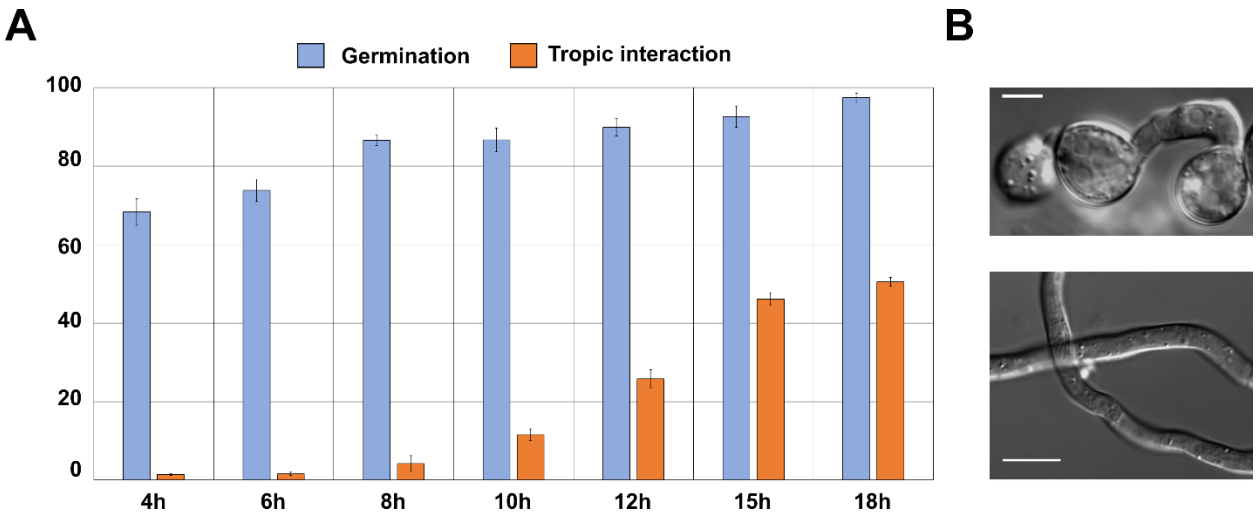

Figure 3.3.2. Quantification of the tropic interactions and germination rates of the wild type B05.10 *B. cinerea* strain at different time points. (A) The wild-type strain B05.10 was inoculated in MM and incubated for 4, 6, 8, 10, 12, 15 and 18 hours and the percentage of tropic interactions and germination were determined. Error bars represent the variation observed in at least 100 germlings per incubation time in three independent experiments. (B) Cell fusion was mostly observed between spores. Hyphal fusion was not observed at any of the times analyzed.

For that reason, we decided to test whether the cell communication mediated by oscillatory membrane recruitment of MAK-2 and SO was conserved among other fungi. We based our research on the plant pathogenic fungus *B. cinerea*. This fungus is an airborne plant pathogen with a necrotrophic lifestyle infecting more than 200 different crop plants (Williamson et al., 2007). In 2012, in a previous study from our laboratory reported that germlings from the wild-type strain, B05.10, undergo cell fusion in a similar manner as *N. crassa* and includes the so-called conidial anastomoses tubes (CATs) (Roca et al., 2012) (Fig. 3.3.1). Interestingly, growth on hydrophobic surfaces suppresses germling fusion and triggers pathogenic development, suggesting that fusion and infectious growth are two alternative, mutualistic exclusive developmental routes in this fungus (Roca et al., 2012).

3.3.1 Cell fusion in B. cinerea peaks at around 15 hours after inoculation.

In order to better understand the cell fusion process in this *B. cinerea*, we first quantified the number of tropic interactions observed in the wild type at different incubation times. To obtain the spore inoculum, a culture on complex medium was incubated for 10 days at room temperature under a full spectrum LED light in a 12 hours light/dark cycle, in order to induce sporulation of the fungus. The spores were harvested and filtered through sterile cheesecloth. A total number of $5x10^6$ spores was inoculated on minimal medium plates and incubated for 4, 6, 8, 10, 12, 15 or 18 hours at 21ºC in dark conditions. Germination rates and cell-cell interactions were quantified by light microscopy. Germination of the spores started after 4 hours and increased gradually until 18 hours, when it almost reached 100%. Tropic interactions were first observed after 10 hours and increased up to 18 hours, when it reached a maximum of about 50%. (Fig. 3.3.2A).

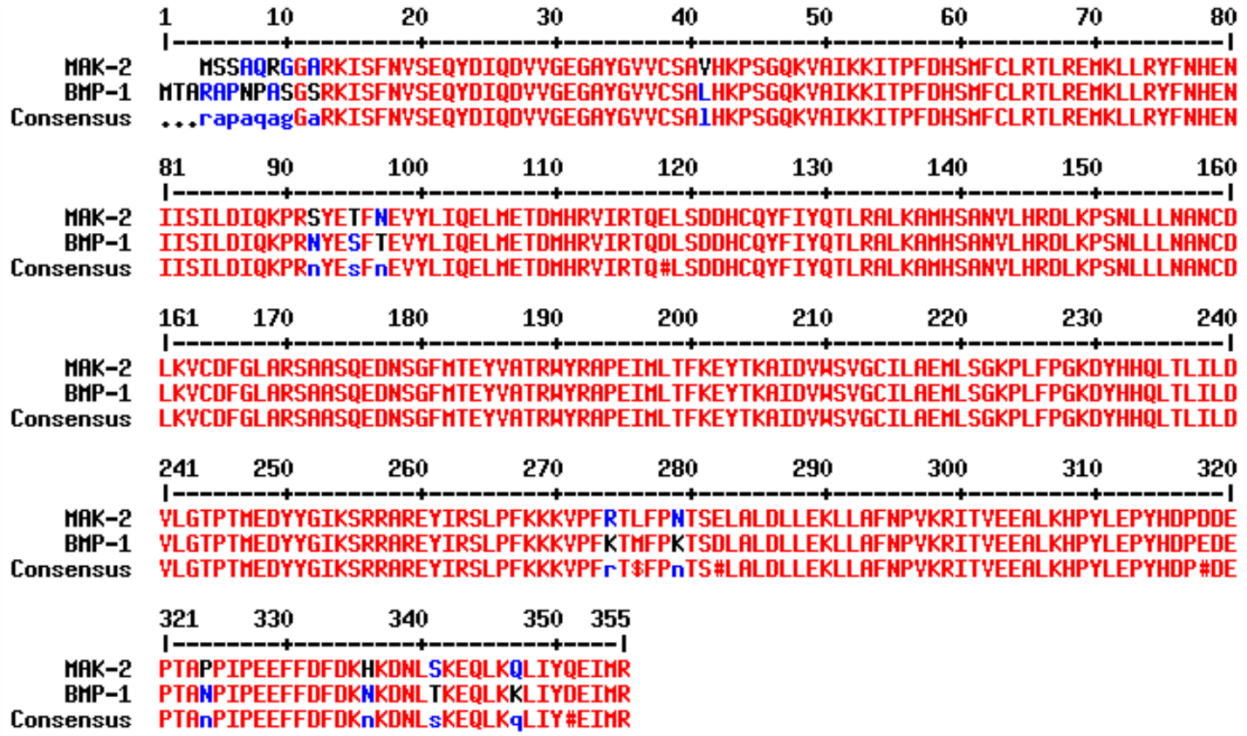

Figure 3.3.3. Alignment of the protein sequences from *N. crassa* MAK-2 and *B. cinerea* BMP-1. The protein sequences are obtained from EnsemblFungi database (MAK-2: NCU02393 and BMP-1: Bcin02g08170) and were aligned by using the Multalin software with default parameters (http://multalin.toulouse.inra.fr/multalin/)

Cell fusion is mostly observed between the spore bodies (not the germ tubes) involving the formation of CATs (Fig. 3.3.2B). In *N. crassa*, fusion is observed between germinating spores and the network formed between them is created soon after germination (Serrano et al., 2017). In contrast, in *B. cinerea* the spores first germinate and later establish the network essentially between the germinated spore bodies. While *N. crassa* cells do not compete but cooperate for the nutrients, *B. cinerea* spores first establish themselves in the medium and only later cooperate and connect into a network.

3.3.2 The MAPK BMP-1 of B. cinerea is homologous to MAK-2 of N. crassa.

To test whether the cell dialog mechanism is conserved in *B. cinerea*, we first identified the proteins involved in the process. We used the two factors that were first shown to oscillate in an antiphase manner during cell fusion in *N. crassa*: the MAP kinase MAK-2 and the SO protein (Fleissner et al., 2009).

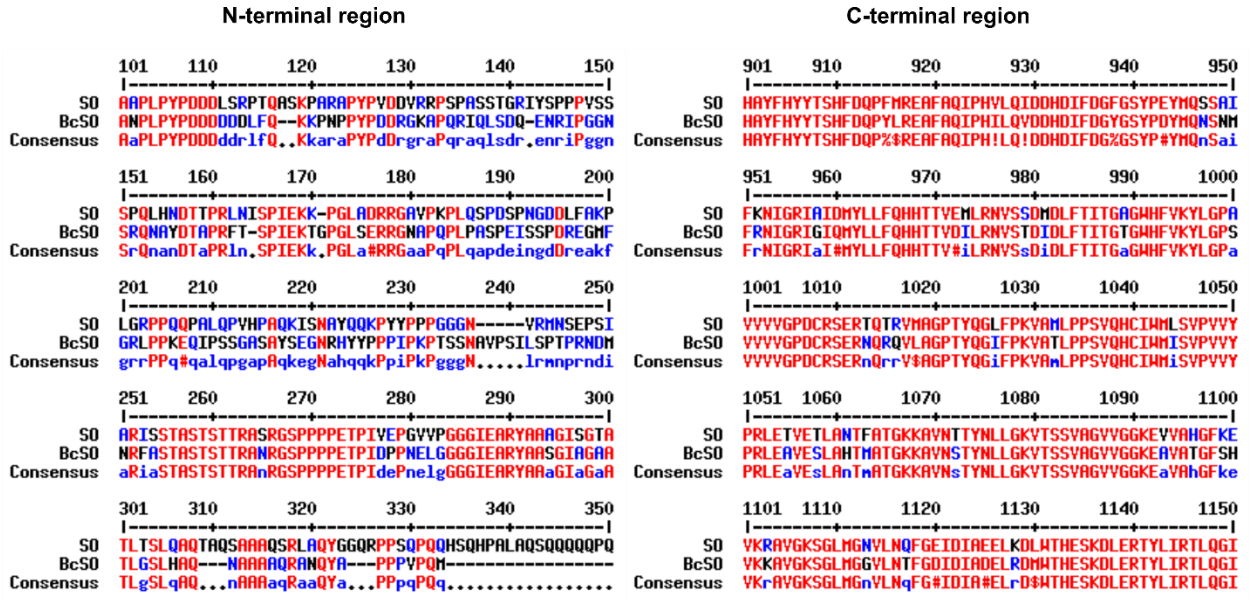

Figure 3.3.4. Alignment of the protein sequences from *N. crassa* SO and *B. cinerea* BcSO. The protein sequences are obtained from EnsemblFungi database (SO: NCU02794 and BcSO: Bcin01g06080). The alignment has been performed by using the Multalin software with default parameters (http://multalin.toulouse.inra.fr/multalin/). Only part of the sequence is shown in the image.

The MAK-2 protein sequence (NCU02393) was obtained from the EnsemblFungi database (***https://fungi.ensembl.org***) and used for a Basic Local Alignment Search Tool (BLAST) search of the "*Botrytis cinerea* B05.10" genome dataset (https://fungi.ensembl.org/Neurospora_crassa/Tools/Blast). As a result, 94 potential hits were identified. From these results, BMP-1 (Bcin02g08170) showed the highest score (1.686) and identity of about 95.4%, followed by the protein BMP-3 (Bcin09g02390), with a score of 463 and 63.8% of identity. The alignment of BMP-1 and MAK-2 clearly showed the high homology between both sequences (Fig. 3.3.3). BMP-1 has been previously described as a homolog of the MAP kinase PMK1 from *Magnaporthe grisea*, which is also homologous to the MAP kinase Fus3p from S. cerevisiae. These data indicate that BMP-1 is homologous to MAK-2 and might therefore have similar functions in cell-cell communication and fusion.

3.3.3 Only the C-terminal region of the SO protein is conserved in B. cinerea.

Following a similar approach, the 1.304 amino acids sequence of the SO protein (NCU02794) was obtained from EnsemblFungi and used for a BLAST search against the genome database of "*Botrytis cinerea* B05.10". Among the 21 potential proteins found, the so far undescribed Bcin01g06080 showed the highest score (2.331) and the best identity alignment (79.9%), followed by another unidentified protein Bcin05g03300 with a score of only 241 and 35.5 % identity. As an additional control, the protein sequence of the potential SO-homologue Bcin01g06080 was also used in a blast search of the "*Fusarium oxysporum f. sp. Lycopersici* 4287" dataset. The highest score (2.552) and identity (80%) was obtained for FSO1, a published homolog of SO from *N. crassa*. Knock-out mutants of *Fso* are fusion defective (Prados Rosales and Di Pietro, 2008). Alignment of the *N. crassa* SO and Bcin01g06080 protein sequences showed low homology in the N-terminal regions of the proteins, but conserved regions in the C-terminus (Fig. 3.3.4). Taken together, these data indicate that the now named BcSO (Bcin01g06080) is a SO homolog.

3.3.4 The MAP kinase BMP-1 and the protein BcSO are essential for cell fusion

In order to test the function of the SO and MAK-2 homologs in *B. cinerea*, a gene knock-out strategy was followed. The Δ*bmp-1* strain had been generated in a previous study and was kindly provided by Prof. Matthias Hahn (Doehlemann et al., 2006). For generation of the Δ*bcso* strain, 1 kb upstream and downstream flanking regions of the open reading frame were amplified by employing the primers pairs 1451/1452 and 1455/1456, respectively and using genomic DNA of B05.10 strain as a template. As a selection marker, the *hph* hygromycin resistance cassette was amplified with the primers 1453/1454. The three fragments were assembled by yeast recombinational cloning, resulting in plasmid *pSCR::BcSo-hph* (number 737). The plasmid was linearized and transformed into the *B. cinerea* wild-type strain as explained in the material and methods section (2.2.10). Primary transformants were isolated and purified by several rounds of single spore isolation until no PCR band was detected for the wild-type gene. Single integration of the knockout construct was tested by Southern blot analysis (Supplementary information 5.5). The resulting strains genotype was *bcso::hph* (strains 908 and 909, only 908 is shown in the following figures).

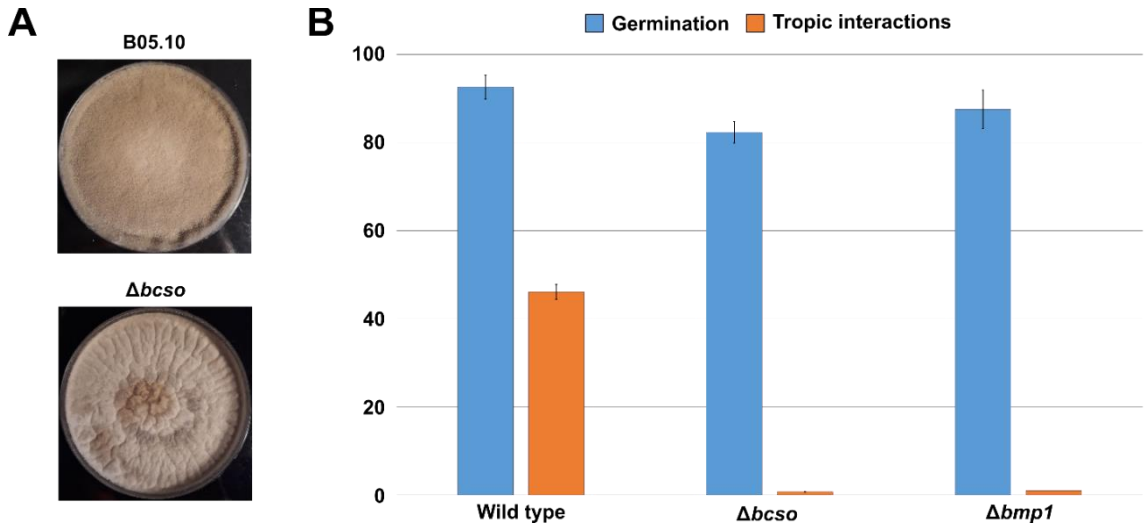

Figure 3.3.5. BMP-1 and BcSO are essential for cell fusion in the plant pathogenic fungus *B. cinerea*. (A) Complex media plates were incubated for 10 days at 21ºC under full spectrum 12 hours conditions. (B) Quantification of germination and tropic interactions of the wild-type strain B05.10, Δ*bcso* and Δ*bmp-1*. Error bars represent the standard variation between 100 cells observed per strain in three independent experiments. Scale bars: 5 µm.

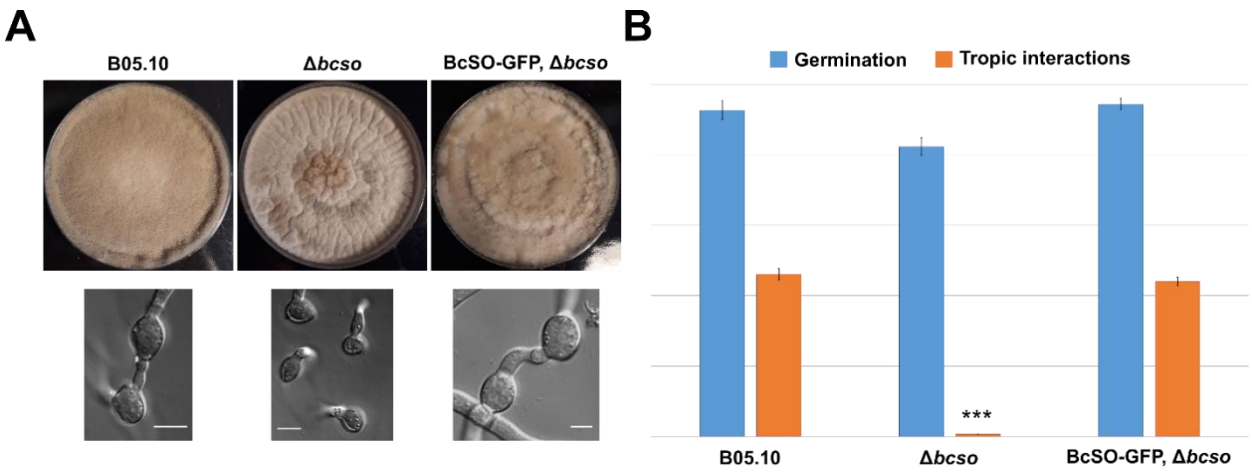

Figure 3.3.6. Expression of BcSO-GFP in Δ*bcso* complements the cell fusion defective phenotype. (A) The macroscopic growth was restored by transformation of *bcso-gfp* into the Δ*bcso* mutant strain. (B) Quantification of germination and tropic interactions after 15 hours of incubation indicates a full recovery of cell fusion by complementation with BcSO-GFP.

In a first step, the growth behavior of both the Δ*bmp-1* and the Δ*bcso* mutants was tested. According to previous reported data, Δ*bmp-1* shows deficiencies of growth on complete medium plates (Doehlemann et al., 2006; Zheng et al., 2000). Δ*bcso* showed similar growth defects, and less sporulation was observed on the plates (Fig. 3.3.5A). Next, both mutants together with the control strain B05.10 were tested for conidial germination and tropic interactions. Fresh spores were harvested and incubated for 15 hours in MM plates at 21ºC. Similar to *N. crassa*, cells lacking the MAP kinase BMP-1 or BcSO showed clear defects in cell fusion (Fig. 3.3.5B). No tropic interactions were observed between germinated spores unlike to the wild type. These data indicate that the MAK-2 homolog BMP-1 and the SO homolog BcSO are essential for the germling fusion process in *B. cinerea* and strains lacking the respective genes do not show any tropic interaction.

3.3.5 BcSO-GFP complements the Δbcso cell fusion defects

In order to test that the cell fusion defects reported by Δ*bcso* were specifically caused by the mutation of the *bcso* gene, a complementation construct was created. Since the mutation of the *bcso* gene was generated with the *hph* cassette, a construct was created in which *bcso-gfp* was integrated with the nourseothricin (*nat*) cassette. Primers 1505 and 1509 were used to amplified the *bcso* gene with overlapping regions with *PoliC* and

gfp of the plasmid pNDN_OGG (Schumacher, 2012). Linearized plasmid (with *Xba*I) and purified fragment were used for yeast recombinational cloning, resulting in a plasmid containing *PoliC-bcso-gfp-Tgluc-nat* (plasmid name 774). The strain 908 (*bcso::*hph) was used as a recipient strain and its transformation with plasmid 774 resulted in strains carrying the genotype *bcso::hph; PoliC-bcso-gfp-Tgluc-nat*. Purification and isolation of the strains were performed by single spore isolation on selection medium containing hygromycine and nourseothricin, generating the purified strain 929.

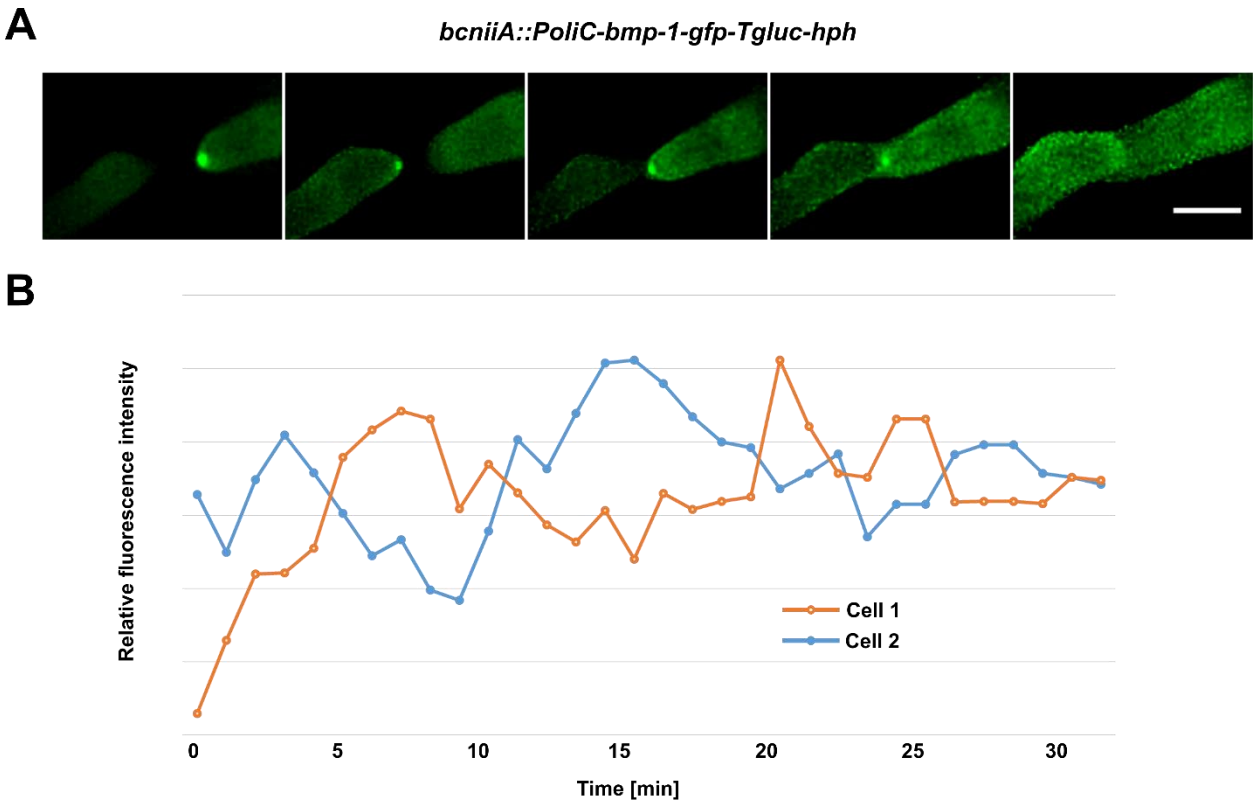

Figure 3.3.7. Oscillatory dynamic localization of the MAK-2 homologous MAP Kinase BMP-1 in *B. cinerea*. (A) Oscillatory dynamic recruitment to the tips of the interacting cells. Scale bar: 5 µm. (B) Quantification of fluorescence intensity at the cell tips normalized to the corresponding fluorescence signal at the cytoplasm of each cell. Pictures were analyzed every minute. Comparable observations were made two more times.

The strain showed a similar phenotype on complex medium plates as the wild type, indicating expression of the *bcso* open reading frame complements the Δ*bcso* mutant (Fig. 3.3.6A). Quantification of germination showed a similar percentage than wild type and Δ*bcso*. The construct fully complemented the cell fusion defect and normal rates of tropic interactions were restored (Fig. 3.3.6B). All these data indicate that the BcSO-GFP construct fully complements Δ*bcso*, proving that the cell fusion defects of the mutant are specifically due to the lack of the *bcso* gene.

3.3.6 The MAP kinase BMP-1 oscillates between the tips of the interacting cells during cell fusion of B. cinerea

As in *N. crassa*¸ the MAK-2 MAPK homolog in *B. cinerea*, BMP-1, is essential for the cell fusion process. As we have previously shown, MAK-2 is recruited to the cell tips of the *N. crassa* fusing cells and oscillate in an antiphase manner to SO.

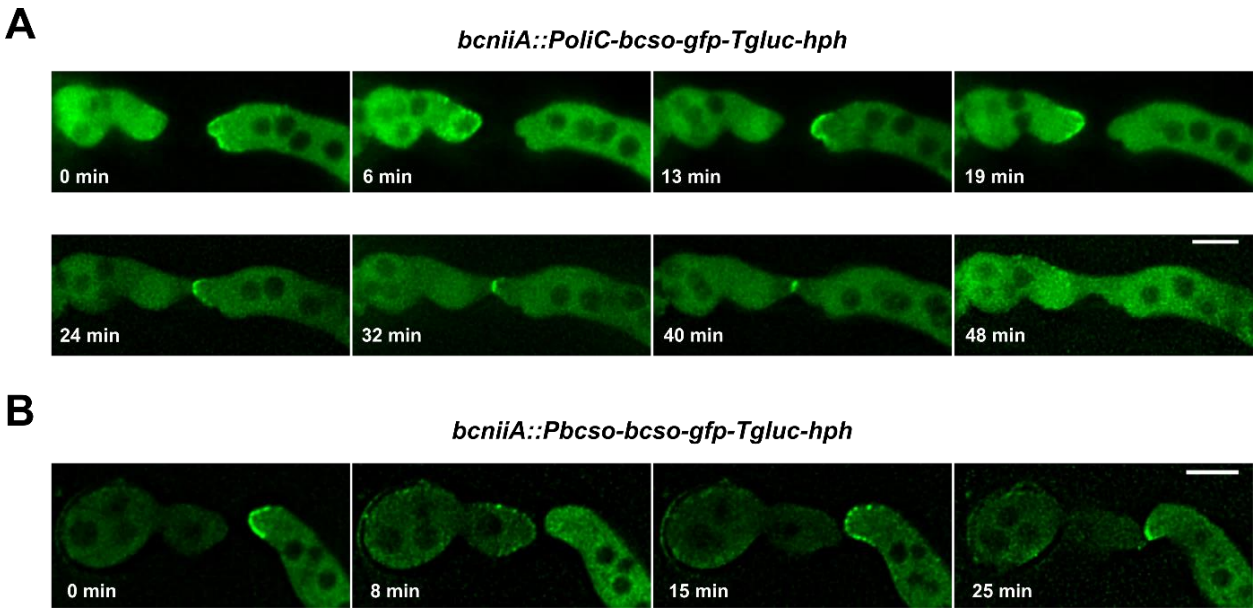

Figure 3.3.8. BcSO localizes in an oscillatory fashion to the tips of interacting germlings. (A) Subcellular localization of BcSO expressed under control of the overexpression promoter *PoliC*. (B) Oscillatory recruitment of BcSO expressed under control of the native promoter *Pbcso*. All scale bars: 5 µm.

To determine whether BMP-1 is also recruited to the cell tips of the interacting cells, we decided to observe the subcellular dynamics of the protein during cell fusion. Dr. Marschall and Prof. Tudzynski kindly provided a strain carrying a *bmp-1-gfp-nat* expression construct integrated into the *bcniiA* gene locus (B05.10 + *bcbmp1_gfp*) (Marschall and Tudzynski, 2016).

Fresh spores from complex media plates were harvested and incubated for 15 hours in MM plates at 21ºC. Images were obtained during the cell communication process mediating cell fusion. Interestingly, in contrast to MAK-2 in *N. crassa*, BMP-1 was accumulated as a single dot in the interacting cells rather than around the cell tips. This signal was first observed in the tip of one of the two cells. After around 6 minutes, the signal disappeared from the cell tip of the previous cell and appeared accumulated at the cell tip of the opposite cell. This oscillation occurred one more time in a period of around 6 minutes. After 10 minutes, the cells established physical contact and the signal accumulated at the contact area of both cells. The signal finally disappeared after 9 minutes (Fig. 3.3.7A). In *N. crassa*, MAK-2 completes a full oscillation process in 6-12 minutes. In order to test the oscillation time of BMP-1, we quantified the signal intensity at the cell tips during tropic growth. Images were obtained every minute and the relative signal intensity was measured in a 3 µm area at the cell tips. For normalization, the fluorescence intensity was then divided by the intensity of the cytoplasmic signal (measured 5 µm away from the cell tip) within the same cell.

The oscillatory membrane recruitment of BMP-1 occurred in a period between 12-15 minutes during the communication process. Period length seemed to decrease when cells were close to making contact, when the oscillation became more rapid with a period of 3-6 minutes (Fig. 3.3.7B).

3.3.7 The protein BcSO localizes in an alternating manner to the tips of interacting cells during germling fusion of B. cinerea

In order to test the subcellular localization of BcSO, the open reading frame of the gene (Bcin01g06080) was amplified with primers 1416 and 1415, which contained overlapping sequences with the *PoliC* promoter and the *gfp* sequence of the plasmid pNAH_OGG (Schumacher, 2012). The linearized plasmid together with the amplified fragment were used for yeast recombinational cloning, resulting in a plasmid containing *PoliC-bcso-gfp-Tgluc* with *hph* as a selection marker for fungal transformation (plasmid 711).

Transformation of strain B05.10 with this plasmid resulted in strains with the genotype: *bcniiA::PoliC-bcso-gfp-Tgluc-hph*. Strains were isolated, purified and integration was tested by PCR as indicated previously (Schumacher, 2012), generating the strain 854. Localization of the protein was analyzed by fluorescence microscopy. The BcSO-GFP signal was completely cytoplasmic in non-interacting cells and no signal was detected inside of the nucleus. During fusion related cell-cell communication and directed growth, the protein accumulated at the cell tips of the interacting cells in an alternating manner (Fig. 3.3.8A). In contrast to the BMP-1 localization and similar to MAK-2 and SO of *N. crassa*, BcSO was observed around the tip rather than concentrated as a single dot. During the communication phase, the signal accumulated at only one cell tip at time and switched after a period of 6-8 minutes. This oscillation was observed until the cells established physical contact, when the protein accumulated at the contact area (Fig. 3.3.8A). To study the localization of this protein, we used an overexpression promoter. The overexpression of a protein could, however, produce artefacts in its subcellular localization. To test that the oscillatory dynamic recruitment was not caused by overexpression, we generated a BcSO-GFP expressing construct under control of the native *bcso* promoter. The region 1 kb upstream of the *bcso* start codon together with the coding region sequence of *bcso* was amplified with primers 1431 and 1415. The plasmid pNAH_OGG (Schumacher, 2012) was cut with the restriction enzymes *Nco*I and *Spe*I in order to exchange the *PoliC* promoter by the fragment containing the native *bcso* promoter and ORF. The PCR fragment and the linearized plasmid were fused by yeast recombinational cloning, resulting in plasmid *Pbcso-bcso-gfp-Tgluc-hph* (799). The new

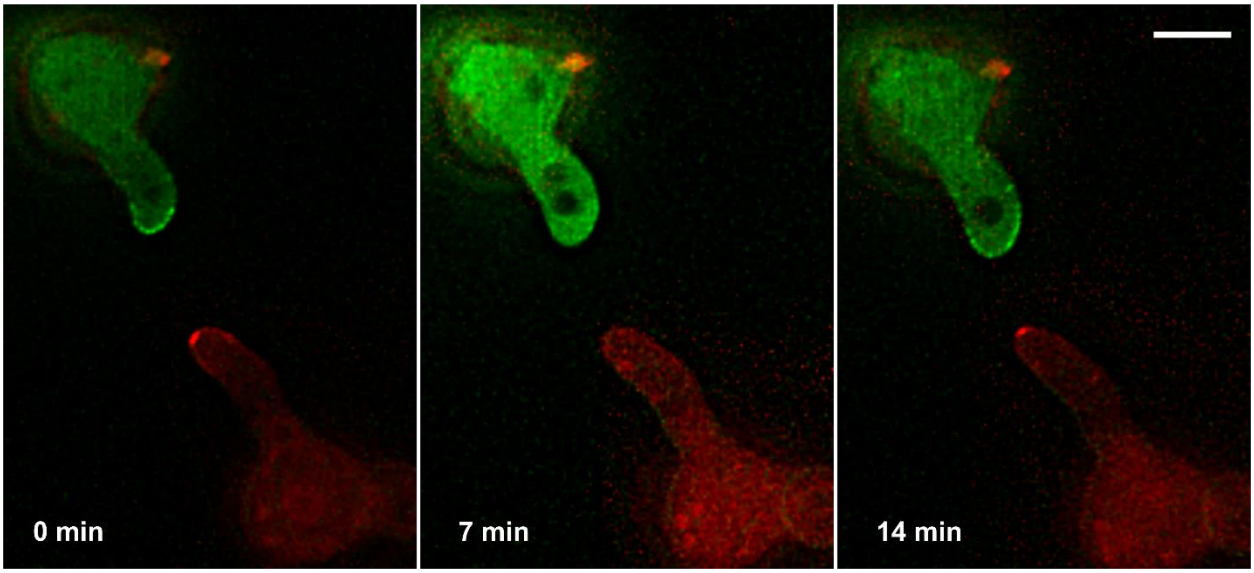

Figure 3.3.9. BMP-1 and BcSO oscillate in an antiphase manner during the cell-cell interaction. Fresh spores from strains 856 (*bcniiA::PoliC-bmp-1-mCherry-Tgluc-hph*) and 854 (*bcniiA::PoliC-bcso-gfp-Tgluc-hph*) were mixed and incubated together to observe cell-cell interactions and localization of BMP-1-mCherry and BcSO-GFP. Scale bar: 5 µm.

plasmid was transformed into B05.10, resulting in strain *bcniiA::Pbcso-bcso-gfp-Tgluc-hph* (strain 910). Fluorescence microscopy revealed that the fluorescence signal was weaker than in the overexpressing strain, but the general localization pattern of the protein was comparable in both strains. During cell fusion, the signal accumulated at the cell tips in a similar manner to the overexpressed BcSO-GFP, and oscillated between the interacting cell tips in a similar period of time (Fig. 3.3.8B).

These data suggest that the expression level of the protein does not affect its localization and BcSO oscillates in an alternating manner during the communication phase.

3.3.8 BMP-1 and BcSO oscillate in antiphase during cell fusion

One of the most interesting features of the cell dialog process in *N. crassa* is the behavior coordination between the two interacting cells. According to the current working model, one cell is sending the unknown signal, while the partner is receiving the signal and after 3-6 minutes these roles switch. This model is based on the colocalization of MAK-2 and SO. When MAK-2 is recruited at one cell tip, SO is recruited at the opposite cell tip and

both proteins do not colocalize before the cells have established physical contact (Fleissner et al., 2009; Serrano et al., 2017). After showing that the homologs of MAK-2 and SO of *B. cinerea*, BMP-1 and BcSO, undergo comparable subcellular dynamics during the cell fusion process, we decided to also colocalize both factors to test if their membrane recruitment also alternates. For this we created a strain expressing a red-labeled BMP-1 protein. We first generated a pNAH_OGG plasmid (number 93) with a poly-linker region to allow us to make recombination of different genes, generating the plasmid 661. This plasmid was used as a backbone and *gfp* was removed by cutting with the restriction enzymes *Nco*I and *Not*I. The *mCherry* encoding sequence was amplified with primers 1411 and 1412. Fragment and plasmid were ligated and cloned in *E. coli* resulting in plasmid 710. The *bmp-1* encoding region was later amplified with primers 1296 and 1297 and the fragment was cloned in plasmid 710, resulting in plasmid *PoliC-bmp-1-mCherry-Tgluc-hph* (727). The new plasmid was linearized with XbaI and transformed into the wild-type strain B05.10. Transformants were isolated and the integration of the construct was tested by PCR as indicated in (Schumacher, 2012), resulting in strain *bcniiA::PoliC-bmp-1-mCherry-Tgluc-hph* (strain 856). Fresh spores from BMP-1-mCherry and BcSO-GFP were mixed and incubated together on a MM plate for 12 hours at 21ºC. Fluorescence microscopy was then employed to analyze the subcellular dynamics of the fluorescently labeled proteins in cell pairs consisting of a green and a red labeled cell. Similar to the observations made in *N. crassa*, the signals from BMP-1-mCherry and BcSO-GFP accumulated at the same time independently in each cell tip.

After around 6-7 minutes, both signals disappeared from the cell tips. 6-7 additional minutes later, signals were again accumulated at the cell tips (Fig. 3.3.9). These data clearly indicate that the two signals of the two different proteins appear at the same time in the two different cell tips. This indirectly confirms that the recruitment of the two proteins oscillate in an antiphase manner during the cell fusion process, exactly like MAK-2 and SO in *N. crassa*.

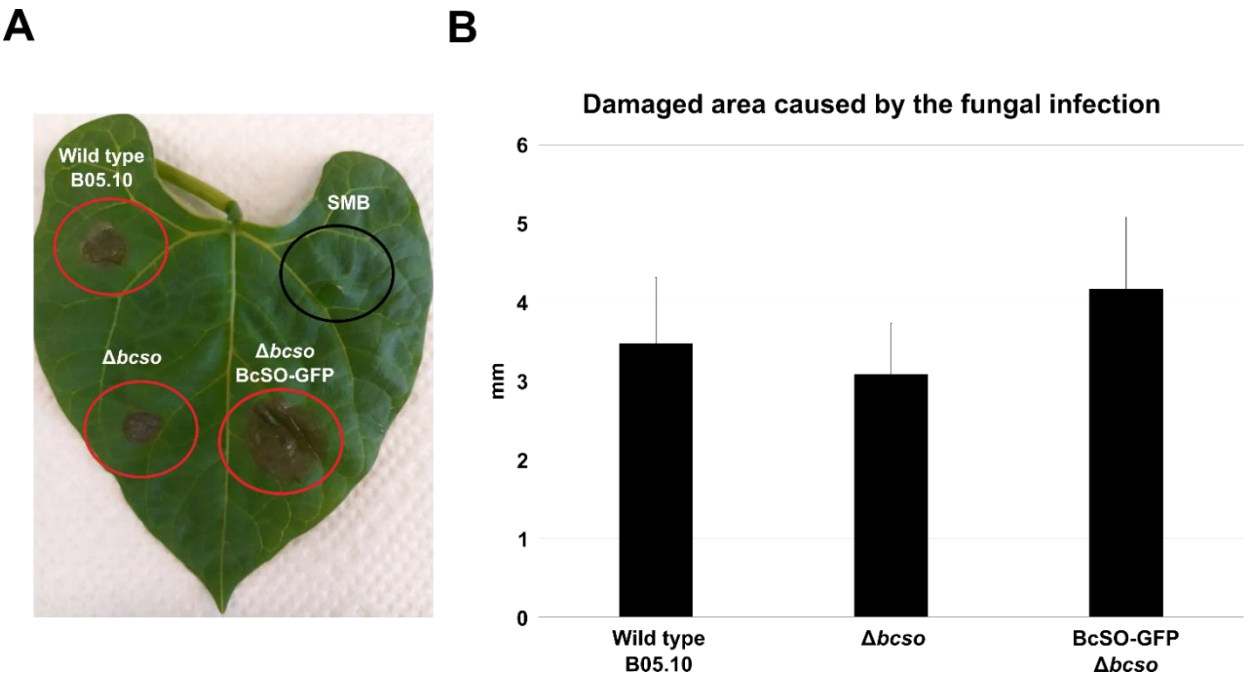

Figure 3.3.10. BcSO is not essential for pathogenicity of the fungus. (A) 10^5 spores from wild type (B05.10, strain 785), Δ*bcso* (strain 908), and Δ*bcso*; BcSO-GFP (strain 929) were placed on French beans leaves to study the fungal pathogenicity. As a control, the infection media alone was applied (SMB). Leaves were incubated for 3 days at room temperature in high humidity chambers. (B) Quantification of the infection area damaged cause by the fungal infection (diameter). Standard deviation was calculated from 10 pairs of leaves from 5 different plants. No significant differences were observed for the three different isolates.

3.3.9 Cell fusion is not essential for pathogenicity of B. cinerea.

The function of the SO protein during cell fusion and virulence has been investigated in different fungi with different outcomes. For example, the lack of the *so* homologous gene in the necrotrophic fungus *A. brassisicola* leads to reduced virulence on cabbage (Craven et al., 2008). In contrast, the mutation of *so* in *F. oxysporum f. sp. Lycopersici* does not affect the virulence and pathogenicity of the fungus (Prados Rosales and Di Pietro, 2008).

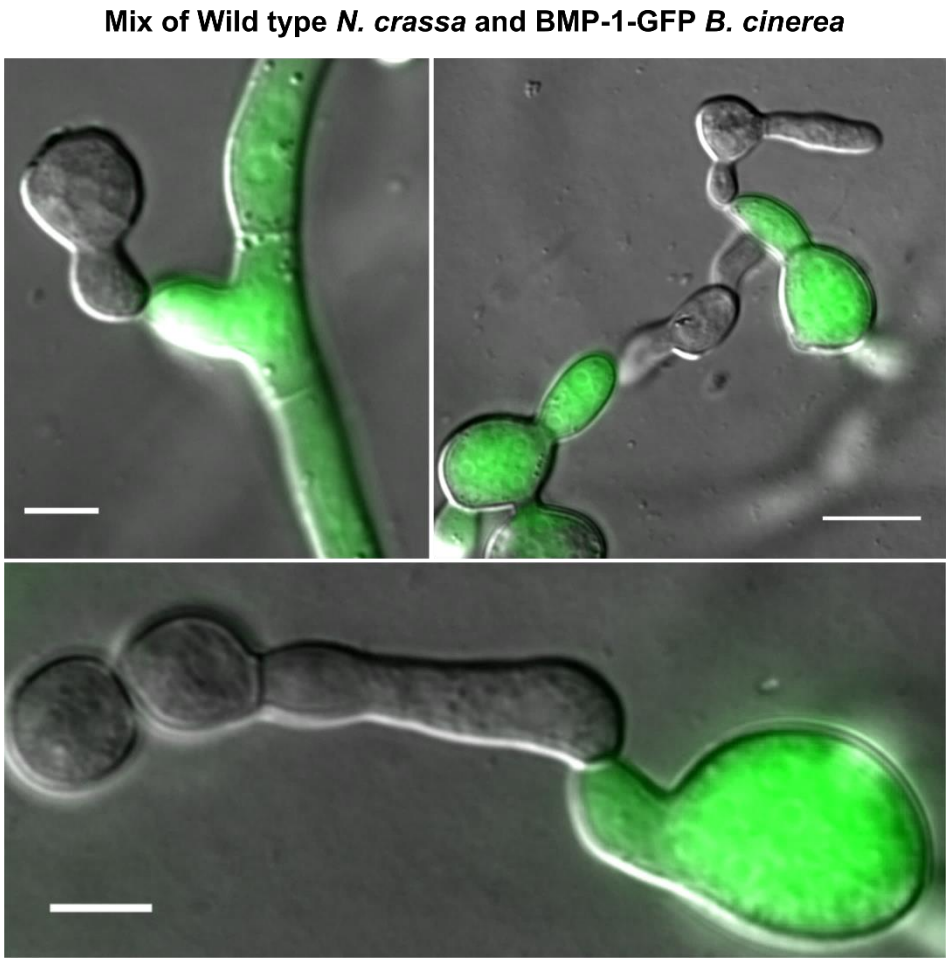

Figure 3.3.11. *N. crassa* and *B. cinerea* share a common molecular language but do not undergo cell fusion. Mix of germlings of wild-type *N. crassa* and BMP-1-GFP expressing *B. cinerea* (Strain 857). In the upper panels N1-01 *mat A* was used from *N. crassa*. In the lower panel, N1-02 *mat a* was used from *N. crassa*. All images are mergers of the DIC and GFP channel images. All scale bars: 5 µm.

In order to test a potential role for SO in the pathogenic development of *B. cinerea*, fresh spores from strains B05.10, Δ*bcso* (Strain 908) and the complemented strain (Strain 929) were harvested from plates previously incubated for 10 days at 21ºC. The pathogenicity assay was performed on detached primary leaves of *Phaseolus vulgaris* (grown from commercial seeds). 10 µl of a 10^5 spores/ml suspension of SMB media (maltose-peptone pH 5.6) were inoculated on the leaves (4 strains per leaf). The infected leaves were incubated in humidity chambers at room temperature under natural light. After 3 days, the infection was quantified by measuring the size of the lesion formed by the fungus. As a result, no differences were observed for the wild-type, the mutant or the complemented strain (Fig. 3.3.10A and B). These data suggest that BcSO is dispensable for infectious growth of *B. cinerea* and, moreover, indicates that cell fusion does not contribute to the virulence of the fungus.

3.3.10 The plant pathogen B. cinerea and N. crassa share a common molecular language

The previous results of this dissertation had revealed that the cell dialog mechanism, which was initially identified in *N. crassa,* is also conserved in *B. cinerea*. The homologs of MAK-2 and SO, BMP-1 and BcSO respectively, are essential for the cell fusion process and are recruited to the growing fusion tips in an alternating manner. We therefore decided to test whether the so far unknown signals and their cognate receptor were also similar between both fungi.

In order to test this hypothesis, fresh spores of the BMP-1-GFP strain were harvested from complex medium plates and 300 µl of a 10^5 spores/ml suspension were inoculated in MM plates. Spores were incubated for 12 hours at 21ºC, afterwards 100 µl of a 10^5 spores/ml suspension from either wild-type *N. crassa* strain N1-01 (*mat A*) or N1-02 (*mat a*) were added to the same plate and incubated for additional 3 hours. We used both strains to investigate if the mating type of the *N. crassa* cell is important for the potential interspecies communication. When analyzed by light microscopy several events were found, in which *N. crassa* germlings were tropically growing towards *B. cinerea* hyphae or germlings and vice versa (Fig. 3.3.11).

Interestingly, no cytoplasmic mixing was observed between these interspecies cell pairs even when cells were incubated for extended times (>9 hours), suggesting that fusion between cells of different species does not take place. These data clearly indicate that the signals and the cognate receptor involved in the cell-cell communication process are highly conserved, but interspecies fusion is probably prevented by additional regulatory systems. In addition, no differences were observed between both mating types of *N. crassa*, suggesting that the interspecies interactions are independent of the mating type.

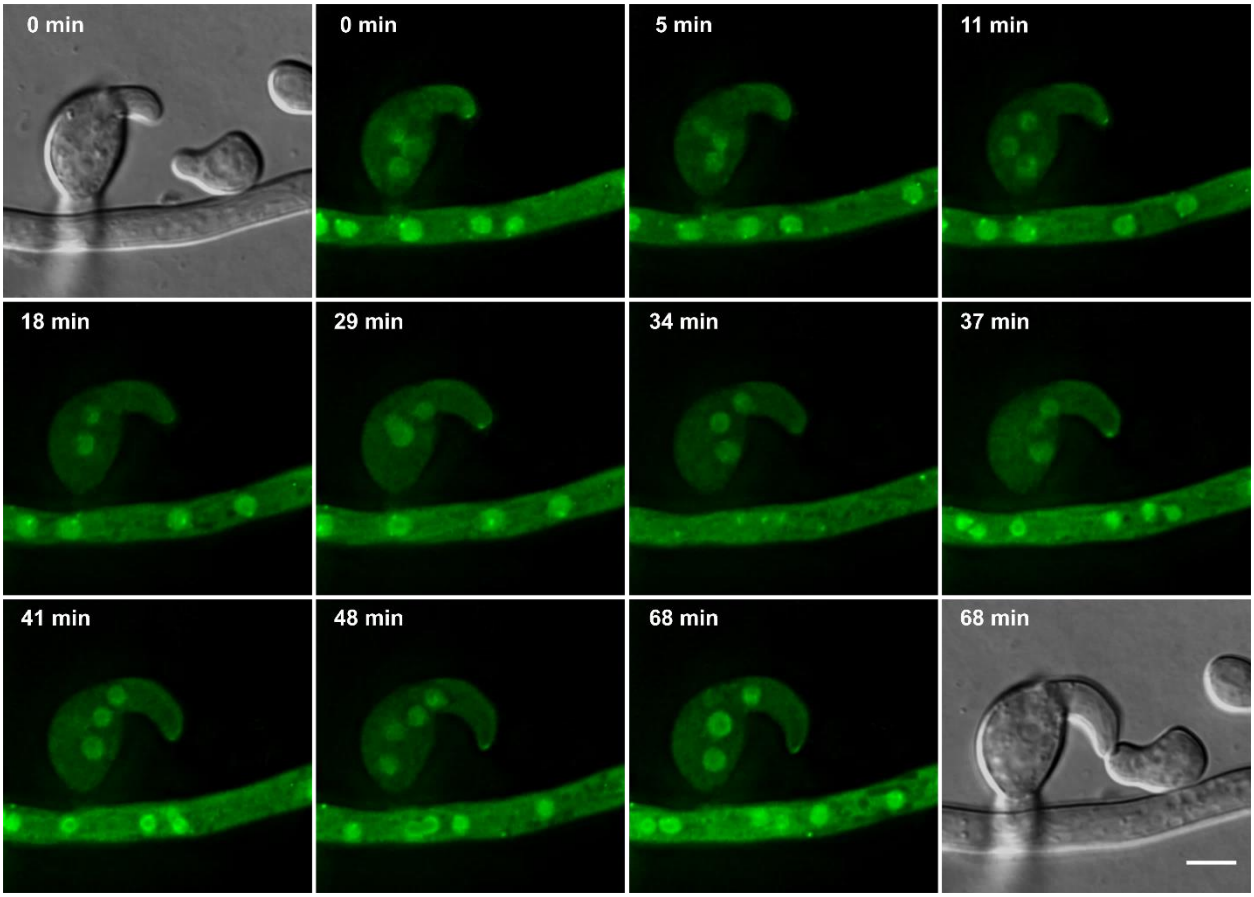

Figure 3.3.12. BMP-1 oscillates in a wild-type manner while interacting with a *N. crassa* germling. Oscillatory recruitment of BMP-1 in an interaction with *N. crassa* wild-type N1-01 germling. Scale bar: 5 µm. Comparable observations were made three more times.

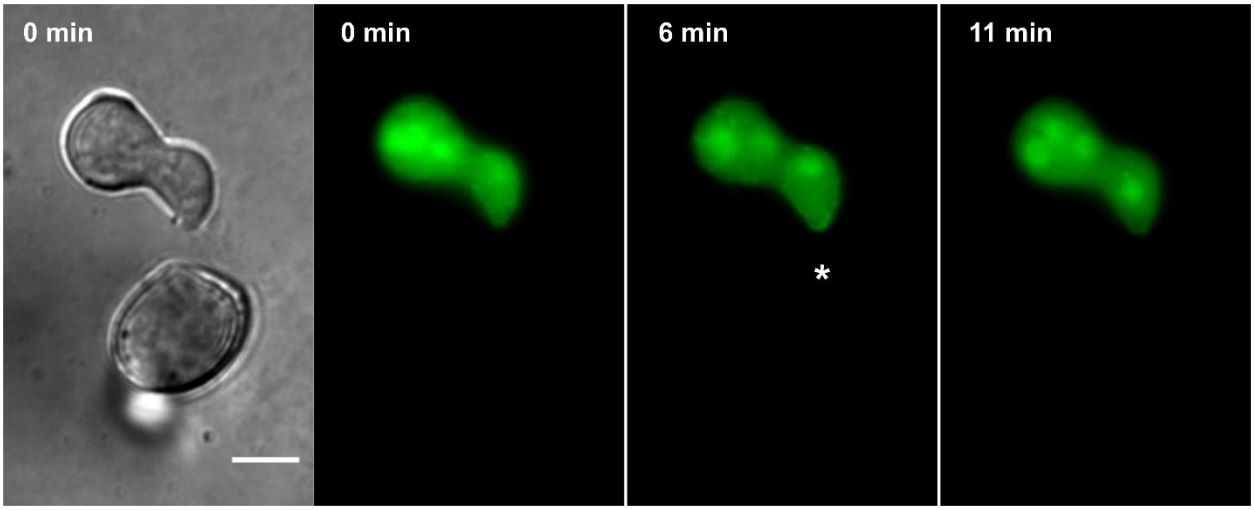

Figure 3.3.13. MAK-2 oscillates in a *N. crassa* germling during the interaction with a *B. cinerea* germling. Spores from strain 665 were mixed with wild-type *B. cinerea* strain (B05.10). Cell-cell interactions were observed after 2 hours of incubation. Scale bar: 5 µm.

3.3.11 The MAP kinase BMP-1 oscillates while interacting with N. crassa

In order to test whether the observed interspecies interactions were also mediated through the cell dialog mechanism, we localized BMP-1 of *B. cinerea* in an interaction with a wild-type *N. crassa* cell. Interestingly, we observed that BMP-1 was recruited to the cell tips in the typical alternating manner. After 5 minutes, the protein disappeared from the cell tips while probably MAK-2 was recruited in the *N. crassa* cell. After 6 more minutes, BMP-1 was again recruited to the *B. cinerea* tip and continued oscillating until the cells established physical contact. The protein then accumulated at the contact area (Fig. 3.3.12).

Interestingly, even 20 minutes after the cells had established physical contact, no green fluorescent was detected in the *N. crassa* germling, indicating again that no successful fusion and subsequent cytoplasmic mixing occurs between the different species.

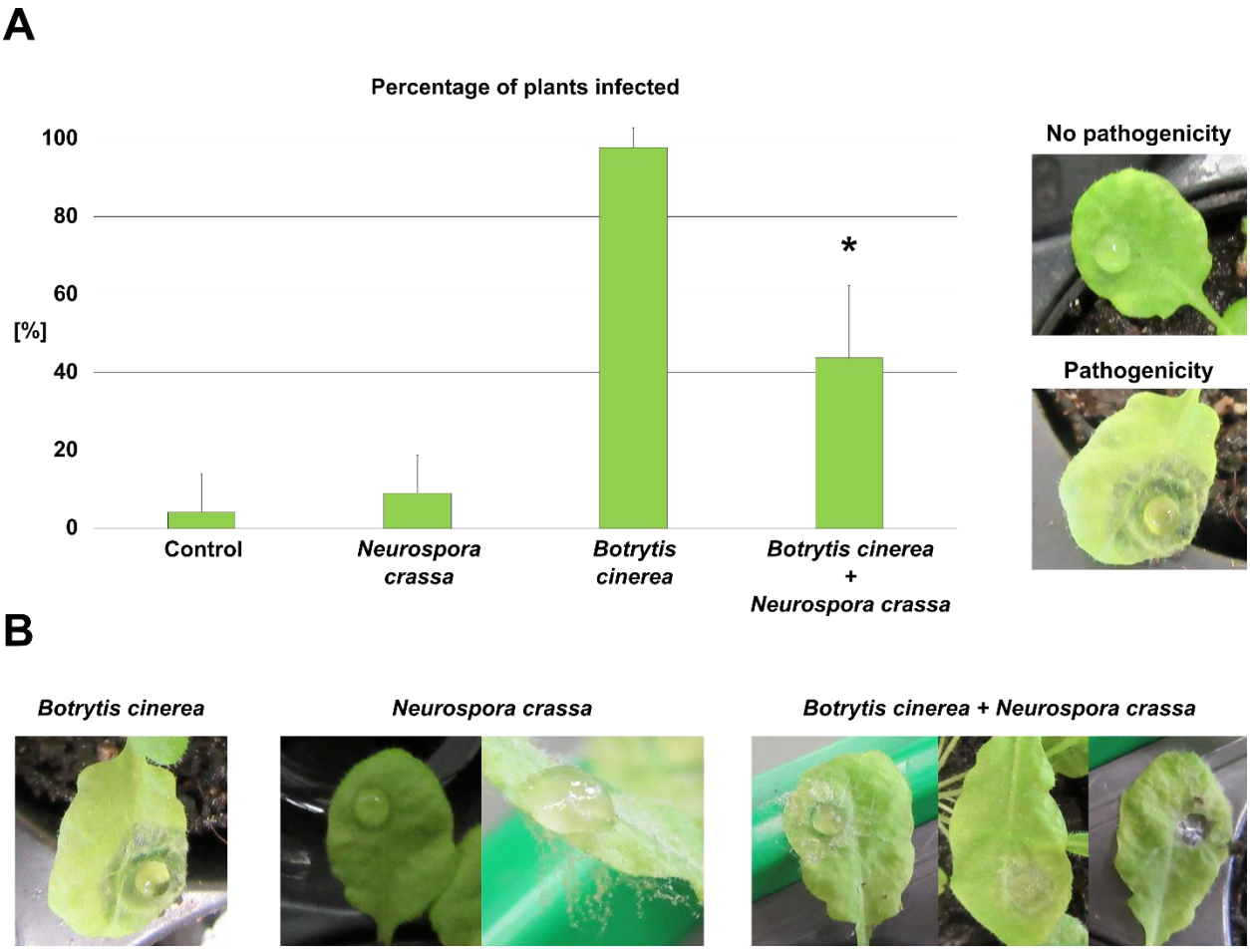

Figure 3.3.14. The presence of *N. crassa* modulate the pathogenicity of *B. cinerea*. (A) The leaves of 16 plants per condition were inoculated with SMB, *N. crassa* (strain N1-01), *B. cinerea* (strain B05.10) and the mix of *B. cinerea* and *N. crassa*. The amount of leaves infected per plant was quantified based on the presence or absence of infection symptoms. A t-test of two-tail paired was calculated and show significance with a significance value $p<0.05$ (B) Examples of the infection assay classified by each condition.

3.3.12 The MAP kinase MAK-2 oscillates in N. crassa while interacting with B. cinerea.

Following the same approach, we decided to also test whether the MAP kinase MAK-2 oscillates in the *N. crassa* partner while interacting with a *B. cinerea* cell. MAK-2 was first absent at the tip of the *N. crassa* cell. After around 5-6 minutes, the signal accumulated at the cell tip of the *N. crassa* germling.

Observing the cells for 6 more minutes showed that signals again disappeared, completing a full oscillation period (Fig. 3.3.13). These data indicate that MAK-2 oscillates to the cell tip of the *N. crassa* cell while interacting with the *B. cinerea* cell. The interspecies interactions are therefore also mediated by the conserved cell dialog mechanism mediating somatic fungal cell fusion.

3.3.13 The presence of N. crassa reduces the infection of A. thaliana by B. cinerea

We have shown that *N. crassa* and *B. cinerea* undergo mutual attraction, which is mediated by the conserved cell fusion machinery. This suggests that the unknown fusion signal and its cognate receptor are conserved between these two-divergent species. Virulence of *B. cinerea* has long been studied because of the huge economical loss that this fungus provokes. Previous studies had shown that *B. cinerea* virulence program is activated by the hydrophobicity of the leaf surface through BMP-1 (Giesbert et al., 2014; Zheng et al., 2000).

It has been shown that *B. cinerea* germlings behaves differently at different growth surfaces. For example, on hydrophobic surfaces, such as leaves, the cells do not undergo cell fusion but the infection program. In contrast, in hydrophilic surfaces, the cell fusion program is triggered and the cells form a network (Roca et al., 2012), suggesting that infection and fusion are two alternative and mutually exclusive developmental programs. We therefore raised the question if the artificial induction of the fusion program might suppress pathogenic growth, even on surfaces, which usually promote pathogenicity. The natural, probably chemical signal inducing fusion and mediating the cellular interaction remains, however, unknown.

Since *N. crassa* and *B. cinerea* do communicate with each other, we hypothesize that *N. crassa* might be able to provide the fusion signal also on plant surfaces. We therefore tested the growth behavior of germinating spores on plant surfaces, specifically on onion epidermal layers. In contrast to *B. cinerea*, *N. crassa* readily undergoes fusion on this surface, indicating that it is also producing the fusion signal on plant leaves (supplementary section 9.26). Next, we hypothesized, that *B. cinerea* cells might be influenced by the presence of *N. crassa* fusing cells and therefore switch its behavior from

infection to cell fusion, which should result in a reduced infection efficiency. In order to test this hypothesis, we tested the infection of *B. cinerea* cells when mixed with *N. crassa* cells in the plant model organism *A. thaliana*.

A total amount of 10^5 spores from the *B. cinerea* wild type B05.10 were harvested from 10 days old plates and mixed with a total amount of 10^6 spores from *N. crassa* N1-01 that were harvested from 5 days old precultures. As controls, 10 µl of SMB without spores was used together with single inoculations of *N. crassa* 10^6 spores and *B. cinerea* 10^5 spores. Every plant was infected with a single type of inoculum by adding a single droplet of spore suspension per leaf.

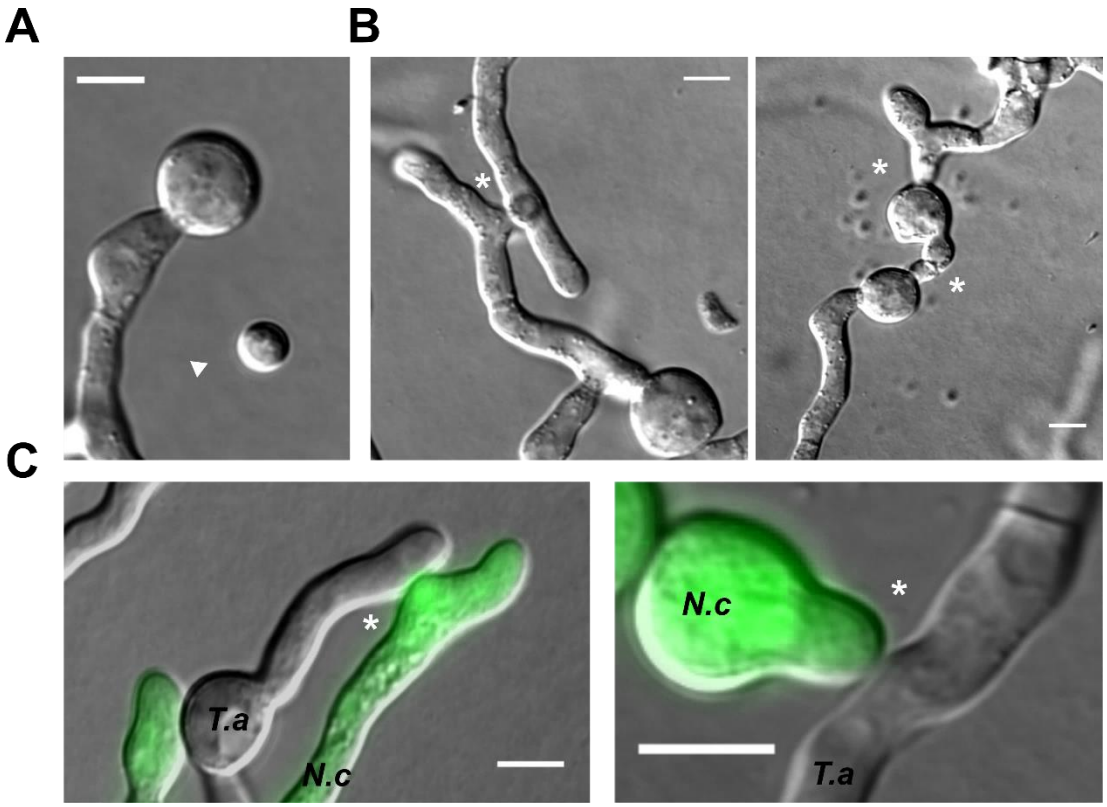

Figure 3.3.15. Cell fusion is observed between germlings of *T. atroviride*. (A) Spores swell during 12 hours until germination is observed. (B) Fusion was detected between germ tubes and between spores of *T. atroviride* cells. (C) Preliminary observation of potential interspecies interactions between *N. crassa* (GFP-labelled; *N.c*) and *T. atroviride* (unlabeled; *T.a*) spores. Scale bars of all images: 5 µm.

For the experiment shown, 16 plants (with an average of 8 leaves per plant) were tested per inoculum/condition (SMB control, *N. crassa* alone, *B. cinerea* alone and mix of both fungal species). Plants were incubated for 3 days at room temperature under natural light. To quantify the effect of the fungus on the plant, the number of inoculated leaves, that presented a damaged area were counted. As expected, we observed that while the control and the single inoculation of *N. crassa* did not have any negative effect on the plant, the inoculation with *B. cinerea* resulted in infection in almost all tested leaves. Surprisingly, the mix of *N. crassa* and *B. cinerea* had a significant impact on the virulence of *B. cinerea* which is observed by a lower number of leaves which showed lesions (Fig. 3.3.14A). Closer observation of the leaves revealed that while *B. cinerea* cells produced the usual lesion at the tissue, the mixed inoculum did not produce a clear lesion and, in general, leaves were healthier (Fig. 3.3.14B). Interestingly, we also observed that *N. crassa* germinated on the leaves and even established a colony and formed aerial hyphae without inducing any visible plant defense reactions (Fig. 3.3.14B).

These data provide a very first and preliminary hint supporting the hypothesis, that fusion signals produced by *N. crassa* placed over the leaf surface modulate the cell fusion program of *B. cinerea* which therefore excludes the activation of the infection program. Furthermore, we had observed in preliminary experiments that when *B. cinerea* spores are mixed together with *N. crassa* spores in an onion epidermis layer, cell fusion is observed between the *B. cinerea* spores, and the virulence program seems to be not activated (supplementary section 9.26). We can, however, not exclude potential secondary effects produced by the presence of both fungi at the leaf surface, such as competition, nutrition starvation, unknown non-fusion related signals, etc., which need to be addressed in further experiments.

3.3.14 Cell fusion and network formation is part of colony establishment in the mycoparasite fungus Trichoderma atroviride

As we have already shown, fungal interspecies interactions occurring between *B. cinerea* and *N. crassa* are mediated through the cell fusion process. Apparently, these interactions seem to be harmless for both cells of the two species in our laboratory conditions. Interestingly, there is a special type of naturally occurring fungal interspecies interactions in which one fungus parasite another one in nature, and is known as mycoparasitism. Therefore, it would be very interesting to test if these fungal interactions are also mediated through the cell fusion process. To investigate it, we decided to first observe whether a mycoparasite fungus such as *Trichoderma atroviride* undergoes cell fusion. This fungus is typically found in the soil and several strains have been developed as biocontrol agents. The strain CBS101525 was purchased from the Westerdijk institute (from the CBS-KNAW collection) and incubated for 7 days at 30ºC in darkness and 3 days at room temperature under natural light. Fresh spores were harvested and inoculated in MM plates.

Interestingly, spores were small and needed an incubation of at least 12 hours for swelling and germination (Fig. 3.3.15A). Once the spores germinated, cell fusion was readily observed within the spore population and networks were established between the cells (Fig. 3.3.15B). As a preliminary experiment, we decided to investigate whether *N. crassa* and *T. atroviride* would undergo cellular mutual interactions, just as we showed between *B. cinerea* and *N. crassa*. Spores of *T. atroviride* were harvested from MM plates previously incubated for 10 days (7 days dark, 3 days natural light; RT), inoculated in MM plates and incubated for 12 hours at 30ºC. Afterwards, *N. crassa* spores of strain 665 (*Ptef-1-mak-2*-gfp) were added to the same MM plate and incubated for 3 hours at 30ºC. As a very preliminary result, we had observed that *N. crassa* can grow towards *T. atroviride* and establish physical contact (3.3.15C). In future experiments, the roles of MAK-2, its localization and its functions need to be addressed to understand whether mycoparasitism has potentially evolved and made use of the cell fusion machinery to detect another fungal species in nature.

Together, all the data present in this chapter show that the cell fusion machinery which involves the alternating oscillatory recruitment of MAK-2 and SO is conserved in the plant pathogenic fungus *B. cinerea*. In addition, we also show that *N. crassa* cells can modulate the decision-making behavior of *B. cinerea* when their spores are encountered in a plant surface, preventing the virulence of *B. cinerea* by promoting its cell fusion program. Our data also suggest that the conservation of the cell dialog process might be part of some opportunistic life styles behavior found in nature, such as mycoparasitism.

DISCUSSION

4 Discussion

4.1 MAK-2 dynamics are essential for the cell fusion process

Membrane-tethering of MAK-2 triggers its phosphorylation but results in a loss of function. It is well established that MAPK translocate into the nucleus after their activation, where they phosphorylate transcriptional factors resulting in appropriate transcriptional responses to the specific extracellular stimulus (Brunet et al., 1999; van Drogen et al., 2001; Van Drogen and Peter, 2001). MAK-2 phosphorylation targets include the transcriptional factors PP-1 and RCM, which are needed for the initiation of the cell fusion program (Aldabbous et al., 2010; Jonkers et al., 2014; Li et al., 2005). Prevention of the nuclear translocation of the protein by membrane tethering therefore prevents the interaction of MAK-2 with its nuclear targets resulting in cell fusion deficiency, although protein activation is intact. In contrast, in *S cerevisiae*, nuclear arrest of the MAPK Fus3 prevents membrane recruitment of the protein in response to pheromone, which reduces MAPK activation and diminishes all responses related to mating (Chen et al., 2010). Together these findings support the idea that the fine-tuned subcellular MAPK dynamics, either in response to the pheromone in yeast or during cell fusion in *N. crassa*, are essential for proper transduction of the input signal through the MAPK cascade.

In yeast, it is well known that the MAPK module is recruited to the plasma membrane in response to pheromone reception. There, the three-tiered MAP kinase phosphorylation cascade induces phosphorylation of the MAPK Fus3, which subsequently phosphorylates the scaffolding protein Ste5 thereby promoting complex disassembly. This allows the MAPK to be translocated into the nucleus where transcriptional factors related to mating are activated and the appropriate transcriptional response is mediated (Merlini et al., 2013; Van Drogen and Peter, 2001). In *N. crassa*, HAM-5 serves as the scaffold for the complex formed by the MAP3K NRC-1, MAP2K MEK-2, and the MAPK MAK-2 (Dettmann et al., 2014, 2012; Jonkers et al., 2014).

Interestingly, MAK-2 also phosphorylates HAM-5 (similarly to the yeast MAPK Fus3 and the scaffold protein Ste5), but so far, the consequences of this phosphorylation remain elusive. Jonkers et al. hypothesize that the phosphorylation of HAM-5 also results in disassembly of the MAPK complex (Jonkers et al., 2014). In our experiments, we created an analog-sensitive variant of MAK-2 linked to GFP, that showed full complementation of the Δ*mak-2* fusion deficiency phenotype and allowed us to analyze the dynamics of the protein after activity inhibition. It is important to highlight that in these experiments phosphorylation of MAK-2 remains intact, and only its activity towards its phosphorylation targets is affected. Upon MAPK inhibition, MAK-2 remains stable at the plasma membrane for long periods of time (>40 mins), which strongly suggests that MAK-2 activity is also essential for the dynamics of the protein. These findings support a model, in which, similar to Fus3 dynamics in budding yeast, MAK-2 phosphorylates HAM-5. As a consequence, the complex disassociates and MAK-2 is released in order to be translocated to the nucleus, where transcriptional factors related to the cell fusion program are activated. At the same time, disassembly of the membrane associated complex might terminate further MAK-2 activation, therefore representing a negative regulatory feedback loop. In future studies it will be necessary to analyze the dynamics of the remaining components of the MAK-2 complex (HAM-5, NRC-1 and MEK-2) after MAK-2 inhibition to test whether similar observations are made. Interestingly, when MEK-2 is tethered to the plasma membrane (as a MEK-2-GFP-CAAX construct) it still allowed partial functioning of the cell fusion process, although in a drastically reduced manner, suggesting that only MAK-2 needs to translocate from the plasma membrane to the nucleus during the cell fusion process (Illgen, 2017; Serrano et al., 2018). However, this finding contrasts with a report on *Aspergillus nidulans*, in which the whole kinase module complex translocates together to the nuclear envelope (Bayram et al., 2012). It will therefore be of great interest to determine the function and dynamics of the upstream components of the MAK-2 kinase complex and their function at different developmental stages.

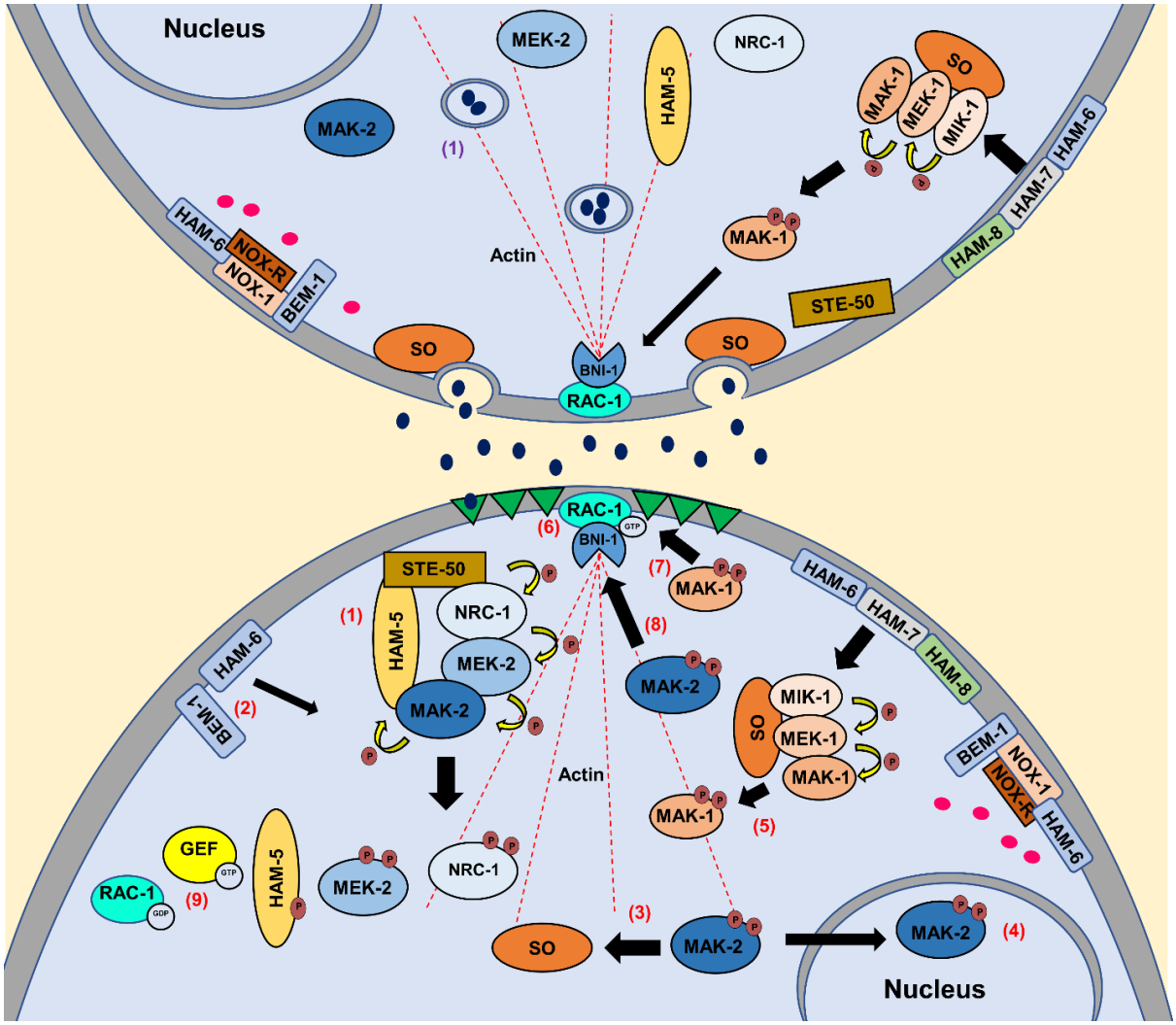

Figure 4.1. Model of cell signaling during cell-cell fusion. The upper cell represents the sending of the signal state. (1) The unknown fusion signals are secreted to the extracellular environment potentially associated with the SO protein. The bottom cell represents the receiving of the signal state. (1) Upon reception of the fusion signal, the HAM-5, NRC-1, MEK-2 and MAK-2 proteins form a complex associated with the membrane-tethered STE-50. Membrane recruitment of the complex induces MAK-2 phosphorylation. Once activated, MAK-2 phosphorylates HAM-5, which induces the complex disassociation. (2) The proteins BEM-1 and HAM-6 promote MAK-2 phosphorylation, independently of the NOX complex. (3) After activation, MAK-2 activity prevents SO membrane recruitment; the protein remains cytoplasmic. (4) Activation of MAK-2 allows its nuclear accumulation, where transcription factors that are fusion-related are activated, such as PP-1. **(Continue next page.)**

(5) The second role of SO is to function as a scaffolding protein to promote MAK-1 phosphorylation. This activation might occur through the fusion-related sensors HAM-6, HAM-7 and HAM-8. **(6)** The Rho-GTPase RAC-1 accumulates at sterol-rich domains after activation. This activation promotes conformational changes in the formin (BNI-1) that allows actin polymerization. **(7)** MAK-1 activity is essential to keep RAC-1 activated, allowing the tropic growth to the other interacting cell. **(8)** MAK-2 functions by locating the RAC-1 protein at the right position to mediate directed growth, probably depending on the direction of reception of the fusion signal. **(9)** RAC-1 activation depends on GEFs proteins, that promotes its membrane recruitment after GTP exchange.

Legend: **Fusion signals.** **Reactive oxygen species.** **Fusion receptor**

4.2 The membrane-tethering of MAK-2 results in hyper-phosphorylation of the protein

It is very interesting that the permanently membrane-tethered MAK-2 is hyper-phosphorylated even in conditions that do not promote cell fusion (hyphae in shaking liquid media), which suggests that its hyper-phosphorylation is somewhat independent of the cell fusion signals that usually trigger MAK-2 phosphorylation. This artificial phosphorylation might be caused by two opposite but not exclusive mechanisms. First, the membrane recruitment of the kinase might prevent the interaction of the protein with inactivating factors, such as phosphatases. In yeast, Fus3 activation is tightly controlled by the phosphatases Msg5, Ptp2 and Ptp3, which are located in the cytoplasm and the nucleus (Doi et al., 1994; Mattison and Ota, 2000). So far, these homologs have not been studied in *N. crassa*. Assuming similar localization patterns, membrane-recruitment could efficiently separate inactivating factors from their MAPK target. Indeed, the propagation of activated Fus3p from the yeast shmoo tip to the nucleus is spatially constrained by a gradient generated through inactivating phosphatases across the cytoplasm (Maeder et al., 2007), which supports our hypothesis that phosphatases have to be spatially separated from the plasma membrane. In future studies, the localization and roles of these inactivating-MAK-2 phosphatases in *N. crassa* need to be addressed. Second, membrane recruitment of MAK-2 might locally concentrate activating factors. In yeast, the Fus3 activating module is recruited to the plasma membrane upon pheromone reception,

which locally concentrates the complex together with its activating factors that leads to an increase in the signal intensity (Lamson et al., 2006). In addition, membrane recruitment of MAPK upon signal reception is essential to produce a proper output response (Harding et al., 2005). We hypothesize that similarly the local concentration of activating factors results in increased MAK-2 phosphorylation. So far, the identity and interaction of these activating factors remains unclear. There are, however, a number of factors, which have been discussed to potentially promote MAK-2 activation, such as the ROS generating NADHP oxidase 1 complex (Cano-domı et al., 2008, Roca, 2012), the Rho type GTPase RAC-1 (A. Lichius et al., 2014), the STE-50 NRC-1-adapter (Dettmann et al., 2014) or the CWI MAPK MAK-1 (Maddi et al., 2012).

Our experiments revealed, that the core components of the ROS generating system, NOR-1 and NOX-1, are not important for MAK-2 phosphorylation, which suggest that they function downstream or independent of MAK-2 (Fig. 4.1). Two more components have been shown to be part of the ROS generating system: BEM-1 and HAM-6 (Lacaze et al., 2015; Takemoto et al., 2011). Interestingly, the protein adapter BEM-1 and the transmembrane protein HAM-6 play an important role in MAK-2 phosphorylation, but independently of the ROS generating system. In yeast, Bem1 physically interacts with the Fus3 MAPK scaffold protein Ste5 and mediates the interaction between Ste5 and the membrane-bound protein Cdc24, which triggers the membrane recruitment of the kinase complex (Lyons et al., 1996). In *N. crassa*, BEM-1 is dispensable for general hyphal polarity, but essential for normal spore formation and for proper and robust MAK-2 recruitment during cell fusion (Schürg et al., 2012). Our data suggest that BEM-1 might play a similar role as the yeast Bem1, mediating the proper formation of the phosphorylation MAPK complex cascade, but not being involved in hyphal polarity establishment. In further experiments, the roles of these proteins and their function related to MAK-2 activation must be addressed. In contrast to BEM-1, HAM-6 has only been identified in filamentous fungi. In *Podospora anserina*, the HAM-6 homolog Nox-D, is part of the ROS generating system and functions in controlling the assembly of the ROS generating complex (Lacaze et al., 2015). In *N. crassa* HAM-6 (NoxD) is a predicted transmembrane protein that has been hypothesized to function together with another transmembrane protein, HAM-8 and the GPI-anchored cell wall protein, HAM-7, as a

complex for sensing extracellular signals that trigger activation of the MAPK CWI MAK-1 (Fu et al., 2014). We hypothesized that the reduction of MAK-2-GFP-CAAX phosphorylation in Δ*ham-6* was caused by a potential reduction in the phosphorylation of MAK-1, which would indicate a defect in the crosstalk between both MAP kinases. However, the phosphorylation of MAK-2 was not affected when MAK-1 was mutated, indicating that HAM-6 might function more directly as an upstream component of MAK-2 activation in a ROS generating system/MAK-1 sensor independent manner. It is now of great interest to test whether HAM-7 and HAM-8 also function upstream of MAK-2 and if they function, as hypothesized, as sensors of the cell fusion signal.

4.3 The dynamic localization SO is controlled by MAK-2 during tropic growth but is independent during the cell-cell merger phase.

In previous studies, Fleißner and colleagues showed that MAK-2 activity is essential for the proper release of SO from the plasma membrane during the cell communication phase. They hypothesized that MAK-2 activity controls SO release from the plasma membrane in wild-type cell-cell interactions (Fleissner et al., 2009). In our study, we made very similar observations when MAK-2^{Q100A} was inhibited and SO localization was tested. In addition, we observed that the permanent presence of MAK-2 at the plasma membrane only disrupts the dynamic SO localization, when the kinase is activated. These findings suggest an intricate regulation of SO recruitment through MAK-2 activation, in order to keep both proteins mutually excluded at the plasma membrane (Fig. 4.1). This process must be tightly controlled to establish the proper oscillatory switching of the cellular behavior. These data indicate that SO is probably always primed for membrane recruitment during the cellular communication, but the presence and activation of MAK-2 controls directly or indirectly a window of time when SO is located there. This hypothesis is supported by the data of chapter 4, where inhibition of either MAK-1 or MAK-2 leads to membrane recruitment of SO in both interacting partners, as if sending of the signal from the cells is always activated and only the presence of activated MAK-2 at the plasma membrane switches off this process. One unsolved issue in this hypothesis is that SO recruitment is only observed after the cellular communication phase has been initiated and it remains unclear how the cellular interaction is started.

Recently, a novel SO-interacting protein (short as SIP-1) was identified by co-immunoprecipitation combined with mass spectrometry (Schumann, 2018). The spatial dynamics of the protein are very similar to SO during cell-cell communication, but surprisingly, SIP-1 is also recruited to the cell tips of non-interacting cells in an oscillatory manner (Schumann, 2018). In the current working model, this protein is hypothesized to function in the controlled sending of signals waves into the extracellular environment in order to find fusion partners. Once a partner is detected, MAK-2 is activated which leads to the disappearance of SIP-1 from the plasma membrane. After MAK-2 is translocated to the nucleus, SIP-1, now together with SO, are recruited to the interacting tip. The protein SO therefore might play a role in the coordination of the cellular behavior, after the interaction has been initiated. To further test this model, SIP-1 localization must be tested after MAK-2 and MAK-1 inhibition. Furthermore, SIP-1 localization should be tested when MAK-2 is permanently tethered to the plasma membrane in non-interacting cells.

A striking observation are the different SO behaviors during the different stages of the cell fusion process. The protein SO has previously been hypothesized to play different roles at these different stages. For example, SO has been shown to serve as a scaffolding protein of the CWI MAPK pathway (Teichert et al., 2014), however, MAK-1 is not observed at the cell tips of the interacting cells and is only recruited once the cells establish physical contact (Weichert et al., 2016). These observations suggest that SO plays at least two different roles: one function, which is independent of the CWI pathway, during the cellular communication phase and a second function after the cells have established physical contact potentially by mediating the recruitment of MAK-1 to the contact area (Fig. 4.1). Permanent membrane tethering of MAK-2 results in a complete deletion of the cell fusion process. However, when MAK-2 is membrane-tethered in a wild-type background (with the wild-type *mak-2* locus intact), the cell fusion rate is significantly reduced but still observed. In these cell-cell interactions, SO is not recruited during the communication phase and only MAK-2 is artificially and permanent present at the plasma membrane while the cells grow towards each other.

However, SO is still recruited once the cells establish physical contact, indicating that the regulation of SO recruitment to the plasma membrane differs before and after cell-cell contact, indicating the presence of these two different functions of SO during the whole cell fusion process.

Interestingly, after cell-cell contact, SO co-localizes for a certain time with MAK-2 at the cell-cell contact area. The importance of MAK-2 at the cell-cell merger phase had not been elucidated until now. We show that MAK-2 activity is also essential at this phase, although the membrane recruitment in this phase is completely independent of the phosphorylation state of the kinase. Important observations have been made for the phospho-negative variants of MAK-2. All of them were not properly recruited to the plasma membrane during the cell communication phase, but their recruitment was very obvious after the cells established physical contact, indicating that the translocation to the fusion point is independent of the phosphorylation state of the kinase. Additionally, MAK-2 is even recruited to the contact area after inhibition of its activity. This is in contrast to the second MAP kinase MAK-1, whose activity is essential for its recruitment to the plasma membrane at this phase (Weichert et al., 2016). These findings suggest that a completely different regulatory program is initiated by cell-cell contact, when SO, MAK-1, and MAK-2 are recruited among other proteins to the contact area and the forming fusion pore. The switch of the cellular behavior after cell contact is probably controlled by the MAPK MAK-1, as it has been shown in a previous study that its activity is essential for the transition from tropic growth to cell-cell merger (Weichert et al., 2016). To further characterize this behavioral switch induced by physical cell-cell contact, future studies could aim to identify targets of MAK-1 but also the upstream regulators involved in the recognition of cell-cell contact.

4.4 MAK-1 plays different roles in CWI regulation and cell fusion

The central and well-described role of the CWI-signaling pathway is to detect and respond to cell wall stresses that arise in the vegetative life cycle of fungi. In yeast, activation of this pathway is well understood and has been reviewed several times (Alonso-monge, 2010; De Nobel et al., 2000; Levin, 2011).

In filamentous fungi, activation of the pathway is mediated by a group of sensor proteins named as WSC (cell wall integrity and stress-response component). These glycosylated transmembrane proteins sense morphological changes induced by cell growth or cell wall stresses. The signal is transduced to the MAPK cascade by the small Rho-GTPase RhoA and the protein kinase C (PkcA). This activation yields a fully phosphorylated MpkA MAPK (homolog to MAK-1) that further activates transcriptional factors mediating the appropriate cellular responses (Yoshimi et al., 2016). In *N. crassa*, WSC-1 and its homolog WSC-2 activate the cell wall integrity MAK-1 MAP kinase pathway when the cell wall is stressed.

Deletion of both genes (*wsc-1* and *wsc-2*) results in strong morphological defects during vegetative growth and colony formation (Maddi et al., 2012), which is very similar to the observations made in the different mutants of the CWI MAP kinase MAK-1 pathway (Maerz et al., 2008; Park et al., 2008; Vogt and Seiler, 2008). In addition to these defects in cell wall stress response, mutation of every component of the MAK-1 MAP kinase module also results in a cell fusion-defective phenotype (Fu et al., 2011). However, while the kinases are essential to undergo cell fusion, WSC-1 and WSC-2 are dispensable for this process, indicating that for the cell fusion process MAK-1 is activated independently of the CWI pathway (Maddi et al., 2012).

Another upstream activator of MAK-1 is the HAM-7 protein. HAM-7 is a GPI-anchored cell wall protein that is required for activation of MAK-1 (Maddi et al., 2012). Together with HAM-7, the proteins HAM-6 and HAM-8 are hypothesized to work together in a complex as a sensor of signals to trigger MAK-1 phosphorylation (Fu et al., 2014). Mutation of either *ham-6*, *ham-7* or *ham-8* results in a cell fusion defective phenotype, therefore suggesting that its function might be related to activation of MAK-1 for cell fusion purposes. All these clearly suggest and support the idea that MAK-1 is activated by two different set of sensors: the WSC complex that mediates the signals related to the cell wall stresses and the HAM-6/HAM-7/HAM-8 sensor which is more associated to the signals coming from the cell fusion process.

4.5 MAK-1 functions in all of the three main cell fusion steps: competence, signaling and pore formation

As shown before, cell fusion comprises several independent steps: first the cells need to acquire a cell fusion competence. Second, the cells recognize the presence of other cells and start the tropic including the membrane recruitment of MAK-2 and SO. Third, the cells establish physical contact, their growth is arrested and the cell wall is remodeled in order to allow the subsequent fusion of the plasma membranes of both interacting cells. Before this thesis, MAK-1 had been shown to play potential functions during competence and pore formation. It is known that the mutation of *mak-1* results in a cell fusion defective phenotype, in which cells fail to initiate interactions (Maerz et al., 2008), indicating that the cells need *mak-1* in order to start the cell fusion process. This also suggests that MAK-1 plays a role in the activation of different factors that allow the acquisition of the competence state by the cell.

One of these potential factors might be the Rho-GTPase RAC-1. As it has been previously shown, mutation of *rac-1* also leads to a fusion defective phenotype and its inhibition results in the loss of the ability of the cells to undergo cell fusion (Alexander Lichius et al., 2014). Our experiments revealed that inhibition of MAK-1 results in inactivation of RAC-1 and the failure of the cells to initiate interactions. We therefore hypothesize that an active version of RAC-1 is needed to establish the cell fusion competence in the cell. This activation is probably mediated by MAK-1. One way to test if a mutant is blocked in the cell fusion competence state is to analyze its ability to form CATs. For example, the mutation of *so* results in spores that are fusion defective, but are still able to form CATs in the presence of wild-type cells, suggesting that the cells are still fusion competent but unable to undergo the subsequent communication process and directed growth (Fleißner et al., 2005). To analyze whether RAC-1 is also affected in this state, a mix of Δ*rac-1* and wild-type spores should be analyzed by light microscopy to observe whether CATs are formed. RAC-1 inhibition studies could also be performed, by mixing of inhibited and uninhibited wild-type cells. These experiments would elucidate whether RAC-1 is essential for cell fusion competence and would also help to solve the implications of MAK-1 to this process.

As previously mentioned, MAK-1 also plays a role after the cells have established physical contact, specifically in growth arrest and fusion pore formation. During the communication phase, when MAK-2 and SO are dynamically recruited to the tips of the interacting cells, MAK-1 remains cytoplasmic. The protein is only localized to the contact area of the cells after establishment of cell-cell contact, once cell growth is arrested and fusion pore is being formed (Weichert et al., 2016). Interestingly, partial inhibition of MAK-1 which still allows fusion competence and the tropic cell-cell interaction, results in a unique phenotype, in which the interaction partners fail to arrest growth after cell-cell contact and twist around each other.

Together these observations suggest a role of MAK-1 in the recognition of cell-cell contact and subsequent growth arrest. (Weichert et al., 2016). A similar failure in cell growth arrest is observed in the Δ*erg-2* strain. The *erg-2* (*ergosterol-2*) gene encodes a sterol reductase, which mediates the last step of the ergosterol biosynthesis in *N. crassa*. In this mutant, MAK-1 is not recruited to the contact area and the twisted phenotype is also observed. Both defects are cause by the accumulation of a specific ergosterol precursor (Weichert et al., 2016). Interestingly, a potential connection between MAK-1 partial inhibition and membrane sterol composition is the Rho GTPase RAC-1. We have shown that MAK-1 is controlling the activation of RAC-1 (Fig. 4.1). In addition, the membrane recruitment of Rho GTPases is dependent of the proper accumulation and synthesis of sterol-rich membrane (SRM) domains which are defined by the sterol composition of the membrane (Makushok et al., 2016). This suggest that the defects reported in the sterol-biosynthesis mutant (Δ*erg-2*) (Weichert et al. 2016), could be caused by defects in the composition and formation of the SRM domains, which may partially affect the proper localization and likely activation of the Rho-GTPase RAC-1. It will also explain why partial inhibition of MAK-1, which we can assume also cause partial inhibition of RAC-1, produced a similar phenotype. In future studies, it will be of great interest to observe whether the localization of activated RAC-1 (CRIB reporter) is affected in the Δ*erg-2* strain. Furthermore, localization of activated RAC-1 should also be studied after partial MAK-1 inhibition.

4.6 MAK-1 is essential for maintenance of the directed growth machinery while MAK-2 controls the direction of the growth

As discussed above, MAK-1 possesses functions during two of the cell communication steps: fusion competence and growth arrest after cell-cell contact. Data of this thesis show for the first time that, in addition, MAK-1 also plays a role during the phase of cell-cell signaling and directed growth.

Specific inhibition of MAK-1 during this stage of the fusion process revealed that the kinase is essential for the maintenance of an actin cluster formed by actin filaments at the growing cell tips. This function seems to be again linked to the small Rho-type GTPase RAC-1, whose inhibition results in a comparable disintegration of the actin aster, suggesting that both factors function in the same pathway. Localization of activated RAC-1 (visualized by the CRIB reporter) at the cell tip also required MAK-1 activity, suggesting that MAK-1 functions upstream of RAC-1.

While the role of RAC-1 and MAK-1 in maintenance of the actin cluster is now established, the factor(s) linking MAK-1 activity to actin assembly remain still unknown. In yeast mating, pheromone reception induces Fus3 (the MAK-2 homolog) activation, which phosphorylates the formin Bni1 to control actin polymerization and shmoo growth towards the mating partner (Matheos et al., 2004). Consistent with our finding that in *N. crassa* not the *fus-3* homologous MAK-2 but MAK-1 is essential for the maintenance of the actin aster, the only formin of this fungus, BNI-1 is also not phosphorylated by MAK-2 (Jonkers et al., 2014). We therefore hypothesize, that in *N. crassa* MAK-1 is playing the role of *fus-3* of yeast in directed growth. To test this hypothesis, future experiments will have to establish if BNI-1 is a direct target of MAK-1. Together these observations suggest that within conserved signaling networks individual factors can adopt different roles, and specific functions can be exchanged between conserved factors. Given sets of proteins can therefore be specifically rewired to serve the specific needs of individual species.

Our testing of the specific function of the *fus-3* homolog MAK-2 in *N. crassa* cell fusion revealed that the kinase is essential for the correct positioning of the actin cluster within the cell.

Consistent with our hypothesis that MAK-1 and RAC-1 function in the same pathway organizing the structure of this aster (see above) also the position of RAC-1 becomes instable after MAK-2 inhibition (Fig. 4.1). Future experiments should co-localize actin, BNI-1, RAC-1 and MAK-1 after MAK-2 inhibition. If our hypothesis is correct, all factors should co-localize in the same instable fashion after MAK-2 inhibition (meaning they should all move around together in the inhibited cell).

A major unanswered question is how MAK-2 is positioning the actin cluster at the proper position in the cell, thereby controlling growth directionality. We hypothesize that MAK-2 is directly involved in the translocation of the cell-cell communication signal and is therefore marking the position of highest signal intensity. Unfortunately, so far this signal and its cognate receptor remain unknown. Common candidates, such as G-Protein coupled receptors or histidine kinases could be excluded (Fleißner and Serrano, 2015). Future experiments should therefore aim to identify the signal, the upstream activators of MAK-2, and MAK-2 targets involved in positioning the actin cluster.

4.7 B. cinerea and N. crassa exhibit different behavior during colony establishment

Vegetative cell fusion between genetically identical cells is not exclusive to *N. crassa*. Many different filamentous fungal species exhibit germling and hyphal fusion and different authors have proposed the potential conservation of the signaling process that was firstly described in *N. crassa* (Fleißner and Serrano, 2015; Glass et al., 2004; Leeder et al., 2011). While germling fusion is common, cell merger can occur at different developmental stages in the different fungi. For example, spores of *N. crassa* germinate quickly after exposure to nutrients, and fusion is induced briefly after germination. The cells cooperate to form a network, which probably enhances survival of the spore population and promotes competitiveness against other organisms in the environment. In *B. cinerea* conidia germinate within a similar time range as *N. crassa* (2-4 hours), however fusion-related interactions are not observed until at least 10 hours. This suggests that the onset of cell fusion competence is delayed in *B. cinerea*.

These observed differences are probably due to the specific environments, in which the two fungi are found in nature. *N. crassa* is considered to grow as a saprophyte, and is mostly found on burned vegetation after forest fires. Recently, however, it has also been described as a potential endophyte of Scots pine, which would explain its occurrence as a first colonizer of burned pine trees (Kuo et al., 2014). Colony formation on burned vegetation is most likely initiated by sexual ascospores, which become activated by heat and chemicals present in burnt wood.

So far, the role of vegetative spores in the endophytic life style is not understood. During the saprophytic colonization of dead organic material by vegetative spores, however, germling fusion appears advantageous. If the germlings would not fuse, they would produce numerous clonal individuals, which would compete with each other for space and nutrients. In contrast, *B. cinerea* is a necrotrophic fungus, which attacks the plants and kills the host cells before feeding on the dead plant material. This suggests that *B. cinerea* cells first infect the plant in order to make the nutrients from the dead cells available as soon as possible to avoid plant defense reactions. Only after the infection is established and the nutrients are available, cells cooperate to share and form the network through cell fusion within the plant tissue. Consistent with this hypothesis, germling fusion is fully suppressed during growth on plant surfaces (Roca et al. 2012). This behavior might have evolved by natural selection, such that the faster the fungus infects the host the higher are the chances for survival. In future studies, the roles of cell fusion for the necrotrophic fungus *B. cinerea* in natural environments need to be addressed in order to understand its implication on plant infection and its potential role in the fungal life cycle.

4.8 Cell fusion is not essential for infectious growth of B. cinerea

In our study, we show that the mutation of the *N. crassa so*-homolog in *B. cinerea*, *bcso*, results in disruption of the cell fusion process. In other fungi, cell fusion and pathogenicity are highly related. For example, mutation of *so* in *A. brassisicola* results in deficiencies in the infection process (Craven et al., 2008). Interestingly, in the plant-endophytic fungus *E. festucae*, mutation of the *so*-homolog leads to disruption of the symbiotic growth, resulting in a surprising pathogenic behavior of the fungus on the host plant (Charlton et al., 2012).

In contrast, however, deletion of *fso* in *F. oxysporum* did not have any effect in pathogenicity. (Prados Rosales and Di Pietro, 2008). In *N. crassa*, the mutation of *so* produces a very pleiotropic phenotype, which indicates that the protein might play a role in many different processes. Therefore, defects in cell fusion and pathogenicity cannot simply be directly correlated in pathogenic fungi, such that the lack of fusion and the suppression of pathogenicity might also represent different, independent functions of the SO protein.

In *B. cinerea*, disruption of the cell fusion process by mutation of *bcso* did not have any effect on the infection process within the first three days after inoculation. As mentioned above an earlier study revealed that during spore germination on hydrophobic plant surfaces, cell-cell fusion is suppressed in *Botrytis cinerea* (Roca et al. 2012), indicating that fusion is dispensable before entering of the host plant. However, infection of a plant does not take place in only three days.

Although no effects in the *bcso* mutant strain become apparent under laboratory conditions, it could be different in nature. For example, the *F. oxysporum f. sp. Lycopersici* infection of tomato plants requires at least 16 days to observe the full virulence of the fungus. Indeed, although mutation of *fso* (homolog to *bcso*) does not affect the ability to infect the plant, it disrupts the hyphal network usually formed by the wild-type strain around the plant root. This network protects the fungus from being removed, and is not formed in cell fusion mutants. This suggests that cell fusion might have a more significant impact in pathogenicity of *F. oxysporum* in nature, but is dispensable under laboratory conditions. Similar defects could also be envisioned for the Δ*bcso* mutant. While pathogenicity at the early stages is wild-type like, longer incubation times in future experiments might reveal important functions of cell fusion, for example in redistributing the nutrients within the hyphal network inside the plant or in response to the plant defenses reactions induced by the fungal pathogen.

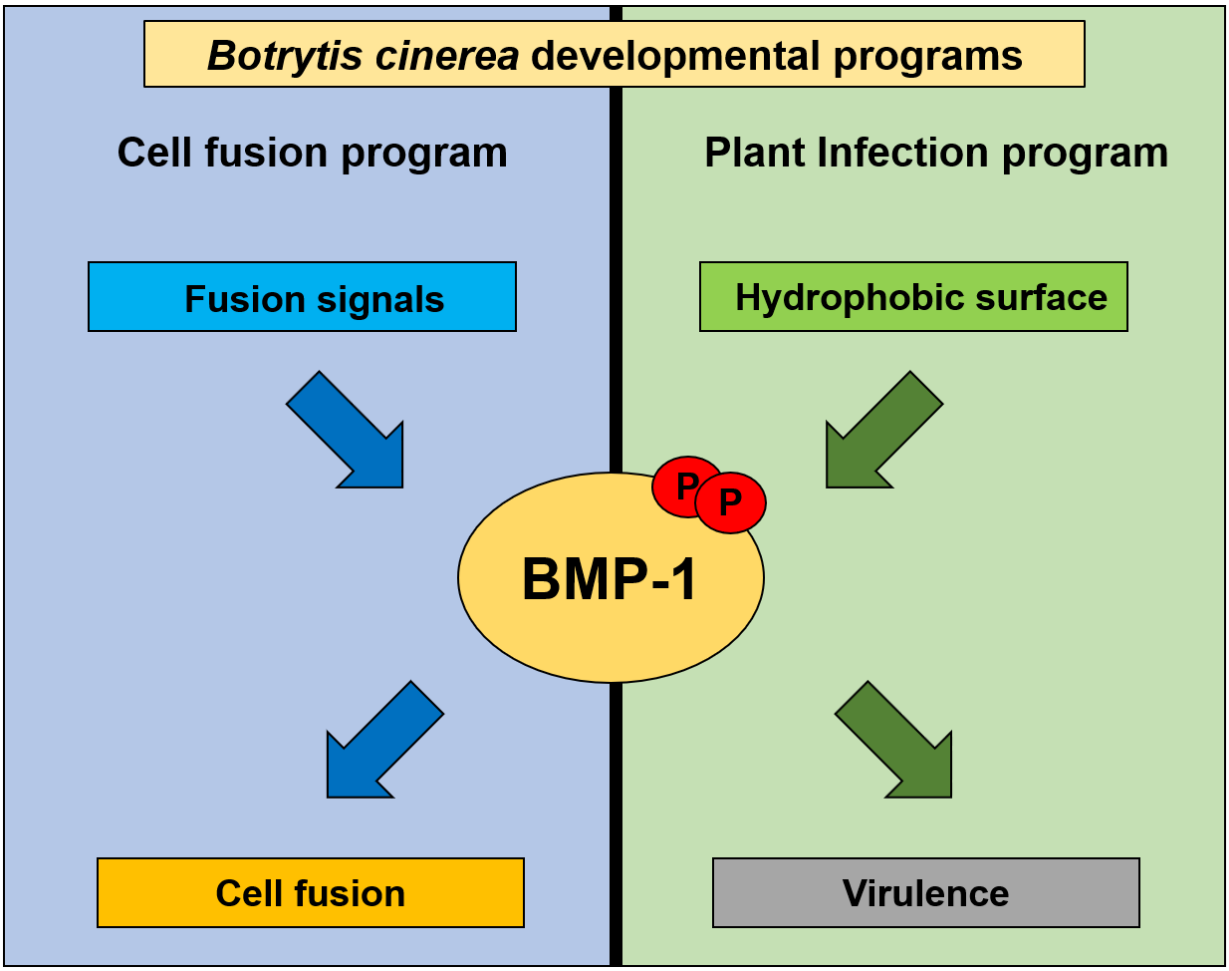

Figure 4.2. Decision making of *B. cinerea* cells when exposed to two different stimuli. Two different stimuli trigger different responses through the same protein, the MAPK BMP-1. The sense of a hydrophobic surface triggers activation of BMP-1 which activates transcriptional factors related to the virulence program of the fungus. In contrast, fusion signals or hydrophilic surfaces activate BMP-1, which therefore activates transcriptional factors that develop the cell fusion program. Both developmental programs are therefore mutually exclusive.

4.9 B. cinerea and N. crassa share a common molecular language

Although germling fusion in *B. cinerea* occurs later after germination than in *N. crassa*, the fusion process itself is very similar in both fungi and involves the following steps: fusion competence, tropic growth, growth arrest, cell wall remodeling and membrane fusion. Also molecular factors, which are essential for cell fusion in *N. crassa,* are also necessary for germling fusion in *B. cinerea,* such as an ROS generating NADPH oxidase complex (Roca et al., 2012).

This highlights already the potential conservation of the signal machinery mediating cell fusion in both fungi. In addition, we report the high conservation in the amino acid sequences of the MAPKs MAK-2 and BMP-1, and the conservation between the C-terminal regions of SO and the now named BcSO. The localization of both *B. cinerea* proteins during cell fusion revealed a dynamic oscillatory and alternating membrane recruitment to the cell tips of the interacting cells, which shares high similarity with MAK-2/SO dynamics in *N. crassa*. Surprisingly, we observed that when *N. crassa* and *B. cinerea* were mixed at the time when cell fusion is usually induced, interactions between both fungi occurred. All these data clearly suggest that the cell dialog mechanism as well as the so far unknown signal and receptor mediating this cellular interaction are conserved between these two divergent fungal species.

In our experiments, we observed that both species undergo cell-cell interactions, which however always halted after physical contact was established. Successful interspecies fusions were never detected. This observation suggests, that while the proposed signal and receptor are conserved, regulatory mechanisms have evolved, that prevent interspecies cell fusion. Recently, the molecular basis of a regulatory mechanism, which suppresses cell-cell interactions even in the presence of the conserved signal and receptor has been identified in *N. crassa* (Heller et al., 2016). In a collection of 110 wild isolates of *N. crassa,* different communication groups were identified, such that germlings within one communication group interacted at high frequency, while germlings from different communication groups avoided each other. Bulk segregant analysis together with whole genome sequencing identified three linked genes (*doc-1*, *doc-2*, and *doc-3*), which were associated with the specific communication groups. Interestingly, by simply exchanging *doc-1* and *doc-2* alleles from different communication groups, strains changed their communication group affiliation, indicating that the three genes function as greenbeard genes. These genes are therefore involved in mediating long-distance kind recognition and regulate the cooperation between non-genealogical relatives, like for example different species (Heller et al., 2016). Blast search analysis revealed that *B. cinerea* does not possess homologs of the *doc* genes, which could explain the fact that *B. cinerea* and *N. crassa* could undergo cellular interactions. Additional layers of regulation might exist that prevent fusion between these two species.

This hypothetical regulation would prevent the exchange of DNA between different species. This process is also known as horizontal gene transfer (HGT). HGT is defined as the stable integration of genetic material originated in different species. This process plays a crucial role in the adaptation of organisms to the changing environments. In the fungal kingdom, there are many different examples of genes homologies that might be explained by HGT. For example, it has been reported that at least 90 genes involved in pathogenicity have been transferred between plant pathogenic *Magnaporthales* and *Colletotrichum* species (Qiu et al., 2016). Several other examples of genes that likely were acquired through HGT are described elsewhere (Fitzpatrick, 2012; Mehrabi et al., 2011).

The main hypothesis that explain how this HGT occurs in nature is based on DNA uptake from the environment. However, in the literature some reports of interspecies interactions that might be mediated by the cell fusion machinery exist. For example, an earlier study already reported potential interactions between closely related different fungal species or incompatible strains. They reported that the mix of different vegetative compatible and incompatible spores of different wild-type isolates of *C. lindemuthianum* form a network through cell fusion without inducing the typical incompatibility response (Ishikawa et al., 2012). Indeed, another report showed that cell fusion interactions have been even observed between two different fungal species, such as *C. lindemuthianum* and *Colletotrichum gossypii* (Roca et al., 2004). In this study, spores from both species were mixed and cell fusion between both species was observed. The most interesting part of this study is the report of a potential exchange of DNA between the two species (HGT). After mixing spores from the *C. gossypii* strain and the *C. lindemuthianum* strain, the occurrence of potential hybrids was observed. These hybrids shared features of both parental strains and were hygromycin resistant (Roca et al., 2004). Although all of these data suggest that the exchange of DNA was performed through cell fusion, it could also be that one of the fungal isolates simply took up DNA, which was released into the environment from the other species. Further analyses of the experiment including fusion incompetent isolates should be performed to elucidate which is the cause of the DNA transmission.

Based on our data and the already mentioned report of interspecies cell fusion of *Colletotrichum spp*. (Ishikawa et al., 2012; Roca et al., 2004), it appears possible that cell fusion might play a role in HGT. In future studies, it will be of great interest to investigate this potential role. For example, the study of the interspecies interactions (between *N. crassa* and *B. cinerea*) under different conditions (starvation, antibiotic pressure, etc.,) could improve our understanding on this topic. In addition, the mixing of closely and further related species would be a good approach to determine how conserved the cell fusion signals are and how commonly interspecies interactions occur.

4.10 Fusion signals might modulate the pathogenic behavior of B. cinerea

B. cinerea is a plant pathogenic fungus which needs the MAP kinase BMP-1 for the infection process (Zheng et al., 2000). Specifically, this MAP kinase is essential for sensing of the hydrophobic surface where the spore is landing (Doehlemann et al., 2006). Pathogenic behavior of the fungus is not observed during growth on the hydrophilic surface of an onion epidermal layer, which, however, it still plant material (Roca et al., 2012). This suggests that the plant-infection program is induced by hydrophobic surfaces, independent of nutrients or other plant signals. Interestingly, we have shown that BMP-1 is also essential for cell fusion. Moreover, cell fusion of *B. cinerea* is not observed in hydrophobic surfaces (Roca et al., 2012). Together these data suggest that BMP-1 is a key MAPK for regulating both infection and cell fusion, which appear to be two mutually exclusive developmental routes (Fig. 4.2). In contrast, *N. crassa* undergoes cell fusion on both hydrophobic and hydrophilic surfaces, even on the top of leaves (Weichert, 2016). Since *N. crassa* and *B. cinerea* share a common molecular language, we hypothesized that fusion signals produced by *N. crassa* could potentially induce fusion in *B. cinerea* even during growth on the plant surface and might therefore reprogram the fungus from infection to fusion. In our experiments, we observed as expected that while the inoculation of *B. cinerea* spores alone at the leave surface produced the usual infection area as a result of the virulence of the fungus, *N. crassa* did not produce any observable response while growing on the plant surface. As we hypothesized, the mix of both fungal strains did, however, result in reduced infection symptoms, suggesting that the cell fusion program of *B. cinerea* was triggered by the fusion signals produced of *N. crassa*.

While this observation in general supported the initial idea, different alternative hypotheses could also explain these preliminary observations. For example, the presence of *N. crassa* might fully suppress the growth of *B. cinerea*. In a preliminary experiment, however, in which spores from both fungal species were mixed on the hydrophobic surface of an onion layer, we observed that germination of *B. cinerea* was unaffected (Supplementary figure 9.26). The growth of *N. crassa* and the related nutrient uptake might, however, induce starvation in *B. cinerea*. Earlier studies showed that a positive correlation between fusion frequency and starvation exists in many fungi including *B. cinerea* (Roca et al. 2012).

In this case fusion would be induced by the presence of the other fungus, however, not by a direct reprogramming through the fusion signal. These issues have to be addressed in future studies. Unfortunately, the nature of the fusion signal remains so far elusive. Identification of the signal would be extremely useful for answering the question if *B. cinerea* can be reprogrammed from infection to fusion. The idea of reprogramming pathogenic fungi instead of killing or inhibiting them, would represent a novel and very attractive new concept of controlling fungi.

4.11 Mycoparasitism: a novel view on the origin of this fungal life style

Mycoparasitism is a form of antagonistic relationship between a fungal parasite and a fungal host. There are two distinct modes of mycoparasitism: biotrophic, in which the host is not severely harmed, for example between *Verticillium biguttatum* on *Rhizoctonia solani* (Van Den Boogert and Deacon, 1994), and necrotrophic, in which the host is killed and the parasite feeds on the dead fungal material. There are several reported mycoparasitic fungal species (Barnett, 1963; Jeffries, 1995; Viterbo and Horwitz, 2010), but the mostly studied species belong to the genus *Trichoderma*. In our study, preliminary experiments have shown that *T. artroviride* cells might share a common molecular language with *N. crassa*. In addition, it has been shown that the transcriptional factor Ste12 and the MAPK Tmk1 (homolog to MAK-2) are essential for cell fusion and mycoparasitism in *T. atroviride*, suggesting that both processes share the same molecular pathway (Gruber and Zeilinger, 2014). Based on these data, we hypothesize that cell fusion might have served as the base for the origin of the mycoparasitic behavior.

In nature, *Trichoderma* is usually found in the soil and it is used as a biocontrol agent due to its prevalence to attack pathogenic fungi such as *F. oxysporum* (Dubey et al., 2007). It is likely that the same machinery, which mediates fusion related cell-cell interactions, guide *Trichoderma* hyphae towards their prey.

To test this hypothesis, several future experiments need to be performed. First of all, mutants of the *so*-homolog in *T. atroviride* must be created and tested for mycoparasitism. If our hypothesis is right, mutants lacking SO should not be able to detect and infect other fungi. Since the function of SO is more specifically related to cell fusion, it will be more interesting to mutate this gene than the MAPK, which are usually involved in multiple processes. Second, localization of MAK-2 and SO in *N. crassa* while interacting with *T. atroviride* must be tested for the typical oscillating dynamics. Third, for the same reason, the subcellular dynamics of the MAK-2 homolog and SO-homolog in *T. atroviride* should be tested. It would be also of great interest to create analog-sensitive variants of the MAK-2-homolog in *T. atroviride* to observe at which stage the protein activity is essential and to study its functions after cell-cell contact is established, and the mycoparasitic program of *T. atroviride* becomes fully activated.

SUMMARY

5 Summary

Cell fusion is essential for the development and propagation of most eukaryotic organisms. In the filamentous fungus *Neurospora crassa*, cell fusion is observed during early colony establishment, when germinating spores fuse into a supracellular network which further develops into the highly interconnected mycelial colony. The interaction of these genetically identical germlings is mediated by an unusual signaling mechanism in which, in order to avoid self-signaling, the cells take turns in signal sending and receiving. The switch between these two physiological states is represented by the alternating membrane recruitment of the SO protein and the MAP kinase MAK-2, respectively. This dialog-like behavior is observed until the cells establish physical contact, when MAK-2 and SO both accumulate at the contact area. At this stage a second MAP kinase, MAK-1, is also recruited to the cell contact area, in order to control the subsequent steps of cell wall remodeling and membrane fusion.

The goal of this thesis was to further characterize the molecular functions of the MAP kinases MAK-2 and MAK-1. A specific focus was the investigation of the relationship between the activity of these kinases and their subcellular spatial and temporal dynamics, by using molecular genetics, protein mislocalization, chemical genetics and live cell imaging. The results revealed that recruitment to and release from the plasma membrane is essential for the function of MAK-2. Membrane recruitment of this kinase results in its phosphorylation and the presence of phosphorylated MAK-2 at the membrane prevents the recruitment of SO. These data provided for the first-time insight into the molecular mechanism coordinating the dynamics of MAK-2 and SO. Analysis of the hyperphosphorylation in different mutant background revealed that activation depends on the up-stream kinases MEK-2 and MIK-2 as well as BEM-1 and HAM-6, which could also be placed upstream of the kinase module. The chemical genetics approaches revealed, that the proper subcellular dynamics of MAK-2 do not only depend on its phosphorylation, but surprisingly also on is enzymatic activity, supporting a model, in which activation of MAK-2 activates positive and negative feedback loops resulting in the observed highly coordinated dynamics of the different signaling factors.

Specific inhibition of MAK-2 further indicated that the kinase has additional functions after cell-cell contact during fusion pore formation.

In this phase, the CWI MAP kinase MAK-1 also plays an important function, which might be related to cell wall remodeling and fusion pore formation. This work, revealed, however, for the first time another additional function of MAK-1 during the tropic growth phase. Specific inhibition of this kinase during tropic growth resulted in disassembly of the actin aster mediating the growth of the cell tips, and mislocalization of SO and MAK-2. Similar defects were observed after the inhibition of the Rho-GTPase RAC-1, suggesting for a first time a functional link between these factors. In contrast, after inhibition of the second kinase MAK-2, the actin aster stayed intact, however, its subcellular localization became instable within the cell. Together these observations led to a new working model, in which MAK-1 promotes the formation and stability of the actin aster, while MAK-2 controls its position and thereby the growth directionality of the cells.

A second independent research project investigated the conservation of cell fusion in other filamentous fungi. While cell fusion has been described in many filamentous fungi, such as *Fusarium oxysporum f. sp. Lycopersici* or *Botrytis cinerea*, the molecular mechanism behind this process has not been described in these other fungi. This study revealed that the MAK-2 and SO homologs in *B. cinerea*, BMP-1 and, BcSO respectively, are both essential for germling fusion. Their subcellular dynamics during the tropic growth phase are comparable to *N. crassa*, indicating high conservation of the cell communication mechanism. When *N. crassa* and *B. cinerea* spore were mixed, interspecies interactions were readily observed indicating that also the so far unknown communication signal and its cognate receptor must be conserved and that both fungi share a common molecular language. Earlier studies reported that fusion of *B. cinerea* spore germlings is suppressed during growth on hydrophobic plant surfaces, suggesting that infection and fusion are two alternative, mutually exclusive developmental routes.

In contrast, *N. crassa* is completely unaffected by hydrophobicity and always induces the cell fusion program after germination. Based on these observations we hypothesized that the induction of fusion by signals produced by *N. crassa* might suppress pathogenic development of *B. cinerea*. First experiments using a mixture of spores from both species clearly supported this hypothesis.

The preliminary data of this second project are of very high relevance as a basis for different future research areas, including fungal developmental decision making, the design of new strategies of fungal control, and the molecular basis of mycoparasitism and horizontal gene transfer.

.

REFERENCES

6 References

Abmayr, S.M., Pavlath, G.K., **2012**. Myoblast fusion: lessons from flies and mice. Development 139, 641–656. https://doi.org/10.1242/dev.068353

Aldabbous, M.S., Roca, M.G., Stout, A., Huang, I.C., Read, N.D., Free, S.J., **2010**. The *ham-5*, *rcm-1* and *rco-1* genes regulate hyphal fusion in *Neurospora crassa*. Microbiology 156, 2621–2629. https://doi.org/10.1099/mic.0.040147-0

Alonso-monge, R., **2010**. MAPK cell-cycle regulation in 1125–1141.

Alonso-Rodríguez, E., Fernández-Piñar, P., Sacristán-Reviriego, A., Molina, M., Martín, H., **2016**. An analog-sensitive version of the protein kinase Slt2 allows identification of novel targets of the yeast cell wall integrity pathway. J. Biol. Chem. 291, 5461–5472. https://doi.org/10.1074/jbc.M115.683680

Araujo-Palomares, C.L., Richthammer, C., Seiler, S., Castro-Longoria, E., **2011**. Functional characterization and cellular dynamics of the CDC-42 - RAC - CDC-24 module in neurospora crassa. PLoS One 6. https://doi.org/10.1371/journal.pone.0027148

Barnett, H.L., **1963**. The Nature of Mycoparasitism by Fungi. Annu. Rev. Microbiol. 17, 1–14. https://doi.org/10.1146/annurev.mi.17.100163.000245

Bayram, Ö., Bayram, Ö.S., Ahmed, Y.L., Maruyama, J. ichi, Valerius, O., Rizzoli, S.O., Ficner, R., Irniger, S., Braus, G.H., **2012**. The Aspergillus nidulans MAPK module AnSte11-Ste50-Ste7-Fus3 controls development and secondary metabolism. PLoS Genet. 8. https://doi.org/10.1371/journal.pgen.1002816

Becker, Y., Eaton, C., Brasell, E., **2014**. The Fungal Cell Wall Integrity MAPK Cascade is Crucial for Hyphal Network Formation and Maintenance of Restrictive Growth of *Epichloë festucae* in Symbiosis With *Lolium perenne*. Mol. Plant. Microbe. Interact. 28, 69–85. https://doi.org/10.1094/MPMI-06-14-0183-R

Berepiki, A., Lichius, A., Read, N.D., **2011**. Actin organization and dynamics in filamentous fungi. Nat. Rev. Microbiol. 9, 876–887. https://doi.org/10.1038/nrmicro2666

Berepiki, A., Lichius, A., Shoji, J.Y., Tilsner, J., Read, N.D., **2010**. F-actin dynamics in *Neurospora crassa*. Eukaryot. Cell 9, 547–557. https://doi.org/10.1128/EC.00253-09

Bernhards, Y., Pöggeler, S., **2011**. The phocein homologue SmMOB3 is essential for vegetative cell fusion and sexual development in the filamentous ascomycete *Sordaria macrospora*. Curr. Genet. 57, 133–149. https://doi.org/10.1007/s00294-010-0333-z

Biosciences, E., Genetics, F., Genetics, F., **2014**. Ajb Centennial Review *Neurospora crassa* : Looking Back and Looking Forward 101, 2022–2035. https://doi.org/10.3732/ajb.1400377

Bishop, A.C., Ubersax, J. a, Petsch, D.T., Matheos, D.P., Gray, N.S., Blethrow, J., Shimizu, E., Tsien, J.Z., Schultz, P.G., Rose, M.D., Wood, J.L., Morgan, D.O., Shokat, K.M., **2000**. A chemical switch for inhibitor-sensitive alleles of any protein kinase. Nature 407, 395–401. https://doi.org/10.1038/35030148

Boyce, B.F., **2013**. Advances in the regulation of osteoclasts and osteoclast functions. J. Dent. Res. 92, 860–867. https://doi.org/10.1177/0022034513500306

Bradford, M.M., **1976**. A rapid and sensitive method for the quantitation of microgram quantities of protein utilizing the principle of protein-dye binding. Anal. Biochem. 72, 248–254. https://doi.org/10.1016/0003-2697(76)90527-3

Brunet, A., Le Roux, D., Lenormand, P., Dowd, S., Keyse, S., Pouyssé Gur, J., **1999**. Nuclear translocation of p42/p44 mitogen-activated protein kinase is required for growth factor-induced gene expression and cell cycle entry. EMBO J. 18, 664–674. https://doi.org/10.1093/emboj/18.3.664

Buchsbaum, R.J., **2007**. Rho activation at a glance. J. Cell Sci. 120, 1149–1152. https://doi.org/10.1242/jcs.03428

Büttner, P., Koch, F., Voigt, K., Quidde, T., Risch, S., Blaich, R., Brückner, B., Tudzynski, P., **1994**. Variations in ploidy among isolates of *Botrytis cinerea*: implications for genetic and molecular analyses. Curr. Genet. 25, 445–450. https://doi.org/10.1007/BF00351784

Cano-domı, N., Karen, A., Cano-Domínguez, N., Álvarez-Delfín, K., Hansberg, W., Aguirre, J., **2008**. NADPH oxidases NOX-1 and NOX-2 require the regulatory subunit NOR-1 to control cell differentiation and growth in *Neurospora crassa*. Eukaryot. Cell 7, 1352–1361. https://doi.org/10.1128/EC.00137-08

Charlton, N.D., Shoji, J.Y., Ghimire, S.R., Nakashima, J., Craven, K.D., **2012**. Deletion of the fungal gene *soft* disrupts mutualistic symbiosis between the grass endophyte *Epichloë festucae* and the host plant. Eukaryot. Cell 11, 1463–1471. https://doi.org/10.1128/EC.00191-12

Chen, R.E., Patterson, J.C., Goupil, L.S., Thorner, J., **2010**. Dynamic localization of Fus3 mitogen-activated protein kinase is necessary to evoke appropriate responses and avoid cytotoxic effects. Mol. Cell. Biol. 30, 4293–4307. https://doi.org/10.1128/MCB.00361-10

Chen, R.E., Thorner, J., **2007**. Function and regulation in MAPK signaling pathways: lessons learned from the yeast *Saccharomyces cerevisiae*. Biochim. Biophys. Acta 1773, 1311–40. https://doi.org/10.1016/j.bbamcr.2007.05.003

Colot, H. V., Park, G., Turner, G.E., Ringelberg, C., Crew, C.M., Litvinkova, L., Weiss, R.L., Borkovich, K.A., Dunlap, J.C., **2006**. A high-throughput gene knockout procedure for *Neurospora* reveals functions for multiple transcription factors. October 103, 16614–16615.

Corvest, V., Bogliolo, S., Follette, P., Arkowitz, R.A., Bassilana, M., **2013**. Spatiotemporal regulation of Rho1 and Cdc42 activity during *Candida albicans* filamentous growth. Mol. Microbiol. 89, 626–648. https://doi.org/10.1111/mmi.12302

Craven, K.D., Vélëz, H., Cho, Y., Lawrence, C.B., Mitchell, T.K., **2008**. Anastomosis is required for virulence of the fungal necrotroph *Alternaria brassicicola*. Eukaryot. Cell 7, 675–683. https://doi.org/10.1128/EC.00423-07

Davis, R.H., Perkins, D.D., **2002**. *Neurospora*: A model of model microbes. Nat. Rev. Genet. 3, 397–403. https://doi.org/10.1038/nrg797

De Nobel, H., Van den Ende, H., Klis, F.M., **2000**. Cell wall maintenance in fungi. Trends Microbiol. 8, 344–345. https://doi.org/10.1016/S0966-842X(00)01805-9

Dean, R., Van Kan, J.A.L., Pretorius, Z.A., Hammond-Kosack, K.E., Di Pietro, A., Spanu, P.D., Rudd, J.J., Dickman, M., Kahmann, R., Ellis, J., Foster, G.D., **2012**. The Top 10 fungal pathogens in molecular plant pathology. Mol. Plant Pathol. 13, 414–430. https://doi.org/10.1111/j.1364-3703.2011.00783.x

Dettmann, A., Heilig, Y., Valerius, O., Ludwig, S., Seiler, S., **2014**. Fungal communication requires the MAK-2 pathway elements STE-20 and RAS-2, the NRC-1 adapter STE-50 and the MAP kinase scaffold HAM-5. PLoS Genet. 10, e1004762. https://doi.org/10.1371/journal.pgen.1004762

Dettmann, A., Illgen, J., März, S., Schürg, T., Fleissner, A., Seiler, S., **2012**. The NDR Kinase Scaffold HYM1/MO25 Is Essential for MAK2 MAP Kinase Signaling in *Neurospora crassa*. PLoS Genet. 8, e1002950. https://doi.org/10.1371/journal.pgen.1002950

Dirschnabel, D.E., Nowrousian, M., Cano-Domínguez, N., Aguirre, J., Teichert, I., Kück, U., **2014**. New insights into the roles of NADPH oxidases in sexual development and ascospore germination in *Sordaria macrospora*. Genetics 196, 729–744. https://doi.org/10.1534/genetics.113.159368/-/DC1

Dittmar, T., Zänker, K., **2011**. Cell Fusion in health and disease.

Doehlemann, G., Berndt, P., Hahn, M., **2006**. Different signalling pathways involving a G protein, cAMP and a MAP kinase control germination of *Botrytis cinerea* conidia. Mol. Microbiol. 59, 821–835. https://doi.org/10.1111/j.1365-2958.2005.04991.x

Doi, K., Gartner, a, Ammerer, G., Errede, B., Shinkawa, H., Sugimoto, K., Matsumoto, K., **1994**. MSG5, a novel protein phosphatase promotes adaptation to pheromone response in *S. cerevisiae*. EMBO J. 13, 61–70.

Dubey, S.C., Suresh, M., Singh, B., **2007**. Evaluation of *Trichoderma* species against *Fusarium oxysporum f. sp. ciceris* for integrated management of chickpea wilt. Biol. Control 40, 118–127. https://doi.org/10.1016/j.biocontrol.2006.06.006

Dudin, O., Bendezu, F.O., Groux, R., Laroche, T., Seitz, A., Martin, S.G., **2015**. A formin-nucleated actin aster concentrates cell wall hydrolases for cell fusion in fission yeast. J. Cell Biol. 208, 897–911. https://doi.org/10.1083/jcb.201411124

Duelli, D.M., Padilla-Nash, H.M., Berman, D., Murphy, K.M., Ried, T., Lazebnik, Y., **2007**. A Virus Causes Cancer by Inducing Massive Chromosomal Instability through Cell Fusion. Curr. Biol. 17, 431–437. https://doi.org/10.1016/j.cub.2007.01.049

Fan, L., Li, R., Pan, J., Ding, Z., Lin, J., **2015**. Endocytosis and its regulation in plants. Trends Plant Sci. 20, 388–397. https://doi.org/10.1016/j.tplants.2015.03.014

Fitzpatrick, D.A., **2012**. Horizontal gene transfer in fungi. FEMS Microbiol. Lett. 329, 1–8. https://doi.org/10.1111/j.1574-6968.2011.02465.x

Fleißner, A., **2013**. Turning the switch : using chemical genetics to elucidate protein kinase functions in filamentous fungi. Fungal Biol. Rev. 27, 25–31. https://doi.org/10.1016/j.fbr.2013.02.001

Fleißner, A., Glass, N.L., **2007**. SO, a protein involved in hyphal fusion in *Neurospora crassa*, localizes to septal plugs. Eukaryot. Cell 6, 84–94. https://doi.org/10.1128/EC.00268-06

Fleissner, A., Leeder, A.C., Roca, M.G., Read, N.D., Glass, N.L., **2009**. Oscillatory recruitment of signaling proteins to cell tips promotes coordinated behavior during cell fusion. Proc. Natl. Acad. Sci. U. S. A. 106, 19387–19392. https://doi.org/10.1073/pnas.0907039106

Fleißner, A., Sarkar, S., Jacobson, D.J., Roca, M.G., Read, N.D., Glass, N.L., **2005**. The so locus is required for vegetative cell fusion and postfertilization events in *Neurospora crassa*. Eukaryot. Cell 4, 920–930. https://doi.org/10.1128/EC.4.5.920-930.2005

Fleißner, A., Serrano, A., **2015**. The Art of Networking : Vegetative Hyphal Fusion in Filamentous Ascomycete Fungi. Mycota - Growth, Differ. Sex. 1–53. https://doi.org/10.1007/978-3-319-25844-7_7

Fu, C., Ao, J., Dettmann, A., Seiler, S., Free, S.J., **2014**. Characterization of the *Neurospora crassa* Cell Fusion Proteins, HAM-6, HAM-7, HAM-8, HAM-9, HAM-10, AMPH-1 and WHI-2. PLoS One 9. https://doi.org/10.1371/journal.pone.0107773

Fu, C., Iyer, P., Herkal, A., Abdullah, J., Stout, A., Free, S.J., **2011**. Identification and characterization of genes required for cell-to-cell fusion in *Neurospora crassa*. Eukaryot. Cell 10, 1100–1109. https://doi.org/10.1128/EC.05003-11

Galagan, J.E., Calvo, S.E., Borkovich, K. a, Selker, E.U., Read, N.D., Jaffe, D., FitzHugh, W., Ma, L.-J., Smirnov, S., Purcell, S., Rehman, B., Elkins, T., Engels, R., Wang, S., Nielsen, C.B., Butler, J., Endrizzi, M., Qui, D., Ianakiev, P., Bell-Pedersen, D., Nelson, M.A., Werner-Washburne, M., Selitrennikoff, C.P., Kinsey, J. a, Braun, E.L., Zelter, A., Schulte, U., Kothe, G.O., Jedd, G., Mewes, W., Staben, C., Marcotte, E., Greenberg, D., Roy, A., Foley, K., Naylor, J., Stange-Thomann, N., Barrett, R., Gnerre, S., Kamal, M., Kamvysselis, M., Mauceli, E., Bielke, C., Rudd, S., Frishman, D., Krystofova, S., Rasmussen, C., Metzenberg, R.L., Perkins, D.D., Kroken, S., Cogoni, C., Macino, G., Catcheside, D., Li, W., Pratt, R.J., Osmani, S. a, DeSouza, C.P.C., Glass, L., Orbach, M.J., Berglund, J.A., Voelker, R., Yarden, O., Plamann, M., Seiler, S., Dunlap, J., Radford, A., Aramayo, R., Natvig, D.O., Alex, L. a, Mannhaupt, G., Ebbole, D.J., Freitag, M., Paulsen, I., Sachs, M.S., Lander, E.S., Nusbaum, C., Birren, B., **2003**. The genome sequence of the filamentous fungus *Neurospora crassa*. Nature 422, 859–868. https://doi.org/10.1038/nature01554

Galletta, B.J., Mooren, O.L., Cooper, J.A., **2010**. Actin dynamics and endocytosis in yeast and mammals. Curr. Opin. Biotechnol. 21, 604–610. https://doi.org/10.1016/j.copbio.2010.06.006

Gao, Y., Dickerson, J.B., Guo, F., Zheng, J., Zheng, Y., **2004**. Rational design and characterization of a Rac GTPase-specific small molecule inhibitor. Proc. Natl. Acad. Sci. U. S. A. 101, 7618–23. https://doi.org/10.1073/pnas.0307512101

Genetics, U.C., Dissect, T., Kinase, P., **2007**. Using Chemical Genetics and ATP Analogues To Dissect Protein Kinase Function 2, 299–314.

Giesbert, S., Siegmund, U., Schumacher, J., Kokkelink, L., Tudzynski, P., **2014**. Functional Analysis of BcBem1 and Its Interaction Partners in *Botrytis cinerea*: Impact on Differentiation and Virulence. PLoS One 9, e95172. https://doi.org/10.1371/journal.pone.0095172

Glass, N.L., Rasmussen, C., Roca, M.G., Read, N.D., **2004**. Hyphal homing, fusion and mycelial interconnectedness. Trends Microbiol. 12, 135–141. https://doi.org/10.1016/j.tim.2004.01.007

Goryachev, A.B., Lichius, A., Wright, G.D., Read, N.D., **2012**. Excitable behavior can explain the “ping-pong” mode of communication between cells using the same chemoattractant. BioEssays 34, 259–266. https://doi.org/10.1002/bies.201100135

Graziano, B.R., DuPage, A.G., Michelot, A., Breitsprecher, D., Moseley, J.B., Sagot, I., Blanchoin, L., Goode, B.L., **2011**. Mechanism and cellular function of Bud6 as an actin nucleation-promoting factor. Mol. Biol. Cell 22, 4016–4028. https://doi.org/10.1091/mbc.E11-05-0404

Gruber, S., Zeilinger, S., **2014**. The transcription factor Ste12 mediates the regulatory role of the Tmk1 MAP kinase in mycoparasitism and vegetative hyphal fusion in the filamentous fungus *Trichoderma atroviride*. PLoS One 9. https://doi.org/10.1371/journal.pone.0111636

Harding, A., Tian, T., Westbury, E., Frische, E., Hancock, J.F., **2005**. Subcellular localization determines MAP kinase signal output. Curr. Biol. 15, 869–873. https://doi.org/10.1016/j.cub.2005.04.020

Havlik, D., Brandt, U., Bohle, K., Fleißner, A., **2017**. Establishment of *Neurospora crassa* as a host for heterologous protein production using a human antibody fragment as a model product. Microb. Cell Fact. 16, 1–15. https://doi.org/10.1186/s12934-017-0734-5

Heller, J., Zhao, J., Rosenfield, G., Kowbel, D.J., Gladieux, P., Glass, N.L., **2016**. Characterization of Greenbeard Genes Involved in Long-Distance Kind Discrimination in a Microbial Eukaryote. PLOS Biol. 14, e1002431. https://doi.org/10.1371/journal.pbio.1002431

Herzog, S., Schumann, M.R., Fleißner, A., **2015**. Cell fusion in *Neurospora crassa*. Curr. Opin. Microbiol. 28, 53–59. https://doi.org/10.1016/j.mib.2015.08.002

Hutchison, E., Brown, S., Tian, C., Glass, N.L., **2009**. Transcriptional profiling and functional analysis of heterokaryon incompatibility in *Neurospora crassa* reveals that reactive oxygen species, but not metacaspases, are associated with programmed cell death. Microbiology 155, 3957–3970. https://doi.org/10.1099/mic.0.032284-0

Hyakumachi, M., Ui, T., **1987**. Non-self-anastomosing isolates of *Rhizoctonia solani* obtained from fields of sugarbeet. Trans. Br. Mycol. Soc. 89, 155–159. https://doi.org/10.1016/S0007-1536(87)80147-X

Illgen, J., **2017**. Untersuchungen zur subzellul ¨aren Dynamik, Funktion und Aktivität von Kinasen des MAK-2 MAP-Kinasen-Moduls während der Zell-Zell-Kommunikation in *Neurospora crassa*. Technische Universität Braunschweig.

Ishikawa, F.H., Souza, E.A., Shoji, J.Y., Connolly, L., Freitag, M., Read, N.D., Roca, M.G., **2012**. Heterokaryon incompatibility is suppressed following conidial anastomosis tube fusion in a fungal plant pathogen. PLoS One 7. https://doi.org/10.1371/journal.pone.0031175

Jeffries, P., **1995**. Biology and ecology of mycoparasitism. Can. J. Bot. 73, 1284–1290. https://doi.org/10.1139/b95-389

Jonkers, W., Fischer, M.S., Do, H.P., Starr, T.L., Louise Glass, N., **2016**. Chemotropism and cell fusion in *Neurospora crassa* relies on the formation of distinct protein complexes by HAM-5 and a novel protein HAM-14. Genetics 203, 334–391. https://doi.org/10.1534/genetics.115.185348

Jonkers, W., Leeder, A.C., Ansong, C., Wang, Y., Yang, F., Starr, T.L., Camp, D.G., Smith, R.D., Glass, N.L., **2014**. HAM-5 Functions As a MAP Kinase Scaffold during Cell Fusion in *Neurospora crassa.* PLoS Genet. 10, e1004783. https://doi.org/10.1371/journal.pgen.1004783

Kondoh, K., Nishida, E., **2007**. Regulation of MAP kinases by MAP kinase phosphatases. Biochim. Biophys. Acta - Mol. Cell Res. 1773, 1227–1237. https://doi.org/10.1016/j.bbamcr.2006.12.002

Kuo, H.-C., Hui, S., Choi, J., Asiegbu, F.O., Valkonen, J.P.T., Lee, Y.-H., **2014**. Secret lifestyles of *Neurospora crassa*. Sci. Rep. 4, 5135. https://doi.org/10.1038/srep05135

Lacaze, I., Lalucque, H., Siegmund, U., Silar, P., Brun, S., **2015**. Identification of NoxD/Pro41 as the homologue of the p22phox NADPH oxidase subunit in fungi. Mol. Microbiol. 95, 1006–24. https://doi.org/10.1111/mmi.12876

Lamson, R.E., Takahashi, S., Winters, M.J., Pryciak, P.M., **2006**. Dual role for membrane localization in yeast MAP kinase cascade activation and its contribution to signaling fidelity. Curr. Biol. 16, 618–623. https://doi.org/10.1016/j.cub.2006.02.060

Leeder, A.C., Jonkers, W., Li, J., Louise Glass, N., **2013**. Early colony establishment in *Neurospora crassa* requires a MAP kinase regulatory network. Genetics 195, 883–898. https://doi.org/10.1534/genetics.113.156984

Leeder, A.C., Palma-Guerrero, J., Glass, N.L., **2011**. The social network: deciphering fungal language. Nat. Rev. Microbiol. 9, 440–451. https://doi.org/10.1038/nrmicro2580

Lehmeyer, M., Kanofsky, K., Hanko, E.K.R., Ahrendt, S., Wehrs, M., Machens, F., Hehl, R., **2016**. Functional dissection of a strong and specific microbe-associated molecular pattern-responsive synthetic promoter. Plant Biotechnol. J. 14, 61–71. https://doi.org/10.1111/pbi.12357

Levin, D.E., **2011**. Regulation of cell wall biogenesis in *Saccharomyces cerevisiae*: The cell wall integrity signaling pathway. Genetics 189, 1145–1175. https://doi.org/10.1534/genetics.111.128264

Li, D., Bobrowicz, P., Wilkinson, H.H., Ebbole, D.J., **2005**. A mitogen-activated protein kinase pathway essential for mating and contributing to vegetative growth in *Neurospora crassa*. Genetics 170, 1091–1104. https://doi.org/10.1534/genetics.104.036772

Lichius, A., **2010**. Cell Fusion in *Neurospora crassa*: Ph.D. Thesis: The University of Edinburgh, Edinburgh, UK.

Lichius, A., Goryachev, A.B., Fricker, M.D., Obara, B., Castro-Longoria, E., Read, N.D., **2014**. CDC-42 and RAC-1 regulate opposite chemotropisms in *Neurospora crassa*. J. Cell Sci. 127, 1953–1965. https://doi.org/10.1242/jcs.141630

Lichius, A., Goryachev, A.B., Fricker, M.D., Obara, B., Castro-Longoria, E., Read, N.D., **2014**. CDC-42 and RAC-1 regulate opposite chemotropisms in *Neurospora crassa*. J. Cell Sci. 127, 1953–65. https://doi.org/10.1242/jcs.141630

Lichius, A., Yáñez-Gutiérrez, M.E., Read, N.D., Castro-Longoria, E., **2012**. Comparative live-cell imaging analyses of SPA-2, BUD-6 and BNI-1 in *Neurospora crassa* reveal novel features of the filamentous fungal polarisome. PLoS One 7, e30372. https://doi.org/10.1371/journal.pone.0030372

Lyons, D.M., Mahanty, S.K., Choi, K., Manandhar, M., Elion, E.A., **1996**. The SH3-Domain Protein Bem1 Coordinates Mitogen-Activated Protein Kinase Cascade Activation with Cell Cycle Control in *Saccharomyces cerevisiae*. Mol. Cell. Biol. 16, 4095–4106. https://doi.org/10.1128/MCB.16.8.4095

Maddi, A., Dettman, A., Fu, C., Seiler, S., Free, S.J., **2012**. WSC-1 and HAM-7 are MAK-1 MAP kinase pathway sensors required for cell wall integrity and hyphal fusion in *Neurospora crassa*. PLoS One 7, 1–10. https://doi.org/10.1371/journal.pone.0042374

Maeder, C.I., Hink, M.A., Kinkhabwala, A., Mayr, R., Bastiaens, P.I.H., Knop, M., **2007**. Spatial regulation of Fus3 MAP kinase activity through a reaction-diffusion mechanism in yeast pheromone signalling. Nat. Cell Biol. 9, 1319–1326. https://doi.org/10.1038/ncb1652

Maerz, S., Ziv, C., Vogt, N., Helmstaedt, K., Cohen, N., Gorovits, R., Yarden, O., Seiler, S., **2008**. The nuclear Dbf2-related kinase COT1 and the mitogen-activated protein kinases MAK-1 and MAK-2 genetically interact to regulate filamentous growth, hyphal fusion and sexual development in *Neurospora crassa*. Genetics 179, 1313–1325. https://doi.org/10.1534/genetics.108.089425

Makushok, T., Alves, P., Huisman, S.M., Kijowski, A.R., Brunner, D., **2016**. Sterol-Rich Membrane Domains Define Fission Yeast Cell Polarity. Cell 165, 1182–1196. https://doi.org/10.1016/j.cell.2016.04.037

Marschall, R., Tudzynski, P., **2016**. BcIqg1, a fungal IQGAP homolog, interacts with NADPH oxidase, MAP kinase and Calcium signaling proteins and regulates virulence and development in *Botrytis cinerea*. Mol. Microbiol. 00, 1–18. https://doi.org/10.1111/mmi.13391

Martin, S.G., Arkowitz, R.A., **2014**. Cell polarization in budding and fission yeasts. FEMS Microbiol. Rev. 38, 228–253. https://doi.org/10.1111/1574-6976.12055

Martine, C., Brenner, S.L., Spector, I., Korn, D.E., **1987**. Inhibition of actin polymerization by latrunculin A 2, 316–318.

Matheos, D., Metodiev, M., Muller, E., Stone, D., Rose, M.D., **2004**. Pheromone-induced polarization is dependent on the Fus3p MAPK acting through the formin Bni1p. J. Cell Biol. 165, 99–109. https://doi.org/10.1083/jcb.200309089

Mattison, C.P., Ota, I.M., **2000**. Two protein tyrosine phosphatases, Ptp2 and Ptp3, modulate the subcellular localization of the Hog1 MAP kinase in yeast. Genes Dev. 14, 1229–1235. https://doi.org/10.1101/gad.14.10.1229

McClean, M.N., Mody, A., Broach, J.R., Ramanathan, S., **2007**. Cross-talk and decision making in MAP kinase pathways. Nat. Genet. 39, 409–414. https://doi.org/10.1038/ng1957

Mehrabi, R., Bahkali, A.H., Abd-Elsalam, K.A., Moslem, M., Ben M'Barek, S., Gohari, A.M., Jashni, M.K., Stergiopoulos, I., Kema, G.H.J., De Wit, P.J.G.M., **2011**. Horizontal gene and chromosome transfer in plant pathogenic fungi affecting host range. FEMS Microbiol. Rev. 35, 542–554. https://doi.org/10.1111/j.1574-6976.2010.00263.x

Merlini, L., Dudin, O., Martin, S.G., **2013**. Mate and fuse: how yeast cells do it. Open Biol. 3, 130008–130008. https://doi.org/10.1098/rsob.130008

Michaelson, D., Silletti, J., Murphy, G., D'Eustachio, P., Rush, M., Philips, M.R., **2001**. Differential localization of Rho GTPases in live cells: Regulation by hypervariable regions and RhoGDI binding. J. Cell Biol. 152, 111–126. https://doi.org/10.1083/jcb.152.1.111

Mishra, M., Huang, J., Balasubramanian, M.K., **2014**. The yeast actin cytoskeleton. FEMS Microbiol. Rev. 38, 213–227. https://doi.org/10.1111/1574-6976.12064

Mooren, O.L., Galletta, B.J., Cooper, J.A., **2012**. Roles for Actin Assembly in Endocytosis. Annu. Rev. Biochem. 81, 661–686. https://doi.org/10.1146/annurev-biochem-060910-094416

Neumann, B., Coakley, S., Giordano-Santini, R., Linton, C., Lee, E.S., Nakagawa, A., Xue, D., Hilliard, M.A., **2015**. EFF-1-mediated regenerative axonal fusion requires components of the apoptotic pathway. Nature 517, 219–222. https://doi.org/10.1038/nature14102

Neumann, B., Nguyen, K.C.Q., Hall, D.H., Ben-Yakar, A., Hilliard, M.A., **2011**. Axonal regeneration proceeds through specific axonal fusion in transected *C. elegans* neurons. Dev. Dyn. 240, 1365–1372. https://doi.org/10.1002/dvdy.22606

Ninomiya, Y., Suzuki, K., Ishii, C., Inoue, H., **2004**. Highly efficient gene replacements in *Neurospora* strains deficient for nonhomologous end-joining. PNAS 101.

Pandey, A., Roca, M.G., Read, N.D., Glass, N.L., **2004**. Role of a Mitogen-Activated Protein Kinase Pathway during Conidial Germination and Hyphal Fusion in *Neurospora crassa*. Eukaryot. Cell 3, 348–358. https://doi.org/10.1128/EC.3.2.348

Park, G., Pan, S., Borkovich, K.A., Al, P.E.T., **2008**. Mitogen-Activated Protein Kinase Cascade Required for Regulation of Development and Secondary Metabolism in *Neurospora crassa* 7, 2113–2122. https://doi.org/10.1128/EC.00466-07

Perkins, D.D., Davis, R.H., **2000**. Evidence for safety of *Neurospora* species for academic and commercial uses. Appl. Environ. Microbiol. 66, 5107–5109. https://doi.org/10.1128/AEM.66.12.5107-5109.2000

Plotnikov, A., Flores, K., Maik-Rachline, G., Zehorai, E., Kapri-Pardes, E., Berti, D. a, Hanoch, T., Besser, M.J., Seger, R., **2015**. The nuclear translocation of ERK1/2 as an anticancer target. Nat. Commun. 6, 6685. https://doi.org/10.1038/ncomms7685

Prados Rosales, R.C., Di Pietro, A., **2008**. Vegetative hyphal fusion is not essential for plant infection by *Fusarium oxysporum*. Eukaryot. Cell 7, 162–171. https://doi.org/10.1128/EC.00258-07

Qi, M., Elion, E.A., **2007**. Formin-induced actin cables are required for polarized recruitment of the Ste5 scaffold and high level activation of MAPK Fus3. J. Cell Sci. 120, 712–712. https://doi.org/10.1242/jcs03398

Qiu, H., Cai, G., Luo, J., Bhattacharya, D., Zhang, N., **2016**. Extensive horizontal gene transfers between plant pathogenic fungi. BMC Biol. 14, 1–11. https://doi.org/10.1186/s12915-016-0264-3

Rasmussen, C.G., Glass, N.L., **2005**. A Rho-Type GTPase , *rho-4*, Is Required for Septation in *Neurospora crassa*. Eukaryot. Cell 4, 1913–1925. https://doi.org/10.1128/EC.4.11.1913

Richard, F., Glass, N.L., Pringle, A., **2012**. Cooperation among germinating spores facilitates the growth of the fungus , *Neurospora crassa* 419–422.

Richthammer, C., Enseleit, M., Sanchez-Leon, E., März, S., Heilig, Y., Riquelme, M., Seiler, S., **2012**. RHO1 and RHO2 share partially overlapping functions in the regulation of cell wall integrity and hyphal polarity in *Neurospora crassa*. Mol. Microbiol. 85, 716–733. https://doi.org/10.1111/j.1365-2958.2012.08133.x

Riedl, J., Crevenna, A.H., Kessenbrock, K., Yu, J.H., Neukirchen, D., Bista, M., Bradke, F., Jenne, D., Holak, T.A., Werb, Z., Sixt, M., Wedlich-Soldner, R., **2008**. Lifeact: A versatile marker to visualize F-actin. Nat. Methods 5, 605–607. https://doi.org/10.1038/nmeth.1220

Robertson, A.S., Smythe, E., Ayscough, K.R., **2009**. Functions of actin in endocytosis. Cell. Mol. Life Sci. 66, 2049–2065. https://doi.org/10.1007/s00018-009-0001-y

Roca, G.M., Weichert, M., Siegmund, U., Tudzynski, P., Fleißner, A., **2012**. Germling fusion via conidial anastomosis tubes in the grey mould *Botrytis cinerea* requires NADPH oxidase activity. Fungal Biol. 116, 379–387. https://doi.org/10.1016/j.funbio.2011.12.007

Roca, M.G., Davide, L.C., Davide, L.M.C., Mendes-costa, M.C., Schwan, R.F., Wheals, A.E., **2004**. Conidial anastomosis fusion between *Colletotrichum* species 108, 1320–1326. https://doi.org/10.1017/S0953756204000838

Roca, M.G., Kuo, H.C., Lichius, A., Freitag, M., Read, N.D., **2010**. Nuclear dynamics, mitosis, and the cytoskeleton during the early stages of colony initiation in *Neurospora crassa*. Eukaryot. Cell 9, 1171–1183. https://doi.org/10.1128/EC.00329-09

Roh, D.-H., Blair Bowers, Martin Schmidt, Enrico Cabib, **2002**. The Septation Apparatus, an Autonomous System in Budding Yeast. Mol. Biol. Cell 5, 2372–2384. https://doi.org/10.1091/mbc.E02

Román, E., Arana, D.M., Nombela, C., Alonso-Monge, R., Pla, J., **2007**. MAP kinase pathways as regulators of fungal virulence. Trends Microbiol. 15, 181–190. https://doi.org/10.1016/j.tim.2007.02.001

Sagot, I., Klee, S.K., Pellman, D., **2002**. Yeast formins regulate cell polarity by controlling the assembly of actin cables. Nat. Cell Biol. 4, 42–50. https://doi.org/10.1038/nc719

Schnabel, R., Hutter, H., Moerman, D., Schnabel, H., **1997**. Assessing Normal Embryogenesis in *Caenorhabditis elegans* Using a 4D Microscope: Variability of Development and Regional Specification. Dev. Biol. 184, 234–265. https://doi.org/10.1006/dbio.1997.8509

Schumacher, J., **2012**. Tools for *Botrytis cinerea*: New expression vectors make the gray mold fungus more accessible to cell biology approaches. Fungal Genet. Biol. 49, 483–497. https://doi.org/10.1016/j.fgb.2012.03.005

Schumann, M., 2018. Identifizierung und Charakterisierung molekularer Faktoren der pilzlichen Zell-Zell-Kommunikation und -Fusion. Techsniche Universität Braunschweig.

Schürg, T., **2012**. Der molekulare Adapter BEM-1 in Zellpolarität , gerichtetem Wachstum und Zell - Fusion in *Neurospora crassa*. Technische Universität Braunschweig.

Schürg, T., Brandt, U., Adis, C., Fleißner, A., **2012**. The *Saccharomyces cerevisiae* BEM1 homologue in *Neurospora crassa* promotes co-ordinated cell behaviour resulting in cell fusion. Mol. Microbiol. 86, 349–366. https://doi.org/10.1111/j.1365-2958.2012.08197.x

Seale, T., **1973**. Life cycle of *Neurospora crassa* viewed by scanning electron microscopy. J. Bacteriol. 113, 1015–1025.

Serrano, A., Hammadeh, H.H., Herzog, S., Illgen, J., Schumann, M.R., Weichert, M., Fleißner, A., **2017**. The dynamics of signal complex formation mediating germling fusion in *Neurospora crassa*. Fungal Genet. Biol. 101, 31–33. https://doi.org/10.1016/j.fgb.2017.02.003

Serrano, A., Illgen, J., Brandt, U., Thieme, N., Letz, A., Lichius, A., Read, N., Fleißner, A., **2018**. Spatio-temporal MAP kinase dynamics mediate cell behavior coordination during fungal somatic cell fusion. J. Cell Sci. jcs.213462. https://doi.org/10.1242/jcs.213462

Shemer, G., Podbilewicz, B., **2000**. Fusomorphogenesis: Cell fusion in organ formation. Dev. Dyn. 218, 30–51. https://doi.org/10.1002/(SICI)1097-0177(200005)218:1<30::AID-DVDY4>3.0.CO;2-W

Smythe, E., Ayscough, K.R., **2006**. Actin regulation in endocytosis. J. Cell Sci. 119, 4589–4598. https://doi.org/10.1242/jcs.03247

Takemoto, D., Kamakura, S., Saikia, S., Becker, Y., Wrenn, R., Tanaka, A., Sumimoto, H., Scott, B., **2011**. Polarity proteins Bem1 and Cdc24 are components of the filamentous fungal NADPH oxidase complex. Proc. Natl. Acad. Sci. U. S. A. 108, 2861–2866. https://doi.org/10.1073/pnas.1017309108

Tatebe, H., Nakano, K., Maximo, R., Shiozaki, K., **2008**. Pom1 DYRK Regulates Localization of the Rga4 GAP to Ensure Bipolar Activation of Cdc42 in Fission Yeast. Curr. Biol. 18, 322–330. https://doi.org/10.1016/j.cub.2008.02.005

Teichert, I., Steffens, E.K., Schnaß, N., Fränzel, B., Krisp, C., Wolters, D.A., Kück, U., **2014**. PRO40 is a scaffold protein of the cell wall integrity pathway, linking the MAP kinase module to the upstream activator protein kinase C. PLoS Genet. 10, e1004582. https://doi.org/10.1371/journal.pgen.1004582

Van Den Boogert, P.H.J.F., Deacon, J.W., **1994**. Biotrophic mycoparasitism by *Verticillium biguttatum* on *Rhizoctonia solani*. Eur. J. Plant Pathol. 100, 137–156. https://doi.org/10.1007/BF01876247

Van Drogen, F., Peter, M., **2001**. MAP kinase dynamics in yeast. Biol. Cell 93, 63–70. https://doi.org/10.1016/S0248-4900(01)01123-6

van Drogen, F., Stucke, V.M., Jorritsma, G., Peter, M., **2001**. MAP kinase dynamics in response to pheromones in budding yeast. Nat. Cell Biol. 3, 1051–1059. https://doi.org/10.1038/ncb1201-1051

Viterbo, A., Horwitz, B.A., **2010**. Mycoparasitism 676–693. https://doi.org/10.1128/9781555816636

Vogt, N., Seiler, S., **2008**. The RHO1-specific GTPase-activating Protein LRG1 Regulates Polar Tip Growth in Parallel to Ndr Kinase Signaling in *Neurospora* 19, 4554–4569. https://doi.org/10.1091/mbc.E07

Wainstein, E., Seger, R., **2016**. The dynamic subcellular localization of ERK: Mechanisms of translocation and role in various organelles. Curr. Opin. Cell Biol. 39, 15–20. https://doi.org/10.1016/j.ceb.2016.01.007

Weichert, M., **2016**. Zelluläres Allgemeingut mit spezifischer Wirkung: Definierte strukturelle Merkmale von Sterolen beeinflussen die Zell-Zell-Kommunikation und -Fusion in *Neurospora crassa.* Technische Universität Braunschweig.

Weichert, M., Lichius, A., Priegnitz, B.-E., Brandt, U., Gottschalk, J., Nawrath, T., Groenhagen, U., Read, N.D., Schulz, S., Fleißner, A., **2016**. Accumulation of specific sterol precursors targets a MAP kinase cascade mediating cell–cell recognition and fusion. Proc. Natl. Acad. Sci. 113, 201610527. https://doi.org/10.1073/pnas.1610527113

Westergaard, M., Mitchell, H.K., **1947**. *Neurospora* V. A Synthetic Medium Favoring Sexual Reproduction. Am. J. Bot. 34, 573–577.

Willet, A.H., McDonald, N.A., Gould, K.L., **2016**. Regulation of contractile ring formation and septation in *Schizosaccharomyces pombe*. Curr Opin Microbiol 37232, 1922–2013. https://doi.org/10.1016/j.mib.2015.08.001

Williamson, B., Tudzynski, B., Tudzynski, P., Van Kan, J.A.L., **2007**. *Botrytis cinerea*: The cause of grey mould disease. Mol. Plant Pathol. 8, 561–580. https://doi.org/10.1111/j.1364-3703.2007.00417.x

Wohlbold, L., Merrick, K.A., De, S., Amat, R., Kim, J.H., Larochelle, S., Allen, J.J., Zhang, C., Shokat, K.M., Petrini, J.H.J., Fisher, R.P., **2012**. Chemical Genetics Reveals a Specific Requirement for Cdk2 Activity in the DNA Damage Response and Identifies Nbs1 as a Cdk2 Substrate in Human Cells. PLoS Genet. 8. https://doi.org/10.1371/journal.pgen.1002935

Wurzinger, B., Mair, A., Pfister, B., Teige, M., **2011**. Cross-talk of calcium-dependent protein kinase and MAP kinase signaling. Plant Signal. Behav. 6, 8–12. https://doi.org/10.4161/psb.6.1.14012

Yoshimi, A., Miyazawa, K., Abe, K., **2016**. Cell wall structure and biogenesis in *Aspergillus* species. Biosci. Biotechnol. Biochem. 80, 1700–1711. https://doi.org/10.1080/09168451.2016.1177446

Young, M.E., Cooper, J.A., Bridgman, P.C., **2004**. Yeast actin patches are networks of branched actin filaments. J. Cell Biol. 166, 629–635. https://doi.org/10.1083/jcb.200404159

Zhan, X., Deschenes, R.J., Kun-liang, G., **1997**. Differential regulation of FUS3 MAP kinase by tyrosine-specificphosphatases in *Saccharomyces cerevisiae* 1690–1702. https://doi.org/10.1101/gad.11.13.1690

Zhao, X., Spraker, J.E., Bok, J.W., Velk, T., Hel, Z.M., Keller, N.P., **2017**. A cellular fusion cascade regulated by laea is required for sclerotial development in *Aspergillus flavus*. Front. Microbiol. 8, 1–12. https://doi.org/10.3389/fmicb.2017.01925

Zheng, L., Campbell, M., Murphy, J., Lam, S., Xu, J.-R., **2000**. The BMP1 Gene Is Essential for Pathogenicity in the Gray Mold Fungus *Botrytis cinerea*. Mol. Plant-Microbe Interact. MPMI 724, 724–732. https://doi.org/10.1094/MPMI.2000.13.7.724

Zito, F., Lampiasi, N., Kireev, I., Russo, R., **2016**. United we stand: Adhesion and molecular mechanisms driving cell fusion across species. Eur. J. Cell Biol. https://doi.org/10.1016/j.ejcb.2016.09.002

SUPPLEMENTARY INFORMATION

7 Supplementary information

The data presented in this section indicate show the raw data obtained for each of the figures.

7.1 Figure 3.1C

	Germination rate		Tropic interactions	
	Average	Standard deviation	Average	Standard deviation
Wild type	87.58	1.54	70.88	5.51
Δ*mak-2*	70.86	5.00	1.00	0.00
MAK-2-GFP, Δ*mak-2*	91.17	1.54	58.29	2.58
MAK-2-GFP-CAAX, Δ*mak-2*	70.33	3.67	1.00	0.00
MAK-2-GFP-SAAX, Δ*mak-2*	89.48	1.77	59.06	1.81

7.2 Figure 3.2B

Blot 1			
	Ratio	normalization	Log10
Lane 1	0.62	1.00	0.00
Lane 2	70.05	113.31	2.05
Lane 3	1.20	1.94	0.29
Lane 4	0.74	1.20	0.08
Lane 5	9.00	14.56	1.16
Lane 6	0.65	1.05	0.02

Blot 2			
	Ratio	normalization	Log10
Lane 1	0.38	1.00	0.00
Lane 2	63.71	169.77	2.23
Lane 3	0.71	1.88	0.28
Lane 4	0.54	1.44	0.16
Lane 5	10.94	29.16	1.46
Lane 6	0.84	2.25	0.35

Blot 3			
	Ratio	normalization	Log10
Lane 1	0.37	1.00	0.00
Lane 2	39.06	105.92	2.02
Lane 3	0.66	1.79	0.25
Lane 4	0.59	1.60	0.20
Lane 5	8.20	22.24	1.35
Lane 6	0.47	1.28	0.11

Blot 4			
	Ratio	normalization	Log10
Lane 1	0.13	1.00	0.00
Lane 2	14.80	114.80	2.06
Lane 3	0.24	1.84	0.26
Lane 4	0.27	2.08	0.32
Lane 5	5.62	43.62	1.64
Lane 6	0.51	3.94	0.59

Average of Log10		
	Average	standard deviation
Lane 1	0.00	0.00
Lane 2	2.09	0.08
Lane 3	0.27	0.01
Lane 4	0.19	0.09
Lane 5	1.40	0.17
Lane 6	0.27	0.22

7.3 Figure 3.2G

	gel 1	gel 2	gel 3	Average	Standard deviation
665	1	1	1	1	0
267	3.53466	3.60878	5.540723	4.228055	1.137408406
361	0.470067	0.342133	0.659965	0.490722	0.159919346
384	0.071655	0.045461	0.024156	0.047091	0.023791481
670	0.177958	0.017751	0.224943	0.140217	0.108629915
770	1.220174	1.664802	2.368712	1.751229	0.579126029

7.4 Figure 3.2H

	Germination rate		Tropic interactions	
	Average	Standard deviation	Average	Standard deviation
Wild type	97.82	0.14	84.13	3.58
Δmik-2	84.55	2.27	0.17	0.03
MAK-2-GFP-CAAX, *Δmik-2*	85.52	3.28	0.96	0.17
Δmek-2	87.62	2.91	0.13	0.03
MAK-2-GFP-CAAX, *Δmek-2*	83.87	2.81	0.79	0.01

7.5 Figure 3.3A

	Germination rate		Tropic interactions	
	Average	Standard deviation	Average	Standard deviation
Wild type	87.58	1.54	70.88	5.51
Δ*mak-2*	70.86	5.00	1.00	0.00
Ptef-1-mak-2-gfp	84.91	2.43	73.77	2.35
Ptef-1-mak-2-gfp-caax	89.98	1.80	34.90	1.83
Pmak-2-mak-2-gfp-caax	97.54	0.79	75.72	1.23
Ptef-1-mak-2-gfp-sax	95.20	0.63	86.23	2.51

7.6 Figure 3.7A

	Germination rate		Tropic interactions	
	Average	Standard deviation	Average	Standard deviation
Wild type	97.54	0.79	75.72	1.23
Ptef-1-mak-2$^{T180A/Y182F}$-gfp, Δmak-2	84.55	2.27	0.17	0.03
Ptef-1-mak-2^{T180A}-gfp, Δmak-2	82.89	4.70	0.19	0.01
Ptef-1-mak-2^{Y182F}-gfp, Δmak-2	84.19	4.90	0.17	0.01

7.7 Figure 3.9B

	Germination rate		Tropic interactions	
	Average	Standard deviation	Average	Standard deviation
DMSO	89.81	0.95	91.17	3.30
1-NM-PP1	89.60	0.82	4.38	2.87

7.8 Figure 3.11A

	Germination		Tropic interactions	
	Average	Standard deviation	Average	Standard deviation
Wild type	93.00	2.65	80.33	1.53
Δ*nox1*	89.33	1.53	1.00	0.00
MAK-2-GFP-CAAX, Δnox1	88.00	2.00	1.00	0.00
Δ*noxr*	91.67	1.53	1.00	0.00
MAK-2-GFP-CAAX, ΔnoxR	88.33	3.06	1.00	0.00
Δ*bem-1*	90.33	2.08	4.67	0.58
MAK-2-GFP-CAAX, Δbem-1	89.00	1.00	4.00	2.00
Δham-6	88.00	1.73	1.00	0.00
MAK-2-GFP-CAAX, Δham-6	89.00	2.00	1.00	0.00

7.9 Figure 3.12B

	Blot 1	Blot 2	Blot 3	Average	Standard deviation
665	1.00	1.00	1.00	1.00	0.00
267	3.53	3.61	5.54	4.23	1.14
361	0.47	0.34	0.66	0.49	0.16
384	0.07	0.05	0.02	0.05	0.02
670	0.18	0.02	0.22	0.14	0.11
770	1.22	1.66	2.37	1.75	0.58
723	3.58	4.56	6.81	4.98	1.65
719	5.71	3.83	4.20	4.58	0.99
569	1.09	1.27	1.59	1.31	0.25
773	1.37	2.66	1.33	1.79	0.76

7.10 Figure 3.13B

	Blot 1	Blot 2	Blot 3	Average	Standard deviation
665	1.00	1.00	1.00	1.00	0.00
267	4.50	5.93	6.95	5.79	1.01
361	0.53	0.51	0.67	0.57	0.07
775	3.49	4.87	7.81	5.39	1.80

7.11 Figure 4.1A

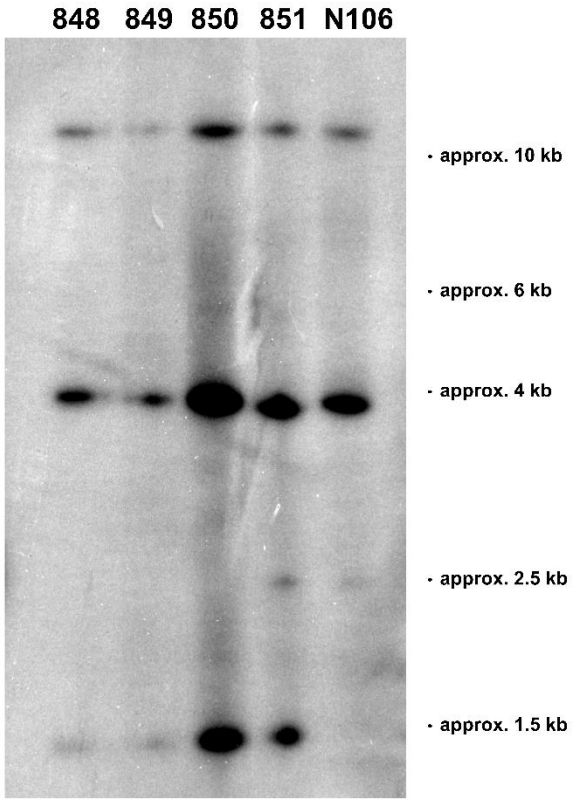

7.12 Figure 4.1D

	Germination		Tropic interactions	
	Average	Standard deviation	Average	Standard deviation
1NM-PP1	90.56	2.57	0.67	0.05
DMSO	87.66	2.19	81.11	1.97

7.13 Figure 4.9B

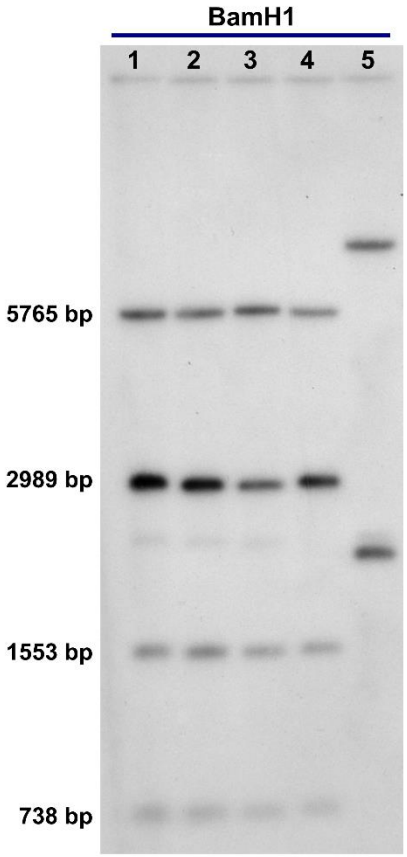

7.14 Figure 4.9D

	Germination		Tropic interactions	
	Average	Standard deviation	Average	Standard deviation
1NM-PP1	86.31	0.86	0.80	0.02
DMSO	84.14	0.42	51.40	1.75

7.15 Figure 4.12A

	Germination		Tropic interactions	
	Average	Standard deviation	Average	Standard deviation
N101	91.00	1.88	73.78	2.67
849	90.56	2.57	81.11	1.97
899	86.31	0.86	51.40	1.75
926	73.39	1.16	60.30	1.95

7.16 Figure 4.12B

	Germination		Tropic interactions	
	Average	Standard deviation	Average	Standard deviation
N101	91.00	1.88	69.14	0.62
849	90.56	2.57	0.67	0.05
899	86.31	0.86	0.80	0.02
926	73.39	1.16	1.20	0.56

7.17 Figure 4.14

	DMSO		1-NM-PP-1	
	Average	Standard deviation	Average	Standard deviation
N101	3.27	0.71	2.99	1.40
849	2.87	0.56	2.81	1.39
899	2.92	1.31	2.97	1.26

7.18 Figure 5.2A

	Germination		Tropic interactions	
	Average	Standard deviation	Average	Standard deviation
4h	68.30	3.37	1.42	0.19
6h	73.82	2.84	1.58	0.45
8h	86.59	1.42	4.21	2.00
10h	86.69	3.02	11.59	1.45
12h	89.91	2.25	25.82	2.29
15h	92.62	2.71	46.11	1.65
18h	97.44	1.17	50.54	1.12

7.19 Supplementary figure chapter 5

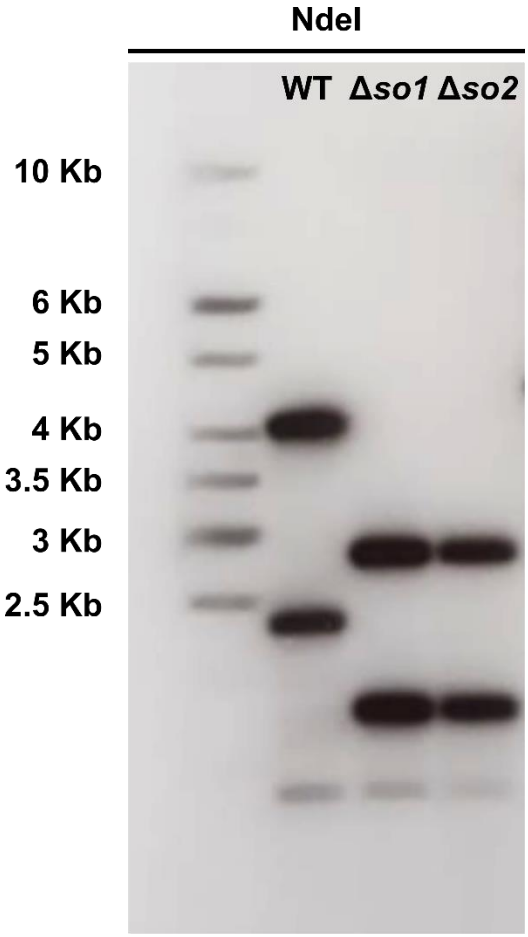

7.20 Figure 5.5B

	Germination		Tropic interactions	
	Average	Standard deviation	Average	Standard deviation
B05.10	92.62	2.71	46.11	1.65
Δ*bcso*	82.31	2.46	0.78	0.04
Δ*bmp1*	87.53	4.36	0.00	0.00

7.21 Figure 5.6B

	Germination		Tropic interactions	
	Average	Standard deviation	Average	Standard deviation
B05.10	92.62	2.71	46.11	1.65
Δ*bcso*	82.31	2.46	0.78	0.04
BcSO-GFP; Δ*bcso*	94.39	1.52	44.08	1.17

7.22 Figure 5.10B

		Area affected	cm to mm	Average	Standard deviation
WT	1	0.35	3.53	3.48	0.84
	2	0.41	4.09		
	3	0.37	3.74		
	4	0.28	2.83		
	5	0.24	2.37		
	6	0.49	4.93		
	7	0.20	2.03		
	8	0.43	4.25		
	9	0.33	3.32		
	10	0.37	3.72		
Δ*bcso*	1	0.30	3.02	3.09	0.65
	2	0.31	3.06		
	3	0.29	2.86		
	4	0.35	3.49		
	5	0.27	2.65		
	6	0.43	4.33		
	7	0.24	2.43		
	8	0.27	2.70		
	9	0.23	2.27		
	10	0.41	4.09		
BcSO-GFP Δ*bcso*	1	0.51	5.07	4.17	0.91
	2	0.43	4.27		
	3	0.53	5.29		
	4	0.48	4.75		
	5	0.31	3.09		
	6	0.50	4.96		
	7	0.24	2.42		
	8	0.47	4.67		
	9	0.34	3.35		
	10	0.39	3.87		

7.23 Figure 5.14A

	Average	Standard deviation
Control	4.23	9.76
N. crassa	9.07	9.75
B. cinerea	97.69	5.12
B. cinerea+N. crassa	43.82	18.51

7.24 Supplementary figure chapter 5

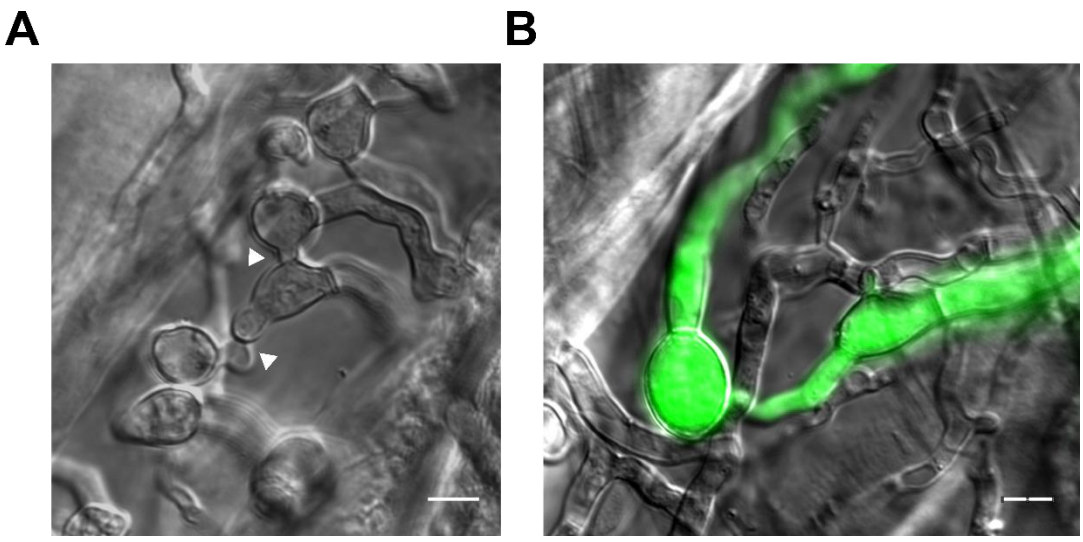

Figure 7.24. Mix of *N. crassa* and *B. cinerea* cells in an onion epidermis layer. (A) *N. crassa* cells undergo cell fusion (arrows) even when they are growing in hydrophobic surfaces, such as the epidermal layer of onion. (B) *B. cinerea* cells are capable of germinate when surrounded by a large number of germinated *N. crassa* cells. Scale bar: 5 µm

8 Acknowledgements

It’s hard to start writing this section. Thinking all the way back of the last 4 years, many people have contributed everyday to make me feel welcome in this country. Being honest, the weather and the language barrier were the hardest part, but knowing that there were always people that I could count with in our department, made me feel part of this “research” family and helped me to always go on.

One of the most important people for me in this family research is Prof. Dr. **André Fleißner**. Your willingness to always listen to us (and I think I can speak for all the students), to help us to create and follow our own ideas in the lab and your way to always bring the group together (field trips, cocktail nights, etc.), is wonderful. I feel very lucky to have been in your lab and grateful for giving me this opportunity 5 years ago. Thank you for giving us the chance to attend to so many conferences. Such wonderful experiences like the trips to San Francisco and Paris were really expensive, but still you always took us together, and this is something that we will always appreciate. To short it up, thank you for being a cool and wise supervisor.

I also would like to thank Prof. Dr. **Norbert F. Käufer**, because of his predisposition to being the referee for this thesis and for all his positive and constructive feedback in all our group seminars. Your comments were always helpful and help me to improve my communication skills and our research.

I would like to thank to Dr. **Barbara Schulz** for kindly accepting being part of my disputation committee.

I am also very grateful for the help and advice provided by Prof. Dr. **Reinhard Hehl** and **Konstantin Kanofsky** in our fungal infection experiments and for sharing the greenhouse for our plants.

I also feel grateful for all the advice and the help provided by Prof. Dr. **Ralf Schnabel** and **Christian Hennig** in the microscopy part and for the installation and guide on how to use the new microscope.

I also would like to thank to Prof. Dr. **Paul Tudzynski**, Dr. **Julia Schumacher** and Dr. **Robert Marschall** from Münster University for their help to manipulate and grow *B. cinerea* in our lab, besides providing plasmids, strains and plants needed for our experiments. Additionally, I am very grateful for letting me stay in their lab as a secondment for one week to learn and practice the transformation technique of this fungus. In this sense, I am also grateful to Prof. Dr. **Matthias Hahn** from the TU Kaiserslautern for providing some strains needed for our experiments.

I also would like to thank to the Marie Skłodowska-Curie actions (MSCA) of the European Commission for giving all the groups of the Initial Training Network "Fungibrain" the opportunity to collaborate and create together a research network. I want to thank to all the professors part of the network for the nice and positive discussion in every meeting and for the very interesting courses that took place in our consortium. I would like to make a special mention to Prof. Dr. **Sophie Martin** from the University of Lausanne for letting me stay in her lab as a secondment for three weeks to learn very useful microscopy techniques. I feel very lucky to have been part of this network during my PhD. Also, I feel very grateful to have meet the amazing students that were part of the consortium. **Pavlos, Tânia, Mariana, Patricia Silva, Valeria, Cassandre, Hugo, Klara, Saskia, Paola, Patricia Hernandez, Stefania and Luigi,** I cannot imagine this PhD without all of you, having tons of fun during our courses and meetings and learning a lot, thank you Fungibrainers!

During my working time in the lab, there was one person that helped me a lot and teach me almost everything I know about cloning. I feel very grateful to **Ulrike Brandt**, she always was there to rescue me when cloning or transformation didn't work, and thanks to her help in creating the strains, I was able to mostly focus in the experimental part of each chapter. Thank you for always being there with a smile and willing to help.

I'd like to make a special mention to our genetics department students, Dr. **Daniela Eckert**, **Nicole Andrée**, **Tanja Sastradihardja**, **Daniel Findeis** and **Konstantin Kanofsky**, for their nice comments and feedback in our PhD seminars and for all their help when needed. Special thanks to all the workers staff of our department, for making our research work much easier every day.

In particular, I would like to thank to **Marion Utecht** and **Carsta Mahnkopf** for being always friendly and very helpful in all the paperwork. I am really thankful for their willingness and patience to always translate everything to me.

I'd like to thanks to all the members of the Braunschweig Fungal Genetics Group. To the former students, Dr. **David Havlik**, Dr. **Julia Illgen**, Dr. **Suellen Finamor** and especially to Dr. **Martin Weichert**. The very nice research discussions that we had together was the start of the third chapter of this thesis. Your positive and constructive feedback in our meetings helped me a lot to become a better scientist. I also want to thank to all the current students of our research family, Dr. **Marcel R. Schumann**, **Stephanie Herzog** and **Hamzeh Haj Hammadeh, Anne Oostlander, Linda Matz and Hannah Knobel**. Thank you for all the funny times in the lab, outside the lab and in our trip conferences. Also thank you for all your help and your always positive feedback in our discussions. I feel very grateful to André for bringing together such an amazing group of people. I'd like to thanks to all the students that contributed to some parts of this thesis: **Hannah, Anne, Bianca, Jin, Larissa, Milan, Miriam and Natalie**. Thank you for your hard work.

Finalmente, me gustaría escribir estas palabras en español. Quiero agradecer a toda mi familia, por el apoyo que me han brindado, y por estar siempre ahí cuando los necesitaba. Estos 4 años han sido muy duros estando lejos de todos vosotros. Gracias por ser siempre un apoyo para continuar y seguir adelante, aún en los momentos más duros. No puedo evitar acordarme de todos mis abuelos, que, aunque ya no puedan leer estas palabras, sé que siempre me acompañarán. Por último, quiero agradecer a mi esposa, Nati, por todo lo que ha hecho por mí. Las circunstancias nos obligaron a vivir separados, pero el amor, el cariño y las decenas de viajes que hicimos para vernos consiguió mantenernos unidos. Esta tesis es tan tuya como mía. Gracias por ser como eres y estar siempre ahí para apoyarme en todo.

Curriculum vitae

Persönliche Daten

Antonio Serrano Salces

16.05.1990, Córdoba – Spain

Current address: C/ Músico Juan del Encina, 7, P.3-2. Córdoba 14011 Spain.

Email: a.serrano@tu-bs.de & antonioserr90@gmail.com

Studium und Schulbildung

From 09/2014	**Promotion (PhD) studies** in the Institut für Genetik at the Technische Universität Braunschweig
From 07/2013 to 07/2014	**Master of Sciences (M. Sc.)** in the Master in Molecular and Cellular Biotechnology and Genetics by the Universidad de Córdoba (Spain). The Master requires the achieve of a Master thesis, title as: "In vivo determination of intracellular pH using phluorin proteins in *Fusarium oxysporum*" and awarded as Outstanding Master's Thesis of 2014 by the Universidad de Córdoba. The research was performed under the supervision of Prof. Dr. Antonio Di Pietro in the same university.
From 09/2008 to 07/2013	**Bachelor of Biology (B. Sc.)** in the Universidad de Córdoba (Spain). The main occupational topics were: biotechnology, molecular biology, genetics, cellular biology, microbiology and immunology.
From 09/2002 to 07/2008	Highschool studies at Instituto de Enseñanza Secundaria "El Tablero".

Work experience

From 09/2014 to 07/2018	**Early stage researcher** (PhD student) at the Institut für Genetik at the TU Braunschweig. My research and salary were funded by the European commission (**Fungibrain** ITN project: 607963).

■ Training

Workshop I. Fungal genetics and Biology. Organizer: J. Wendland, Carlsberg Laboratory, Copenhagen. 10-14th June 2014.

Workshop II. Microfabrication for Microbiology. Organizer: N. Minc, Institut Jacques Monrod, Paris. 4th-6th May 2015.

Workshop III. Scientific Writing I. Organizer: P. Follette, CNRS, Nice. 11-12th May 2015

Workshop IV: Scientific Writing II. Organizer: P. Follette, hosted in University of Manchester, 25th- 5th May 2016

Workshop V: Systems Biology of Fungi. Hosted in University of Aberdeen, 12th-15th Sept. 2016.

Workshop VI: Chemical Genetics. Organizer: André Fleißner, TU Braunschweig, May 2017.

Workshop VII: Medical Mycology. Organizer: N. Gow and A. Brand, University of Aberdeen, 12th-15th Sept. 2016.

Workshop VIII: Grant Writing Skills. Organizer: N. Gow and A. Brand, University of Aberdeen, 12th-15th Sept. 2016.

Workshop IX: Antifungal discovery and company start-up. Organizer: J. Oliver, F2G, Manchester.

Summer School I. Phospholipid signaling and imaging. Organizer: R. Arkowitz and M. Bassilana, CNRS, Nice. 8th-13th May 2015.

Summer School II: Proteomics and Mass Spectrometry. Organizer: G. Braus, 19th-23rd Oct 2015, University Göttingen.

Summer School III: Calcium and Signaling and Live Cell imaging. Organizer: N. Read, 25th- 5th May 2016, University of Manchester.

Intensive Course. Industrial Agricultural and Fungicide Research. Organizer: M.Busch and P. Perret, BCS, Lyon. 7th May 2015

■ Veröffentlichungen und Tagungsbeiträge

Publications

Fleißner, A. and Serrano, A. The art of Networking: Vegetative Hyphal Fusion in Filamentous Ascomycete Fungi**.** The Mycota Vol. I: Growth, Differentiation and Sexuality, 3rd ed., ed. by Jürgen Wendland. 2015

Serrano, A., Hammadeh, H., Herzog, S., Illgen, J., Schumann, M., Weichert, M., Fleißner, A., The dynamics of signal complex formation mediating germling fusion in *Neurospora crassa*, Fungal Genetics and Biology (2017).

Serrano, A., Illgen, J., Brandt, U., Thieme, N., Letz, A., Lichius, A., Read, N., Fleißner, A., 2018. Spatio-temporal MAP kinase dynamics mediate cell behavior coordination during fungal somatic cell fusion. J. Cell Sci. jcs.213462. doi:10.1242/jcs.213462

Conferences

Subcellular dynamics of MAPKs mediating tropism and cell fusion in *Neurospora crassa*. Oral presentation in the **ITN Fungibrain Network meeting II**. 19.09.14**,** Salamanca, Spain.

Subcellular dynamics of MAPKs mediating tropism and cell fusion in *Neurospora crassa*. Oral presentation in the **VAAM Mini-Symposium of the Special Group "Fungal Biology and Biotechnology".** 02.03.2015 Marburg, Germany.

Subcellular dynamics of MAPKs mediating tropism and cell fusion in *Neurospora crassa*. Oral presentation in the **ITN Fungibrain Network meeting III.** 15.06.15, Nice, France**.**

Role of different NAPDH oxidase components in the regulation of the MAP kinase MAK-2 during cell fusion in *Neurospora crassa*. Poster presentation in the **11th VAAM Conference Molecular Biology of Fungi,** 7-9.10.15, Berlin, Germany.

Role of different NAPDH oxidase components in the regulation of the MAP kinase MAK-2 during cell fusion in *Neurospora crassa*. Poster presentation in the **ITN Fungibrain Mid Term Review Meeting,** 16.10.15 Göttingen, Germany

Subcellular localization influences the activity of the MAP Kinase MAK-2 during cell fusion in *Neurospora crassa*. Oral presentation in the **European "Neurospora Meeting" at ECFG13 Workshop,** 3 April 2016, Paris, France.

Subcellular localization influences the activity of the MAP Kinase MAK-2 during cell fusion in *Neurospora crassa***.** Poster presentation in the **13th European Conference on Fungal Genetics (ECFG13),** 4-6 April 2016, Paris, France.

Roles of the MAP Kinase MAK-2 during cell fusion in *Neurospora crassa*. Oral presentation in the **ITN Fungibrain Network Meeting IV,** 16.09.16, Aberdeen, UK.

Subcellular dynamics of the MAP kinase MAK-2 correlate with its activity during germling fusion, thereby mediating a conserved cell-cell signaling mechanism. Oral and poster presentation in the **29th Fungal Genetics Conference.** 14-19 March 2017 in the Asilomar conference center, California, USA.

Cell fusion in filamentous fungi. Oral presentation in the **ITN Fungibrain Final Meeting**, 14-15.09.17, Córdoba, Spain.

Cell fusion in filamentous fungi. Oral presentation at the **12th conference of the VAAM special group Molecular Biology of Fungi**, 28-30 September 2017 in Jena, Germany.

Identification of novel functions of the cell wall integrity MAP kinase MAK-1 during cell polarity and cell fusion. Poster presentation at the **12th conference of the VAAM special group Molecular Biology of Fungi**, 28-30 September 2017 in Jena, Germany.

The cell dialog mechanism mediating vegetative cell fusion in fungi is conserved in the plant pathogen *Botrytis cinerea*. Oral presentation at the **Annual Conference 2018 of the Association for General and Applied Microbiology**, 15-18 April 2018 in Wolfsburg, Germany.